ORGANISATION EUROPÉENNE POUR LA RECHERCHE NUCLÉAIRE

CERN **EUROPEAN ORGANIZATION FOR NUCLEAR RESEARCH**

Handbook of LHC Higgs cross sections:
1. Inclusive observables

Report of the LHC Higgs Cross Section Working Group

Editors: S. Dittmaier
C. Mariotti
G. Passarino
R. Tanaka

GENEVA
2011

Conveners

Gluon-Fusion process: M. Grazzini, F. Petriello, J. Qian, F. Stöckli

Vector-Boson-Fusion process: A. Denner, S. Farrington, C. Hackstein, C. Oleari, D. Rebuzzi

WH/ZH *production mode:* S. Dittmaier, R. Harlander, C. Matteuzzi, J. Olsen, G. Piacquadio

ttH *process:* C. Neu, C. Potter, L. Reina, M. Spira

MSSM neutral Higgs: M. Spira, M. Vazquez Acosta, M. Warsinsky, G. Weiglein

MSSM charged Higgs: M. Flechl, M. Krämer, S. Lehti, T. Plehn

PDF: S. Forte, J. Huston, K. Mazumdar, R. Thorne

Branching ratios: A. Denner, S. Heinemeyer, I. Puljak, D. Rebuzzi

NLO MC: M. Felcini, F. Maltoni, P. Nason, J. Yu

Higgs Pseudo-Observables: M. Dührssen, M. Felcini, S. Heinemeyer, G. Passarino

This Report should be cited as:

LHC Higgs Cross Section Working Group, S. Dittmaier, C. Mariotti, G. Passarino, R. Tanaka (Eds.), *Handbook of LHC Higgs Cross Sections: 1. Inclusive Observables*, CERN-2011-002 (CERN, Geneva, 2011).

Abstract

This Report summarizes the results of the first 10 months' activities of the LHC Higgs Cross Section Working Group. The main goal of the working group was to present the state of the art of Higgs Physics at the LHC, integrating all new results that have appeared in the last few years. The Report is more than a mere collection of the proceedings of the general meetings. The subgroups have been working in different directions. An attempt has been made to present the first Report from these subgroups in a complete and homogeneous form. The subgroups' contributions correspondingly comprise the main parts of the Report. A significant amount of work has been performed in providing higher-order corrections to the Higgs-boson cross sections and pinning down the theoretical uncertainty of the Standard Model predictions. This Report comprises explicit numerical results on total cross sections, leaving the issues of event selection cuts and differential distributions to future publications. The subjects for further study are identified.

We, the authors, would like to dedicate this Report to the memory of
Nicola Cabibbo and Georges Charpak.

S. Dittmaier[1], C. Mariotti[2], G. Passarino[2,3] and R. Tanaka[4] (eds.);
J. Baglio[5], P. Bolzoni[6], R. Boughezal[7], O. Brein[1], C. Collins-Tooth[8], S. Dawson[9], S. Dean[10],
A. Denner[11], S. Farrington[12], M. Felcini[13], M. Flechl[1], D. de Florian[14], S. Forte[15], M. Grazzini[16],
C. Hackstein[17], T. Hahn[18], R. Harlander[19], T. Hartonen[20], S. Heinemeyer[13], J. Huston[21],
A. Kalinowski[22], M. Krämer[23], F. Krauss[24], J.S. Lee[25], S. Lehti[20], F. Maltoni[26], K. Mazumdar[27],
S.-O. Moch[28], A. Mück[23], M. Mühlleitner[17], P. Nason[29], C. Neu[30], C. Oleari[29], J. Olsen[31],
S. Palmer[30], F. Petriello[7,32], G. Piacquadio[33], A. Pilaftsis[34], C.T. Potter[35], I. Puljak[36], J. Qian[37],
D. Rebuzzi[38], L. Reina[39], H. Rzehak[1,17], M. Schumacher[1], P. Slavich[40], M. Spira[41], F. Stöckli[33],
R.S. Thorne[10], M. Vazquez Acosta[42] T. Vickey[12,43], A. Vicini[15], D. Wackeroth[44], M. Warsinsky[1],
M. Weber[18], G. Weiglein[45], C. Weydert[46], J. Yu[47], M. Zaro[26], and T. Zirke[19].

[1] Physikalisches Institut, Albert-Ludwigs-Universität Freiburg, D-79104 Freiburg, Germany

[2] INFN, Sezione di Torino, Via P. Giuria 1, 10125 Torino, Italy

[3] Dipartimento di Fisica Teorica, Università di Torino, Via P. Giuria 1, 10125 Torino, Italy

[4] Laboratoire de l'Accélérateur Linéaire, CNRS/IN2P3, F-91898 Orsay CEDEX, France

[5] Laboratoire de Physique Théorique, Universite Paris XI et CNRS, F-91405 Orsay, France

[6] II. Institut für Theoretische Physik, Universität Hamburg,
Luruper Chaussee 149, D-22761 Hamburg, Germany

[7] High Energy Physics Division, Argonne National Laboratory,
Argonne, IL 60439, USA

[8] Department of Physics and Astronomy, University of Glasgow,
Glasgow G12 8QQ, UK

[9] Department of Physics, Brookhaven National Laboratory,
Upton, NY 11973, USA

[10] Department of Physics and Astronomy, University College London,
Gower Street, London WC1E 6BT, UK

[11] Institut für Theoretische Physik und Astrophysik, Universität Würzburg,
Am Hubland, D-97074 Würzburg, Germany

[12] Department of Physics, University of Oxford, Denys Wilkinson Building,
Keble Road, Oxford OX1 3RH, UK

[13] Instituto de Física de Cantabria (IFCA), CSIC-Universidad de Cantabria,
Santander, Spain

[14] Departamento de Física, Facultad de Ciencias Exactas y Naturales
Universidad de Buenos Aires, Pabellon I, Ciudad Universitaria (1428)
Capital Federal, Argentina

[15] Dipartimento di Fisica, Università degli Studi di Milano and INFN,
Sezione di Milano, Via Celoria 16, I-20133 Milan, Italy

[16] INFN, Sezione di Firenze and Dipartimento di Fisica e Astronomia, Università di Firenze,
I-50019 Sesto Fiorentino, Florence, Italy

[17] Institut für Theoretische Physik und Institut für Experimentelle Teilchenphysik,
Karlsruhe Institut of Technology, D-76131 Karlsruhe, Germany

[18] Max-Planck-Institut für Physik, Werner-Heisenberg-Institut,
Föhringer Ring 6, D-80805 München, Germany

[19] Bergische Universität Wuppertal, D-42097 Wuppertal, Germany

[20] Helsinki Institute of Physics, P.O. Box 64, FIN-00014 University of Helsinki, Finland

[21] Department of Physics and Astronomy, Michigan State University,
East Lansing, MI 48824, USA

[22] Faculty of Physics, University of Warsaw, Hoza 69, 00-681 Warsaw, Poland

[23] Institut für Theoretische Teilchenphysik und Kosmologie, RWTH Aachen University, D-52056 Aachen, Germany

[24] Institute for Particle Physics Phenomenology, Department of Physics, University of Durham, Durham DH1 3LE, UK

[25] National Center for Theoretical Sciences, 101, Section 2 Kuang Fu Road Hsinchu, Taiwan 300, Republic of China

[26] Centre for Cosmology, Particle Physics and Phenomenology (CP3), Université Catholique de Louvain, B-1348 Louvain-la-Neuve, Belgium

[27] Tata Institute of Fundamental Research, Homi Bhabha Road, Mumbai 400 005, India

[28] DESY, Zeuthen, Platanenallee 6, D-15738 Zeuthen, Germany

[29] Università di Milano-Bicocca and INFN, Sezione di Milano-Bicocca, Piazza della Scienza 3, 20126 Milan, Italy

[30] University of Virginia, Charlottesville, VA 22906, USA

[31] Department of Physics, Princeton University, Princeton, NJ 08542, USA

[32] Department of Physics & Astronomy, Northwestern University, Evanston, IL 60208, USA

[33] CERN, CH-1211 Geneva 23, Switzerland

[34] School of Physics and Astronomy, University of Manchester, Manchester M13 9PL, UK

[35] Department of Physics, University of Oregon, Eugene, OR 97403-1274, USA

[36] University of Split, FESB, R. Boskovica bb, 21 000 Split, Croatia

[37] Department of Physics, University of Michigan, Ann Arbor, MI 48109, USA

[38] Università di Pavia and INFN, Sezione di Pavia, Via A. Bassi, 6, 27100 Pavia, Italy

[39] Physics Department, Florida State University, Tallahassee, FL 32306-4350, USA

[40] Laboratoire de Physique Théorique et des Hautes Energies, 4 Place Jussieu, F-75252 Paris CEDEX 05, France

[41] Paul Scherrer Institut, CH–5232 Villigen PSI, Switzerland

[42] Physics Dept., Blackett Laboratory, Imperial College London, Prince Consort Rd, London SW7 2BW, UK

[43] School of Physics, University of the Witwatersrand, Private Bag 3, Wits 2050, Johannesburg, South Africa

[44] Department of Physics, SUNY at Buffalo, Buffalo, NY 14260-1500, USA

[45] DESY, Notkestrasse 85, D-22607 Hamburg, Germany

[46] Laboratory for Subatomic Physics and Cosmology, Université Joseph Fourier, (Grenoble 1), F-38026 Grenoble CEDEX, France

[47] Department of Physics, Univ. of Texas at Arlington, SH108, University of Texas, Arlington, TX 76019, USA

Prologue

The implementation of spontaneous symmetry breaking in the framework of gauge theories in the 1960s triggered the breakthrough in the construction of the standard electroweak theory, as it still persists today. The idea of driving the spontaneous breakdown of a gauge symmetry by a self-interacting scalar field, which thereby lends mass to gauge bosons, is known as the *Higgs mechanism* and goes back to the early work of Refs. [1–5]. The postulate of a new scalar neutral boson, known as the *Higgs particle*, comes as a phenomenological imprint of this mechanism. Since the birth of this idea, the Higgs boson has successfully escaped detection in spite of tremendous search activities at the high-energy colliders LEP and Tevatron, leaving open the crucial question whether the Higgs mechanism is just a theoretical idea or a 'true model' for electroweak symmetry breaking. The experiments at the Large Hadron Collider (LHC) will answer this question, either positively upon detecting the Higgs boson, or negatively by ruling out the existence of a particle with properties attributed to the Higgs boson within the Standard Model. In this sense the outcome of the Higgs search at the LHC will either carve our present understanding of electroweak interactions in stone or will be the beginning of a theoretical revolution.

Contents

---

[1]S. Dittmaier, C. Mariotti, G. Passarino and R. Tanaka

[2]M. Grazzini, F. Petriello, J. Qian, F. Stoeckli (eds.); J. Baglio, R. Boughezal and D. de Florian.

[3]A. Denner, S. Farrington, C. Hackstein, C. Oleari, D. Rebuzzi (eds.); P. Bolzoni, S. Dittmaier, F. Maltoni, S.-O. Moch, A. Mück, S. Palmer and M. Zaro.

[4]S. Dittmaier, R.V. Harlander, J. Olsen, G. Piacquadio (eds.); O. Brein, M. Krämer and T. Zirke.

[5]C. Collins-Tooth, C. Neu, L. Reina, M. Spira (eds.); S. Dawson, S. Dean, S. Dittmaier, M. Krämer, C.T. Potter and D. Wackeroth.

[6]M. Spira, M. Vazquez Acosta, M. Warsinsky, G. Weiglein (eds.); S. Dittmaier, R. Harlander, S. Heinemeyer, A. Kalinowski, M. Mühlleitner, M. Krämer, H. Rzehak, M. Schumacher, P. Slavich and T. Vickey.

[7]M. Flechl, M. Krämer, S. Lehti (eds.); S. Dittmaier, T. Hahn, T. Hartonen, S. Heinemeyer, J. S. Lee, A. Pilaftsis, M. Spira and C. Weydert.

[8]S. Forte, J. Huston, K. Mazumdar, R.S. Thorne and A. Vicini.

---

[9]A. Denner, S. Heinemeyer, I. Puljak, D. Rebuzzi (eds.); S. Dittmaier, A. Mück, M. Spira, M. Weber and G. Weiglein.

[10]M. Felcini, F. Krauss, F. Maltoni, P. Nason and J. Yu.

[11]S. Heinemeyer and G. Passarino.

[12]A. Denner, S. Dittmaier, S. Forte and G. Passarino.

[13]S. Dittmaier, C. Mariotti, G. Passarino and R. Tanaka.

1 Introduction[1]

After the start of pp collisions at the LHC the natural question is: Why precision Higgs physics now? The LHC successfully started at the end of 2009 colliding two proton beams at centre-of-mass energies of $\sqrt{s} = 0.9$ TeV and 2.36 TeV. In 2010 the energy has been raised up to 7 TeV.

By the end of the 7 TeV run in 2011 and (likely at 8 TeV) in 2012 each experiment aims to collect an integrated luminosity of a few inverse femtobarns. Then a long shutdown will allow the implementation of necessary modifications to the machine, to restart again at the design energy of 14 TeV. By the end of the life of the LHC, each experiment will have collected 3000 fb^{-1} on tape. The luminosity that the experiments expect to collect with the 7 TeV run will allow us to probe a wide range of the Higgs-boson mass. Projections of ATLAS and CMS when combining only the three main channels (H → $\gamma\gamma$, H → ZZ, H → WW), indicate that in case of no observed excess, the Standard Model (SM) Higgs boson can be excluded in the range between 140 GeV and 200 GeV. A 5σ significance can be reached for a Higgs-boson mass range between 160 GeV and 170 GeV. The experiments (ATLAS, CMS, and LHCb) are now analysing more channels in order to increase their potential for exclusion at lower and higher masses. For these reasons an update of the discussion of the proper definition of the Higgs-boson mass and width has become necessary. Indeed, in this scenario, it is of utmost importance to access the best theory predictions for the Higgs cross sections and branching ratios, using definitions of the Higgs-boson properties that are objective functions of the experimental data while respecting first principles of quantum field theory. In all parts we have tried to give a widely homogeneous summary for the precision observables. Comparisons among the various groups of authors are documented reflecting the status of our theoretical knowledge. This may be understood as providing a common opinion about the present situation in the calculation of Higgs cross sections and their theoretical and parametric errors.

The experiments have a coherent plan for using the input suggestions of the theoretical community to facilitate the combination of the individual results. Looking for precision tests of theoretical models at the level of their quantum structure requires the highest standards on the theoretical side as well. Therefore, this Report is the result of a workshop started as an appeal by experimentalists. Its progress over the subsequent months to its final form was possible only because of a close contact between the experimental and theory communities.

The major sections of this Report are devoted to discussing the computation of cross sections and branching ratios for the SM Higgs and for the Minimal Supersymmetric Standard Model (MSSM) Higgs bosons, including the still-remaining theoretical uncertainties. The idea of presenting updated calculations on Higgs physics was triggered by experimentalists and is substantiated as far as possible in this Report. The working group was organized in 10 subgroups. The first four address different Higgs production modes: gluon–gluon fusion, vector-boson fusion, Higgs-strahlung, and associated production with top-quark pairs. Two more groups are focusing on MSSM neutral and MSSM charged Higgs production. One group is dedicated to the prediction of the branching ratios (BR) of Higgs bosons in the SM and MSSM. Another group studies predictions from different Monte Carlo (MC) codes at next-to-leading order (NLO) and their matching to parton-shower MCs. The definition of Higgs pseudo-observables is also a relevant part of this analysis, in order to correctly match the experimental observables and the theoretical definitions of physical quantities. Finally, a group is devoted to parton density functions (PDFs), in particular to the issue of new theoretical input related to PDFs, in order to pin down the theoretical uncertainty on cross sections.

To discover or exclude certain Higgs-boson mass regions different inputs are needed:

- SM cross sections and BR in order to produce predictions;
- theoretical uncertainties on these quantities. These uncertainties enter also the determination of systematic errors of the mean value.

---

[1]S. Dittmaier, C. Mariotti, G. Passarino and R. Tanaka

Furthermore, common and correlated theoretical inputs (cross sections, PDFs, SM and MSSM parameters, etc.) require the highest standards on the theoretical side. The goal has been to give precise common inputs to the experiments to facilitate the combination of multiple Higgs search channels.

The structure of this Report centres on a description of cross sections computed at next-to-next-to-leading order (NNLO) or NLO, for each of the production modes. Comparisons among the various groups of authors for the central value and the range of uncertainty are documented and reflect the status of our theoretical knowledge. Note that all the central values have been computed using the same SM parameters input, as presented in table Table A of the Appendix. An update of the previous discussions of theoretical uncertainties has become necessary for several reasons:

- The PDF uncertainty has been computed following the PDF4LHC prescription as described in Section 8 of this Report.
- The α_s uncertainty has been added in quadrature to the PDF variation.
- The renormalization and factorization QCD scales have been varied following the criterion of pinning down, as much as possible, the theoretical uncertainty. It often remains the largest of the uncertainties.

A final major point is that, for this Report, all cross sections have been computed within an inclusive setup, not taking into account the experimental cuts and the acceptance of the apparatus. A dedicated study of these effects (cuts on the cross sections and on K-factors) will be presented in a future publication.

The final part of this Report is devoted to describing a new direction of work: what the experiments observe in the final state is not always directly connected to a well defined theoretical quantity. We have to take into account the acceptance of the detector, the definition of *signal*, the interference *signal–background*, and all sorts of approximations built into the Monte Carlo codes. As an example at LEP, the line shape of the Z for the final state with two electrons has to be extracted from the cross section of the process ($e^+e^- \to e^+e^-$), after having subtracted the contribution of the photon and the interference between the photon and the Z. A corrected definition of the Higgs-boson mass and width is needed. Both are connected to the corresponding complex pole in the p^2 plane of the propagator with momentum transfer p. We claim that the correct definition of mass of an unstable particle has to be used in Monte Carlo generators.

Different Monte Carlo generators exist at LO and NLO. It was important to compare their predictions and to stress the corresponding differences, also taking into account the different algorithms used for parton shower. Note that NLO matrix-element generators matched with a parton shower are the tools for the future. Beyond the goals of this Report remains the agreement between NLO MC predictions and NNLO calculations within the acceptance of the detectors. The next step in the activities of this working group will be the computation of cross sections that include acceptance cuts and differential distributions for all final states that will be considered in the Higgs search at the LHC. Preferably this should be carried out with the same set of (benchmark) cuts for ATLAS and CMS. The goal is to understand how the K-factors from (N)LO to (N)NLO will change after introduction of cuts and to compare the NNLO differential distributions with the ones from Monte Carlo generators at NLO. There is a final comment concerning the SM background: we plan to estimate theoretical predictions for the most important backgrounds in the signal regions. This means that a *background control region* has to be defined, and there the experiments will measure a given source of background directly from data. The *control region* can be in the bulk of the background production phase space, but can also be in the tail of the distributions. Thus it is important to define the precision with which the SM background will be measured and the theoretical precision available for that particular region. Then the background uncertainty should be extrapolated back to the *signal region*, using available theoretical predictions and their uncertainty. It will be important to compute the interference between signal and background and try to access this at NLO.

The (N)LO Monte Carlos will be used to simulate this background and determine how the K-factor is changing with the chosen kinematic cuts.

The present documentation is the result of a workshop that started in January 2010 as a new joint effort for Higgs cross sections between ATLAS, CMS, and the theory community.

In this Report the Higgs-boson cross section calculations are presented at the energy of the first pp run, 7 TeV, as well as at the nominal one (14 TeV). Updated tables at the future energy will be made available at the twiki page: https://twiki.cern.ch/twiki/bin/view/LHCPhysics/CrossSections .

2 Gluon-Fusion process[2]

2.1 Higgs-boson production in gluon–gluon fusion

Gluon fusion through a heavy-quark loop [6] (see Fig. 1) is the main production mechanism of the Standard Model Higgs boson at hadron colliders. When combined with the decay channels H → γγ, H → WW, and H → ZZ, this production mechanism is one of the most important for Higgs-boson searches and studies over the entire mass range, $100\text{ GeV} \lesssim M_{\text{H}} \lesssim 1\text{ TeV}$, to be investigated at the LHC.
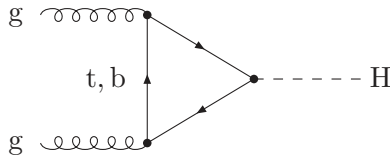
Fig. 1: Feynman diagram contributing to gg → H at lowest order.

The dynamics of the gluon-fusion mechanism is controlled by strong interactions. Detailed studies of the effect of QCD radiative corrections are thus necessary to obtain accurate theoretical predictions. In QCD perturbation theory, the leading order (LO) contribution [6] to the gluon-fusion cross section is proportional to α_{s}^2, where α_{s} is the QCD coupling constant. The main contribution arises from the top quark, due to its large Yukawa coupling to the Higgs boson. The QCD radiative corrections to this process at next-to-leading order (NLO) have been known for some time, both in the large-m_{t} limit [7,8] and maintaining the full top- and bottom-quark mass dependence [9,10]. They increase the LO cross section by about $80-100\%$ at the LHC. The exact calculation is very well approximated by the large-m_{t} limit. When the exact Born cross section with the full dependence on the mass of the top quark is used to normalize the result, the difference between the exact and the approximated NLO cross sections is only a few percent. The next-to-next-to-leading order (NNLO) corrections have been computed only in this limit [11–17], leading to an additional increase of the cross section of about 25%. The NNLO calculation has been consistently improved by resumming the soft-gluon contributions up to NNLL [18]. The result leads to an additional increase of the cross section of about $7-9\%$ ($6-7\%$) at $\sqrt{s} = 7$ (14) TeV. The NNLL result is nicely confirmed by the evaluation of the leading soft contributions at N^3LO [19–23].

Recent years have seen further progress in the computation of radiative corrections and in the assessment of their uncertainties. The accuracy of the large-m_{t} approximation at NNLO has been studied in Refs. [24–29]. These papers have definitely shown that if the Higgs boson is relatively light ($M_{\text{H}} \lesssim 300\text{ GeV}$), the large-$m_{\text{t}}$ approximation works extremely well, to better than 1%. As discussed below, these results allow us to formulate accurate theoretical predictions where the top and bottom loops are treated exactly up to NLO, and the higher-order corrections to the top contribution are treated in the large-m_{t} approximation [30].

Considerable work has also been done in the evaluation of electroweak (EW) corrections. Two-loop EW effects are now known [31–35]. They increase the cross section by a factor that strongly depends on the Higgs-boson mass, changing from $+5\%$ for $M_{\text{H}} = 120\text{ GeV}$ to about -2% for $M_{\text{H}} = 300\text{ GeV}$ [35]. The main uncertainty in the EW analysis comes from the fact that it is not obvious how to combine them with the large QCD corrections. In the *partial factorization* scheme of Ref. [35] the EW correction applies only to the LO result. In the *complete factorization* scheme, the EW correction instead multiplies the full QCD-corrected cross section. Since QCD corrections are sizeable, this choice has a non-negligible effect on the actual impact of EW corrections in the computation. The computation of the dominant mixed QCD–EW effects due to light quarks [30], performed using an effective-Lagrangian

---

[2]M. Grazzini, F. Petriello, J. Qian, F. Stoeckli (eds.); J. Baglio, R. Boughezal and D. de Florian.

approach, supports the complete factorization hypothesis, suggesting that EW corrections become a multiplicative factor times the full QCD expansion. This result should be interpreted carefully since the effective theory is strictly valid only when $M_H \ll M_W$. However, as discussed later, it is expected to be a good approximation to the exact result for Higgs-boson masses below several hundred GeV for the same reasons that the large-m_t limit furnishes a good approximation to the exact top-mass dependent calculation up to nearly $M_H = 1$ TeV. Very recently, EW effects for Higgs production at finite transverse momentum [36,37] have also been studied. Their effect is at the 1% level or smaller.

In the following we present the results of three updated computations, based on the work presented in Refs. [30,38] (see Section 2.2) and Refs. [39,40] (see Section 2.4).[3] These calculations use MSTW2008 NNLO parton distribution functions (PDFs) [41].

2.2 Cross-section predictions I

The following predictions are based on calculations by Anastasiou/Boughezal/Petriello/Stoeckli and by de Florian/Grazzini.

The calculation by Anastasiou, Boughezal, Petriello and Stoeckli (ABPS) [30] starts from the exact NLO cross section with full dependence on the top- and bottom-quark masses and includes the NNLO top-quark contribution in the large-m_t limit. The result includes EW contributions [32–35] according to Refs. [34,35], evaluated in the complete factorization scheme. Mixed QCD–EW contributions [30] are also accounted for, together with some effects from EW corrections at finite transverse momentum [36]. The effect of soft-gluon resummation is mimicked by choosing the central value of the renormalization and factorization scales as $\mu_R = \mu_F = M_H/2$. The latter choice is also motivated by an improved convergence of the fixed-order QCD perturbative expansion.

The calculation by de Florian and Grazzini (dFG) is a slightly improved version on the calculation presented in Ref. [38]. The starting point is the exact NLO cross section with full dependence on the top- and bottom-quark masses, computed with the program HIGLU [9,10], on top of which the NLL resummation of soft-gluon contributions is included. Then, the top-quark contribution is considered and the NNLL+NNLO corrections [18] are consistently added in the large-m_t limit. The result is finally corrected for EW contributions [32–35] according to Refs. [34,35] in the complete factorization scheme. The central value of factorization and renormalization scales is chosen to be $\mu_F = \mu_R = M_H$. The results of this calculation are available through an online calculator [42].

The results of the dFG and ABPS calculations are reported in Tables 1,3 and 2,4, respectively. For each Higgs-boson mass the corresponding cross section is reported. We also quote three uncertainties: Scale uncertainty, PDF+α_s uncertainty, and the latter uncertainty according to the PDF4LHC recipe, computed as discussed below. In Fig. 2 we present a comparison of ABPS and dFG results, including scale uncertainties. We see that the results are perfectly consistent and show a very good agreement over a wide range of Higgs-boson masses. At $\sqrt{s} = 7$ TeV the difference between ABPS and dFG central values ranges from $+3.5\%$ for $M_H = 100$ GeV to -6% for $M_H = 1$ TeV. In the range $M_H = 115-300$ GeV the difference ranges from $+3\%$ to $+1\%$. At $\sqrt{s} = 14$ TeV the difference between ABPS and dFG central values ranges from $+3.7\%$ for $M_H = 100$ GeV to -3% for $M_H = 1$ TeV. In the range $M_H = 115-300$ GeV the difference ranges from $+3\%$ to $+2\%$.

---

[3]The central values of these cross-section predictions are in good mutual agreement, but the error assessment – in particular of theoretical errors that go beyond mere scale uncertainties – is still under debate, leading to this splitting of cross-section predictions into parts I and II. It is worth noting that both calculations (ABPS and dFG) include the exact NLO mass dependence already. Also, the b mass parametric error should be accounted for by scale variations. The combined numbers in the Summary, Section 13, are based on the two predictions (ABPS and dFG) of the next section; the inclusion of the BD analysis described in Section 2.4, with a common combination of all uncertainties, is in progress.

Table 1: Results on $pp(gg) \rightarrow H + X$ cross sections with $\sqrt{s} = 7$ TeV based on dFG calculation, using MSTW2008 NNLO PDFs.

M_H[GeV]	σ[pb]	Scale [%]	PDF+α_s [%]	PDF4LHC [%]
90	29.48	+8.2 −8.7	+4.0 −3.1	+7.8 −6.7
95	26.48	+8.0 −8.6	+4.0 −3.0	+7.8 −6.7
100	23.97	+7.8 −8.4	+4.0 −3.0	+7.7 −6.8
105	21.74	+7.7 −8.3	+4.0 −3.0	+7.7 −6.9
110	19.81	+7.5 −8.1	+4.0 −3.0	+7.7 −6.9
115	18.12	+7.4 −8.0	+4.0 −3.0	+7.7 −7.0
120	16.63	+7.2 −7.9	+4.0 −3.0	+7.6 −7.0
125	15.31	+7.1 −7.8	+4.0 −3.1	+7.6 −7.1
130	14.13	+7.0 −7.7	+4.0 −3.1	+7.6 −7.2
135	13.08	+6.9 −7.6	+3.9 −3.1	+7.6 −7.3
140	12.14	+6.8 −7.5	+3.9 −3.1	+7.6 −7.3
145	11.29	+6.7 −7.5	+3.9 −3.1	+7.6 −7.4
150	10.52	+6.6 −7.4	+3.9 −3.1	+7.6 −7.5
155	9.80	+6.5 −7.3	+3.9 −3.1	+7.5 −7.5
160	9.08	+6.4 −7.2	+3.9 −3.1	+7.5 −7.6
165	8.35	+6.4 −7.2	+3.9 −3.2	+7.5 −7.7
170	7.76	+6.3 −7.1	+3.9 −3.2	+7.5 −7.8
175	7.24	+6.2 −7.0	+3.9 −3.2	+7.5 −7.8
180	6.76	+6.2 −7.0	+3.9 −3.2	+7.5 −7.8
185	6.32	+6.1 −6.9	+3.9 −3.2	+7.5 −7.8
190	5.92	+6.1 −6.9	+3.9 −3.3	+7.5 −7.8
195	5.57	+6.1 −6.8	+4.0 −3.3	+7.5 −7.8
200	5.27	+6.0 −6.8	+4.0 −3.3	+7.6 −7.8
210	4.74	+6.0 −6.7	+4.0 −3.4	+7.5 −7.9
220	4.29	+6.5 −6.6	+4.0 −3.4	+7.6 −7.9
230	3.92	+5.9 −6.5	+4.0 −3.4	+7.7 −8.0
240	3.59	+5.9 −6.4	+4.0 −3.5	+7.7 −8.0
250	3.32	+5.8 −6.3	+4.1 −3.5	+7.8 −8.1
260	3.08	+5.8 −6.3	+4.1 −3.6	+7.8 −8.1
270	2.87	+5.8 −6.2	+4.1 −3.6	+7.9 −8.1
280	2.70	+5.8 −6.1	+4.2 −3.7	+7.9 −8.2
290	2.55	+5.8 −6.1	+4.2 −3.7	+8.0 −8.3
300	2.42	+5.8 −6.0	+4.2 −3.8	+8.0 −8.3
320	2.25	+5.8 −6.0	+4.3 −3.9	+8.2 −8.4
340	2.20	+5.8 −5.9	+4.4 −4.0	+8.3 −8.4
360	2.36	+5.8 −5.9	+4.5 −4.1	+8.4 −8.5
380	2.26	+5.9 −5.6	+4.5 −4.2	+8.4 −8.6
400	2.03	+5.9 −5.4	+4.7 −4.3	+8.8 −8.6
450	1.37	+5.9 −5.3	+5.0 −4.5	+9.2 −8.7
500	0.865	+6.0 −5.2	+5.4 −4.8	+9.5 −8.9
550	0.538	+6.0 −5.2	+5.8 −5.0	+9.7 −9.0
600	0.336	+6.1 −5.2	+6.2 −5.3	+10.1 −9.4
650	0.212	+6.2 −5.2	+6.5 −5.5	+10.4 −9.7
700	0.136	+6.3 −5.3	+6.9 −5.8	+10.7 −9.9
750	0.0889	+6.4 −5.4	+7.2 −6.1	+10.9 −10.1
800	0.0588	+6.5 −5.4	+7.6 −6.3	+11.2 −10.4
850	0.0394	+6.5 −5.5	+8.0 −6.6	+11.8 −11.0
900	0.0267	+6.7 −5.6	+8.3 −6.9	+12.6 −11.8
950	0.0183	+6.8 −5.7	+8.8 −7.2	+13.5 −12.7
1000	0.0127	+7.0 −5.7	+9.1 −7.5	+14.2 −13.5

Table 2: Results on $pp(gg) \rightarrow H + X$ cross sections with $\sqrt{s} = 7$ TeV based on ABPS calculation, using MSTW2008 NNLO PDFs.

M_{H}[GeV]	σ[pb]	Scale [%]	PDF+α_{s} [%]	PDF4LHC [%]
90	30.70	+10.2 −11.9	+4.2 −3.1	+8.0 −6.9
95	27.54	+9.9 −10.8	+4.1 −3.1	+8.0 −6.9
100	24.81	+9.7 −10.5	+4.1 −3.1	+7.9 −7.0
105	22.47	+9.4 −10.3	+4.1 −3.1	+7.9 −7.0
110	20.44	+9.2 −10.1	+4.1 −3.1	+7.9 −7.1
115	18.67	+8.9 −10.0	+4.1 −3.1	+7.9 −7.2
120	17.12	+8.7 −9.8	+4.1 −3.1	+7.8 −7.2
125	15.74	+8.6 −9.7	+4.0 −3.1	+7.8 −7.3
130	14.52	+8.3 −9.6	+4.0 −3.1	+7.8 −7.4
135	13.43	+8.2 −9.4	+4.0 −3.1	+7.7 −7.4
140	12.45	+8.1 −9.3	+4.0 −3.1	+7.8 −7.5
145	11.58	+8.0 −9.3	+4.0 −3.2	+7.8 −7.5
150	10.79	+7.9 −9.3	+4.0 −3.2	+7.8 −7.6
155	10.08	+7.7 −9.2	+4.0 −3.2	+7.7 −7.7
160	9.36	+7.6 −9.2	+4.0 −3.2	+7.7 −7.7
165	8.54	+7.5 −9.2	+4.0 −3.2	+7.7 −7.8
170	7.92	+7.5 −9.2	+4.0 −3.2	+7.7 −7.9
175	7.40	+7.4 −9.2	+4.0 −3.3	+7.7 −7.9
180	6.93	+7.3 −9.1	+4.0 −3.3	+7.7 −7.9
185	6.44	+7.2 −9.1	+4.0 −3.3	+7.7 −8.0
190	6.03	+7.2 −9.1	+4.0 −3.3	+7.7 −8.0
195	5.67	+7.2 −9.1	+4.0 −3.4	+7.7 −8.0
200	5.36	+7.1 −9.1	+4.1 −3.4	+7.8 −8.0
210	4.82	+7.0 −9.1	+4.0 −3.4	+7.7 −8.0
220	4.37	+7.0 −9.0	+4.1 −3.5	+7.8 −8.1
230	3.98	+6.8 −9.0	+4.1 −3.5	+7.8 −8.1
240	3.65	+6.8 −9.0	+4.1 −3.5	+7.9 −8.2
250	3.37	+6.7 −9.0	+4.2 −3.6	+7.9 −8.2
260	3.12	+6.6 −9.0	+4.2 −3.6	+8.0 −8.3
270	2.91	+6.5 −9.0	+4.2 −3.7	+8.0 −8.3
280	2.73	+6.6 −9.0	+4.2 −3.7	+8.1 −8.3
290	2.58	+6.6 −8.9	+4.3 −3.8	+8.1 −8.4
300	2.45	+6.5 −8.9	+4.3 −3.8	+8.2 −8.4
320	2.28	+6.5 −9.0	+4.4 −3.9	+8.3 −8.5
340	2.25	+6.7 −9.2	+4.5 −4.0	+8.4 −8.6
360	2.44	+6.8 −9.2	+4.5 −4.1	+8.5 −8.6
380	2.31	+6.1 −8.9	+4.6 −4.2	+8.7 −8.7
400	2.05	+5.7 −8.6	+4.8 −4.3	+8.9 −8.7
450	1.35	+4.8 −8.2	+5.2 −4.6	+9.5 −8.9
500	0.844	+4.2 −7.9	+5.5 −4.8	+9.7 −9.0
550	0.522	+3.8 −7.7	+6.0 −5.1	+10.0 −9.2
600	0.325	+3.5 −7.5	+6.4 −5.4	+10.5 −9.6
650	0.205	+3.3 −7.4	+6.8 −5.6	+10.8 −9.9
700	0.131	+3.2 −7.3	+7.1 −5.9	+11.1 −10.2
750	0.0850	+3.1 −7.2	+7.5 −6.2	+11.3 −10.4
800	0.0560	+3.0 −7.2	+7.9 −6.5	+11.6 −10.8
850	0.0374	+2.9 −7.1	+8.3 −6.8	+12.3 −11.4
900	0.0253	+2.8 −7.1	+8.7 −7.2	+13.1 −12.2
950	0.0173	+2.8 −7.1	+9.1 −7.5	+14.0 −13.1
1000	0.0119	+2.7 −7.1	+9.5 −7.8	+14.9 −14.0

Table 3: Results on $\mathrm{pp(gg)} \to \mathrm{H} + X$ cross sections with $\sqrt{s} = 14$ TeV based on dFG calculation, using MSTW2008 NNLO PDFs.

M_H[GeV]	σ[pb]	Scale [%]	PDF+α_s [%]	PDF4LHC [%]
90	87.68	+8.7 −9.0	+4.0 −3.0	+7.3 −6.0
95	79.95	+8.5 −8.8	+3.9 −3.0	+7.3 −6.0
100	73.38	+8.3 −8.6	+3.9 −3.0	+7.2 −6.0
105	67.47	+8.1 −8.5	+3.9 −3.0	+7.2 −6.0
110	62.28	+7.9 −8.3	+3.9 −2.9	+7.2 −6.0
115	57.69	+7.8 −8.2	+3.8 −2.9	+7.2 −6.0
120	53.62	+7.6 −8.1	+3.8 −2.9	+7.2 −6.0
125	49.97	+7.5 −8.0	+3.8 −2.9	+7.2 −6.0
130	46.69	+7.3 −7.9	+3.8 −2.9	+7.2 −6.0
135	43.74	+7.2 −7.8	+3.7 −2.8	+7.1 −6.0
140	41.05	+7.1 −7.7	+3.7 −2.8	+7.1 −6.0
145	38.61	+7.0 −7.6	+3.7 −2.8	+7.1 −6.1
150	36.38	+6.9 −7.5	+3.7 −2.8	+7.1 −6.1
155	34.26	+6.8 −7.5	+3.7 −2.8	+7.1 −6.1
160	32.08	+6.7 −7.4	+3.7 −2.8	+7.1 −6.1
165	29.84	+6.7 −7.4	+3.6 −2.8	+7.0 −6.1
170	28.01	+6.6 −7.2	+3.6 −2.8	+7.0 −6.2
175	26.41	+6.5 −7.2	+3.6 −2.8	+7.0 −6.2
180	24.92	+6.4 −7.1	+3.6 −2.8	+7.0 −6.2
185	23.53	+6.4 −7.1	+3.6 −2.8	+7.0 −6.3
190	22.26	+6.3 −7.0	+3.6 −2.8	+7.0 −6.3
195	21.15	+6.2 −7.0	+3.6 −2.7	+7.0 −6.3
200	20.18	+6.2 −6.9	+3.6 −2.7	+7.0 −6.3
210	18.50	+6.1 −6.8	+3.6 −2.7	+6.9 −6.4
220	17.08	+6.0 −6.7	+3.6 −2.8	+6.9 −6.4
230	15.86	+5.9 −6.6	+3.6 −2.8	+6.9 −6.5
240	14.82	+5.8 −6.5	+3.5 −2.8	+6.9 −6.6
250	13.92	+5.8 −6.4	+3.5 −2.8	+6.9 −6.7
260	13.15	+5.7 −6.4	+3.5 −2.8	+6.9 −6.8
270	12.48	+5.7 −6.3	+3.5 −2.8	+6.9 −6.8
280	11.91	+5.7 −6.2	+3.5 −2.8	+6.8 −6.9
290	11.44	+5.7 −6.2	+3.5 −2.8	+6.8 −6.9
300	11.07	+5.6 −6.1	+3.5 −2.9	+6.8 −7.0
320	10.60	+5.6 −6.0	+3.5 −2.9	+6.8 −6.9
340	10.69	+5.6 −6.0	+3.5 −2.9	+6.8 −7.0
360	11.81	+5.6 −5.9	+3.5 −3.0	+6.8 −7.0
380	11.66	+5.6 −5.7	+3.6 −3.0	+6.8 −7.1
400	10.76	+7.3 −5.5	+3.6 −3.0	+6.9 −7.1
450	7.80	+5.5 −5.1	+3.6 −3.2	+6.9 −7.2
500	5.31	+5.5 −5.0	+3.7 −3.3	+7.0 −7.2
550	3.54	+5.4 −4.9	+3.8 −3.4	+7.3 −7.5
600	2.37	+5.4 −4.8	+3.9 −3.5	+7.3 −7.4
650	1.60	+5.3 −4.7	+4.0 −3.6	+7.5 −7.5
700	1.10	+5.3 −4.7	+4.1 −3.8	+7.7 −7.5
750	0.765	+5.4 −4.7	+4.3 −3.9	+8.0 −7.6
800	0.539	+5.3 −4.6	+4.5 −4.0	+8.2 −7.7
850	0.385	+5.3 −4.6	+4.7 −4.1	+8.4 −7.8
900	0.279	+5.3 −4.6	+4.9 −4.2	+8.6 −8.0
950	0.204	+5.4 −4.7	+5.1 −4.4	+8.8 −8.1
1000	0.151	+5.4 −4.6	+5.3 −4.5	+8.9 −8.2

Table 4: Results on $pp(gg) \rightarrow H + X$ cross sections with $\sqrt{s} = 14$ TeV based on ABPS calculation, using MSTW2008 NNLO PDFs.

| M_{H}[GeV]	σ[pb]	Scale [%]	PDF+α_{s} [%]	PDF4LHC [%]
90	91.49	+10.5 −14.0	+4.1 −3.1	+7.5 −6.2
95	83.22	+10.1 −13.5	+4.0 −3.1	+7.4 −6.1
100	76.07	+9.9 −13.1	+4.0 −3.1	+7.4 −6.1
105	69.84	+9.6 −12.7	+4.0 −3.0	+7.4 −6.1
110	64.38	+9.3 −12.3	+3.9 −3.0	+7.3 −6.1
115	59.56	+9.1 −11.9	+3.9 −3.0	+7.3 −6.1
120	55.29	+8.9 −11.6	+3.9 −2.9	+7.3 −6.1
125	51.47	+8.7 −11.3	+3.9 −2.9	+7.3 −6.1
130	48.06	+8.6 −11.1	+3.8 −2.9	+7.3 −6.1
135	44.98	+8.4 −10.8	+3.8 −2.9	+7.3 −6.1
140	42.21	+8.2 −10.5	+3.8 −2.9	+7.3 −6.2
145	39.71	+8.1 −10.3	+3.8 −2.9	+7.3 −6.2
150	37.43	+8.0 −10.1	+3.8 −2.8	+7.2 −6.2
155	35.34	+7.8 −9.9	+3.8 −2.8	+7.2 −6.2
160	33.19	+7.7 −9.7	+3.7 −2.8	+7.2 −6.2
165	30.60	+7.6 −9.5	+3.7 −2.8	+7.2 −6.2
170	28.69	+7.5 −9.4	+3.7 −2.8	+7.2 −6.3
175	27.09	+7.5 −9.2	+3.7 −2.8	+7.2 −6.3
180	25.65	+7.4 −9.1	+3.7 −2.8	+7.2 −6.3
185	24.09	+7.3 −8.9	+3.7 −2.8	+7.1 −6.4
190	22.75	+7.3 −8.8	+3.7 −2.8	+7.1 −6.4
195	21.63	+7.2 −8.7	+3.7 −2.8	+7.1 −6.4
200	20.64	+7.1 −8.5	+3.7 −2.8	+7.1 −6.4
210	18.92	+7.0 −8.3	+3.6 −2.8	+7.1 −6.5
220	17.47	+6.9 −8.1	+3.6 −2.8	+7.1 −6.6
230	16.22	+6.8 −8.0	+3.6 −2.8	+7.0 −6.6
240	15.15	+6.7 −7.9	+3.6 −2.8	+7.0 −6.7
250	14.23	+6.6 −7.9	+3.6 −2.8	+7.0 −6.8
260	13.43	+6.5 −7.8	+3.6 −2.8	+7.0 −6.9
270	12.74	+6.4 −7.8	+3.6 −2.8	+7.0 −6.9
280	12.15	+6.4 −7.8	+3.6 −2.8	+7.0 −7.0
290	11.67	+6.3 −7.7	+3.6 −2.9	+6.9 −7.0
300	11.28	+6.2 −7.7	+3.6 −2.9	+6.9 −7.0
320	10.81	+6.2 −7.7	+3.6 −2.9	+6.9 −7.0
340	11.00	+6.2 −7.7	+3.6 −2.9	+6.9 −7.1
360	12.30	+6.1 −7.7	+3.6 −3.0	+6.9 −7.1
380	12.01	+5.7 −7.4	+3.6 −3.0	+6.9 −7.1
400	10.98	+5.3 −7.1	+3.6 −3.1	+6.9 −7.2
450	7.81	+4.7 −6.7	+3.7 −3.2	+7.0 −7.2
500	5.24	+4.3 −6.4	+3.7 −3.3	+7.1 −7.3
550	3.48	+4.0 −6.2	+3.8 −3.4	+7.3 −7.5
600	2.32	+3.8 −6.0	+3.9 −3.5	+7.4 −7.5
650	1.57	+3.6 −5.9	+4.0 −3.6	+7.5 −7.5
700	1.07	+3.5 −5.8	+4.1 −3.8	+7.7 −7.6
750	0.746	+3.3 −5.7	+4.3 −3.9	+7.8 −7.7
800	0.525	+3.2 −5.7	+4.4 −4.0	+7.9 −7.8
850	0.374	+3.2 −5.6	+4.5 −4.1	+8.0 −7.9
900	0.270	+3.1 −5.6	+4.6 −4.3	+8.1 −8.0
950	0.197	+3.0 −5.5	+4.8 −4.4	+8.2 −8.1
1000	0.146	+3.0 −5.5	+4.9 −4.5	+8.3 −8.3
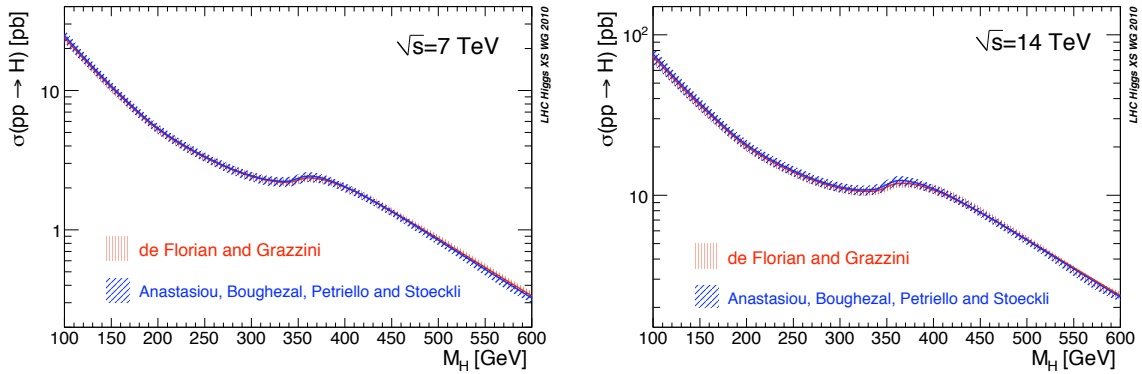
Fig. 2: Comparison of ABPS [30] and dFG [38] results, including scale uncertainty bands.

2.3 Uncertainties

We now discuss the various sources of uncertainty affecting the cross sections presented in Tables 1–4. The uncertainty has two primary origins: From missing terms in the partonic cross sections and from our limited knowledge of the PDFs.

- Uncalculated higher-order QCD radiative corrections are one of the most important sources of uncertainty on the partonic cross section. The customary method used in perturbative QCD calculations to estimate their size is to vary the renormalization and factorization scales around a central value μ_0, which is chosen to be of the order of the hard scale of the process. The uncertainty of the ABPS and dFG calculations is quantified in this way. The factorization and renormalization scales μ_F and μ_R are varied in the range $0.5\mu_0 < \mu_F, \mu_R < 2\mu_0$, with the constraint $0.5 < \mu_F/\mu_R < 2$. The choice of the central scale μ_0 is instead different: dFG choose $\mu_0 = M_H$, whereas ABPS choose $\mu_0 = M_H/2$. The structure of the scale dependent logarithmic contributions in the fixed-order calculation of ABPS suggests that the central value of the scale should be chosen parametrically smaller than M_H. This is supported by the better convergence of the cross section through NNLO and also after including the leading N^{3}LO terms [19]. The resummation implemented in the NNLL result of dFG minimizes the sensitivity to the choice of central scale. This is clearly shown in Fig. 3, where the scale dependent bands for different values of the reference scale μ_0 are shown. The results of dFG show a remarkable stability with respect to the choice of μ_0 both at 7 TeV and at 14 TeV.

  In principle, the uncertainty obtained through scale variations can only give a lower limit on the *true* uncertainty. Nonetheless, we point out that the results of ABPS and dFG are consistent with those obtained at the previous order (i.e., dFG NNLL bands overlap with the NNLO band, and ABPS NNLO band overlap with the NLO band), thus suggesting that the uncertainty obtained with this procedure provides a reasonable estimate of the true perturbative uncertainty. At $\sqrt{s} = 7$ (14) TeV the scale uncertainty of the ABPS result is about $\pm 9-10\%$ ($\pm 8-13\%$) in the range $M_H = 100-300$ GeV, and it decreases to about $\pm 7\%$ ($\pm 5\%$) as M_H increases. At $\sqrt{s} = 7$ (14) TeV the scale uncertainty of the dFG result is about $\pm 6-8\%$ ($\pm 6-9\%$) in the range $M_H = 100-300$ GeV, and it decreases slightly to about $\pm 5-7\%$ ($\pm 5\%$) as M_H increases.

- Another source of perturbative uncertainty on the partonic cross sections comes from the implementation of the EW corrections. Both ABPS and dFG results are obtained in the complete factorization scheme discussed above. The partial factorization scheme would lead to a change of the results ranging from about -3% ($M_H = 110$ GeV) to $+1\%$ ($M_H = 300$ GeV). We note that the effective-theory calculation of Ref. [30] supports the use of the complete factorization scheme. When the three-loop mixed QCD–EW correction derived there is normalized with the
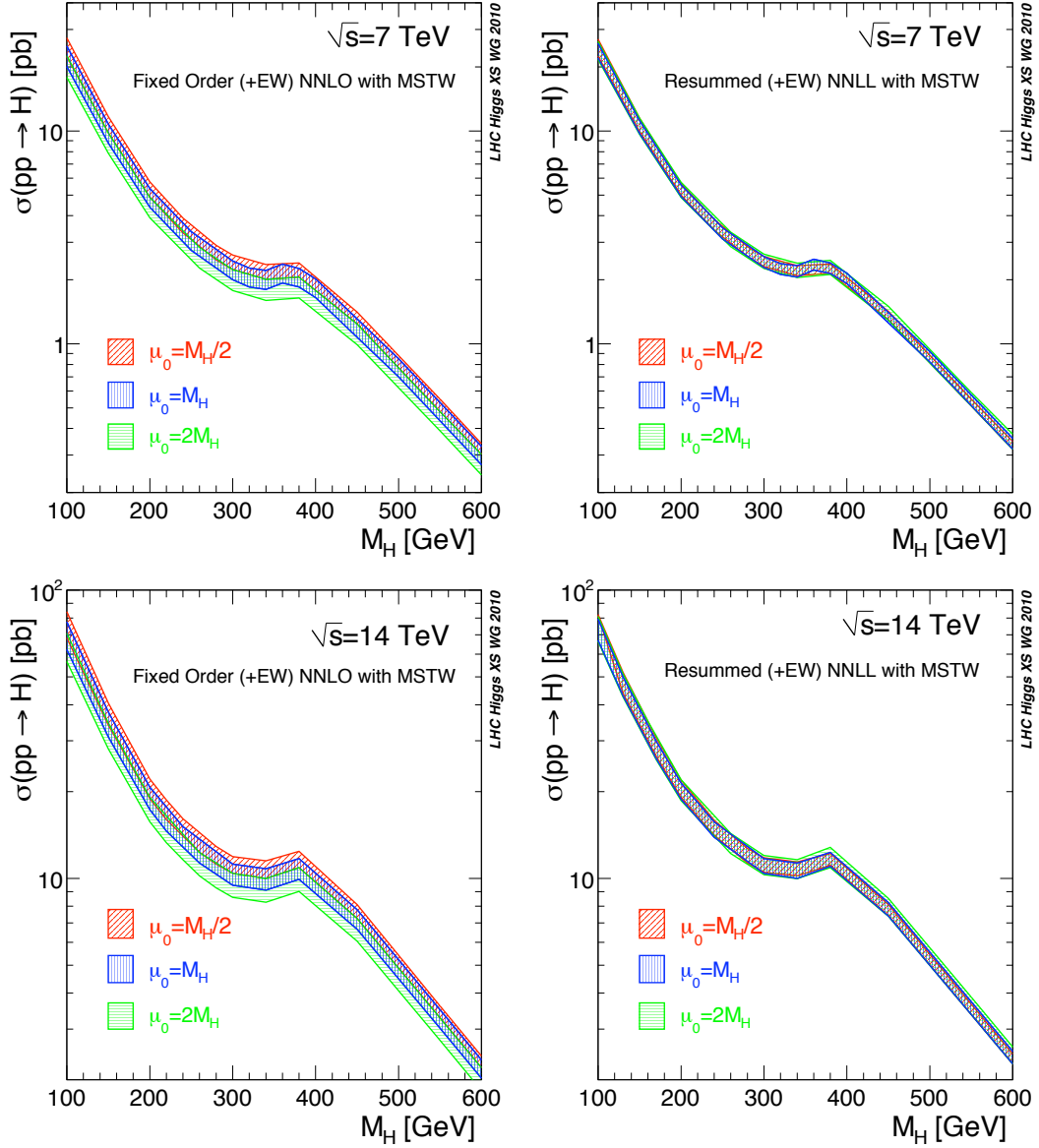
Fig. 3: Comparison of NNLO and NNLL bands with different choice of the central scale.

exact two-loop light-quark terms derived in Refs. [34, 35], the dominant parts of the exact QCD corrections to the EW contributions are properly included. This is the same reason that the NLO correction found using the large-m_t approximation only differs from the exact result by $10-15\%$ even for $M_H \sim 1$ TeV, well outside the expected range of validity $M_H < 2m_t$. We expect that the exact three-loop mixed QCD–EW correction is estimated with a similar $\pm 10\%$ uncertainty using the effective-theory calculation of Ref. [30]. As the two-loop EW contribution to the cross section reaches a maximum of only $+5\%$, we estimate an uncertainty of $\pm 1\%$ coming from missing EW corrections for $M_H \lesssim 300$ GeV.

- The use of the large-m_t approximation induces another source of uncertainty. The ABPS and dFG calculations both include the exact NLO corrections with full dependence on the masses of the top and bottom quarks. The NNLO (NNLL) top-quark contributions are instead evaluated in the large-m_t limit. In Refs. [24–29] subleading corrections to the large-m_t limit have been computed. These works have shown that for a relatively light Higgs boson ($M_H \lesssim 300$ GeV),

the approximation works to better than 1%. For a heavier Higgs boson ($M_\mathrm{H} \gtrsim 300$ GeV), the accuracy of the large-m_t approximation is expected to be worse, but still within a few percent.

- Different choices of the input quark masses m_t and m_b lead to a scheme dependence in the cross section. We have checked that different values of m_t produce a negligible effect on the final cross section. Although the contribution of the bottom quark to the production rate is much smaller than that of the top quark, large logarithms of the form $\ln(M_\mathrm{H}/m_\mathrm{b})$ lead to a non-negligible shift in the cross section. We estimate this by evaluating the cross section using both the pole mass and the $\overline{\mathrm{MS}}$ mass for the b quark, and interpreting the difference as a measure of uncertainty. We use the $\overline{\mathrm{MS}}$ mass evaluated at the renormalization scale, $m_\mathrm{b}(\mu_R)$. This leads to an uncertainty estimate of approximately $\pm 1-2\%$ on the final result.

- The other important source of uncertainty in the cross section is the one coming from PDFs. Modern PDF sets let the user estimate the experimental uncertainty originating from the accuracy of the data points used to perform the fit. The MSTW2008 NNLO set [41] provides 40 different grids that allow evaluation of the experimental uncertainties according to the procedure discussed in Ref. [43]. A related and important uncertainty is the one coming from the value of the QCD coupling. Higgs production through gluon fusion starts at $\mathcal{O}(\alpha_\mathrm{s}^2)$ and thus this uncertainty is expected to have a sizeable effect on the production rate. Recently, the MSTW collaboration has studied the combined effect of PDF+α_s uncertainties [44]. The PDF+α_s uncertainties at 68% confidence limit (CL) of the ABPS and dFG calculations are reported in Tables 1–4. The uncertainties turn out to be quite similar, being about $\pm 3-4\%$ in the range $M_\mathrm{H} = 100-300$ GeV both at $\sqrt{s} = 7$ TeV and 14 TeV. At $\sqrt{s} = 7$ (14) TeV they increase to about $\pm 8-9\%$ ($\pm 5\%$) at high Higgs-boson masses. In Tables 1–4 we also report the uncertainties (see Section 8.5) obtained through the PDF4LHC recommendation[4] [45]. At 7 (14) TeV the uncertainties are about $\pm 7-8\%$ ($\pm 6-7\%$) in the range $M_\mathrm{H} = 100-300$ GeV, and increase at high Higgs-boson masses. This is not completely unexpected: as the Higgs mass increases, larger values of x are probed, where the gluon distribution is more uncertain.

  We finally point out that, besides MSTW, we have at present three other NNLO parton analyses: ABKM09 [46], JR09VFNNLO [47], and HERAPDF [48]. These PDF sets tend to give smaller cross sections both at 7 TeV and 14 TeV with respect to MSTW. For example, at 14 TeV the ABKM09 (JR09) result is smaller than the MSTW result by about $6-10\%$ ($13-8\%$) in the range $M_\mathrm{H} = 100-300$ GeV. At 7 TeV the ABKM09 (JR09) cross section is smaller than the MSTW cross section by $9-16\%$ ($12-4\%$) in the same range of Higgs-boson masses. HERAPDF has released two NNLO PDF sets corresponding to $\alpha_\mathrm{s}(M_\mathrm{Z}) = 0.1145$ and $\alpha_\mathrm{s}(M_\mathrm{Z}) = 0.1176$. At 14 TeV the result corresponding to $\alpha_\mathrm{s}(M_\mathrm{Z}) = 0.1145$ ($\alpha_\mathrm{s}(M_\mathrm{Z}) = 0.1176$) is smaller than the MSTW result by about $8-10\%$ ($4-5\%$). At 7 TeV the cross section corresponding to $\alpha_\mathrm{s}(M_\mathrm{Z}) = 0.1145$ ($\alpha_\mathrm{s}(M_\mathrm{Z}) = 0.1176$) is smaller than the MSTW result by about $10-14\%$ ($5-7\%$).

2.4 Cross-section predictions II

A study of both the central value and uncertainty of Higgs production cross sections at the Tevatron was performed in Ref. [39]. We refer to this analysis with the acronym BD. The BD study was later extended to cover LHC production [40], and the results are reported in Tables 5 and 6. BD use a fixed-order calculation with the exact top- and bottom-quark mass effects at NLO, and then add on the NNLO top contributions in the large-m_t limit as well as the electroweak corrections at NLO and NNLO, as done in ABPS. They assume a central scale value $\mu_0 = M_\mathrm{H}/2$, as also do ABPS. This leads to an excellent agreement in central value and relatively good agreement in the estimated scale variation error with the dFG and ABPS results. BD estimate the error arising from the PDFs and α_s differently than do dFG and ABPS. They first choose to consider the 90% CL PDF+$\Delta^\mathrm{exp}\alpha_\mathrm{s}$ uncertainty and then define an

---

[4]We thank A. Vicini for providing us with the PDF4LHC correction factors.

additional theoretical error of $\Delta^{\text{th}}\alpha_{\text{s}} = 0.002$ on the strong coupling constant and use PDF grids with a fixed α_{s} provided by MSTW to define a resulting uncertainty on the production cross section. The resulting BD uncertainty is then added in quadrature with the combined PDF+$\Delta^{\text{exp}}\alpha_{\text{s}}$ uncertainty (at 90% CL) obtained by using the MSTW procedure [44], giving a combined PDF+$\Delta^{\text{exp+th}}\alpha_{\text{s}}$ uncertainty estimate of $\pm 10\%$ for Higgs masses below 350 GeV. The BD procedure is motivated by having the PDF+α_{s} uncertainty bands obtained using MSTW to be consistent with those obtained with the PDF set of Ref. [46]. The ensuing BD uncertainty is only slightly larger than the one obtained by following the PDF4LHC recommendation. BD finally combine the uncertainties as follows: the PDF+α_{s} uncertainties are evaluated directly on the maximum and minimum cross sections that arise from scale variation. This gives a combined BD uncertainty that is comparable to that obtained with a linear sum of the scale and PDF+α_{s} uncertainties.

The major difference between the BD estimate for the theory uncertainty compared to dFG and ABPS, is that an additional uncertainty, which is mainly due to the use of the effective-field-theory approach beyond NLO, is considered. It consists of three main components: i) the difference between the partial and complete factorisation schemes in the NLO electroweak corrections [35] which approximately is equivalent to the contributions of the mixed NNLO QCD–electroweak corrections obtained in the limit $M_{\text{H}} \ll M_{\text{W}}$ [30]; ii) the missing b-quark loop contribution at NNLO (and its interference with the top-quark loop) and the scheme dependence in the renormalisation of the b-quark mass in the NLO QCD contributions; iii) the use of the $m_{\text{t}} \to \infty$ effective approximation for Higgs masses beyond the $2m_{\text{t}}$ threshold in the NNLO QCD contribution. The (linear) sum of these three uncertainties turns out to be quite large: it is at the level of about $6-7\%$ in the mass range $M_{\text{H}} \lesssim 160$ GeV where the difference between the partial and complete factorisation approaches is significant and becomes even larger for $M_{\text{H}} \gtrsim 600$ GeV where the $m_{\text{t}} \to \infty$ approximation starts to fail badly.

When the EFT uncertainty is added linearly with the combined scale and PDF+α_{s} uncertainty, the total BD theoretical uncertainties become definitely large, being at $\sqrt{s} = 7$ TeV, about $\pm 25-30\%$ in the low- and high-Higgs mass ranges.

2.5 An alternative cross-section calculation based on an effective field theory

In Ref. [49] updated predictions for Higgs-boson production at the Tevatron and the LHC were presented. The results of Ref. [49] are based on the work of Refs. [50, 51], where a new calculation of the Higgs production cross section was presented. This calculation supplements the NNLO result, obtained in the large-m_{t} approximation, with soft-gluon resummation done in the framework of an effective field theory (EFT) approach, and with the resummation of some "π^2-terms" originating from the analytic continuation of the gluon form factor. These additional terms are obtained in the EFT formalism by choosing an imaginary matching scale, and are included by the authors to improve the convergence of the perturbative series. The update of Ref. [49] treats both top- and bottom-quark loops in the heavy-quark approximation, and includes EW corrections assuming complete factorization. In the range $M_{\text{H}} = 115-200$ GeV the central values of Ref. [49] are in good agreement with those of the ABPS and dFG calculations (for example, the difference with the dFG results is at $1-2\%$ level). However, we note that the reliability of π^2 resummation has been questioned, and that there are puzzling differences between this approach and the standard soft-gluon resummation. The effect of resummation in Ref. [49] is driven by the π^2 terms; without them, the effect of resummation is much smaller than the one obtained using the standard approach [51]. The numerical agreement between central values therefore appears accidental. Soft-gluon resummations typically deal with logarithmically terms that are enhanced in some region of the phase space. As an example, in the soft-gluon resummation of Ref. [18] the logarithmic terms are $\log^n(1-z)$ where $1 - z = 1 - M_{\text{H}}^2/\hat{s}$ is the distance from the partonic threshold. These logarithmic terms can be precisely traced back and identified at each perturbative order. On the contrary, π^2 terms are just numbers, and there is no limit in which they can dominate. Moreover, only those π^2 terms coming from the analytic continuation of the gluon form factor can actually be controlled in this way. Other π^2 terms are

Table 5: Results on $pp(gg) \rightarrow H + X$ cross sections with $\sqrt{s} = 7$ TeV based on BD calculation with MSTW PDFs.

M_{H}[GeV]	σ[pb]	Scale [%]	PDF+$\Delta_{\alpha_{\mathrm{s}}}^{exp+th}$ [%]	EFT [%]
90	29.79	$+10.4 - 12.1$	$+9.3 - 8.9$	± 7.8
95	26.77	$+10.1 - 11.$	$+9.2 - 8.9$	± 7.7
100	24.25	$+9.9 - 10.7$	$+9.2 - 8.8$	± 7.6
105	22.01	$+9.6 - 10.5$	$+9.2 - 8.8$	± 7.5
110	20.06	$+9.4 - 10.3$	$+9.1 - 8.8$	± 7.4
115	18.35	$+9.1 - 10.2$	$+9.1 - 8.8$	± 7.3
120	16.84	$+8.9 - 10.2$	$+9.1 - 8.8$	± 7.3
125	15.51	$+8.8 - 9.9$	$+9.1 - 8.8$	± 7.2
130	14.32	$+8.5 - 9.8$	$+9.1 - 8.8$	± 7.1
135	13.26	$+8.4 - 9.6$	$+9.1 - 8.8$	± 7.0
140	12.31	$+8.3 - 9.5$	$+9.1 - 8.8$	± 7.0
145	11.45	$+8.2 - 9.5$	$+9.1 - 8.8$	± 6.9
150	10.67	$+8.1 - 9.5$	$+9.1 - 8.8$	± 6.8
155	9.94	$+7.9 - 9.4$	$+9.1 - 8.8$	± 6.6
160	9.21	$+7.8 - 9.4$	$+9.1 - 8.8$	± 5.9
165	8.47	$+7.7 - 9.4$	$+9.1 - 8.8$	± 4.9
170	7.87	$+7.7 - 9.4$	$+9.1 - 8.8$	± 4.2
175	7.35	$+7.6 - 9.4$	$+9.1 - 8.9$	± 3.7
180	6.86	$+7.5 - 9.3$	$+9.2 - 8.9$	± 3.1
185	6.42	$+7.4 - 9.3$	$+9.2 - 8.9$	± 3.0
190	6.01	$+7.4 - 9.3$	$+9.2 - 8.9$	± 3.4
195	5.65	$+7.4 - 9.3$	$+9.2 - 8.9$	± 3.6
200	5.34	$+7.3 - 9.3$	$+9.3 - 9.0$	± 3.7
210	4.81	$+7.2 - 9.3$	$+9.3 - 9.0$	± 3.7
220	4.36	$+7.2 - 9.2$	$+9.3 - 9.1$	± 3.6
230	3.97	$+7.0 - 9.2$	$+9.4 - 9.2$	± 3.5
240	3.65	$+7.0 - 9.2$	$+9.5 - 9.2$	± 3.3
250	3.37	$+6.9 - 9.2$	$+9.5 - 9.3$	± 3.1
260	3.11	$+6.8 - 9.2$	$+9.6 - 9.4$	± 3.0
270	2.89	$+6.7 - 9.2$	$+9.7 - 9.5$	± 2.8
280	2.71	$+6.8 - 9.2$	$+9.8 - 9.5$	± 2.6
290	2.55	$+6.8 - 9.1$	$+9.8 - 9.6$	± 2.4
300	2.42	$+6.7 - 9.1$	$+9.9 - 9.7$	± 2.3
320	2.23	$+6.7 - 9.2$	$+10.1 - 9.9$	± 2.3
340	2.19	$+6.9 - 9.2$	$+10.3 - 10.1$	± 3.0
360	2.31	$+7.0 - 9.2$	$+10.5 - 10.3$	± 4.1
380	2.18	$+6.3 - 9.1$	$+10.7 - 10.5$	± 2.5
400	1.93	$+5.9 - 8.8$	$+11.0 - 10.7$	± 3.1
450	1.27	$+5.0 - 8.4$	$+11.6 - 11.3$	± 4.0
500	0.79	$+4.4 - 8.1$	$+12.2 - 11.9$	± 4.5
550	0.49	$+4.0 - 7.9$	$+12.7 - 12.4$	± 5.5
600	0.31	$+3.7 - 7.7$	$+13.3 - 13.0$	± 6.6
650	0.20	$+3.5 - 7.6$	$+14.0 - 13.5$	± 7.5
700	0.13	$+3.4 - 7.5$	$+14.7 - 14.1$	± 8.3
750	0.08	$+3.3 - 7.4$	$+15.4 - 14.6$	± 9.0
800	0.06	$+3.1 - 7.4$	$+16.2 - 15.1$	± 9.7
850	0.04	$+3.1 - 7.3$	$+17.1 - 15.7$	± 10.2
900	0.03	$+3.0 - 7.3$	$+18.0 - 16.2$	± 10.8
950	0.02	$+3.0 - 7.3$	$+18.9 - 16.8$	± 11.3
1000	0.01	$+2.9 - 7.2$	$+19.9 - 17.3$	± 11.8

Table 6: Results on $\mathrm{pp(gg)} \to \mathrm{H} + X$ cross sections with $\sqrt{s} = 14$ TeV based on BD calculation with MSTW PDFs.

M_{H}[GeV]	σ[pb]	Scale [%]	PDF+$\Delta_{\alpha_{\mathrm{s}}}^{exp+th}$ [%]	EFT [%]
90	90.02	$+10.8 - 14.3$	$+9.1 - 8.9$	± 8.3
95	82.09	$+10.4 - 13.8$	$+9.0 - 8.8$	± 8.2
100	75.41	$+10.2 - 13.4$	$+8.9 - 8.7$	± 8.1
105	69.38	$+9.9 - 13.0$	$+8.8 - 8.7$	± 8.0
110	64.07	$+9.6 - 12.6$	$+8.7 - 8.6$	± 7.9
115	59.37	$+9.4 - 12.2$	$+8.7 - 8.5$	± 7.8
120	55.20	$+9.2 - 11.9$	$+8.6 - 8.4$	± 7.7
125	51.45	$+9.0 - 11.6$	$+8.5 - 8.4$	± 7.6
130	48.09	$+8.9 - 11.4$	$+8.5 - 8.3$	± 7.5
135	45.06	$+8.7 - 11.1$	$+8.4 - 8.2$	± 7.5
140	42.30	$+8.5 - 10.8$	$+8.4 - 8.2$	± 7.4
145	39.80	$+8.4 - 10.6$	$+8.3 - 8.1$	± 7.3
150	37.50	$+8.3 - 10.4$	$+8.3 - 8.1$	± 7.2
155	35.32	$+8.1 - 10.2$	$+8.3 - 8.1$	± 7.0
160	33.08	$+8.0 - 10.0$	$+8.2 - 8.0$	± 6.3
165	30.77	$+7.9 - 9.8$	$+8.2 - 8.0$	± 5.3
170	28.89	$+7.8 - 9.7$	$+8.2 - 8.0$	± 4.5
175	27.24	$+7.8 - 9.5$	$+8.2 - 7.9$	± 4.0
180	25.71	$+7.7 - 9.4$	$+8.2 - 7.9$	± 3.5
185	24.28	$+7.6 - 9.1$	$+8.1 - 7.9$	± 3.3
190	22.97	$+7.6 - 9.1$	$+8.1 - 7.9$	± 3.8
195	21.83	$+7.5 - 9.0$	$+8.1 - 7.9$	± 4.0
200	20.83	$+7.4 - 8.8$	$+8.1 - 7.9$	± 4.1
210	19.10	$+7.3 - 8.6$	$+8.1 - 7.8$	± 4.1
220	17.64	$+7.2 - 8.4$	$+8.1 - 7.8$	± 4.0
230	16.38	$+7.1 - 8.3$	$+8.0 - 7.8$	± 3.8
240	15.30	$+7.0 - 8.2$	$+8.0 - 7.8$	± 3.7
250	14.38	$+6.9 - 8.2$	$+8.0 - 7.8$	± 3.5
260	13.52	$+6.8 - 8.1$	$+8.0 - 7.8$	± 3.3
270	12.79	$+6.7 - 8.1$	$+8.0 - 7.8$	± 3.1
280	12.17	$+6.7 - 8.1$	$+8.0 - 7.8$	± 2.9
290	11.65	$+6.6 - 8.0$	$+8.0 - 7.8$	± 2.8
300	11.22	$+6.5 - 8.0$	$+8.0 - 7.8$	± 3.4
320	10.70	$+6.5 - 8.0$	$+8.1 - 7.9$	± 3.1
340	10.83	$+6.5 - 8.0$	$+8.1 - 7.9$	± 2.8
360	11.77	$+6.4 - 8.0$	$+8.1 - 8.0$	± 3.5
380	11.46	$+6.0 - 7.7$	$+8.2 - 8.1$	± 4.4
400	10.46	$+5.6 - 7.4$	$+8.2 - 8.1$	± 5.0
450	7.42	$+5.0 - 7.0$	$+8.4 - 8.3$	± 6.0
500	4.97	$+4.6 - 6.7$	$+8.6 - 8.6$	± 6.4
550	3.32	$+4.3 - 6.5$	$+8.9 - 8.8$	± 7.4
600	2.24	$+4.1 - 6.3$	$+9.2 - 9.1$	± 8.3
650	1.53	$+3.9 - 6.2$	$+9.5 - 9.4$	± 9.0
700	1.05	$+3.8 - 6.1$	$+9.8 - 9.6$	± 9.6
750	0.74	$+3.6 - 6.0$	$+10.1 - 9.9$	± 10.1
800	0.52	$+3.5 - 6.0$	$+10.4 - 10.2$	± 10.5
850	0.38	$+3.5 - 5.9$	$+10.7 - 10.5$	± 11.0
900	0.27	$+3.4 - 5.9$	$+11.0 - 10.7$	± 11.3
950	0.20	$+3.3 - 5.8$	$+11.3 - 11.0$	± 11.7
1000	0.15	$+3.3 - 5.8$	$+11.5 - 11.3$	± 12.0

present at each order in perturbation theory, and they can be obtained only through an explicit computation. We add a final comment on the perturbative uncertainties quoted in the calculation of Ref. [49]. The scale uncertainty of the results are of the order of $\pm 3\%$ or smaller. This should be contrasted with the uncertainties of the ABPS and dFG calculations, which are a factor of $2-3$ larger. Since the calculation of Ref. [49] does not contain new information beyond NNLO with respect to those of ABPS, dFG, and BD, we feel uncomfortable with such a small uncertainty and believe it is underestimated. For comparison, it should be noticed that the perturbative uncertainty of a full N^3LO calculation, estimated through scale variations, would be of the order of about $\pm 5\%$ [19].

3 Vector-Boson-Fusion process[5]

3.1 Higgs-boson production in vector-boson fusion

The production of a Standard Model Higgs boson in association with two hard jets in the forward and backward regions of the detector, frequently quoted as the "vector-boson fusion" (VBF) channel, is a cornerstone in the Higgs-boson search both in the ATLAS [52] and CMS [53] experiments at the LHC. Higgs-boson production in the VBF channel plays also an important role in the determination of Higgs-boson couplings at the LHC (see e.g., Ref. [54]). Bounds on non-standard couplings between Higgs and electroweak (EW) gauge bosons can be imposed from precision studies in this channel [55]. In addition this channel contributes in a significant way to the inclusive Higgs production over the full Higgs-mass range.

The production of a Higgs boson + 2 jets receives two contributions at hadron colliders. The first type, where the Higgs boson couples to a weak boson that links two quark lines, is dominated by t- and u-channel-like diagrams and represents the genuine VBF channel. The hard jet pairs have a strong tendency to be forward–backward directed in contrast to other jet-production mechanisms, offering a good background suppression (transverse-momentum and rapidity cuts on jets, jet rapidity gap, central-jet veto, etc.).

If one is interested in the measurement of the Higgs-boson couplings in VBF, especially for the measurement of the HWW and HZZ couplings, cuts should be applied in order to suppress events from Higgs + 2 jet production via gluon fusion, which become a background to the signal VBF production. In the gluon-fusion channel, the Higgs boson is radiated off a heavy-quark loop that couples to any parton of the incoming hadrons via gluons [56,57]. Although the final states are similar, the kinematic distributions of jets are very different. Applying appropriate event selection criteria, called VBF cuts (see e.g., Refs. [58–62]), it is possible to sufficiently suppress the gluon-fusion Higgs-boson production mechanism with respect to the VBF one. According to a recent estimate [63], gluon fusion contributes about $4-5\%$ to the Higgs + 2 jet events for a Higgs-boson mass of $120\,\text{GeV}$, after applying VBF cuts. A next-to-leading order (NLO) analysis of the gluon-fusion contribution [57] shows that its residual scale dependence is still of the order of 35%.

Electroweak Higgs-boson production at leading order (LO) involve only quark and antiquark initial states, qq $\to$ qqH. The topologies of the LO Feynman diagrams contributing to various partonic processes are shown in Fig. 4. As s-channel diagrams and interferences tend to be suppressed when imposing VBF cuts, the cross section can be approximated by the contribution of squared t- and u-channel diagrams only without their interference. The corresponding QCD corrections reduce to vertex corrections to the weak-boson–quark coupling. Explicit NLO QCD calculations in this approximation [64–68] confirm the expectation that these QCD corrections are small, because they are shifted to the parton distribution functions (PDFs) via QCD factorization to a large extent. The resulting QCD corrections are of the order of $5-10\%$ and reduce the remaining factorization and renormalization scale dependence of the NLO cross section to a few percent. For the NLO QCD predictions from HAWK [69–71], VBFNLO [66,72], and VV2H [73] (this last program calculates only total cross sections without cuts), a tuned comparison has been performed in Ref. [74], neglecting s-channel diagrams and interferences. Recently, VBF@NNLO [75] was also run in the same setup. The results of all four codes were found to agree within the statistical errors at the level of 0.1%.

In Refs. [69,70] the full NLO EW + QCD corrections have been computed with HAWK, including the complete set of t-, u-, and s-channel Feynman diagrams and taking into account real corrections induced by photons in the initial state and QED corrections implicitly contained in the DGLAP evolution of PDFs. The size of the electroweak corrections sensitively depends on the chosen renormalization scheme to define the weak couplings, most notably on the chosen value for the electromagnetic coupling

---

[5]A. Denner, S. Farrington, C. Hackstein, C. Oleari, D. Rebuzzi (eds.); P. Bolzoni, S. Dittmaier, F. Maltoni, S.-O. Moch, A. Mück, S. Palmer and M. Zaro.
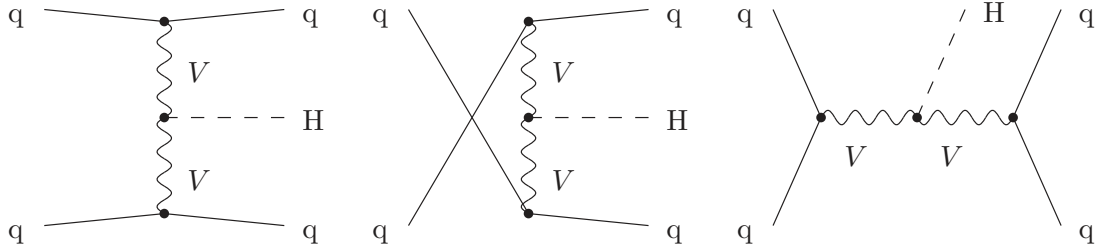
Fig. 4: Topologies of t-, u-, and s-channel contributions for electroweak Higgs-boson production, $qq \to qqH$ at LO, where q denotes any quark or antiquark and V stands for W and Z boson.

α. The preferred choice, which should be most robust with respect to higher-order corrections, is the so-called G_F scheme, where α is derived from Fermi's constant G_F. The impact of EW and QCD corrections in the favoured Higgs-mass range between 100 and 200 GeV are of order 5% and negative, and thus as important as the QCD corrections. Photon-induced processes lead to corrections at the percent level.

Approximate next-to-next-to-leading order (NNLO) QCD corrections to the total inclusive cross section for VBF have been presented in Ref. [75]. The theoretical predictions are obtained using the structure-function approach [65]. Upon including the NNLO corrections in QCD for the VBF production mechanism via the structure-function approach the theoretical uncertainty for this channel, i.e. the scale dependence, reduces from the $5-10\%$ of the NLO QCD and electroweak combined computations [65,70] down to $1-2\%$. The uncertainties due to parton distributions are estimated to be at the same level.

3.2 Higher-order calculations

In order to study the NLO corrections to Higgs-boson production in VBF, we have used two existing partonic Monte Carlo programs: HAWK and VBFNLO, which we now present. Furthermore we also give results of the NNLO QCD calculation based on VBF@NNLO and combine them with the electroweak corrections obtained from HAWK.

3.2.1 HAWK – NLO QCD and EW corrections

HAWK [69–71] is a Monte Carlo event generator for $pp \to H + 2\,jets$. It includes the complete NLO QCD and electroweak corrections and all weak-boson fusion and quark–antiquark annihilation diagrams, i.e. t-channel and u-channel diagrams with VBF-like vector-boson exchange and s-channel Higgs-strahlung diagrams with hadronic weak-boson decay. Also, all interferences at LO and NLO are included. If it is supported by the PDF set, contributions from incoming photons, which are at the level of $1-2\%$, can be taken into account. Leading heavy-Higgs-boson effects at two-loop order proportional to $G_F^2 M_H^4$ are included according to Refs. [76,77]. While these contributions are negligible for small Higgs-boson masses, they become important for Higgs-boson masses above 400 GeV. For $M_H = 700$ GeV they yield $+4\%$, i.e. about half of the total EW corrections. This signals a breakdown of the perturbative expansion, and these contributions can be viewed as an estimate of the theoretical uncertainty. Contributions of b-quark PDFs and final-state b quarks can be taken into account at LO. While the effect of only initial b quarks is negligible, final-state b quarks can increase the cross section by up to 4%. While s-channel diagrams can contribute up to 25% for small Higgs-boson masses in the total cross section without cuts, their contribution is below 1% once VBF cuts are applied. Since the s-channel diagrams are actually a contribution to WH and ZH production, they are switched off in the following.

The code is interfaced to LHAPDF and allows to evaluate the PDF uncertainties in a single run. The calculation can be performed for an on-shell Higgs boson or for an off-shell Higgs boson decaying into a pair of gauge singlets, thus mimicking an off-shell Higgs boson. While the effects of the off-shellness are negligible for small Higgs-boson masses, they should be taken into account for $M_H \gtrsim 400$ GeV. As a flexible partonic Monte Carlo generator, HAWK allows to apply phase-space cuts on the jets and the Higgs-boson decay products and to switch off certain contributions.

3.2.2 VBFNLO – NLO QCD and EW corrections

VBFNLO [78] is a fully flexible partonic Monte Carlo program for VBF, double and triple vector-boson production processes at NLO QCD accuracy. Arbitrary cuts can be specified as well as various scale choices: in fact, VBFNLO can use fixed or dynamical renormalization and factorization scales. Any currently available parton distribution function set can be used through the LHAPDF library. For processes implemented at leading order, the program is capable of generating event files in the Les Houches Accord (LHA) format [79].

Since, in the phase-space regions which are accessible at hadron colliders, VBF reactions are dominated by t-channel electroweak gauge-boson exchange, in VBFNLO, s-channel exchange contributions and kinematically-suppressed fermion-interference contributions [80,81] are disregarded. While the interference effects are always well below 1%, they are entirely negligible once VBF cuts are applied. Here, even the s-channel contributions which, with excellent accuracy, can be regarded as a separate "Higgs-strahlung" process, drop below 1%. The subsequent decay of the Higgs boson is simulated in the narrow-width approximation. For the H $\rightarrow$ W$^+$W$^-$ and the H $\rightarrow$ ZZ modes, full off-shell effects and spin correlations of the decay leptons are included. Details of the calculation can be found in Ref. [66]. Very recently, the EW corrections to VBF Higgs-boson production have been added to the code [82].

3.2.3 VBF@NNLO – NNLO QCD corrections

VBF@NNLO [75] computes VBF Higgs cross sections at LO, NLO, and NNLO in QCD via the structure-function approach. This approach [65] consists basically in viewing the VBF process as a double deep-inelastic scattering (DIS) attached to the colourless pure electroweak vector-boson fusion into a Higgs boson. According to this approach one can include NLO QCD corrections to the VBF process employing the standard DIS structure functions $F_i(x, Q^2)$; $i = 1, 2, 3$ at NLO [83] or similarly the corresponding structure functions [84–87].

The structure-function approach does not include all types of contributions. At LO a structure-function-violating contribution comes from the interferences between identical final-state quarks (e.g., uu $\rightarrow$ Huu) or between processes where either a W or a Z can be exchanged (e.g., ud $\rightarrow$ Hud). These LI contributions have been included in the NNLO results. Apart from such contributions, the structure-function approach represents an exact approach also at NLO. At NNLO, however, several types of diagrams violate it. Some are colour suppressed and kinematically suppressed [88–90], others have been shown in Ref. [91] to be small enough not to produce a significant deterioration of the VBF signal. A first rough estimation for a third set showed that their contribution is small and can be safely neglected. At NNLO in QCD, the theoretical uncertainty is reduced to be less than 2%.

3.3 Results

In the following, we present VBF results for LHC at 7 TeV and 14 TeV calculated at NLO, from HAWK and VBFNLO [78], and at NNLO, from VBF@NNLO [92].

All results have been computed using the values of the electroweak parameters given in Appendix A. The renormalization and factorization scales have been fixed to M_W, and both the scales varied in the range $M_W/2 < \mu < 2M_W$. The Higgs boson has been treated as stable on on-shell, and the contributions from s-channel diagrams have been neglected.

19
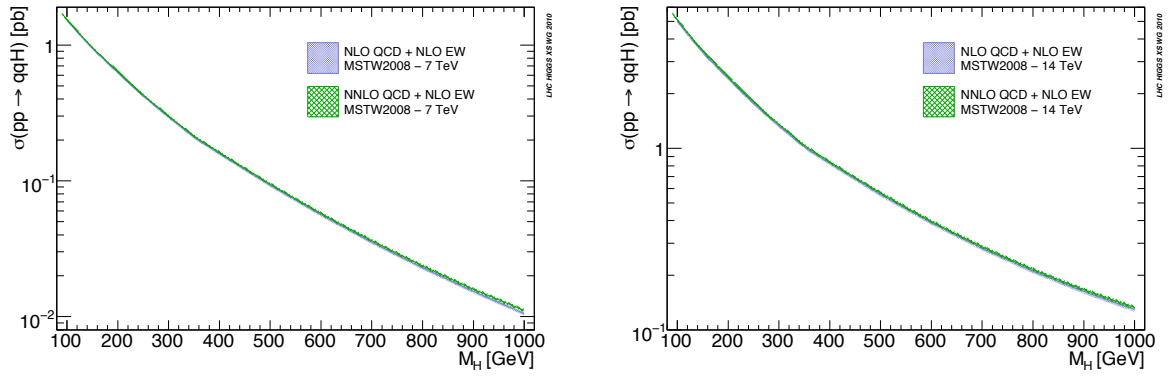
Fig. 5: VBF cross sections at the LHC at 7 TeV (left) and 14 TeV (right) estimated with MSTW2008 PDF set. NLO QCD results and NNLO QCD results are shown both with the EW corrections. The bands represent the PDF + α_s 68% CL uncertainty.
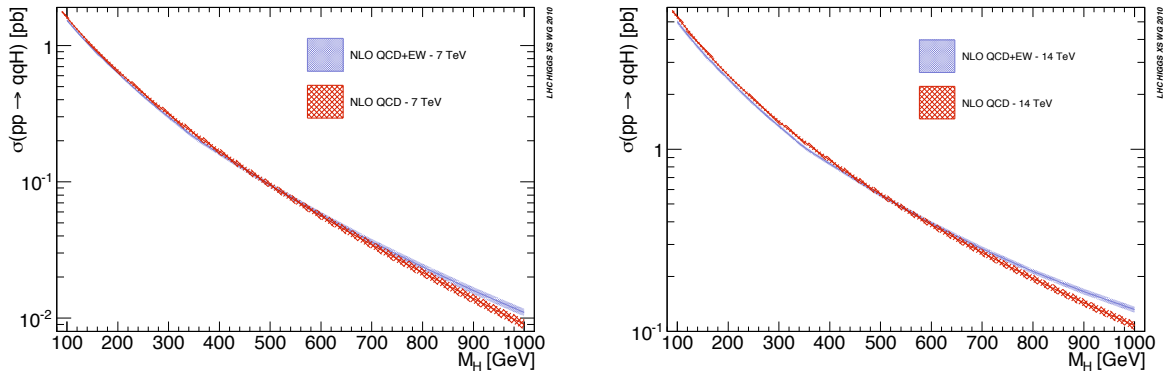
Fig. 6: NLO VBF cross sections at the LHC at 7 TeV (left) and 14 TeV (right). Results with and without the EW corrections are plotted. The bands represent the PDF + α_s 68% CL uncertainty coming from the *envelope* of three PDF sets (see text for details).

Figures 5 and 6 summarize the VBF results at the LHC at 7 TeV and 14 TeV. In Fig. 5, the cross section results at NLO QCD and NNLO QCD both with EW corrections are shown as a function of the Higgs-boson mass. Calculations are performed with the MSTW2008 68% CL PDF set. In Fig. 6, the NLO and NNLO results, with and without the EW corrections, are shown as a function of the Higgs-boson mass. For these calculations, the full estimation of central values and α_s + PDF uncertainty over three PDF sets (namely MSTW2008, CTEQ6.6, and NNPDF2.0, combined according to the PDF4LHC prescription) is available and represented in the plots by the error bands.

In Tables 7 and 9, we collect the NLO QCD + EW results, for the LHC at 7 TeV and 14 TeV, respectively. Numbers have been obtained with HAWK. VBFNLO results (obtained with CTEQ6.6 PDF set) are listed in the rightmost column, for the sake of comparison. For some of the mass points, a full PDF + α_s uncertainty estimation has been performed according to the PDF4LHC prescription. In this case, the uncertainty comes from the *envelope* among three PDF sets (namely CTEQ6.6, MSTW2008NLO, and NNPDF2.0), and the central cross section values are taken from the mid-point of the envelope width. Integration errors, affecting the last shown digit, are below 0.1%. The integration error for the VBFNLO results is of order 0.3%.

In Tables 8 and 10 we collect the results on NLO QCD correction for the LHC at 7 TeV and 14 TeV, respectively. Numbers have been obtained with VBFNLO. In Table 8, HAWK results (obtained with

20

MSTW2008 PDF set) are listed in the rightmost column, for the sake of comparison.

In Tables 11 and 12 we show the NNLO QCD results (second column), obtained with VBF@NNLO, and the combination of NNLO QCD and NLO EW corrections (third column). The combination has been performed under the assumption that QCD and EW corrections factorize completely, i.e. the cross section has been obtained as

$$\sigma = \sigma_{\mathrm{NNLO}} \times (1 + \delta_{\mathrm{EW}}) \,, \tag{1}$$

where σ_{NNLO} is the NNLO QCD result and δ_{EW} the relative EW correction determined in the limit $\alpha_{\mathrm{s}} = 0$. To estimate the uncertainties coming from the parton distributions, we have employed the MSTW 68% confidence level PDF sets [41] and compared with other NNLO PDF sets, i.e. ABKM09 [46] and JR09VF [47]. The results show that an almost constant 2% PDF uncertainty can be associated to the cross section for the LHC. The above discussed NNLO results calculated with MSTW2008 PDFs are similar to the ones based on ABKM09, both in central values and PDF uncertainties of $\mathcal{O}(2\%)$, over the whole mass range. JR09 is in agreement with this for small Higgs masses ($100-200$ GeV) and predicts $\mathcal{O}(10\%)$ larger cross sections at high masses (1 TeV). The numbers of the NNLO calculation presented here can also be obtained via the web interface [92], where the code VBF@NNLO can be run online.

Table 7: NLO QCD + EW results on VBF cross sections at $\sqrt{s} = 7$ TeV: central values and relative uncertainties from HAWK. Integration errors, affecting the last shown digit, are below 0.1%. In the last column, VBFNLO results obtained with CTEQ6.6, for the sake of comparison (integration errors at the 0.3% level).

M_{H}[GeV]	σ[fb]	Scale uncert. [%]	PDF4LHC [%]	VBFNLO [fb]
90	1682	+0.8 −0.2		1706
95	1598	+0.8 −0.3		1613
100	1530	+0.8 −0.1	±2.2	1531
105	1445	+0.7 −0.2		1450
110	1385	+0.7 −0.1	±2.2	1385
115	1312	+0.7 −0.1		1314
120	1257	+0.7 −0.0	±2.1	1253
125	1193	+0.6 −0.0		1193
130	1144	+0.6 −0.0	±2.1	1138
135	1087	+0.6 −0.1		1085
140	1042	+0.6 −0.0	±2.1	1037
145	992	+0.6 −0.1		989
150	951	+0.6 −0.1	±2.1	946
155	907	+0.5 −0.1		903
160	869	+0.5 −0.1	±2.2	864
165	842	+0.5 −0.1		836
170	808	+0.4 −0.1	±2.2	802
175	772	+0.4 −0.1		767
180	738	+0.4 −0.1	±2.2	735
185	713	+0.3 −0.1		709
190	684	+0.3 −0.1	±2.2	680
195	658	+0.3 −0.1		652
200	630	+0.3 −0.1	±2.2	625
210	580	+0.3 −0.0	±2.2	576
220	535	+0.4 −0.0	±2.3	531
230	495	+0.3 −0.0	±2.3	490
240	458	+0.3 −0.0	±2.4	453
250	425	+0.3 −0.0	±2.4	422
260	395	+0.3 −0.0	±2.5	392
270	368	+0.4 −0.0	±2.6	364
280	343	+0.4 −0.0	±2.7	340
290	320	+0.4 −0.0	±2.7	316
300	298	+0.5 −0.0	±2.8	296
320	260	+0.4 −0.1	±2.9	257
340	227	+0.4 −0.1	±3.0	225
360	200	+0.4 −0.0	±3.1	198
380	180	+0.6 −0.1	±3.3	178
400	161	+0.8 −0.1	±3.4	159
450	125	+1.1 −0.2		122
500	94.6	+1.4 −0.2	±4.0	93.4
550	74.8	+1.7 −0.2		72.8
600	57.6	+2.0 −0.3	±4.5	56.9
650	46.6	+2.3 −0.3		44.7
700	36.4	+2.6 −0.3	±5.1	35.7
750	30.0	+2.9 −0.4		28.6
800	23.7	+3.3 −0.4	±5.6	23.5
850	19.9	+3.9 −0.4		18.9
900	15.9	+4.3 −0.4	±6.1	15.5
950	13.6	+4.9 −0.5		13.0
1000	11.0	+5.6 −0.5	±6.6	10.6

Table 8: NLO QCD results on VBF cross sections (NLO EW corrections not included) at $\sqrt{s} = 7$ TeV: central values and relative uncertainties from VBFNLO. Integration errors, affecting the last shown digit, are below 0.3%. In the last column, HAWK results obtained with MSTW2008NLO, for the sake of comparison (integration errors at the 0.1% level).

M_H[GeV]	σ[fb]	Scale uncert. [%]	PDF4LHC [%]	HAWK[fb]
90	1776	+0.0 −0.5	±2.4	1772
95	1685	+0.1 −0.3	±2.5	1682
100	1601	+0.1 −0.4	±2.5	1597
105	1522	+0.1 −0.4	±2.5	1519
110	1448	+0.2 −0.4	±2.5	1445
115	1377	+0.1 −0.3	±2.6	1375
120	1312	+0.2 −0.3	±2.6	1310
125	1251	+0.2 −0.3	±2.6	1249
130	1193	+0.3 −0.3	±2.6	1190
135	1139	+0.3 −0.2	±2.6	1136
140	1088	+0.4 −0.2	±2.7	1084
145	1040	+0.4 −0.2	±2.7	1036
150	994	+0.4 −0.3	±2.8	990
155	951	+0.5 −0.2	±2.8	947
160	910	+0.5 −0.1	±2.9	906
165	872	+0.6 −0.1	±3.0	867
170	836	+0.6 −0.2	±3.0	831
175	801	+0.7 −0.1	±3.0	796
180	768	+0.6 −0.0	±3.1	763
185	737	+0.7 −0.1	±3.1	732
190	707	+0.7 −0.1	±3.1	702
195	679	+0.6 −0.0	±3.2	674
200	653	+0.7 −0.0	±3.2	648
210	603	+0.8 −0.1	±3.3	598
220	558	+0.9 −0.0	±3.4	553
230	517	+1.0 −0.0	±3.5	512
240	480	+1.0 −0.0	±3.6	475
250	446	+1.2 −0.0	±3.6	440
260	415	+1.1 −0.1	±3.7	410
270	386	+1.1 −0.1	±3.8	382
280	360	+1.2 −0.1	±3.9	356
290	336	+1.3 −0.1	±3.9	332
300	314	+1.4 −0.1	±4.0	310
320	275	+1.4 −0.1	±4.2	271
340	242	+1.5 −0.2	±4.3	238
360	213	+1.5 −0.2	±4.4	209
380	189	+1.7 −0.2	±4.5	185
400	167	+1.7 −0.3	±4.7	163
500	94.9	+2.2 −0.4	±5.3	92.0
600	56.3	+2.5 −0.6	±5.9	54.3
650	43.9	+2.7 −0.7	±6.2	42.2
700	34.5	+2.9 −0.7	±6.5	33.1
750	27.3	+3.0 −0.8	±6.8	26.1
800	21.7	+3.1 −1.0	±7.1	20.7
850	17.3	+3.3 −1.1	±7.4	16.5
900	13.9	+3.5 −1.2	±7.7	13.2
950	11.2	+3.7 −1.2	±8.0	10.6
1000	9.03	+3.9 −1.2	±8.3	8.51

Table 9: NLO QCD + EW results on VBF cross sections at $\sqrt{s} = 14\,\mathrm{TeV}$: central values and relative uncertainties for HAWK. Integration errors, affecting the last shown digit, are below 0.1%. In the last column, the VBFNLO results obtained with CTEQ6.6, for the sake of comparison (integration errors at the 0.3% level).

$M_\mathrm{H}[\mathrm{GeV}]$	$\sigma[\mathrm{fb}]$	Scale uncert. [%]	PDF4LHC [%]	VBFNLO [fb]
90	5375	$+1.0\ -0.5$		5517
95	5156	$+0.9\ -0.5$		5272
100	5004	$+1.0\ -0.4$	± 2.6	5057
105	4746	$+1.0\ -0.4$		4839
110	4607	$+1.0\ -0.5$	± 2.6	4642
115	4373	$+0.9\ -0.5$		4455
120	4254	$+0.9\ -0.4$	± 2.6	4272
125	4048	$+0.8\ -0.4$		4109
130	3938	$+1.0\ -0.3$	± 2.5	3952
135	3754	$+0.9\ -0.4$		3807
140	3651	$+0.8\ -0.3$	± 2.5	3666
145	3485	$+0.8\ -0.3$		3431
150	3394	$+0.7\ -0.3$	± 2.5	3403
155	3237	$+0.8\ -0.3$		3277
160	3147	$+1.0\ -0.2$	± 2.4	3156
165	3047	$+0.8\ -0.3$		3083
170	2975	$+0.8\ -0.3$	± 2.4	2978
175	2842	$+0.8\ -0.3$		2866
180	2765	$+0.9\ -0.3$	± 2.3	2764
185	2667	$+0.9\ -0.3$		2679
190	2601	$+1.0\ -0.0$	± 2.3	2595
195	2494	$+0.8\ -0.2$		2512
200	2432	$+0.8\ -0.0$	± 2.3	2437
210	2279	$+0.8\ -0.0$	± 2.2	2274
220	2135	$+0.6\ -0.2$	± 2.3	2135
230	2006	$+0.7\ -0.3$	± 2.2	1999
240	1885	$+0.7\ -0.2$	± 2.3	1883
250	1777	$+0.6\ -0.1$	± 2.2	1770
260	1675	$+0.7\ -0.1$	± 2.1	1668
270	1581	$+0.7\ -0.1$	± 2.1	1575
280	1494	$+0.7\ -0.0$	± 2.1	1488
290	1413	$+0.8\ -0.0$	± 2.1	1407
300	1338	$+0.7\ -0.0$	± 2.1	1329
320	1202	$+0.6\ -0.1$	± 2.1	1195
340	1077	$+0.6\ -0.1$	± 2.1	1069
360	977	$+0.6\ -0.2$	± 2.1	973
380	901	$+0.5\ -0.0$	± 2.1	893
400	830	$+0.4\ -0.2$	± 2.2	826
450	681	$+0.5\ -0.2$		673
500	560	$+0.6\ -0.0$	± 2.3	561
550	469	$+0.6\ -0.1$		463
600	391	$+0.8\ -0.1$	± 2.6	388
650	335	$+1.2\ -0.0$		330
700	284	$+1.4\ -0.0$	± 3.0	282
750	248	$+1.8\ -0.0$		242
800	213	$+1.9\ -0.0$	± 3.2	212
850	189	$+2.4\ -0.0$		185
900	165	$+2.6\ -0.1$	± 3.6	164
950	149	$+3.0\ -0.0$		146
1000	132	$+3.6\ -0.1$	± 3.9	130

Table 10: NLO QCD results on VBF cross sections (NLO EW corrections not included) at $\sqrt{s} = 14$ TeV: central values and relative uncertainties from VBFNLO. Integration errors, affecting the last shown digit, are below 0.3%.

$M_{\mathrm{H}}[\mathrm{GeV}]$	$\sigma[\mathrm{fb}]$	Scale uncert. [%]	PDF4LHC [%]
90	5792	$+1.0 \ -0.9$	± 3.0
95	5550	$+0.8 \ -0.9$	± 3.0
100	5320	$+0.8 \ -0.7$	± 2.9
105	5104	$+0.7 \ -0.9$	± 2.9
110	4898	$+0.7 \ -0.7$	± 2.8
115	4702	$+0.8 \ -0.6$	± 2.8
120	4521	$+0.7 \ -0.8$	± 2.8
125	4344	$+0.7 \ -0.6$	± 2.7
130	4182	$+0.5 \ -0.8$	± 2.7
135	4025	$+0.5 \ -0.8$	± 2.7
140	3874	$+0.5 \ -0.7$	± 2.6
145	3734	$+0.4 \ -0.8$	± 2.6
150	3599	$+0.5 \ -0.6$	± 2.6
155	3472	$+0.4 \ -0.7$	± 2.6
160	3349	$+0.4 \ -0.7$	± 2.5
165	3234	$+0.3 \ -0.6$	± 2.5
170	3124	$+0.3 \ -0.6$	± 2.5
175	3017	$+0.3 \ -0.6$	± 2.4
180	2917	$+0.4 \ -0.6$	± 2.4
185	2819	$+0.3 \ -0.5$	± 2.4
190	2726	$+0.3 \ -0.5$	± 2.4
195	2639	$+0.2 \ -0.5$	± 2.4
200	2553	$+0.2 \ -0.5$	± 2.4
210	2395	$+0.1 \ -0.5$	± 2.4
220	2248	$+0.1 \ -0.4$	± 2.5
230	2115	$+0.1 \ -0.4$	± 2.5
240	1991	$+0.0 \ -0.4$	± 2.5
250	1877	$+0.1 \ -0.5$	± 2.5
260	1771	$+0.1 \ -0.4$	± 2.5
270	1673	$+0.2 \ -0.4$	± 2.5
280	1583	$+0.2 \ -0.3$	± 2.5
290	1498	$+0.1 \ -0.3$	± 2.6
300	1419	$+0.2 \ -0.2$	± 2.5
320	1279	$+0.3 \ -0.3$	± 2.7
340	1156	$+0.4 \ -0.4$	± 2.7
360	1048	$+0.5 \ -0.3$	± 2.8
380	953	$+0.5 \ -0.1$	± 3.0
400	869	$+0.6 \ -0.2$	± 3.0
500	566	$+0.9 \ -0.2$	± 3.4
600	385	$+1.2 \ -0.1$	± 3.8
650	322	$+1.4 \ -0.0$	± 4.0
700	271	$+1.4 \ -0.1$	± 4.2
750	229	$+1.5 \ -0.1$	± 4.4
800	195	$+1.6 \ -0.1$	± 4.5
850	167	$+1.7 \ -0.2$	± 4.7
900	144	$+1.8 \ -0.1$	± 4.9
950	124	$+1.9 \ -0.2$	± 5.0
1000	108	$+2.0 \ -0.2$	± 5.1

Table 11: NNLO QCD results on VBF cross sections at $\sqrt{s} = 7$ TeV: central values and relative uncertainties. PDF uncertainties are evaluated with MSTW2008NNLO PDF set. Integration errors are below the 0.1% level.

$M_{\mathrm{H}}[\,\mathrm{GeV}]$	$\sigma[\mathrm{fb}]$	$(1 + \delta_{\mathrm{EW}})\,\sigma[\mathrm{fb}]$	Scale uncert. [%]	PDF + α_{s}[%]	PDF4LHC [%]
90	1788	1710	+0.6 −0.2	+1.8 −1.8	+2.1 −2.1
95	1703	1628	+0.4 −0.4	+1.8 −1.8	+2.1 −2.1
100	1616	1546	+0.4 −0.3	+1.8 −1.8	+2.2 −2.1
105	1539	1472	+0.3 −0.3	+1.8 −1.8	+2.2 −2.1
110	1461	1398	+0.5 −0.2	+1.8 −1.8	+2.3 −2.1
115	1393	1332	+0.2 −0.2	+1.8 −1.8	+2.3 −2.1
120	1326	1269	+0.3 −0.4	+1.8 −1.8	+2.4 −2.1
125	1265	1211	+0.3 −0.3	+1.8 −1.8	+2.5 −2.1
130	1205	1154	+0.3 −0.2	+1.8 −1.8	+2.5 −2.1
135	1148	1100	+0.5 −0.1	+1.8 −1.8	+2.6 −2.1
140	1099	1052	+0.2 −0.2	+1.8 −1.8	+2.6 −2.1
145	1048	1004	+0.4 −0.0	+1.9 −1.9	+2.7 −2.1
150	1004	961.7	+0.2 −0.1	+1.9 −1.9	+2.7 −2.1
155	959.6	918.0	+0.3 −0.0	+1.9 −1.9	+2.8 −2.1
160	920.0	878.7	+0.1 −0.2	+1.9 −1.9	+2.8 −2.1
165	880.0	851.7	+0.2 −0.1	+1.9 −1.9	+2.9 −2.1
170	843.9	817.3	+0.2 −0.2	+1.9 −1.9	+3.0 −2.1
175	808.2	781.4	+0.2 −0.1	+1.9 −1.9	+3.0 −2.1
180	776.0	748.0	+0.0 −0.3	+1.9 −1.9	+3.1 −2.1
185	742.1	719.3	+0.3 −0.1	+1.9 −1.9	+3.1 −2.0
190	713.5	692.5	+0.1 −0.2	+1.9 −1.9	+3.2 −2.0
195	685.0	664.3	+0.2 −0.4	+1.9 −1.9	+3.2 −2.0
200	657.9	637.1	+0.1 −0.2	+1.9 −1.9	+3.3 −2.0
210	607.6	586.9	+0.1 −0.3	+2.0 −2.0	+3.4 −2.0
220	562.3	542.0	+0.0 −0.4	+2.0 −2.0	+3.5 −2.0
230	520.8	501.1	+0.1 −0.4	+2.0 −2.0	+3.6 −2.0
240	483.2	464.1	+0.1 −0.5	+2.0 −2.0	+3.7 −2.0
250	448.7	430.4	+0.1 −0.6	+2.0 −2.0	+3.8 −2.0
260	416.2	398.8	+0.3 −0.4	+2.0 −2.0	+3.9 −2.0
270	388.1	371.5	+0.1 −0.6	+2.0 −2.0	+4.0 −2.0
280	361.9	346.1	+0.2 −0.7	+2.0 −2.0	+4.2 −2.0
290	337.7	322.6	+0.2 −0.7	+2.1 −2.1	+4.3 −2.0
300	315.4	301.0	+0.2 −0.8	+2.1 −2.1	+4.4 −2.0
320	275.4	262.2	+0.3 −0.7	+2.1 −2.1	+4.6 −1.9
340	241.9	228.6	+0.3 −0.9	+2.1 −2.1	+4.8 −1.9
360	213.2	201.8	+0.3 −1.1	+2.2 −2.2	+5.0 −1.9
380	188.2	180.7	+0.4 −1.1	+2.2 −2.2	+5.2 −1.9
400	166.6	161.9	+0.4 −1.2	+2.2 −2.2	+5.5 −1.9
450	124.4	123.5	+0.6 −1.3	+2.2 −2.2	+6.0 −1.8
500	94.07	94.91	+0.7 −1.6	+2.3 −2.3	+6.6 −1.8
550	71.90	73.56	+0.8 −1.7	+2.3 −2.3	+7.1 −1.8
600	55.52	57.63	+1.0 −2.0	+2.4 −2.4	+7.6 −1.7
650	43.22	45.56	+1.1 −2.2	+2.4 −2.4	+8.2 −1.7
700	33.89	36.35	+1.2 −2.4	+2.5 −2.5	+8.7 −1.6
750	26.74	29.24	+1.4 −2.6	+2.5 −2.5	+9.3 −1.6
800	21.21	23.71	+1.5 −2.8	+2.6 −2.6	+9.8 −1.6
850	16.90	19.37	+1.6 −3.0	+2.6 −2.6	+10.4 −1.5
900	13.52	15.95	+1.7 −3.2	+2.7 −2.7	+10.9 −1.5
950	10.86	13.21	+2.0 −3.3	+2.7 −2.7	+11.5 −1.4
1000	8.752	11.03	+2.2 −3.5	+2.8 −2.8	+12.0 −1.4

Table 12: NNLO QCD results on VBF cross sections at $\sqrt{s} = 14$ TeV: central values and relative uncertainties. PDF uncertainties are evaluated with MSTW2008NNLO PDF set. Integration errors are below the 0.1% level.

M_{H}[GeV]	σ[fb]	$(1 + \delta_{\mathrm{EW}})\,\sigma$[fb]	Scale uncert. [%]	PDF + α_{s}[%]	PDF4LHC [%]
90	5879	5569	+1.0 −0.4	+1.6 −1.6	+1.9 −2.6
95	5637	5338	+1.0 −0.5	+1.6 −1.6	+2.0 −2.6
100	5401	5114	+0.8 −0.5	+1.6 −1.6	+2.0 −2.6
105	5175	4900	+1.2 −0.3	+1.6 −1.6	+2.0 −2.6
110	5015	4750	+0.2 −1.3	+1.6 −1.6	+2.0 −2.6
115	4771	4520	+0.9 −0.4	+1.6 −1.6	+2.0 −2.6
120	4603	4361	+0.4 −0.9	+1.6 −1.6	+2.1 −2.6
125	4412	4180	+0.7 −0.4	+1.6 −1.6	+2.1 −2.6
130	4252	4029	+0.4 −0.5	+1.6 −1.6	+2.1 −2.6
135	4076	3862	+0.9 −0.2	+1.6 −1.6	+2.2 −2.6
140	3938	3732	+0.5 −0.8	+1.6 −1.6	+2.2 −2.6
145	3789	3590	+0.8 −0.4	+1.6 −1.6	+2.2 −2.6
150	3653	3460	+0.6 −0.4	+1.6 −1.6	+2.2 −2.6
155	3522	3332	+0.7 −0.4	+1.6 −1.6	+2.2 −2.6
160	3386	3198	+0.9 −0.2	+1.6 −1.6	+2.3 −2.6
165	3278	3137	+0.7 −0.3	+1.7 −1.7	+2.3 −2.6
170	3168	3033	+0.5 −0.4	+1.7 −1.7	+2.3 −2.6
175	3058	2922	+1.1 −0.2	+1.7 −1.7	+2.3 −2.6
180	2945	2805	+0.9 −0.2	+1.7 −1.7	+2.4 −2.6
185	2860	2740	+0.4 −0.3	+1.7 −1.7	+2.4 −2.6
190	2766	2652	+0.3 −0.3	+1.7 −1.7	+2.4 −2.6
195	2678	2566	+0.4 −0.3	+1.7 −1.7	+2.4 −2.6
200	2583	2472	+0.7 −0.1	+1.7 −1.7	+2.5 −2.6
210	2425	2315	+0.7 −0.1	+1.7 −1.7	+2.5 −2.6
220	2280	2171	+0.4 −0.5	+1.7 −1.7	+2.6 −2.6
230	2142	2036	+0.6 −0.2	+1.7 −1.7	+2.6 −2.6
240	2021	1918	+0.4 −0.1	+1.7 −1.7	+2.7 −2.6
250	1908	1807	+0.2 −0.4	+1.7 −1.7	+2.7 −2.6
260	1809	1711	+0.2 −1.1	+1.8 −1.8	+2.8 −2.6
270	1699	1606	+0.2 −0.3	+1.8 −1.8	+2.8 −2.6
280	1603	1514	+0.4 −0.1	+1.8 −1.8	+2.8 −2.6
290	1522	1436	+0.3 −0.2	+1.8 −1.8	+2.9 −2.6
300	1441	1358	+0.2 −0.3	+1.8 −1.8	+2.9 −2.6
320	1298	1220	+0.2 −0.2	+1.8 −1.8	+3.0 −2.6
340	1173	1094	+0.2 −0.2	+1.8 −1.8	+3.1 −2.6
360	1063	993.0	+0.1 −0.2	+1.9 −1.9	+3.2 −2.6
380	965.3	914.8	+0.1 −0.1	+1.9 −1.9	+3.3 −2.6
400	878.6	842.2	+0.2 −0.1	+1.9 −1.9	+3.4 −2.6
450	703.6	689.3	+0.2 −0.4	+1.9 −1.9	+3.7 −2.6
500	570.7	568.4	+0.1 −0.3	+2.0 −2.0	+3.9 −2.6
550	467.6	472.4	+0.3 −0.4	+2.0 −2.0	+4.1 −2.6
600	386.9	396.5	+0.3 −0.5	+2.0 −2.0	+4.4 −2.6
650	322.8	336.0	+0.3 −0.6	+2.1 −2.1	+4.6 −2.6
700	271.3	287.2	+0.4 −0.8	+2.1 −2.1	+4.9 −2.6
750	229.3	247.6	+0.5 −0.9	+2.1 −2.1	+5.1 −2.6
800	195.1	215.5	+0.5 −1.1	+2.2 −2.2	+5.3 −2.6
850	166.5	188.5	+0.7 −1.0	+2.2 −2.2	+5.6 −2.6
900	143.0	166.6	+0.6 −1.2	+2.2 −2.2	+5.8 −2.6
950	123.4	148.4	+0.5 −1.4	+2.2 −2.2	+6.1 −2.6
1000	106.7	133.0	+0.7 −1.4	+2.3 −2.3	+6.3 −2.6

4 WH/ZH production mode[6]

4.1 Experimental overview

Searches for the Higgs boson in the WH and ZH production modes, usually defined as Higgs-strahlung processes, have been considered mainly by exploiting two decay modes, $H \rightarrow W^+W^-$ and $H \rightarrow b\bar{b}$. While the former is looked for mainly because it could contribute to the measurement of the Higgs-boson coupling to W bosons, the latter decay mode might contribute to the discovery of a low-mass Higgs boson and later allow to measure the coupling of the Higgs boson to b quarks. The experimental sensitivity to $H \rightarrow W^+W^-$ is highest for Higgs-boson masses above about 160 GeV, while the $H \rightarrow b\bar{b}$ decay modes are investigated for the low Higgs-boson mass region, below about 130 GeV.

The $WH \rightarrow WWW$ channel in the tri-lepton mode was explored with a parton-level study in Ref. [93], while a first estimate of the discovery sensitivity at the LHC was presented in Refs. [94, 95], based on a fast simulation of the ATLAS detector only. In the latter document the statistical discovery significance of the ATLAS detector with an integrated luminosity of 30 fb^{-1} was estimated to be above 3σ for Higgs-boson masses in the range $160-170$ GeV. However, a more realistic study based on samples of fully simulated Monte Carlo events, presented in Ref. [96], shows that the extraction of this signal might be significantly harder than previously thought, in particular due to the very high $t\bar{t}$ background, although a precise quantitative estimate of the discovery significance suffers from the limited available statistics of the samples and from the fact that the continuum WWW background was not considered in the study.

The decay channel $H \rightarrow b\bar{b}$ is dominant at low Higgs-boson masses, below about 130 GeV. Given the large $b\bar{b}$ backgrounds from pure QCD-driven processes, this decay mode is not accessible in gluon-fusion production mode and is only marginally accessible in combination with the vector-boson fusion. The most promising sensitivity studies rely on the associated production of a Higgs boson either with a Z or W boson (WH or ZH) or with a $t\bar{t}$ pair. The WH and ZH channels with $H \rightarrow b\bar{b}$ are the main search channels at the Tevatron for a Higgs boson with low mass, but at the LHC it is significantly more challenging to extract these signals from the backgrounds. A first study of the sensitivity to a Higgs boson in the WH and ZH channels was presented in the ATLAS TDR [94] and one year later in Refs. [97, 98]. The channel with the most significant predicted signal is WH, which however results in a predicted discovery significance of about 2 after 30 fb^{-1} and a signal to background ratio of about 2%. Under these conditions, the extraction of the signal is extremely challenging, since the significance is low and the normalization of the backgrounds in the signal region must be controlled at the percent level.

More recently, in Ref. [99], it has been proposed to focus the search for a Higgs boson in the WH and ZH channels with the decay $H \rightarrow b\bar{b}$ into the very specific kinematic region where both the Higgs boson and the W or Z boson produced in association with it are emitted at high p_T (e.g. $p_T > 200$ GeV), i.e. in a topological configuration where they are back-to-back in the transverse plane and highly boosted. As a first consequence, the intermediate virtual W or Z boson producing the Higgs boson and the associated vector boson must be very massive, thus even with the LHC center-of-mass energy it will produced quite centrally, so that the kinematic acceptance of its decay products, the Higgs and the W bosons, will be significantly improved. In addition, for various reasons, the signal-to-background ratio is significantly improved, reducing the impact of background uncertainties onto the discovery significance. A first study based on a realistic simulation of the ATLAS detector, but based only on *LO* Monte Carlo generators, was performed in Ref. [100], where it was found that after 30 fb^{-1} of data collected at a center-of-mass energy of 14 TeV a discovery significance above 3 should be achievable and that these channels might contribute, in combination with others, to the discovery of a low-mass Higgs boson with around 10 fb^{-1} of integrated luminosity.

In the past months the expected sensitivity in the WH and ZH channels has been re-evaluated for lower center-of-mass energies, by both the ATLAS and CMS Collaborations. With 1 fb^{-1} of data and

---

[6]S. Dittmaier, R.V. Harlander, J. Olsen, G. Piacquadio (eds.); O. Brein, M. Krämer and T. Zirke.
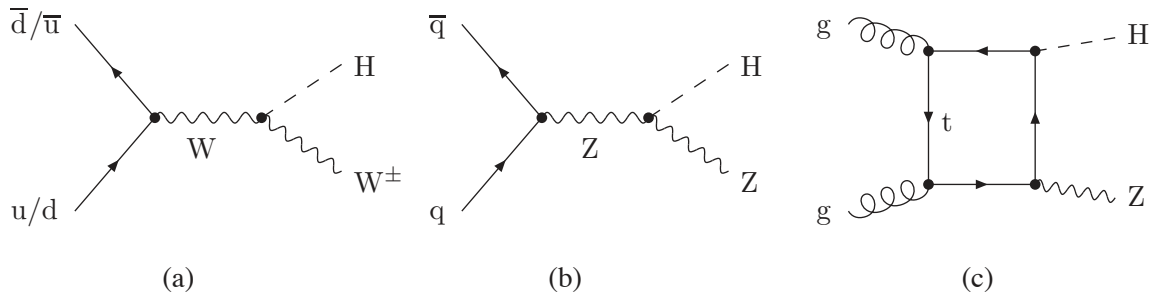
Fig. 7: (a), (b) LO diagrams for the partonic processes $pp \rightarrow VH$ ($V = W, Z$); (c) diagram contributing to the $gg \rightarrow HZ$ channel.

$\sqrt{s} = 7$ TeV ATLAS expects to exclude a Higgs boson at 95% CL with a cross section equivalent to about 6 times the SM one [101], while with 5 fb^{-1} of data and $\sqrt{s} = 8$ TeV CMS expects to exclude a Higgs boson at 95% CL with a cross section equivalent to about 2 times the SM one [102]. These results are very preliminary and partially rely on analyses which have not been re-optimized for the lower center-of-mass energy.

One of the main challenges of these searches is to control the backgrounds down to a precision of about 10% or better in the very specific kinematic region where the signal is expected. Precise differential predictions for these backgrounds as provided by theoretical perturbative calculations and parton-shower Monte Carlo generators are therefore crucial. Further studies (e.g. in Ref. [103]) suggest that with data corresponding to an integrated luminosity of the order of 30 fb^{-1} the $t\bar{t}$ background might be extracted from data in a signal-free control region, while this seems to be significantly harder for the $W b\bar{b}$ or $Z b\bar{b}$ irreducible backgrounds, even in the presence of such a large amount of data.

For all search channels previously mentioned, a precise prediction of the signal cross section and of the kinematic properties of the produced final-state particles is of utmost importance, together with a possibly accurate estimation of the connected systematic uncertainties. The scope of this section is to present the state-of-the-art inclusive cross sections for the WH and ZH Higgs-boson production modes at different LHC center-of-mass energies and for different possible values of the Higgs-boson mass and their connected uncertainties.

4.2 Theoretical framework

The inclusive partonic cross section for associated production of a Higgs boson (H) and a weak gauge boson (V) can be written as

$$\hat{\sigma}(\hat{s}) = \int_0^{\hat{s}} \mathrm{d}k^2 \, \sigma(V^*(k)) \frac{\mathrm{d}\Gamma}{\mathrm{d}k^2}(V^*(k) \rightarrow HV) + \Delta\sigma \,, \tag{2}$$

where $\sqrt{\hat{s}}$ is the partonic center-of-mass energy. The first term on the r.h.s. arises from terms where a virtual gauge boson V^* with momentum k is produced in a Drell–Yan-like process, which then radiates a Higgs boson. The factor $\sigma(V^*)$ is the total cross section for producing the intermediate vector boson and is fully analogous to the Drell–Yan expression. The second term on the r.h.s., $\Delta\sigma$, comprises all remaining contributions. The hadronic cross section is obtained from the partonic expression of Eq. (2) by convoluting it with the parton densities in the usual way.

The LO prediction for $pp \rightarrow VH$ ($V = W, Z$) is based on the Feynman diagrams shown in Fig. 7 (a),(b) and leads to a LO cross section of $\mathcal{O}(G_F^2)$. Through NLO, the QCD corrections are fully given by the NLO QCD corrections to the Drell–Yan cross section $\hat{\sigma}(V^*)$ [104–106]. For $V = W$, this

observation carries over to NNLO[7], so that the corresponding QCD corrections can be easily derived by integrating the classic Drell–Yan result [14,107] over the virtuality of the intermediate gauge boson. For that purpose, the program VH@NNLO has been developed [108], building on the publicly available code ZWPROD.F [107].

The Drell–Yan-like corrections that determine the NNLO result for WH production also give the bulk of the ZH contribution. However, in that case, there are gluon–gluon-induced terms that do not involve a virtual weak gauge boson; both Z and H couple to the gluons via a top-quark loop in this case, see Fig. 7(c). This class of diagrams is not taken into account in VH@NNLO; it was computed in Ref. [108], and the numbers included in the results below are based on the corresponding numerical code.

As every hadron collider observable that is evaluated at fixed order perturbation theory, the cross section depends on the unphysical renormalization and factorization scales μ_R and μ_F. Since the QCD corrections mostly affect the production of the intermediate gauge boson, a natural choice for the central value of μ_F and μ_R is the virtuality k^2 of this gauge boson.

NLO electroweak (EW) corrections have been evaluated in Ref. [109]. In contrast to the NLO QCD corrections, EW corrections do not respect a factorization into Drell–Yan-like production and decay, since there are irreducible (box) corrections to $qq^{(\prime)} \to VH$ already at one loop. Note also that the size of the EW corrections (as usual) sensitively depend on the chosen renormalization scheme to define the weak couplings, most notably on the choice for the electromagnetic couplings α. The preferred choice, which should be most robust with respect to higher-order corrections, is the so-called G_F scheme, where α is derived from Fermi's constant G_F.

The combination of QCD and EW corrections poses the question on whether factorization of the EW and QCD effects is a valid approximation to the actual mixed $\mathcal{O}(G_F\alpha_{\mathrm{s}})$ corrections. Following Ref. [110], we present our result based on the assumption that full factorization of the two effects is valid, i.e., the cross section is determined as

$$\sigma_{\mathrm{WH}} = \sigma_{\mathrm{WH}}^{\mathrm{VH@NNLO}} \times (1 + \delta_{\mathrm{WH,EW}})\,, \qquad \sigma_{\mathrm{ZH}} = \sigma_{\mathrm{ZH}}^{\mathrm{VH@NNLO}} \times (1 + \delta_{\mathrm{ZH,EW}}) + \sigma_{\mathrm{gg}\to\mathrm{ZH}}\,, \quad (3)$$

where $\sigma_{VH}^{\mathrm{VH@NNLO}}$ is the NNLO QCD result of VH@NNLO through $\mathcal{O}(\alpha_{\mathrm{s}}^2)$, $\delta_{VH,\mathrm{EW}}$ is the relative EW correction factor determined in the limit $\alpha_{\mathrm{s}} = 0$, and $\sigma_{\mathrm{gg}\to\mathrm{ZH}}$ is the NNLO contribution to ZH production induced by gg fusion.

The PDF+α_{s} uncertainties are evaluated according to the recipe proposed in Section 8.5 of this report. The uncertainties due to the residual dependence on the renormalization and factorization scales are determined by considering the cross section when mutually fixing one of μ_R and μ_F at the central scale $\sqrt{k^2}$ (the mass of the intermediate gauge boson, see above), and varying the other scale between $\sqrt{k^2}/3$ and $3\sqrt{k^2}$. The EW factor $\delta_{VH,\mathrm{EW}}$ is always calculated in the same way as the central value of the cross section, because the relative EW correction is insensitive to the PDF and/or scale choices.

In principle there are also real NLO EW corrections induced by initial-state photons, which are ignored, since current PDF sets do not deliver a photon PDF. The photon PDF is, however, strongly suppressed, so that an uncertainty of not more than 1% should arise from this approximation. This estimated percent uncertainty, which rests on the comparison with other cross sections such as vector-boson fusion [69,70] where these effects have been calculated, also includes the neglect of NLO EW corrections in the evolution of current PDFs.

---

[7]This statement holds up to two-loop diagrams where the Higgs boson is attached to a one-loop Drell–Yan diagram via the loop-induced ggH coupling. Such diagrams, which are neglected so far, are believed to have only a small impact; their calculation is in progress.

4.3 Numerical results

The results for the NLO and the NNLO QCD cross sections for WH production, including NLO EW effects, are shown in Fig. 8, both at 7 TeV and 14 TeV. The numbers are obtained by summing over W^+H and W^-H production. The corresponding K-factors, obtained by normalizing the cross section to the LO value (at central scales and PDFs), are shown in Fig. 9. The little kinks at around 160 GeV and, somewhat smaller, 180 GeV are due to the WW and ZZ thresholds that occur in the EW radiative corrections (see also Ref. [109]). The present prediction does not properly describe the threshold behaviour, which is in fact singular on threshold. Therefore, in practice, Higgs mass windows of $\sim \pm 5$ GeV around the thresholds should be obtained upon interpolation unless the threshold regions are properly described (e.g. by complex masses), a task which is in progress. The uncertainty of the threshold interpolation is about 1%.

The plots for ZH production are shown in Figs. 10 and 11. The fact that the uncertainty bands at NNLO are of the same order of magnitude as at NLO is due to the gg channel that occurs only at NNLO and is absent in the WH case. In more detail, for the centre-of-mass energy of 7 TeV (14 TeV) the gg channel contributes to ZH production by $2-6\%$ ($4-12\%$) with an uncertainty of $20-30\%$ from scale variation and of 4% (2%) from PDF, translating roughly into a $0.5-1.5\%$ ($1-3\%$) uncertainty on the full result.

We have checked the NLO numbers against V2HV [111] and find agreement at the permille level, once CKM mixing is included in V2HV. Also, we find satisfactory agreement of the NLO result when comparing to MCFM [112]. However, the comparison is less strict in this case as MCFM does not allow the same scale choice as used here.

The results for the central values of the cross section and the corresponding theoretical uncertainties are shown in Tables 13 and 14 for 7 TeV and 14 TeV, respectively. Notice that the scale uncertainties for ZH production are consistently larger than for WH production, because they are dominated by the uncertainties of the gg channel.
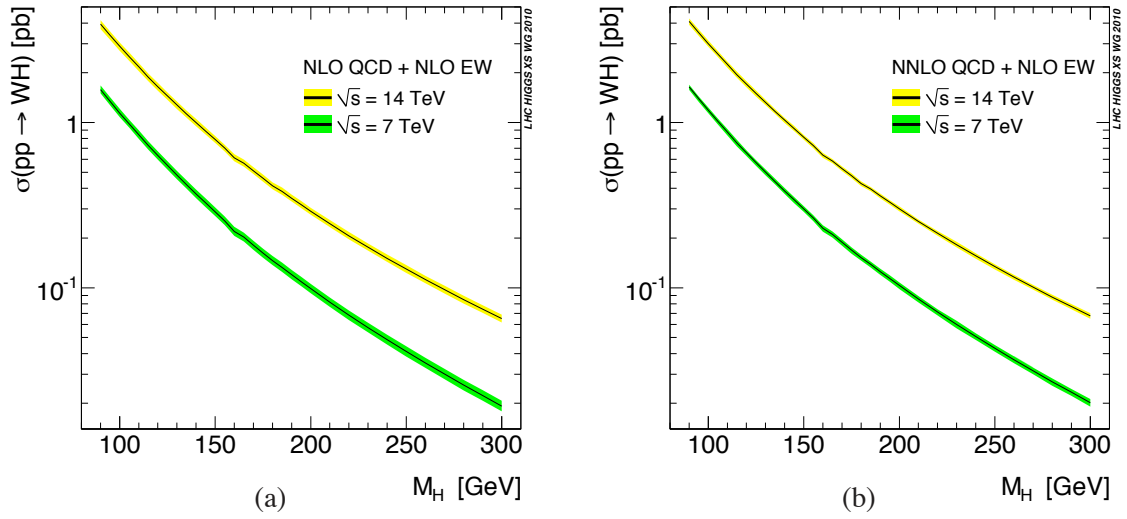
Fig. 8: Cross section for the sum of W^+H and W^-H production for 7 TeV and 14 TeV at (a) NLO and (b) NNLO QCD, including NLO EW effects in both cases.
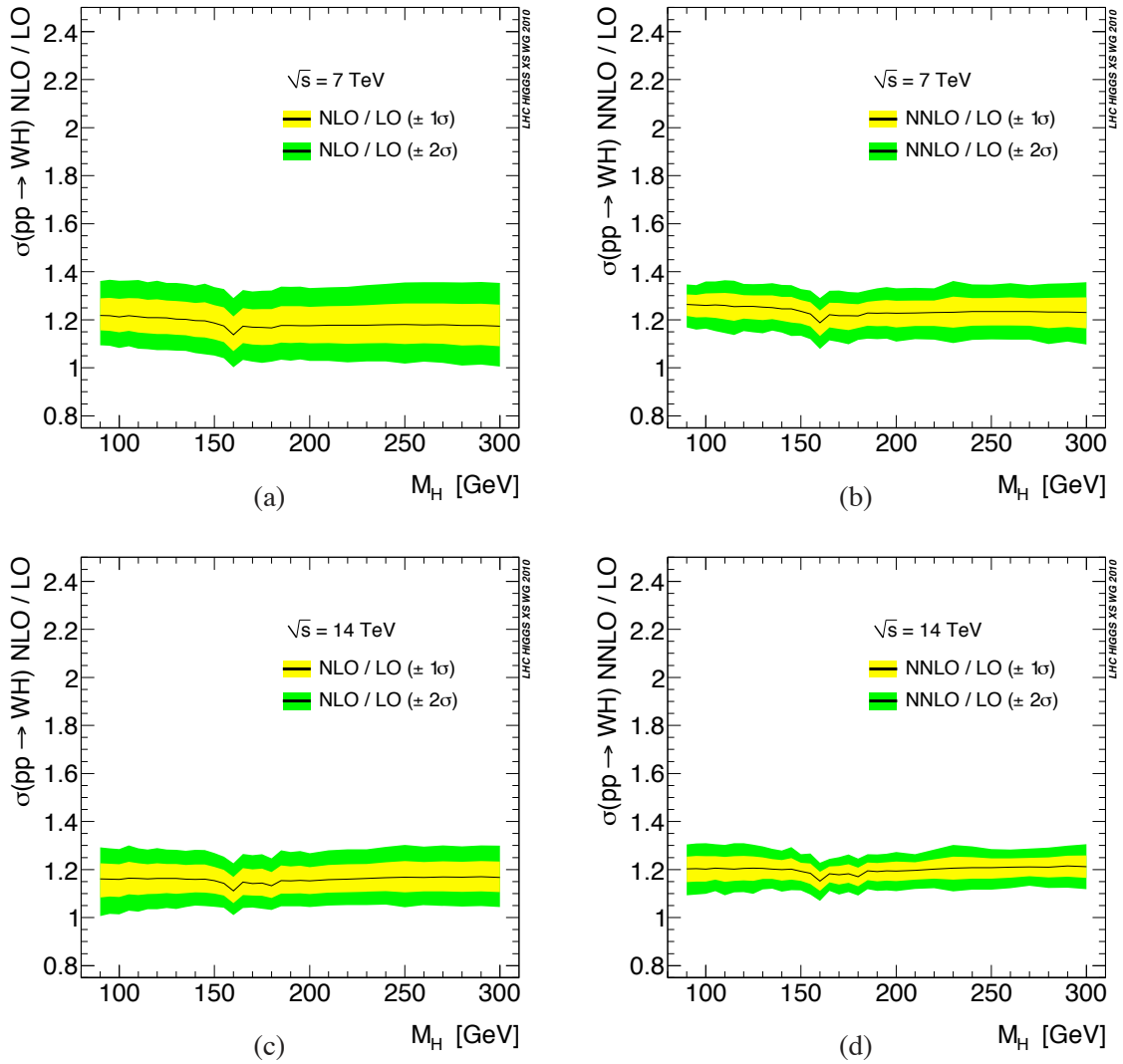
Fig. 9: K-factors (ratio to LO prediction) for the NLO and NNLO cross sections of Fig. 8.
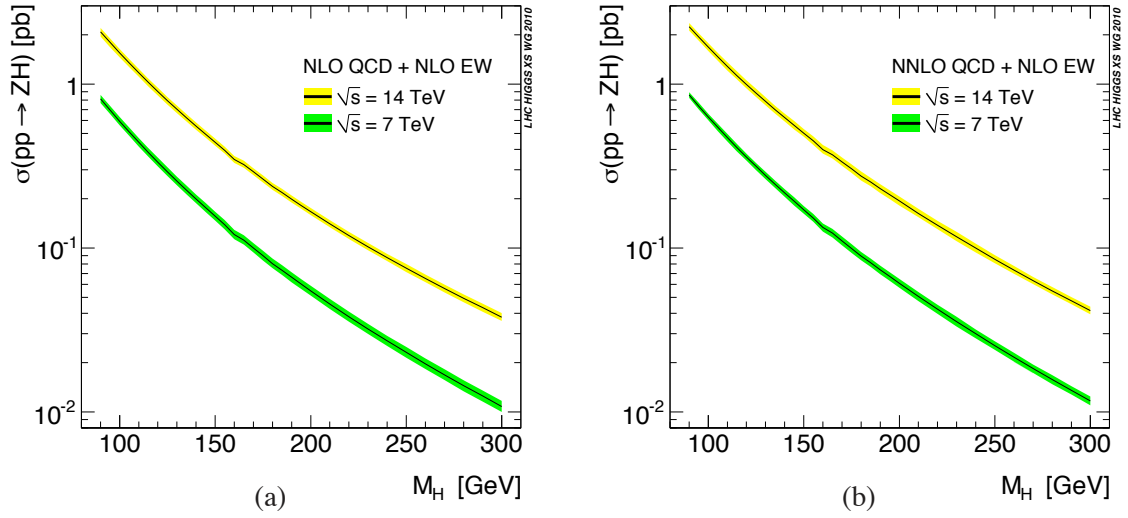
Fig. 10: Cross section for ZH production for 7 TeV and 14 TeV at (a) NLO and (b) NNLO QCD, including NLO EW effects in both cases.

Fig. 11: K-factors (ratio to LO prediction) for the NLO and NNLO cross sections of Fig. 10.

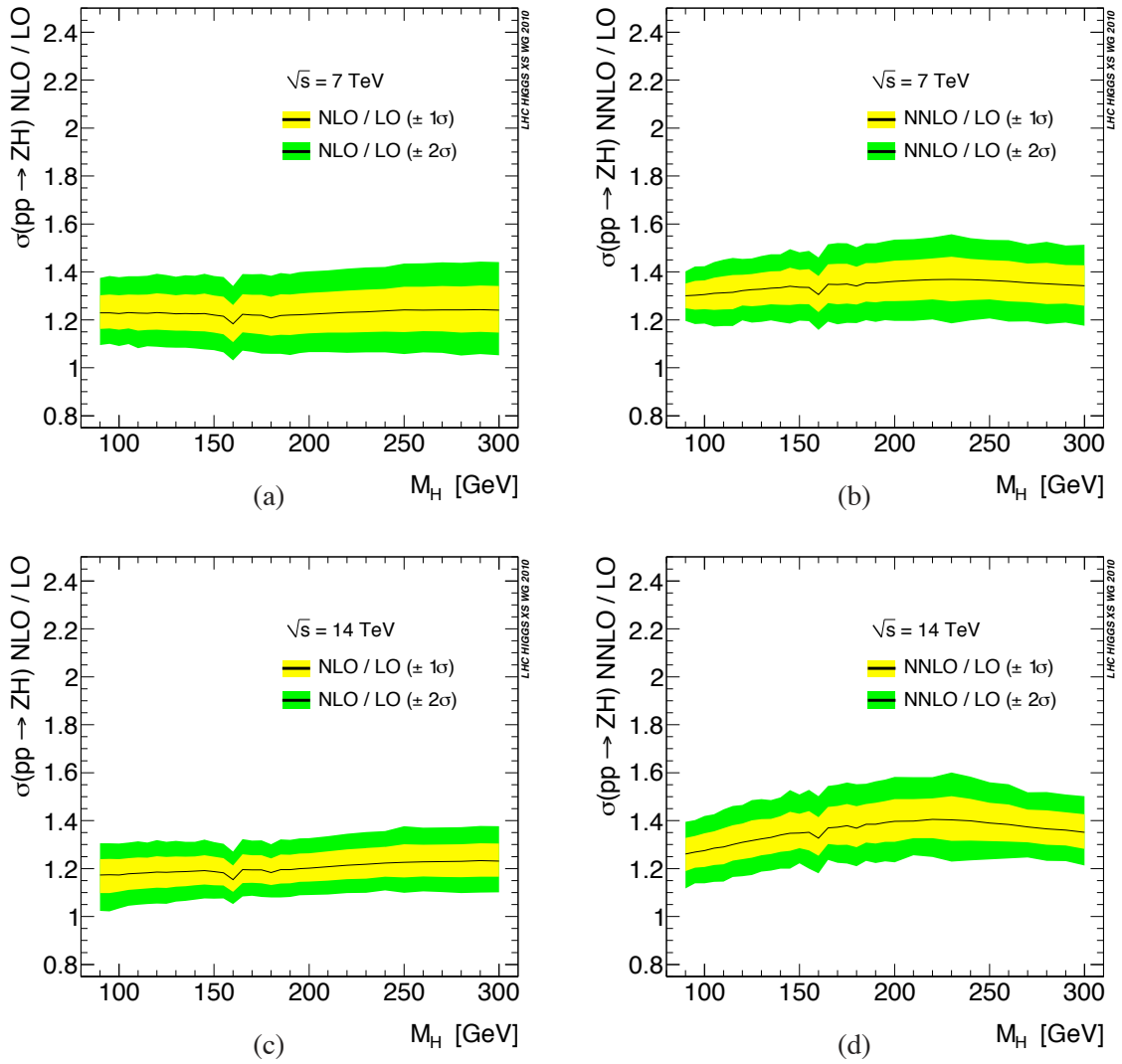**Table 13:** Total inclusive cross section at 7 TeV for WH and ZH production at NNLO QCD + NLO EW. The first error indicates the uncertainty from the renormalization and factorization scale variation, the second from the PDF+α_s variation.

| M_H[GeV]	σ(WH)[pb]	Scale [%]	PDF4LHC [%]	σ(ZH)[pb]	Scale [%]	PDF4LHC [%]
90	1.640	+0.3 −0.8	±3.0	0.8597	+0.9 −1.0	±3.0
95	1.392	+0.1 −0.9	±3.2	0.7348	+1.0 −1.1	±3.6
100	1.186	+0.6 −0.5	±3.4	0.6313	+1.1 −1.2	±3.4
105	1.018	+0.3 −0.8	±3.5	0.5449	+1.3 −1.6	±3.7
110	0.8754	+0.3 −0.7	±3.8	0.4721	+1.2 −1.2	±4.1
115	0.7546	+0.4 −0.8	±3.9	0.4107	+1.3 −1.2	±4.2
120	0.6561	+0.4 −0.7	±3.4	0.3598	+1.5 −1.2	±3.5
125	0.5729	+0.2 −0.8	±3.5	0.3158	+1.4 −1.6	±3.5
130	0.5008	+0.3 −0.8	±3.5	0.2778	+1.5 −1.4	±3.7
135	0.4390	+0.7 −0.4	±3.4	0.2453	+1.7 −1.4	±3.6
140	0.3857	+0.5 −0.5	±3.5	0.2172	+1.5 −1.6	±3.7
145	0.3406	+0.2 −0.8	±3.8	0.1930	+1.8 −1.8	±4.0
150	0.3001	+0.4 −0.8	±3.3	0.1713	+1.8 −1.6	±3.6
155	0.2646	+0.5 −0.8	±3.5	0.1525	+2.1 −1.6	±3.6
160	0.2291	+0.5 −0.7	±3.8	0.1334	+2.0 −1.7	±4.0
165	0.2107	+0.5 −0.7	±3.6	0.1233	+2.1 −1.7	±4.1
170	0.1883	+0.5 −0.7	±3.8	0.1106	+2.2 −1.9	±4.2
175	0.1689	+0.3 −1.1	±3.8	0.09950	+2.1 −1.9	±4.1
180	0.1521	+0.6 −0.6	±3.5	0.08917	+2.2 −1.9	±3.8
185	0.1387	+0.4 −0.9	±3.5	0.08139	+2.3 −2.0	±3.8
190	0.1253	+0.5 −0.7	±3.7	0.07366	+2.2 −2.1	±3.9
195	0.1138	+0.7 −0.6	±3.7	0.06699	+2.3 −1.9	±4.0
200	0.1032	+0.4 −1.0	±3.8	0.06096	+2.3 −1.9	±4.1
210	0.08557	+0.5 −0.7	±3.7	0.05068	+2.1 −2.0	±4.2
220	0.07142	+0.3 −0.9	±3.7	0.04235	+2.2 −1.9	±4.2
230	0.06006	+0.7 −0.7	±4.5	0.03560	+2.1 −1.9	±4.8
240	0.05075	+0.5 −0.7	±4.0	0.02999	+1.9 −1.8	±4.4
250	0.04308	+0.5 −0.7	±4.0	0.02540	+2.0 −1.6	±4.2
260	0.03674	+0.8 −0.7	±4.0	0.02158	+1.8 −1.7	±4.5
270	0.03146	+0.6 −0.9	±3.8	0.01839	+1.7 −1.7	±4.3
280	0.02700	+0.4 −1.0	±4.4	0.01575	+1.6 −1.3	±4.9
290	0.02333	+0.7 −0.8	±4.2	0.01355	+1.5 −1.3	±4.5
300	0.02018	+0.6 −0.9	±4.5	0.01169	+1.4 −1.2	±5.0

Table 14: Total inclusive cross section at 14 TeV for WH and ZH production at NNLO QCD + NLO EW. The first error indicates the uncertainty from the renormalization and factorization scale variation, the second from the PDF+α_s variation.

M_H[GeV]	σ(WH)[pb]	Scale [%]	PDF4LHC [%]	σ(ZH)[pb]	Scale [%]	PDF4LHC [%]
90	4.090	+0.4 −0.7	±3.9	2.245	+1.3 −1.7	±4.0
95	3.499	+0.6 −0.7	±3.8	1.941	+1.6 −1.6	±3.6
100	3.002	+0.8 −0.6	±3.7	1.683	+1.9 −1.5	±3.8
105	2.596	+0.6 −0.5	±3.5	1.468	+1.7 −1.7	±3.7
110	2.246	+0.3 −0.8	±3.8	1.283	+2.1 −1.6	±4.0
115	1.952	+0.7 −0.2	±3.8	1.130	+2.5 −1.5	±3.7
120	1.710	+0.6 −0.3	±3.8	0.9967	+2.4 −1.8	±3.6
125	1.504	+0.3 −0.6	±3.8	0.8830	+2.7 −1.8	±3.7
130	1.324	+0.5 −0.4	±3.3	0.7846	+2.9 −1.8	±3.4
135	1.167	+0.6 −0.5	±2.9	0.6981	+2.9 −2.2	±3.0
140	1.034	+0.2 −0.7	±3.1	0.6256	+2.8 −2.2	±3.0
145	0.9200	+0.5 −0.4	±3.3	0.5601	+3.3 −2.1	±3.4
150	0.8156	+0.3 −0.6	±2.7	0.5016	+3.3 −2.0	±2.7
155	0.7255	+0.4 −0.6	±3.1	0.4513	+3.3 −2.4	±3.2
160	0.6341	+0.2 −0.5	±3.1	0.3986	+3.5 −2.4	±3.1
165	0.5850	+0.2 −0.6	±2.4	0.3705	+3.8 −2.3	±2.6
170	0.5260	+0.3 −0.7	±2.8	0.3355	+3.5 −2.4	±3.0
175	0.4763	+0.5 −0.3	±2.9	0.3044	+3.5 −2.6	±3.1
180	0.4274	+0.4 −0.6	±2.8	0.2744	+3.7 −2.8	±3.0
185	0.3963	+0.4 −0.7	±2.5	0.2524	+3.5 −2.9	±2.6
190	0.3600	+0.2 −0.6	±2.8	0.2301	+3.5 −2.9	±3.0
195	0.3291	+0.3 −0.7	±2.7	0.2112	+3.5 −2.9	±2.9
200	0.3004	+0.4 −0.5	±3.0	0.1936	+3.6 −3.0	±3.1
210	0.2526	+0.2 −0.7	±2.6	0.1628	+3.9 −2.5	±2.6
220	0.2138	+0.6 −0.5	±2.8	0.1380	+3.4 −2.7	±2.9
230	0.1826	+0.4 −0.5	±3.5	0.1173	+3.4 −2.6	±3.6
240	0.1561	+0.4 −0.5	±3.3	0.09996	+3.1 −2.5	±3.4
250	0.1343	+0.2 −0.7	±3.0	0.08540	+3.0 −2.3	±3.2
260	0.1161	+0.2 −0.7	±2.8	0.07341	+3.0 −2.1	±3.1
270	0.1009	+0.5 −0.6	±2.6	0.06325	+2.5 −1.9	±2.8
280	0.08781	+0.4 −0.6	±3.0	0.05474	+2.5 −1.8	±3.2
290	0.07714	+0.3 −0.6	±3.2	0.04769	+2.2 −1.5	±3.2
300	0.06755	+0.6 −0.5	±3.3	0.04156	+2.0 −1.6	±3.6

5 ttH process[8]

5.1 Higgs-boson production in association with $t\bar{t}$ pairs

Higgs radiation off top quarks $q\bar{q}/gg \to Ht\bar{t}$ (see Fig. 12) plays a role for light Higgs masses below ~ 150 GeV at the LHC. The measurement of the $t\bar{t}H$ production rate can provide relevant information on the top–Higgs Yukawa coupling. The leading-order (LO) cross section was computed a long time ago [113–117]. These LO results are plagued by large theoretical uncertainties due to the strong dependence on the renormalization scale of the strong coupling constant and on the factorization scales of the parton density functions inside the proton, respectively. For the LO cross section there are several public codes available, as e.g. HQQ [64, 118], MADGRAPH/MADEVENT [119, 120], MCFM [112], or PYTHIA [121]. The dominant background processes for this signal process are $t\bar{t}b\bar{b}$, $t\bar{t}jj$, $t\bar{t}\gamma\gamma$, $t\bar{t}Z$, and $t\bar{t}W^{+}W^{-}$ production depending on the final-state Higgs-boson decay.
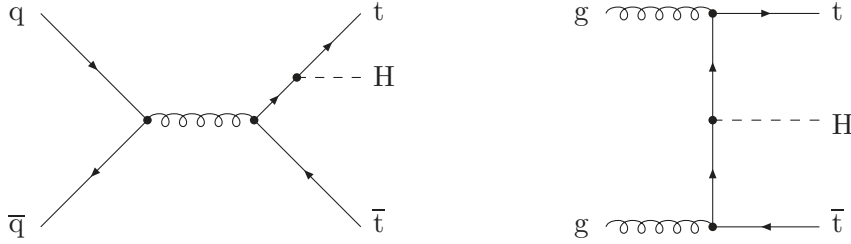
Fig. 12: Examples of LO Feynman diagrams for the partonic processes $q\bar{q}, gg \to t\bar{t}H$.

The full next-to-leading-order (NLO) QCD corrections to $t\bar{t}H$ production have been calculated [122–125] resulting in a moderate increase of the total cross section at the LHC by at most $\sim 20\%$, depending on the value of M_{H} and on the PDF set used. Indeed, when using CTEQ6.6 the NLO corrections are always positive and the K-factor varies between 1.14 and 1.22 for $M_{\mathrm{H}} = 90, \ldots, 300$ GeV, while when using MSTW2008 the impact of NLO corrections is much less uniform: NLO corrections can either increase or decrease the LO cross section by a few percents and result in K-factors between 1.05 and 0.98 for $M_{\mathrm{H}} = 90, \ldots, 300$ GeV.

The residual scale dependence has decreased from $\mathcal{O}(50\%)$ to a level of $\mathcal{O}(10\%)$ at NLO, if the renormalization and factorization scales are varied by a factor 2 up- and downwards around the central scale choice, thus signalling a significant improvement of the theoretical prediction at NLO. The full NLO results confirm former estimates based on an effective-Higgs approximation [126] which approximates Higgs radiation as a fragmentation process in the high-energy limit. The NLO effects on the relevant parts of final-state particle distribution shapes are of moderate size, i.e. $\mathcal{O}(10\%)$, so that former experimental analyses are not expected to change much due to these results. There is no public NLO code for the signal process available yet.

5.2 Background processes

Recently the NLO QCD corrections to the $t\bar{t}b\bar{b}$ production background have been calculated [127–131]. By choosing $\mu_R^2 = \mu_F^2 = m_{\mathrm{t}}\sqrt{p_{T\mathrm{b}}p_{T\bar{\mathrm{b}}}}$ as the central renormalization and factorization scales the NLO corrections increase the background cross section within the signal region by about 20–30%. The scale dependence is significantly reduced to a level significantly below 30%. The new predictions for the NLO QCD cross sections with the new scale choice $\mu_R^2 = \mu_F^2 = m_{\mathrm{t}}\sqrt{p_{T\mathrm{b}}p_{T\bar{\mathrm{b}}}}$ are larger than the old LO predictions with the old scale choice $\mu_R = \mu_F = m_{\mathrm{t}} + m_{\mathrm{b}\bar{\mathrm{b}}}/2$ by more than 100% within the typical

---

[8]C. Collins-Tooth, C. Neu, L. Reina, M. Spira (eds.); S. Dawson, S. Dean, S. Dittmaier, M. Krämer, C.T. Potter and D. Wackeroth.

Table 15: LO cross sections of $pp \to t\bar{t}H$ for $\sqrt{s} = 7$ TeV using MSTW2008 and CTEQ6.6 PDFs. The scale dependence is given for the scale variation $\mu_0/2 < \mu_R, \mu_F < 2\mu_0$ with $\mu_0 = m_t + M_H/2$. The PDF uncertainties are defined at 68% CL using MSTW2008.

M_H [GeV]	LO [fb], MSTW2008	LO [fb], CTEQ6L1	Scale [%]	PDF[%]
90	213.2	174.2	$+40.0 - 26.3$	$+2.5 - 2.6$
100	162.7	133.0	$+39.9 - 26.3$	$+2.5 - 2.6$
110	126.1	102.8	$+39.9 - 26.2$	$+2.5 - 2.5$
120	98.66	80.43	$+39.8 - 26.2$	$+2.5 - 2.6$
130	78.09	63.62	$+39.8 - 26.2$	$+2.5 - 2.5$
140	62.43	50.79	$+39.9 - 26.2$	$+2.5 - 2.6$
150	50.35	40.94	$+39.8 - 26.2$	$+2.6 - 2.6$
160	40.98	33.29	$+39.8 - 26.2$	$+2.6 - 2.6$
170	33.62	27.30	$+39.8 - 26.2$	$+2.6 - 2.6$
180	27.83	22.57	$+39.8 - 26.2$	$+2.6 - 2.6$
190	23.20	18.80	$+39.8 - 26.2$	$+2.7 - 2.6$
200	19.48	15.78	$+39.9 - 26.2$	$+2.7 - 2.7$

experimental cuts [129]. In addition the signal process $pp \to t\bar{t}H \to t\bar{t}b\bar{b}$ has been added to these background calculations in the narrow-width approximation [131]. This makes it possible to study the signal and background processes including the final-state Higgs decay into $b\bar{b}$ with cuts at the same time at NLO. However, it should be noted that the final-state top decays have not been included at NLO so that a full NLO signal and background analysis including all experimental cuts is not possible yet. The top-quark decays are expected to affect the final-state distributions more than the Higgs decays into $b\bar{b}$ pairs. For highly boosted Higgs bosons the shapes of the background distributions are affected by the QCD corrections which thus have to be taken into account properly. The effects of a jet veto for the boosted-Higgs regime require further detailed investigations. Very recently the NLO QCD corrections to $t\bar{t}jj$ production have been calculated [132]. However, a full numerical analysis of these results has not been performed so far. As it is the case for the signal process, there is no public code available for the NLO calculations of the background processes $pp \to t\bar{t}b\bar{b}, t\bar{t}jj$.

5.3   Numerical analysis and results

In the following we provide results for the inclusive NLO signal cross section for different values of Higgs masses. The central scale has been chosen as $\mu_R = \mu_F = \mu_0 = m_t + M_H/2$. In addition, the uncertainties due to scale variations of a factor of two around the central scale μ_0 as well as the 68% CL uncertainties due to the PDFs and the strong coupling α_s are given explicitly. In this study we used the on-shell top-quark mass and did not include the parametric uncertainties due to the experimental error on the top-quark mass. Loop diagrams with a bottom-quark loop were calculated using the b-quark pole mass. The top-quark Yukawa coupling was defined in terms of the top pole mass. The values for the top and bottom masses are chosen according to the parameters given in Appendix A. We have used the MSTW2008 [41, 44], CTEQ6.6 [133], and NNPDF2.0 [134] sets of parton density functions. The central values of the strong coupling constant have been implemented according to the corresponding PDFs for the sake of consistency. In Table 15 we show the LO cross sections for the signal process and their respective scale and PDF uncertainties calculated with MSTW2008 PDFs. For comparison we also show the central LO cross sections obtained with CTEQ6L1 PDFs. It is remarkable that the numbers using the LO PDFs of MSTW2008 and CTEQ6L1 differ by about 20%. The scale uncertainties at LO are typically of the order of $30-40\%$, while the PDF uncertainties amount to about $2-3\%$.

In Table 16 the NLO signal cross section is listed including the scale, α_s, and PDF uncertainties at 68% CL for MSTW2008 PDFs. It should be noted that the LO and NLO cross sections are very similar so that the K-factor is about unity for the central scale choice with MSTW2008 PDFs. The scale un-

certainties amount to $5-10\%$ at NLO typically, while the PDF uncertainties range at the level of $3-5\%$. The uncertainties induced by the strong coupling α_s turn out to be of $\mathcal{O}(2-3\%)$ for MSTW2008 PDFs, while the combined PDF+α_s errors range at the level of $4-6\%$. In Table 17 we show the corresponding NLO numbers for the CTEQ6.6 PDFs and in Table 18 for the NNPDF2.0 parton densities. The difference of about 20% between MSTW2008 and CTEQ6L1 at LO reduces to a level of $7-8\%$ at NLO between MSTW2008 and CTEQ6.6. The PDF and α_s uncertainties are larger with CTEQ6.6 PDFs than with MSTW2008. For the NNPDF2.0 sets we obtain the smallest α_s uncertainties. The PDF uncertainties are comparable to MSTW2008.

Tables 19 and 20 contain our final results for $\sqrt{s} = 7$ TeV and 14 TeV, respectively. We exhibit the central values and the PDF+α_s uncertainties according to the envelope method of the PDF4LHC recommendation and the relative scale variations using MSTW2008 PDFs (see Table 16 for $\sqrt{s} = 7$ TeV). The last column displays the total uncertainties by adding the final errors linearly. The cross sections for $\sqrt{s} = 14$ TeV are $7-10$ times larger than the corresponding values for $\sqrt{s} = 7$ TeV. The total uncertainties amount to typically $10-15\%$ apart from Higgs masses beyond 200 GeV where they are slightly larger.

In Fig. 13a we show the LO and NLO QCD cross sections for $\sqrt{s} = 7$ TeV for the MSTW2008, CTEQ6.6, and NNPDF2.0 PDF sets individually. It is clearly visible that the LO and NLO cross sections nearly coincide for the central scale choice with MSTW2008 PDFs, while there are corrections of $\mathcal{O}(20\%)$ with CTEQ6.6 PDFs. At NLO all three PDF sets yield consistent values within less than 10%.

The final total cross sections for $pp \to t\bar{t}H + X$ are shown in Fig. 13b for both energies $\sqrt{s} = 7, 14$ TeV. The error bands include the total uncertainties according to the PDF4LHC recommendation as given in Tables 19 and 20.
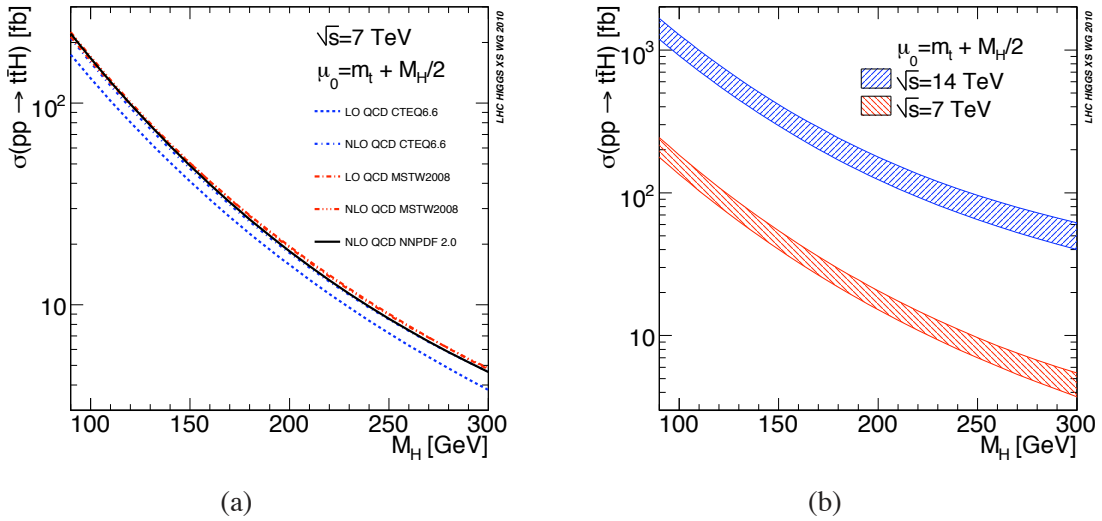
Fig. 13: (a) Total production cross sections of $pp \to t\bar{t}H + X$ for $\sqrt{s} = 7$ TeV at LO and NLO QCD for the different sets of PDFs. (b) Total production cross sections of $pp \to t\bar{t}H + X$ for $\sqrt{s} = 7$ TeV and 14 TeV at NLO QCD including the total uncertainties according to the PDF4LHC recommendation.

Table 16: LO and NLO QCD cross sections of pp $\to$ t$\bar{\text{t}}$H for $\sqrt{s} = 7$ TeV using MSTW2008 PDFs. The scale dependence is given for the scale variation $\mu_0/2 < \mu_R, \mu_F < 2\mu_0$ with $\mu_0 = m_{\text{t}} + M_{\text{H}}/2$. The α_{s} and PDF uncertainties are defined at 68% CL. The last column contains the combined PDF+α_{s} uncertainties obtained with combined PDF sets.

M_{H}[GeV]	LO[fb]	NLO QCD[fb]	Scale [%]	α_{s} [%]	PDF [%]	PDF+α_{s} [%]
90	213.2	224.8	$+4.1 - 9.7$	$+2.2 - 2.7$	$+2.9 - 3.4$	$+4.2 - 3.9$
95	186.1	195.6	$+4.0 - 9.6$	$+2.2 - 2.7$	$+2.9 - 3.4$	$+4.3 - 3.9$
100	162.7	170.4	$+3.9 - 9.6$	$+2.2 - 2.7$	$+2.9 - 3.4$	$+4.3 - 3.9$
105	143.1	149.0	$+3.7 - 9.5$	$+2.2 - 2.7$	$+2.9 - 3.4$	$+4.3 - 3.9$
110	126.1	130.8	$+3.6 - 9.5$	$+2.2 - 2.7$	$+2.9 - 3.4$	$+4.3 - 3.9$
115	111.4	115.0	$+3.5 - 9.4$	$+2.2 - 2.7$	$+3.0 - 3.4$	$+4.3 - 3.9$
120	98.66	101.4	$+3.4 - 9.4$	$+2.2 - 2.7$	$+3.0 - 3.4$	$+4.3 - 3.9$
125	87.66	89.8	$+3.3 - 9.3$	$+2.2 - 2.7$	$+3.0 - 3.4$	$+4.3 - 3.9$
130	78.09	79.57	$+3.2 - 9.3$	$+2.2 - 2.7$	$+3.0 - 3.3$	$+4.3 - 3.9$
135	69.71	70.75	$+3.1 - 9.2$	$+2.2 - 2.7$	$+3.0 - 3.4$	$+4.3 - 3.9$
140	62.43	63.06	$+3.0 - 9.2$	$+2.2 - 2.7$	$+3.0 - 3.4$	$+4.4 - 3.9$
145	55.96	56.50	$+2.9 - 9.1$	$+2.2 - 2.7$	$+3.1 - 3.4$	$+4.4 - 3.9$
150	50.35	50.59	$+2.9 - 9.1$	$+2.2 - 2.7$	$+3.1 - 3.4$	$+4.4 - 3.9$
155	45.37	45.49	$+2.8 - 9.1$	$+2.2 - 2.7$	$+3.1 - 3.4$	$+4.4 - 3.9$
160	40.98	41.01	$+2.8 - 9.1$	$+2.2 - 2.7$	$+3.1 - 3.4$	$+4.4 - 3.9$
165	37.09	36.99	$+2.7 - 9.1$	$+2.2 - 2.6$	$+3.2 - 3.4$	$+4.5 - 3.9$
170	33.62	33.47	$+2.7 - 9.0$	$+2.2 - 2.6$	$+3.2 - 3.4$	$+4.5 - 3.9$
175	30.56	30.31	$+2.6 - 9.0$	$+2.2 - 2.6$	$+3.2 - 3.4$	$+4.5 - 3.9$
180	27.83	27.55	$+2.6 - 9.0$	$+2.2 - 2.7$	$+3.2 - 3.4$	$+4.6 - 4.0$
185	25.38	25.09	$+2.6 - 9.0$	$+2.2 - 2.7$	$+3.3 - 3.5$	$+4.6 - 4.0$
190	23.20	22.93	$+2.6 - 9.0$	$+2.2 - 2.7$	$+3.3 - 3.5$	$+4.6 - 4.0$
195	21.25	20.94	$+2.6 - 9.0$	$+2.2 - 2.7$	$+3.4 - 3.5$	$+4.7 - 4.0$
200	19.48	19.20	$+2.6 - 9.1$	$+2.2 - 2.7$	$+3.4 - 3.6$	$+4.7 - 4.1$
210	16.49	16.23	$+2.8 - 9.2$	$+2.2 - 2.7$	$+3.5 - 3.7$	$+4.8 - 4.1$
220	14.04	13.81	$+2.9 - 9.3$	$+2.2 - 2.7$	$+3.6 - 3.7$	$+4.9 - 4.2$
230	12.04	11.86	$+3.2 - 9.4$	$+2.3 - 2.7$	$+3.7 - 3.9$	$+5.0 - 4.3$
240	10.38	10.24	$+3.2 - 9.5$	$+2.3 - 2.7$	$+3.8 - 4.0$	$+5.2 - 4.4$
250	9.011	8.899	$+3.5 - 9.7$	$+2.3 - 2.7$	$+4.0 - 4.1$	$+5.3 - 4.5$
260	7.850	7.777	$+3.9 - 9.9$	$+2.3 - 2.8$	$+4.1 - 4.3$	$+5.5 - 4.6$
270	6.888	6.866	$+4.3 - 10.1$	$+2.4 - 2.8$	$+4.2 - 4.4$	$+5.6 - 4.7$
280	6.075	6.092	$+4.7 - 10.4$	$+2.4 - 2.8$	$+4.4 - 4.6$	$+5.8 - 4.9$
290	5.376	5.405	$+5.2 - 10.6$	$+2.4 - 2.8$	$+4.6 - 4.7$	$+6.0 - 5.0$
300	4.780	4.848	$+5.6 - 10.9$	$+2.5 - 2.9$	$+4.7 - 4.9$	$+6.2 - 5.2$

Table 17: LO and NLO QCD cross sections of $\mathrm{pp} \to \mathrm{t\bar{t}H}$ for $\sqrt{s} = 7$ TeV using CTEQ6.6 PDFs. The scale dependence is given for the scale variation $\mu_0/2 < \mu_R, \mu_F < 2\mu_0$ with $\mu_0 = m_\mathrm{t} + M_\mathrm{H}/2$. The α_s and PDF uncertainties are defined at 68% CL.

M_H [GeV]	LO [fb]	NLO QCD [fb]	Scale [%]	α_s [%]	PDF [%]
90	174.2	210.0	+4.2 −9.4	+3.5 −2.5	+5.9 −5.1
95	151.9	182.5	+4.1 −9.4	+3.5 −2.5	+5.9 −5.1
100	133.0	159.1	+4.0 −9.3	+3.5 −2.5	+6.0 −5.1
105	116.7	139.3	+3.8 −9.2	+3.5 −2.5	+6.1 −5.2
110	102.8	122.1	+3.7 −9.2	+3.6 −2.5	+6.1 −5.2
115	90.81	107.5	+3.6 −9.2	+3.5 −2.5	+6.2 −5.2
120	80.43	94.91	+3.5 −9.1	+3.5 −2.6	+6.2 −5.3
125	71.44	83.94	+3.5 −9.1	+3.6 −2.5	+6.3 −5.3
130	63.62	74.54	+3.4 −9.0	+3.6 −2.5	+6.4 −5.3
135	56.77	66.32	+3.3 −9.0	+3.6 −2.5	+6.4 −5.4
140	50.79	59.16	+3.2 −9.0	+3.6 −2.5	+6.5 −5.4
145	45.55	52.92	+3.2 −8.9	+3.6 −2.5	+6.6 −5.5
150	40.94	47.45	+3.1 −8.9	+3.6 −2.5	+6.6 −5.5
155	36.88	42.60	+3.1 −8.9	+3.6 −2.5	+6.7 −5.6
160	33.29	38.38	+3.0 −8.9	+3.6 −2.6	+6.8 −5.6
165	30.12	34.68	+3.0 −8.9	+3.7 −2.6	+6.9 −5.7
170	27.30	31.38	+3.0 −8.9	+3.7 −2.6	+7.0 −5.7
175	24.81	28.47	+3.0 −8.9	+3.7 −2.6	+7.0 −5.8
180	22.57	25.88	+3.0 −8.9	+3.7 −2.6	+7.1 −5.8
185	20.58	23.56	+3.0 −8.9	+3.7 −2.6	+7.2 −5.9
190	18.80	21.52	+3.0 −8.9	+3.8 −2.6	+7.3 −6.0
195	17.20	19.70	+3.0 −8.9	+3.8 −2.6	+7.4 −6.0
200	15.78	18.06	+3.1 −9.0	+3.8 −2.6	+7.5 −6.1
210	13.33	15.27	+3.2 −9.1	+3.9 −2.6	+7.8 −6.3
220	11.32	13.02	+3.3 −9.1	+3.9 −2.6	+8.0 −6.4
230	9.696	11.20	+3.5 −9.3	+4.0 −2.7	+8.3 −6.6
240	8.344	9.685	+3.6 −9.4	+4.1 −2.7	+8.5 −6.8
250	7.227	8.450	+3.9 −9.6	+4.2 −2.7	+8.8 −7.0
260	6.286	7.418	+4.1 −9.7	+4.3 −2.8	+9.1 −7.2
270	5.501	6.541	+4.4 −9.9	+4.4 −2.8	+9.5 −7.4
280	4.837	5.809	+4.6 −10.1	+4.5 −2.9	+9.8 −7.7
290	4.267	5.186	+4.9 −10.3	+4.6 −2.9	+10.1 −7.9
300	3.785	4.653	+5.2 −10.5	+4.7 −3.0	+10.5 −8.2

Table 18: NLO QCD cross sections of $pp \to t\bar{t}H$ for $\sqrt{s} = 7$ TeV using NNPDF2.0 PDFs. The scale dependence is given for the scale variation $\mu_0/2 < \mu_R, \mu_F < 2\mu_0$ with $\mu_0 = m_t + M_H/2$. The α_s and PDF uncertainties are defined at 68% CL.

M_H [GeV]	NLO QCD [fb]	Scale [%]	α_s [%]	PDF [%]
90	221.3	$+4.8 - 10.7$	$+1.6 - 2.3$	± 4.1
95	192.0	$+4.7 - 10.6$	$+1.6 - 2.3$	± 4.1
100	167.1	$+4.5 - 10.6$	$+1.6 - 2.2$	± 4.1
105	145.9	$+4.4 - 10.5$	$+1.6 - 2.2$	± 4.1
110	127.8	$+4.3 - 10.4$	$+1.6 - 2.2$	± 4.2
115	112.3	$+4.2 - 10.4$	$+1.6 - 2.2$	± 4.2
120	99.01	$+4.1 - 10.3$	$+1.6 - 2.2$	± 4.2
125	87.50	$+4.1 - 10.2$	$+1.6 - 2.2$	± 4.2
130	77.54	$+4.0 - 10.2$	$+1.6 - 2.2$	± 4.2
135	68.89	$+3.9 - 10.1$	$+1.6 - 2.1$	± 4.2
140	61.37	$+3.8 - 10.1$	$+1.6 - 2.1$	± 4.3
145	54.81	$+3.8 - 10.0$	$+1.6 - 2.1$	± 4.3
150	49.07	$+3.7 - 10.0$	$+1.6 - 2.1$	± 4.3
155	44.03	$+3.7 - 9.9$	$+1.6 - 2.1$	± 4.3
160	39.61	$+3.6 - 9.9$	$+1.6 - 2.1$	± 4.4
165	35.72	$+3.6 - 9.9$	$+1.6 - 2.1$	± 4.4
170	32.28	$+3.6 - 9.9$	$+1.6 - 2.1$	± 4.5
175	29.24	$+3.6 - 9.9$	$+1.6 - 2.1$	± 4.5
180	26.55	$+3.6 - 9.8$	$+1.6 - 2.1$	± 4.5
185	24.16	$+3.6 - 9.8$	$+1.6 - 2.1$	± 4.6
190	22.03	$+3.6 - 9.9$	$+1.6 - 2.0$	± 4.6
195	20.13	$+3.6 - 9.9$	$+1.6 - 2.0$	± 4.7
200	18.44	$+3.7 - 9.9$	$+1.6 - 2.0$	± 4.7
210	15.56	$+3.8 - 10.0$	$+1.6 - 2.0$	± 4.9
220	13.24	$+3.9 - 10.0$	$+1.6 - 2.0$	± 5.0
230	11.35	$+4.1 - 10.1$	$+1.6 - 2.0$	± 5.2
240	9.805	$+4.3 - 10.3$	$+1.6 - 2.0$	± 5.3
250	8.527	$+4.5 - 10.4$	$+1.6 - 2.0$	± 5.5
260	7.465	$+4.8 - 10.6$	$+1.6 - 2.1$	± 5.7
270	6.575	$+5.1 - 10.7$	$+1.6 - 2.1$	± 5.9
280	5.824	$+5.4 - 10.9$	$+1.6 - 2.1$	± 6.1
290	5.187	$+5.7 - 11.1$	$+1.5 - 2.1$	± 6.4
300	4.642	$+6.0 - 11.3$	$+1.5 - 2.1$	± 6.6

Table 19: NLO QCD cross sections of pp $\to$ t$\bar{\text{t}}$H for $\sqrt{s} = 7$ TeV obtained according to the envelope method of the PDF4LHC group.

M_{H} [GeV]	NLO QCD [fb]	Scale [%]	PDF4LHC [%]
90	216.2	$+4.1 -9.7$	± 8.4
95	188.0	$+4.0 -9.6$	± 8.4
100	163.8	$+3.9 -9.6$	± 8.4
105	143.3	$+3.7 -9.5$	± 8.4
110	125.7	$+3.6 -9.5$	± 8.5
115	110.6	$+3.5 -9.4$	± 8.4
120	97.56	$+3.4 -9.4$	± 8.4
125	86.34	$+3.3 -9.3$	± 8.5
130	76.58	$+3.2 -9.3$	± 8.4
135	68.10	$+3.1 -9.2$	± 8.4
140	60.72	$+3.0 -9.2$	± 8.4
145	54.35	$+2.9 -9.1$	± 8.5
150	48.69	$+2.9 -9.1$	± 8.4
155	43.74	$+2.8 -9.1$	± 8.6
160	39.42	$+2.8 -9.1$	± 8.6
165	35.59	$+2.7 -9.1$	± 8.6
170	32.19	$+2.7 -9.0$	± 8.6
175	29.18	$+2.6 -9.0$	± 8.6
180	26.52	$+2.6 -9.0$	± 8.6
185	24.14	$+2.6 -9.0$	± 8.7
190	22.06	$+2.6 -9.0$	± 8.7
195	20.16	$+2.6 -9.0$	± 8.7
200	18.49	$+2.6 -9.1$	± 8.7
210	15.62	$+2.8 -9.2$	± 8.9
220	13.30	$+2.9 -9.3$	± 8.9
230	11.43	$+3.2 -9.4$	± 9.0
240	9.873	$+3.2 -9.5$	± 9.1
250	8.593	$+3.5 -9.7$	± 9.1
260	7.524	$+3.9 -9.9$	± 9.0
270	6.636	$+4.3 -10.1$	± 9.3
280	5.889	$+4.7 -10.4$	± 9.5
290	5.256	$+5.2 -10.6$	± 9.7
300	4.719	$+5.6 -10.9$	± 10.0

Table 20: NLO QCD cross sections of $pp \to t\bar{t}H$ for $\sqrt{s} = 14$ TeV obtained according to the envelope method of the PDF4LHC goup.

M_H [GeV]	NLO QCD [fb]	Scale [%]	PDF4LHC [%]
90	1449	$+6.2 - 9.3$	± 8.7
95	1268	$+6.1 - 9.3$	± 8.7
100	1114	$+6.1 - 9.3$	± 8.7
105	981.6	$+6.0 - 9.3$	± 8.7
110	868.1	$+6.0 - 9.3$	± 8.8
115	769.9	$+6.0 - 9.3$	± 8.8
120	685.0	$+5.9 - 9.3$	± 8.8
125	611.3	$+5.9 - 9.3$	± 8.9
130	547.2	$+5.9 - 9.3$	± 8.9
135	491.0	$+5.9 - 9.3$	± 8.9
140	441.9	$+5.9 - 9.3$	± 8.9
145	398.9	$+5.9 - 9.3$	± 9.0
150	360.9	$+5.9 - 9.3$	± 9.0
155	327.5	$+5.9 - 9.4$	± 9.0
160	298.0	$+5.9 - 9.4$	± 9.1
165	271.8	$+6.0 - 9.4$	± 9.1
170	248.7	$+6.5 - 9.7$	± 9.2
175	227.9	$+6.6 - 9.7$	± 9.2
180	209.5	$+6.6 - 9.8$	± 9.2
185	193.0	$+6.6 - 9.8$	± 9.2
190	178.3	$+6.7 - 9.9$	± 9.3
195	165.0	$+6.7 - 9.9$	± 9.3
200	153.2	$+6.8 - 10.0$	± 9.4
210	132.9	$+7.0 - 10.1$	± 9.4
220	116.2	$+7.2 - 10.3$	± 9.5
230	102.5	$+7.5 - 10.4$	± 9.6
240	91.09	$+7.6 - 10.6$	± 9.7
250	81.56	$+8.0 - 10.8$	± 9.7
260	73.51	$+8.3 - 11.0$	± 9.8
270	66.67	$+8.6 - 11.2$	± 9.9
280	60.81	$+9.0 - 11.4$	± 10.0
290	55.75	$+9.3 - 11.6$	± 10.1
300	51.33	$+9.7 - 11.8$	± 10.1

6 MSSM neutral Higgs production processes[9]

6.1 Higgs phenomenology in the MSSM

The Higgs sector of the Minimal Supersymmetric Standard Model (MSSM) with two scalar doublets accommodates five physical Higgs bosons. In lowest order these are the light and heavy CP-even h and H, the CP-odd A, and the charged Higgs bosons $H^{\pm}$. The MSSM Higgs sector can be expressed at lowest order in terms of the gauge couplings and two further input parameters, conventionally chosen as $\tan\beta \equiv v_2/v_1$, the ratio of the two vacuum expectation values, and either M_A or $M_{H^{\pm}}$. All other masses and mixing angles can therefore be predicted. However, the Higgs sector of the MSSM is affected by large higher-order corrections, which have to be taken into account for reliable phenomenological predictions. In particular, owing to the large top Yukawa coupling, loop contributions from the top and stop sector to the Higgs masses and couplings can be numerically very important. For large values of $\tan\beta$ also effects from the bottom/sbottom sector can be large. The relation between the bottom-quark mass and the bottom Yukawa coupling is affected by a $\tan\beta$-enhanced contribution Δ_b [135–144], which is non-vanishing even in the limit of asymptotically large values of the SUSY mass parameters (an analogous contribution also exists for the τ lepton). While the MSSM Higgs sector is CP-conserving at lowest order, CP-violating effects can enter via the potentially large loop corrections, giving rise to a mixing between all three neutral mass eigenstates. In the following we will focus on the CP-conserving case and use M_A as input parameter.

Higgs phenomenology in the MSSM can differ very significantly from the SM case. The relevant couplings entering production and decay processes of an MSSM Higgs boson can be much different from the corresponding couplings in the SM case. The lower bound on the Higgs mass in the SM from the searches at LEP cannot directly be applied to the MSSM case [145, 146], and in fact much lighter Higgs masses are possible in the MSSM without being in conflict with the present search limits. The presence of more than one Higgs boson in the spectrum can give rise to overlapping signals in the Higgs searches, in particular in parameter regions where the Higgs-boson widths are large. On the other hand, in the decoupling limit, $M_A \gg M_Z$ (in practice realised already for $M_A \gtrsim 2M_Z$), the couplings of the light CP-even Higgs boson to gauge bosons and fermions become SM-like. In this parameter region the light CP-even Higgs boson of the MSSM resembles the Higgs boson of the SM. In addition to the production and decay processes present for a SM Higgs, further channels are possible in the MSSM case. In particular, MSSM Higgs bosons can be produced in association with or in decays of SUSY particles, and decays of MSSM Higgs bosons into SUSY particles, if kinematically allowed, can have a large impact on the Higgs branching ratios. In some parameter regions even decays of heavy MSSM Higgs bosons into lighter Higgs states can be relevant, which if detectable could be of great interest to gain information on the Higgs self-couplings. In the following we will mainly focus on the production processes that are expected to be most relevant for early searches for MSSM Higgs bosons at the LHC, namely Higgs production in gluon fusion and in association with bottom quarks.

It is customary to discuss searches for MSSM Higgs bosons in terms of benchmark scenarios where the lowest-order input parameters $\tan\beta$ and M_A (or $M_{H^{\pm}}$) are varied, while the other SUSY parameters entering via radiative corrections are set to certain benchmark values. In the following we will focus on the $m_h^{\max}$ benchmark scenario [147], which in the on-shell scheme is defined as

$$M_{\text{SUSY}} = 1 \,\text{TeV}, \ X_t = 2M_{\text{SUSY}}, \ \mu = 200\,\text{GeV}, \ M_{\widetilde{g}} = 800\,\text{GeV}, \ M_2 = 200\,\text{GeV}, \ A_b = A_t, \quad (4)$$

where M_{SUSY} denotes the common soft-SUSY-breaking squark mass of the third generation, $X_t = A_t - \mu/\tan\beta$ the stop mixing parameter, A_t and A_b the stop and sbottom trilinear couplings, respectively, μ the Higgsino mass parameter, $M_{\widetilde{g}}$ the gluino mass, and M_2 the SU(2)-gaugino mass parameter. M_1 is fixed via the GUT-relation $M_1 = 5/3M_2 \sin\theta_w/\cos\theta_w$.

---

[9]M. Spira, M. Vazquez Acosta, M. Warsinsky, G. Weiglein (eds.); S. Dittmaier, R. Harlander, S. Heinemeyer, A. Kalinowski, M. Mühlleitner, M. Krämer, H. Rzehak, M. Schumacher, P. Slavich and T. Vickey.

In contrast to the SM case, where the Higgs mass is a free input parameter, calculations of Higgs-boson production and decay processes in the MSSM require as a first step the evaluation of the Higgs-boson masses and mixing contributions in terms of M_A, $\tan\beta$, and all other SUSY parameters that enter via radiative corrections. The mixing between the CP-even states h and H (in the approximation where CP-violating effects are neglected; in general mixing between h, H, and A has to be considered) must be taken into account correctly in order to ensure the correct on-shell properties of the Higgs fields appearing in the S-matrix elements of Higgs-boson production or decay processes.

Two dedicated codes exist for calculating the Higgs-boson masses and mixing contributions in terms of the MSSM input parameters, FEYNHIGGS [148–151] and CPSUPERH [152, 153], which incorporate higher-order corrections in the MSSM Higgs sector up to the two-loop level. In the case of real parameters a more complete set of higher-order corrections is included in FEYNHIGGS. We will therefore use FEYNHIGGS for evaluating the Higgs-boson masses and effective couplings in the MSSM. We have performed a comparison between the predictions of FEYNHIGGS and CPSUPERH (using an appropriate parameter transformation to take account of the different renormalization schemes used in the calculations incorporated in the two codes) in the m_h^{max} and no-mixing benchmark scenarios [147, 154]. We have found in general good agreement, with deviations in the prediction of the lightest MSSM Higgs mass, M_{h}, of $\mathcal{O}(1)$ GeV, and deviations of up to $\sim 10\%$ in the effective mixing angle of the neutral CP-even Higgs sector for large values of $\tan\beta$. The deviations can nevertheless be relevant in the parameter regions that are tested first by the LHC: relatively low M_A and large $\tan\beta$. A numerical comparison of FEYNHIGGS and CPSUPERH with the program HDECAY [64, 155, 156], which performs the calculation of Higgs-boson masses and mixings in the MSSM using a less complete set of higher-order corrections, is in progress.

In making predictions for Higgs-boson production or decay processes in the MSSM one has to face the fact that certain types of higher-order corrections have only been calculated in the SM case up to now, while their counterpart for the case of the MSSM is not yet available. Instead of starting from dedicated MSSM calculations for Higgs cross sections or decay widths, which treat higher-order corrections of SM-type and SUSY-type on the same footing but may be lacking the most up-to-date SM-type corrections, it can be advantageous to start from SM-type processes including the relevant higher-order corrections and to dress suitable building blocks with appropriate MSSM coupling factors (using also the MSSM predictions for the Higgs masses). For the numerical results presented below on MSSM Higgs production in gluon fusion and in association with bottom quarks we have followed the latter approach, as explained in more detail below.

6.2 Overview about the most relevant MSSM Higgs production processes

The dominant neutral MSSM Higgs production mechanisms for small and moderate values of $\tan\beta$ are the gluon-fusion processes (see Fig. 14)

$$\mathrm{gg} \to \mathrm{h, H, A}$$

which are mediated predominantly by top and bottom loops as in the SM case, but in addition by stop
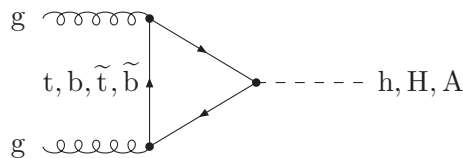
**Fig. 14:** Typical diagram contributing to $\mathrm{gg} \to \mathrm{h, H, A}$ at lowest order.

and sbottom loops for the scalar Higgs bosons h, H, if the squarks are light [157]. The NLO QCD

corrections to the quark loops are known in the heavy-quark limit [7, 8, 158, 159] as well as including the full quark mass dependence [9, 10, 160–164]. They increase the cross sections by up to about 100% for smaller $\tan\beta$ and up to about 50% for large $\tan\beta$, where the bottom loop contributions become dominant due to the strongly enhanced bottom Yukawa couplings (for the light CP-even Higgs this enhancement is only present away from the decoupling limit, i.e. for relatively small M_A). The limit of heavy quarks is only applicable for $\tan\beta \lesssim 5$ within about $20-25\%$, if the full mass dependence of the LO terms is taken into account [64, 165–167]. Thus the available NNLO QCD corrections in the heavy-quark limit [14–16, 168, 169] can only be used for small and moderate $\tan\beta$, while for large $\tan\beta$ one has to rely on the NLO results including the full mass dependence [9, 10, 160, 162–164]. The QCD corrections to the squark loops are known in the heavy-squark limit [157] and including the full mass dependence [162–164, 170]. The full SUSY QCD corrections have been obtained in the limit of heavy squarks and gluinos [171–177] and recently including the full mass dependences, too [178, 179]. The pure QCD corrections are of about the same size as those to the quark loops thus rendering the total K-factor of similar size as for the quark loops alone with a maximal deviation of about 10% [157]. The pure SUSY QCD corrections are small for small values of $\tan\beta$ [171–174, 178]. For large values of $\tan\beta$ sizable corrections arise due to $\tan\beta$-enhanced corrections [177, 179]. The NNLL resummation of the SM Higgs cross section [18, 19, 22] can also be applied to the scalar MSSM Higgs cross sections in the regions where the heavy-quark limit is valid. For the pseudoscalar Higgs-boson production the NNLL resummation has not been performed so far.

The vector-boson fusion processes [180–182] (see Fig. 15)

$$qq \to qq + W^*W^*/Z^*Z^* \to qq + h/H$$

play an important role for the light CP-even Higgs boson h in the decoupling limit, $M_A \gg M_Z$, where it becomes SM-like, and for the heavy CP-even Higgs boson H for small M_A, where H becomes SM-like. In the other regions the cross sections are suppressed by the additional SUSY factors of the Higgs couplings. The NLO and approximate NNLO QCD corrections to the total cross section and the distributions can be taken from the SM Higgs case and are small [65, 66, 68–70, 75]. The SUSY QCD corrections mediated by virtual gluino and squark exchange at the vertices turned out to be small [183, 184]. The SUSY electroweak corrections are typically at the level of 1% with up to $2-4\%$ at the edge of the SUSY exclusion limits [184].
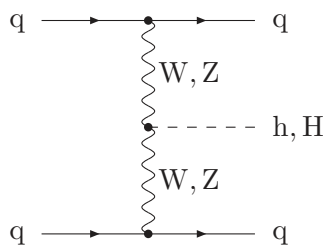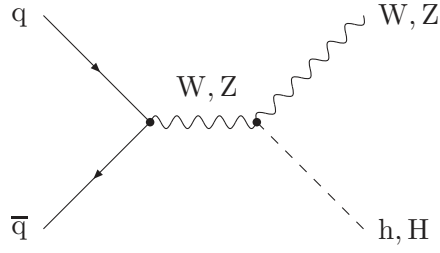

Fig. 15: Diagram contributing to $qq \to qqV^*V^* \to qq + h/H$ ($V = W, Z$) at lowest order.

Higgs-strahlung off W, Z gauge bosons [185, 186] (see Fig. 16)

$$q\bar{q} \to Z^*/W^* \to Z/W + h/H$$

is most relevant for SM-like Higgs states. This class of processes gained renewed attention at the LHC in the context of possible improvements of jet reconstruction and decomposition techniques [99]. The NLO [64, 104] and NNLO [108] QCD corrections can be translated from the SM to the MSSM case, and the SUSY QCD corrections are small [183]. The SUSY electroweak corrections are unknown.

Fig. 16: Diagram contributing to $q\bar{q} \to V^* \to V + h/H$ ($V = W, Z$) at lowest order.

Higgs-boson radiation off top quarks [113–117] (see Fig. 17)

$$q\bar{q}/gg \to t\bar{t} + h/H/A$$

plays a significant role at the LHC for the light scalar Higgs particle only. The NLO QCD corrections are the same as for the SM Higgs boson with modified top and bottom Yukawa couplings and are thus of moderate size [122–125]. The SUSY QCD corrections have been computed recently [187–190]. They are of moderate size, too.
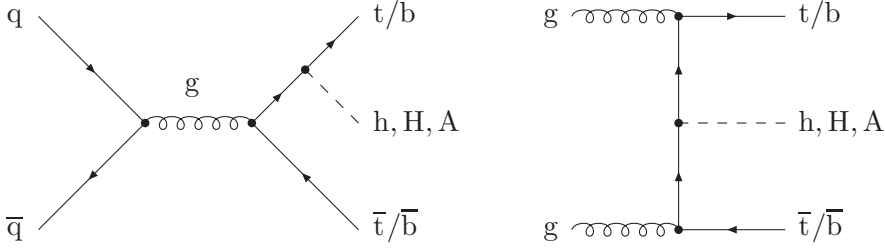
**Fig. 17:** Typical diagrams contributing to $q\bar{q}/gg \to Q\bar{Q} + h/H/A$ ($Q = t, b$) at lowest order.

For large values of $\tan\beta$ Higgs-boson radiation off bottom quarks [113–117] (see Fig. 17)

$$q\bar{q}/gg \to b\bar{b} + h/H/A$$

constitute the dominant Higgs-boson production processes. The NLO QCD corrections can be taken from the analogous calculation involving top quarks. However, they turn out to be large [191, 192]. The main reason is that the integration over the transverse momenta of the final-state bottom quarks generates large logarithmic contributions. The resummation of the latter can be established by the introduction of bottom-quark densities in the proton, since the large logarithms correspond to the DGLAP evolution of these densities. Their DGLAP evolution resums them. This leads to an approximate approach starting from the process [193] (see Fig. 18a)

$$b\bar{b} \to h/H/A$$

at LO, where the transverse momenta of the incoming bottom quarks, their masses and their off-shellness are neglected at LO. The NLO [194, 195] and NNLO [196] QCD corrections to these bottom-initiated processes are known and of moderate size, if the running bottom Yukawa coupling is introduced at the scale of the corresponding Higgs-boson mass. At NNLO the full process $gg \to b\bar{b} + h/H/A$ (see Fig. 18b) contributes to the real corrections for the first time. The fully exclusive $gg \to b\bar{b} + h/H/A$ process, calculated with four active parton flavours in a four-flavour scheme (4FS), and the result, calculated with five active parton flavours in the five-flavour scheme (5FS), will converge against the same value at higher perturbative orders. Reasonable agreement between the NLO 4FS and NNLO 5FS is
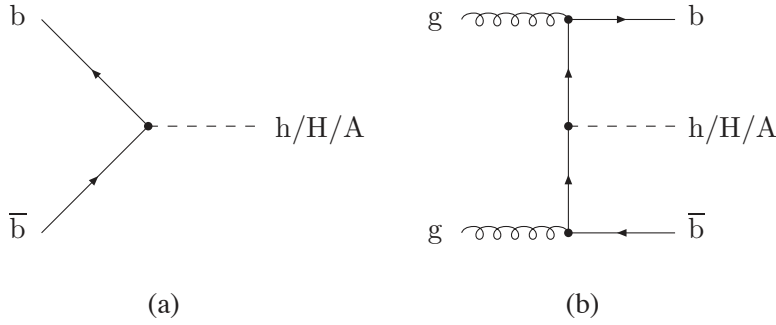
Fig. 18: Typical diagrams for the Higgs-boson production mechanisms related to Higgs radiation off bottom quarks in the 5FS and 4FS at leading order: (a) $b\bar{b} \to h/H/A$ (5FS) and (b) $gg \to b\bar{b} + h/H/A$ (4FS).

achieved if the factorization scale of the bottom-quark densities is chosen as about a quarter of the Higgs mass [197,198]. If both bottom jets accompanying the Higgs boson in the final state are tagged, one has to rely on the fully exclusive calculation for $gg \to b\bar{b} + h/H/A$. For the case of a single b-tag in the final state the corresponding calculation in the 5FS starts from the process $bg \to b + h/H/A$ with the final-state bottom quark carrying finite transverse momentum. The NLO QCD and electroweak corrections to this process have been calculated [199–201] supplemented by the NLO SUSY QCD corrections recently [202].

In our study we concentrated on the gluon-fusion processes and neutral Higgs-boson radiation off bottom quarks as the first step. We have focused on the $m_h^{\max}$ scenario [147, 154], which is characterised by rather heavy SUSY particles. Genuine SUSY QCD and SUSY electroweak corrections in this scenario are below the 10% level for Higgs-boson radiation off bottom quarks as well as the gluon-fusion processes. For the calculation of the MSSM Higgs-boson masses and couplings we have used the program FEYNHIGGS 2.7.4 [148–151] which includes the most up-to-date radiative corrections to the MSSM Higgs sector up to the two-loop level and the Δ_b terms as an approximation of the SUSY QCD and electroweak corrections to the bottom Yukawa couplings. In further steps we will have to include the full SUSY QCD and SUSY electroweak corrections where available and in addition allow for complex MSSM parameters which leads to additional complications of the Higgs sector, since the mass eigenstates will no longer be CP-eigenstates. Moreover, for this study we have fixed the MSSM scenario, since otherwise general predictions as in the SM case will not be possible due to the huge variety of the MSSM parameter space. However, the results in the $m_h^{\max}$ scenario will not be representative for all possible MSSM scenarios. In the further progress of this work we will develop the machinery to be able to cover as many aspects of the MSSM as possible. This requires the combination of the most advanced results and tools available in our HEP community for neutral MSSM Higgs-boson production.

6.3 Gluon fusion

The gluon-fusion processes $gg \to \phi$ ($\phi = h, H, A$) have been calculated by generating grids for the individual contributions of the top and bottom-quark loops. Stop and sbottom loops have been neglected in this first step but will be included in the next steps. We have generated grids for the scalar and pseudoscalar Higgs bosons individually with Yukawa couplings of SM-like strength. The MSSM cross sections can then be obtained by rescaling the individual parts by the corresponding MSSM Yukawa coupling factors,

$$\sigma^{\text{MSSM}}(gg \to \phi) = \left(\frac{g_t^{\text{MSSM}}}{g_t^{\text{SM}}}\right)^2 \sigma_{tt}(gg \to \phi) + \left(\frac{g_b^{\text{MSSM}}}{g_b^{\text{SM}}}\right)^2 \sigma_{bb}(gg \to \phi)$$

$$+ \frac{g_{\mathrm{t}}^{\mathrm{MSSM}}}{g_{\mathrm{t}}^{\mathrm{SM}}} \frac{g_{\mathrm{b}}^{\mathrm{MSSM}}}{g_{\mathrm{b}}^{\mathrm{SM}}} \sigma_{\mathrm{tb}}(\mathrm{gg} \rightarrow \phi), \tag{5}$$

where $\sigma_{\mathrm{tt}}, \sigma_{\mathrm{bb}}$, and σ_{tb} denote the square of the top contributions, the square of the bottom contributions, and the top–bottom interference, respectively. For σ_{bb} and σ_{tb} we have used the full NLO QCD calculation of HIGLU [203]. For σ_{tt} we have used the full NLO QCD result of HIGLU and added the NNLO corrections in the heavy-top-quark limit by using the program GGH@NNLO [14, 168] in the following way: $\sigma_{\mathrm{LO}}^0, \sigma_{\mathrm{NLO}}^0$, and σ_{NNLO}^0 have been calculated by GGH@NNLO. The additional part added to the full NLO result of σ_{tt} is then given by

$$\Delta\sigma_{\mathrm{tt}}^{\mathrm{NNLO}}(\mathrm{gg} \rightarrow \phi) = \Delta K_{\mathrm{NNLO}} \, \sigma_{\mathrm{tt}}^{\mathrm{LO}}(\mathrm{gg} \rightarrow \phi),$$
$$\Delta K_{\mathrm{NNLO}} = \frac{\sigma_{\mathrm{NNLO}}^0 - \sigma_{\mathrm{NLO}}^0}{\sigma_{\mathrm{LO}}^0}, \tag{6}$$

where the individual cross sections $\sigma_{\mathrm{LO}}^0, \sigma_{\mathrm{NLO}}^0, \sigma_{\mathrm{NNLO}}^0$ have been evaluated consistently with LO, NLO, and NNLO PDFs, respectively. Since top mass effects are small at NNLO [24–29] this procedure provides a result that is expected to be very close to full NNLO QCD accuracy for the σ_{tt} parts. Electroweak corrections to MSSM Higgs-boson production via gluon fusion have not been calculated. The corresponding electroweak corrections in the SM case [31–33, 35] cannot be translated easily to the MSSM and have thus been neglected. Moreover, we have neglected the NNLL resummation effects [18, 19, 22] on the σ_{tt} part for two reasons: (i) The NNLL resummation has not been calculated for the pseudoscalar Higgs boson so far so that in order to treat the scalar and pseudoscalar Higgs bosons at the same level, the NNLL effects should be neglected. (ii) For a completely consistent NNLL prediction also NNLL PDFs would be needed which, however, are not available. To use NNLO PDFs instead is not fully consistent.

The top and bottom-quark masses have been introduced as pole masses in the calculation including the corresponding Yukawa couplings. The MSSM Yukawa coupling ratios to the SM couplings in Eq. (5) have been taken from the program FEYNHIGGS 2.7.4 [148–151] . As mentioned above, for the numerical MSSM results we have chosen the m_h^{max} benchmark scenario as specified in Eq. (4). As the central choices of the renormalization and factorization scales we adopted the corresponding Higgs-boson mass M_ϕ. For the NLO pieces of the cross section we used the NLO MSTW2008 PDFs, while for the NNLO contributions the NNLO MSTW2008 PDFs have been used appropriately. The strong coupling constant has been normalized according to the PDFs, i.e. $\alpha_{\mathrm{s}}(M_{\mathrm{Z}}) = 0.12018$ at NLO and $\alpha_{\mathrm{s}}(M_{\mathrm{Z}}) = 0.11707$ at NNLO [41, 44]. The scale uncertainty has been determined by varying the renormalization and factorization scales between $M_\phi/2$ and $2M_\phi$. It amounts to about $10 - 15\%$ for the whole Higgs mass and $\tan\beta$ range although for large values of $\tan\beta$ the results are dominated by the bottom-quark loops which are only known at NLO, unless the light (heavy) scalar Higgs mass is close to its upper (lower) bound, where the top loops are dominant for large values of $\tan\beta$, too. However, the scale dependence of the bottom-quark contributions is considerably smaller than that of the top quark ones [10, 160]. We have added the 68% CL PDF$+\alpha_{\mathrm{s}}$ uncertainties of the MSTW2008 PDFs to the scale uncertainties linearly. Since there are no NNLO PDF sets of CTEQ and NNPDF we did not include those sets in this uncertainty.

We have generated grids of the three cross section parts $\sigma_{\mathrm{tt}}^{\mathrm{NNLO}}, \sigma_{\mathrm{bb}}^{\mathrm{NLO}}$, and $\sigma_{\mathrm{tb}}^{\mathrm{NLO}}$ for the mass ranges from 70 GeV up to 1 TeV in steps of 1 GeV for the scalar and pseudoscalar Higgs bosons separately. These grids are then used for interpolation and the resulting numbers rescaled and added according to the coupling ratios of FEYNHIGGS. For the m_h^{max} scenario we have included the $\tan\beta$-enhanced Δ_{b} corrections in the effective MSSM bottom Yukawa couplings, since we expect them to dominate the full SUSY QCD corrections for squark and gluino masses much larger than the Higgs masses [177]. The resulting cross sections for the pseudoscalar Higgs boson are shown for various values of $\tan\beta$ in Fig. 19, while Figs. 20 and 21 display the corresponding results for the light and heavy CP-even MSSM Higgs bosons. The overall scale and PDF$+\alpha_{\mathrm{s}}$ uncertainties amount to about 15%. It is visible that for small and moderate values of $\tan\beta$ virtual $\mathrm{t\bar{t}}$ thresholds develop for Higgs masses $M_\phi = 2m_{\mathrm{t}}$, while

for large values of $\tan\beta$ this threshold behaviour is strongly suppressed due to the dominance of the bottom-quark contributions. For the light CP-even Higgs boson most of the displayed parameter region corresponds to rather low values of M_A (which is the input parameter that has been varied in the plots), while the decoupling region where $M_A \gg M_Z$ corresponds to the region of the highest M_h values in the plots. It should be noted that in this limit, i.e. for the upper bound of the light CP-even Higgs-boson mass in the plots, the light scalar Higgs-boson production cross section approaches the NNLO SM result by construction. Note that the full MSSM result including stop and sbottom loop contributions does *not* approach the SM cross section for the light scalar Higgs boson at its upper mass bound in general. The additional contributions from the stops and sbottoms impose a mismatch between the MSSM cross section in the decoupling limit and the corresponding SM cross section. This differs from the results of Section 2 which include the NNLL resummation effects by less than 10%, i.e. less than the residual scale uncertainties.

As the next step the inclusion of the full stop and sbottom loop contributions has to be performed. This requires the generation of multi-dimensional grids of the squark contributions including their interference terms with the top and bottom contributions as well as among each other along the same lines as in Eq. (5). This step, however, is beyond the present write-up. The omission of the squark contributions as well as the full SUSY QCD corrections to the gluon-fusion cross sections has to be interpreted as an additional theoretical uncertainty on top of the scale and PDF+α_s uncertainties. Since the corrections originating from the Δ_b terms are smaller than about 10% in the m_h^{max} scenario, their impact on the overall uncertainties is of moderate size. Since the full SUSY QCD corrections to the gluon-fusion cross sections have not been included in our analysis, we take the contribution of the Δ_b terms as an estimate of the uncertainties related to these corrections. The total uncertainties of our gluon-fusion results can be estimated as $\sim 25-30\%$ within the m_h^{max} scenario.

6.4 Higgs radiation off bottom quarks

We have generated grids for the 5FS calculation of $b\bar{b} \to \phi$ and the 4FS calculation of $gg, q\bar{q} \to b\bar{b}\phi$. The Higgs mass range $80-200\,\mathrm{GeV}$ has been covered with steps of 5 GeV and the range $200\,\mathrm{GeV}-1\,\mathrm{TeV}$ with steps of 20 GeV.

For the 5FS calculation we have used the program BBH@NNLO [196]. Scalar and pseudoscalar Higgs-boson production are identical for the same masses and the same coupling factors due to the chiral symmetry of massless bottom quarks. The input value of the $\overline{\mathrm{MS}}$ bottom mass has been chosen as $\overline{m}_b(\overline{m}_b) = 4.213$ GeV which corresponds to a NNLO pole mass of $m_b = 4.75$ GeV, i.e. the bottom mass value of the MSTW2008 PDF sets [41, 44]. For the 5FS the NNLO PDFs of MSTW2008 have been adopted with the strong coupling adjusted accordingly, i.e. $\alpha_s(M_Z) = 0.11707$. As central scales we have chosen $\mu_R = M_\phi$ for the renormalization scale and $\mu_F = M_\phi/4$ for the factorization scale, respectively. For the scale uncertainties of the 5FS we have varied the scales in the intervals $M_\phi/5 < \mu_R < 5M_\phi$ and $M_\phi/10 < \mu_F < 0.7M_\phi$. These ranges cover the maximal and minimal values of the cross sections within the 5FS. The central predictions of the 5FS calculation are shown in Fig. 22a for SM-like couplings. These cross sections have to be multiplied with the ratios $\left(g_b^{\mathrm{MSSM}}/g_b^{\mathrm{SM}}\right)^2$ of the MSSM and SM Yukawa couplings. The MSSM couplings g_b^{MSSM} should contain the Δ_b terms [135–143], since they approximate the full genuine SUSY QCD [189,190] and SUSY electroweak [204] corrections within the percent level. The corresponding scale uncertainties are shown in Fig. 22b. They amount to less than 10% for Higgs masses above about 200 GeV, while for smaller Higgs masses they can reach a level of $30-40\%$ as can be inferred from Fig. 22b. The 68% CL PDF+α_s uncertainties are displayed in Fig. 22c and the 90% CL uncertainties in Fig. 22d. The 68% CL uncertainties amount to less than about 10% in the relevant Higgs mass range below $\sim 500-600$ GeV, while they are enhanced
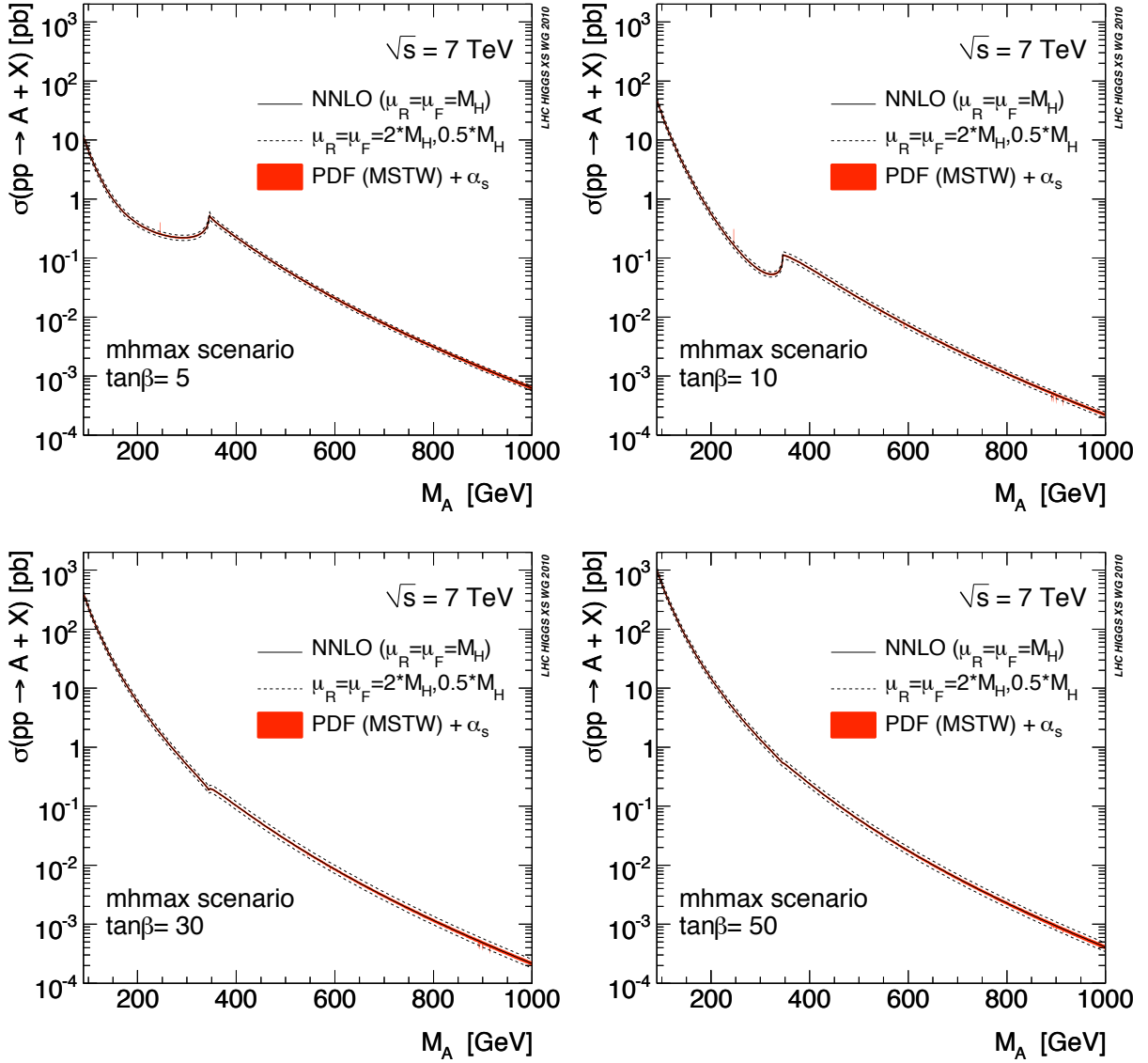
Fig. 19: Total gluon-fusion cross sections of the pseudoscalar MSSM Higgs boson A for four values of $\tan\beta$ within the $m_h^{\max}$ scenario for $\sqrt{s} = 7$ TeV using MSTW2008 PDFs [41,44]. The NNLO results for the SM-type contributions have been obtained from the programs HIGLU and GGH@NNLO, while the rescaling with MSSM coupling factors has been done with FEYNHIGGS.

to a level below about 20% at 90% CL as shown in Fig. 22d. It is also visible that these uncertainties are dominated by the pure PDF uncertainties, while the α_s variation adds only a moderate contribution.

In the corresponding 4FS calculation we have chosen the bottom-quark pole mass as $m_b = 4.75$ GeV which corresponds to a NLO $\overline{\text{MS}}$ mass $\overline{m}b(\overline{m}b) = 4.40$ GeV. The closed top loop contributions appearing in the virtual one-loop contributions have been neglected for consistency, since for large values of $\tan\beta$ they are strongly suppressed and in the 5FS calculation they vanish for strictly massless bottom quarks. In the further progress of this study we will generate separate grids for these top loop contributions so that they can be included in the MSSM calculations consistently. The running bottom-quark Yukawa coupling, expressed in terms of the $\overline{\text{MS}}$ bottom mass, has been chosen at the scale of the Higgs mass M_ϕ. The central scales $\mu_R = \mu_F = M_\phi/4$ have been adopted for the renormalization and factorization scales, respectively. The scale uncertainties have been obtained for scale variations
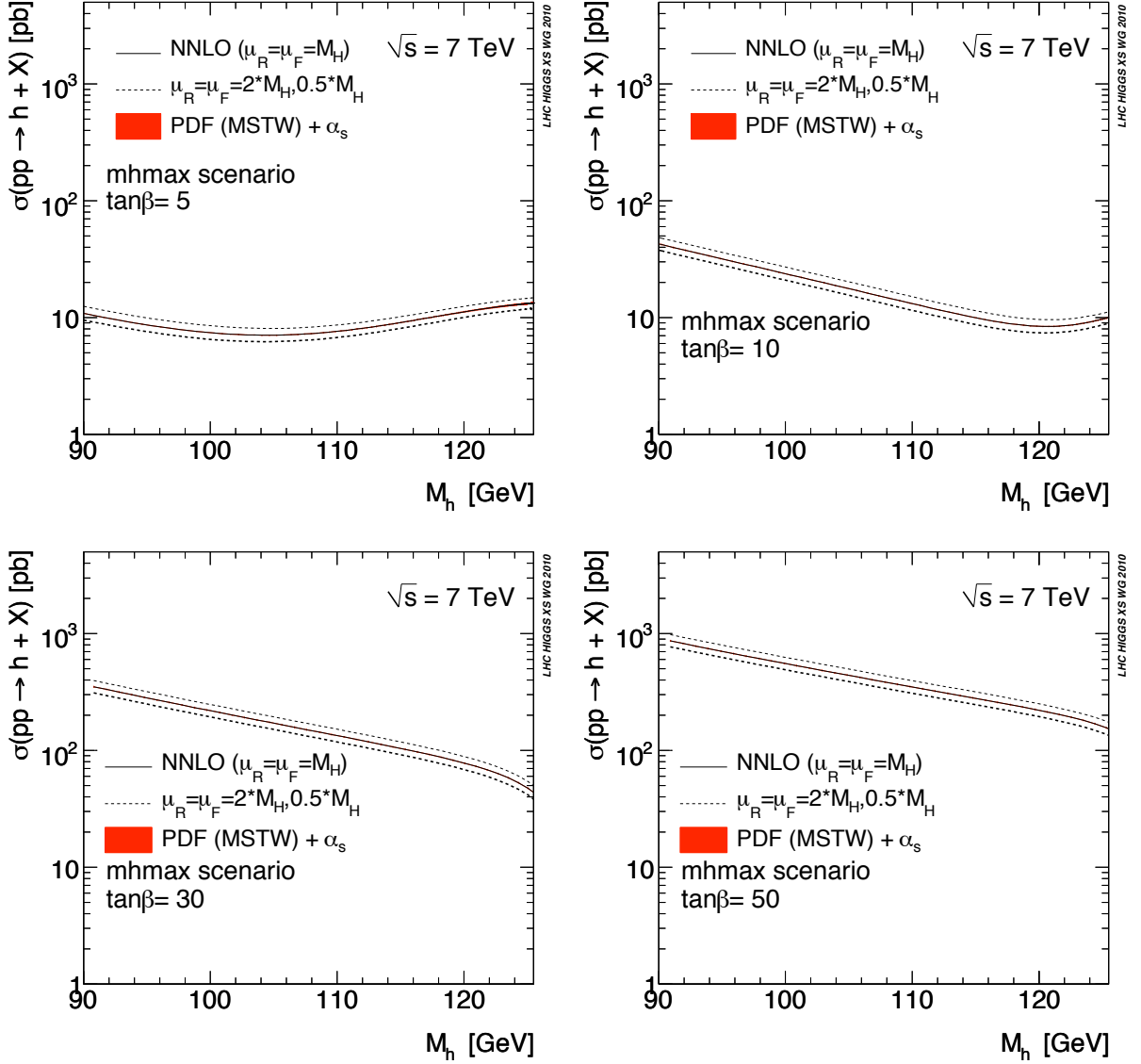
Fig. 20: Total gluon-fusion cross sections of the light scalar (CP-even) MSSM Higgs boson h for four values of $\tan\beta$ within the $m_h^{\max}$ scenario for $\sqrt{s} = 7$ TeV using MSTW2008 PDFs [41,44]. The NNLO results for the SM-type contributions have been obtained from the programs HIGLU and GGH@NNLO, while the rescaling with MSSM coupling factors has been done with FEYNHIGGS.

$M_\phi/8 < \mu_R, \mu_F < M_\phi/2$ where the choice $\mu_R = \mu_F = M_\phi/8$ corresponds to the maximal cross sections and $\mu_R = \mu_F = M_\phi/2$ to the minimal cross sections for all Higgs masses. The four-flavour PDFs of MSTW2008 [205] have been used for the numerical analysis within the 4FS. Error PDFs within this scheme have only been published very recently so that a full PDF uncertainty analysis could not be performed for the 4FS yet. However, the scale uncertainties of $25-30\%$ are expected to dominate the overall uncertainties of the 4FS calculation so that the additional PDF+α_s uncertainties will be expected to modify the overall uncertainties only mildly. The comparison of the 4FS and the 5FS for SM-like couplings is shown in Fig. 23 for scalar and pseudoscalar Higgs-boson production in association with bottom quarks. The scalar and pseudoscalar cross sections for the same mass differ by less than 2% within the 4FS thanks to the approximate chiral symmetry for the light bottom quarks compared to the Higgs-boson masses. Fig. 23 shows good agreement of the 5FS and 4FS results for smaller Higgs masses
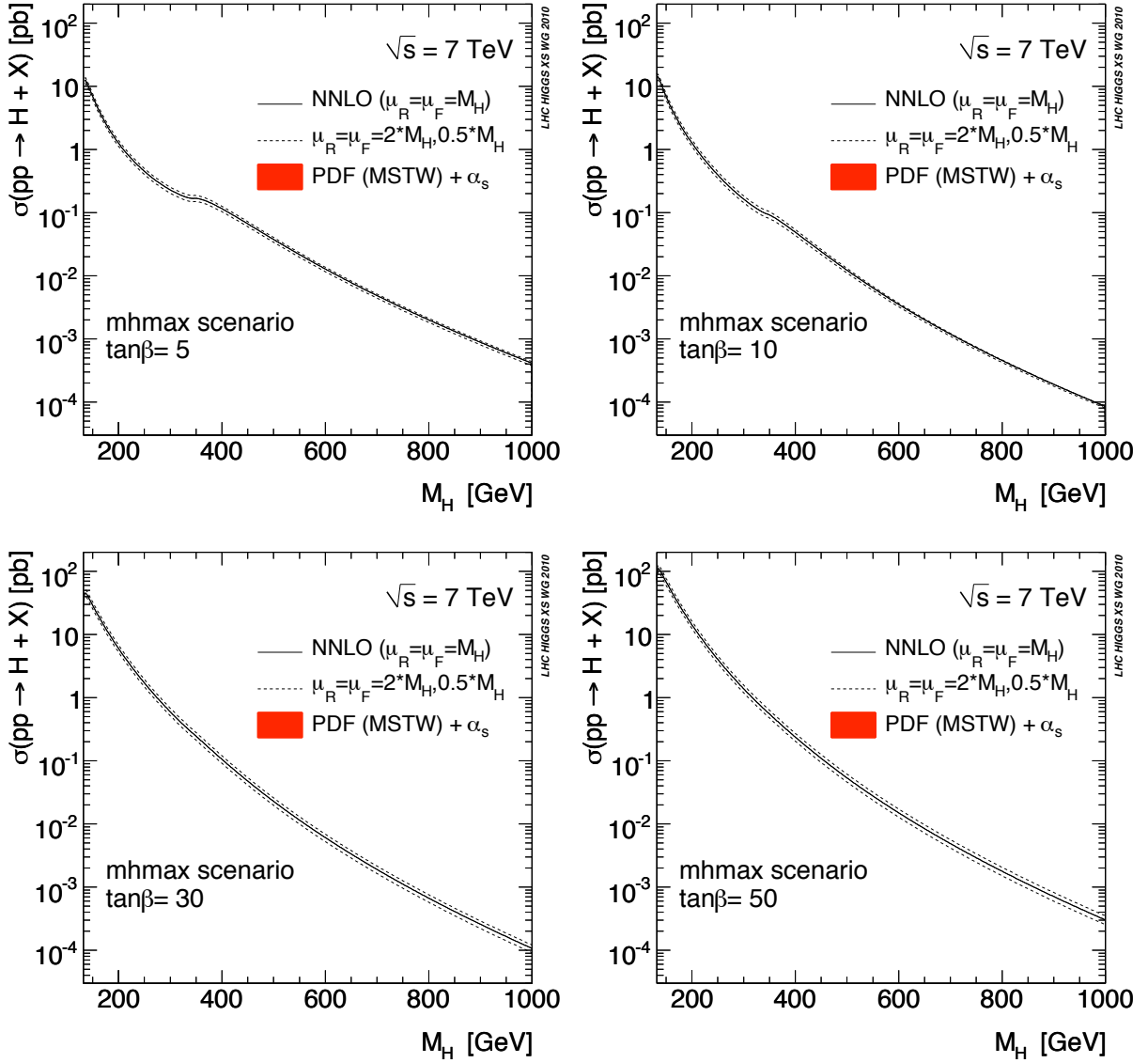
Fig. 21: Total gluon-fusion cross sections of the heavy scalar (CP-even) MSSM Higgs boson H for four values of $\tan\beta$ within the $m_h^{\max}$ scenario for $\sqrt{s} = 7$ TeV using MSTW2008 PDFs [41,44]. The NNLO results for the SM-type contributions have been obtained from the programs HIGLU and GGH@NNLO, while the rescaling with MSSM coupling factors has been done with FEYNHIGGS.

while for large Higgs-boson masses the 5FS cross sections are considerably larger than the corresponding 4FS results. However, an overlap of both uncertainty bands is visible for the whole mass range. This is the first completely consistent comparison of both schemes resulting in a much better agreement of both schemes than in all former studies [197]. The central values of the 4FS and 5FS differ by up to 30%. In order to decide which of the two prescriptions is closer to the experimentally relevant values of these production cross sections, the comparison of the 4FS and 5FS calculations of $b\bar{b}+Z$ production with the forthcoming experimental data will be of big help.

In Fig. 24 the central predictions for the gluon-fusion processes $gg \to h, H, A$ and neutral Higgs radiation off bottom quarks within the 5FS are shown as a function of the corresponding Higgs mass within the $m_h^{\max}$ scenario for two values of $\tan\beta = 5, 30$. These results have been obtained from the grids generated by GGH@NNLO and HIGLU for the gluon-fusion process and BBH@NNLO for
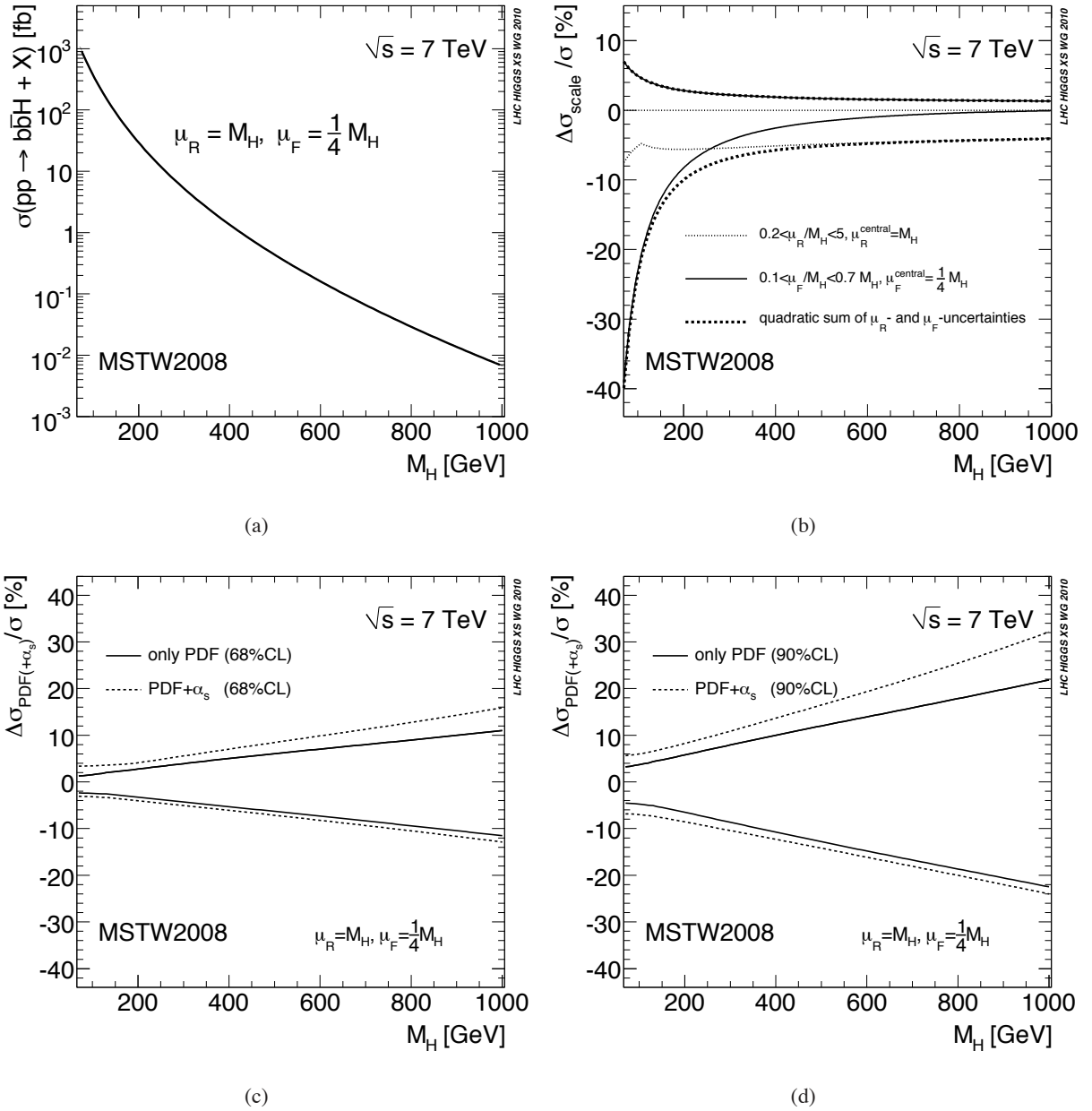
Fig. 22: Total bottom-quark-fusion cross sections of $b\bar{b} \rightarrow H/A + X$ within the 5FS for $\sqrt{s} = 7$ TeV with SM-like couplings using MSTW2008 PDFs [41,44]; (a) central prediction, (b) scale uncertainties, (c) 68% CL PDF+α_s uncertainties, (d) 90% CL PDF+α_s uncertainties.

$b\bar{b} \rightarrow \phi$ and rescaling the corresponding Yukawa couplings by the MSSM factors calculated with FEYN-HIGGS[10]. It is clearly visible that Higgs-boson radiation off bottom quarks plays the dominant role for $\tan \beta = 30$ while for $\tan \beta = 5$ the gluon fusion is either dominant or competitive.

---

[10]Two complete scans of the $(M_A, \tan \beta)$ plane for $\sqrt{s} = 7$ and 14 TeV are available in electronic format on `https://twiki.cern.ch/twiki/bin/view/LHCPhysics/MSSMNeutral` for the m_h^{max} scenario.
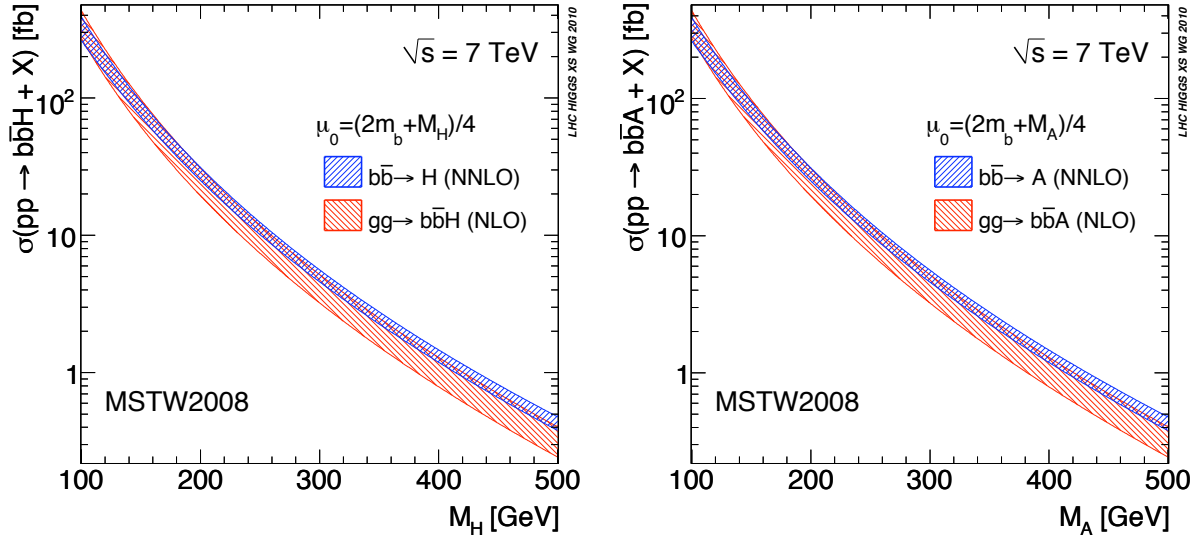
Fig. 23: Total production cross sections of $pp \to b\bar{b}H/A + X$ for $\sqrt{s} = 7$ TeV within the 5FS and the 4FS using MSTW2008 PDFs [41,44]. The upper bands (blue bands) exhibit the combined scale and 68% CL PDF+α_s uncertainties of the 5FS, while the lower bands (red bands) include the scale uncertainties of the 4FS only.

(a)

(b)
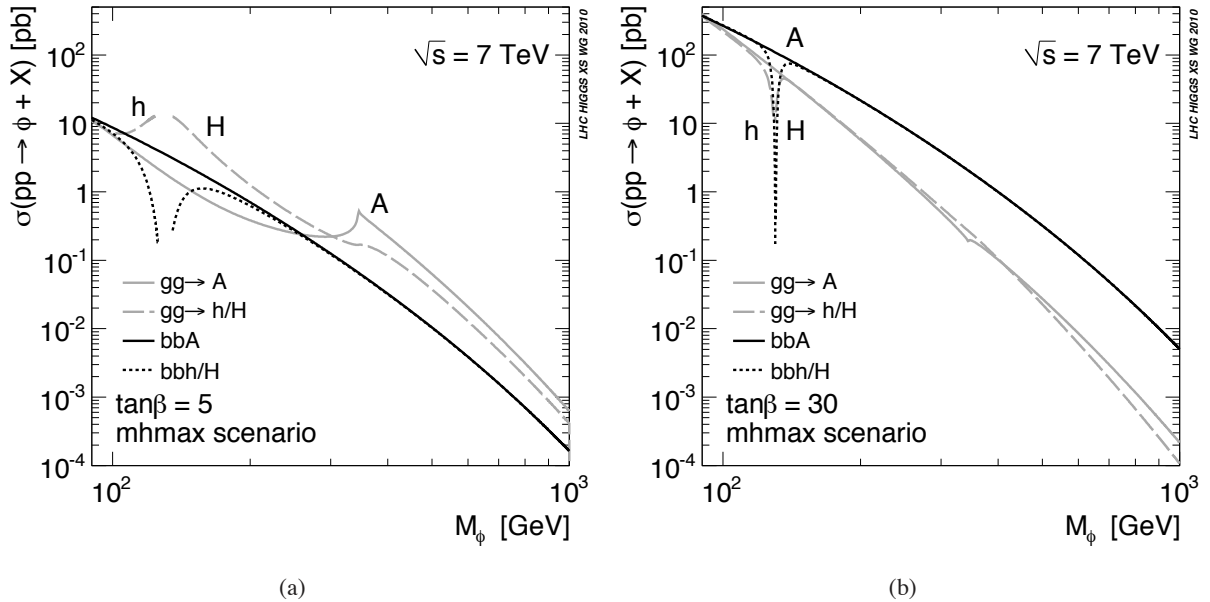
Fig. 24: Central predictions for the total MSSM production cross sections via gluon fusion and Higgs radiation off bottom quarks within the 5FS for $\sqrt{s} = 7$ TeV using NNLO and NLO MSTW2008 PDFs [41,44] for the $m_h^{\max}$ scenario; (a) $\tan\beta = 5$, (b) $\tan\beta = 30$.

7 MSSM charged Higgs production process[11]

Many extensions of the Standard Model, in particular supersymmetric theories, require two Higgs doublets leading to five physical scalar Higgs bosons, including two (mass-degenerate) charged particles $H^\pm$. The discovery of a charged Higgs boson would provide unambiguous evidence for an extended Higgs sector beyond the Standard Model. Searches at LEP have set a limit $M_{H^\pm} > 79.3$ GeV on the mass of a charged Higgs boson in a general two-Higgs-doublet model [206]. Within the MSSM, the charged Higgs-boson mass is constrained by the pseudoscalar Higgs mass and the W-boson mass through $M_{H^\pm}^2 = M_A^2 + M_W^2$ at tree level, with only moderate higher-order corrections [151, 207–209]. A mass limit on the MSSM charged Higgs boson can thus be derived from the limit on the pseudoscalar Higgs boson, $M_A > 93.4$ GeV [146], resulting in $M_{H^\pm} \gtrsim 120$ GeV. At the Tevatron, searches for light charged Higgs bosons in top-quark decays $t \to bH^\pm$ [210, 211] have placed some constraints on the MSSM parameter space, but do not provide any further generic bounds on $M_{H^\pm}$.

There are two main mechanisms for charged Higgs-boson production at the LHC:

$$\begin{aligned}
\text{top-quark decay:} \quad & t \to bH^\pm + X \quad && \text{if } M_{H^\pm} \lesssim m_t\,, \\
\text{associated production:} \quad & pp \to tbH^\pm + X \quad && \text{if } M_{H^\pm} \gtrsim m_t\,.
\end{aligned}$$

Alternative production mechanisms like quark–antiquark annihilation $q\bar{q}' \to H^\pm$ and $H^\pm +$ jet production [212], associated $H^\pm W^\mp$ production [213], or Higgs pair production [214, 215] have suppressed rates, and it is not yet clear whether a signal could be established in any of those channels. Some of the above production processes may, however, be enhanced in models with non-minimal flavour violation.

In this section we discuss charged Higgs-boson production in $t \to bH^\pm$ decays and compare the results of different software packages for the calculation of this branching ratio. Furthermore, we present NLO QCD predictions for the process $pp \to tbH^\pm + X$ in the four- and five-flavour schemes.

7.1 Light charged Higgs production from top-quark decays

If the charged Higgs boson is light, $M_{H^\pm} \lesssim m_t$, it is produced in top-quark decays. The branching ratio calculation of the top quark to a light charged Higgs boson is compared for two different programs, FEYNHIGGS, version 2.7.3 [148–151], and CPSUPERH, version 2.2 [152, 153]. We note that the decay $t \to H^+ b$ is also included in HDECAY [155], which has however not been included in the comparison presented here. The m_h^{max} benchmark scenario was used [147], which in the on-shell scheme is defined as described in Eq. (4). In addition to $\tan\beta$ and $M_{H^\pm}$, the μ parameter was varied with values $\pm 1000, \pm 200$ GeV [216]. The Standard Model parameters were taken as given in the Appendix Table A.

The calculation within FEYNHIGGS is based on the evaluations of $\Gamma(t \to W^+ b)$ and $\Gamma(t \to H^+ b)$. The former is calculated at NLO according to Ref. [217]. The decay to the charged Higgs boson and the bottom quark uses $m_t(m_t)$ and $m_b(m_t)$ in the Yukawa coupling, where the latter receives the additional correction factor $1/(1 + \Delta_b)$. The leading contribution to Δ_b is given by [139]

$$\Delta_b = \frac{C_F}{2}\frac{\alpha_s}{\pi} m_{\tilde{g}} \mu \tan\beta \, I(m_{\tilde{b}_1}, m_{\tilde{b}_2}, m_{\tilde{g}})\,, \tag{7}$$

with $C_F = 4/3$ and the auxiliary function

$$I(a, b, c) = \frac{1}{(a^2 - b^2)(b^2 - c^2)(a^2 - c^2)}\left(a^2 b^2 \ln\frac{a^2}{b^2} + b^2 c^2 \ln\frac{b^2}{c^2} + c^2 a^2 \ln\frac{c^2}{a^2}\right)\,. \tag{8}$$

Here, $\tilde{b}_{1,2}$ are the sbottom mass eigenstates, and $m_{\tilde{g}}$ is the gluino mass. The numerical results presented here have been based on the evaluation of Δ_b in Ref. [144]. Furthermore additional QCD corrections taken from Ref. [139] are included.

---

[11]M. Flechl, M. Krämer, S. Lehti (eds.); S. Dittmaier, T. Hahn, T. Hartonen, S. Heinemeyer, J. S. Lee, A. Pilaftsis, M. Spira and C. Weydert.

The calculation within CPSUPERH is also based on the top-quark decays $t \to W^+ b$ and $t \to H^+ b$. The decay width $\Gamma(t \to W^+ b)$ is calculated by including $\mathcal{O}(\alpha_s)$ corrections [218]. The partial decay width of the decay $t \to H^+ b$ is given by

$$\Gamma(t \to H^+ b) = \frac{g_{tb}^2 m_t}{16\pi} \left(|g_{H^+\bar{t}b}^S|^2 + |g_{H^+\bar{t}b}^P|^2 \right) \left(1 - \frac{M_{H^\pm}^2}{m_t^2} \right)^2 , \qquad (9)$$

where $g_{tb} = -g m_t/\sqrt{2} M_W$, $g_{H^+\bar{t}b}^S = (g_{H^+\bar{t}b}^L + \frac{m_b}{m_t} g_{H^+\bar{t}b}^R)/2$, and $g_{H^+\bar{t}b}^P = i(g_{H^+\bar{t}b}^L - \frac{m_b}{m_t} g_{H^+\bar{t}b}^R)/2$. In the couplings $g_{H^+\bar{t}b}^{L,R}$, all the threshold corrections (both those enhanced and not enhanced by $\tan\beta$) have been included as described in Appendix A of Ref. [152] and Refs. [219, 220], see also Ref. [140]. For m_t and m_b appearing in the couplings, we use the quark masses evaluated at the scale $M_{H^\pm}$.

The comparison started by running FEYNHIGGS with a selected set of parameters. The FEYN-HIGGS output was used to set the values for the CPsuperH input parameters. Due to differences in the parameter definitions, the bottom-quark mass was changed from FEYNHIGGS $m_b(m_b) = 4.16$ GeV to $m_b(m_t) = 2.64$ GeV which is taken as input by CPSUPERH. The main result from the comparison is shown in Figs. 25 and 26. A very good agreement within typically $0-2\%$ can be observed, except if simultaneously very small values of μ, high $\tan\beta$, and relatively small $M_{H^\pm}$ are chosen.

7.2 Heavy charged Higgs production with top and bottom quarks

For heavy charged Higgs bosons, $M_{H^\pm} \gtrsim m_t$, associated production $pp \to tbH^\pm + X$ is the dominant production mode. Two different formalisms can be employed to calculate the cross section for associated $tbH^\pm$ production. In the four-flavour scheme (4FS) with no b quarks in the initial state, the lowest-order QCD production processes are gluon–gluon fusion and quark–antiquark annihilation, $gg \to tbH^\pm$ and $q\bar{q} \to tbH^\pm$, respectively. Potentially large logarithms $\propto \ln(\mu_F/m_b)$, which arise from the splitting of incoming gluons into nearly collinear $b\bar{b}$ pairs, can be summed to all orders in perturbation theory by introducing bottom parton densities. This defines the five-flavour scheme (5FS) [221]. The use of bottom distribution functions is based on the approximation that the outgoing b quark is at small transverse momentum and massless, and the virtual b quark is quasi on shell. In this scheme, the leading-order (LO) process for the inclusive $tbH^\pm$ cross section is gluon–bottom fusion, $gb \to tH^\pm$. The next-to-leading order (NLO) cross section in the 5FS includes $\mathcal{O}(\alpha_s)$ corrections to $gb \to tH^\pm$ and the tree-level processes $gg \to tbH^\pm$ and $q\bar{q} \to tbH^\pm$. To all orders in perturbation theory the four- and five-flavour schemes are identical, but the way of ordering the perturbative expansion is different, and the results do not match exactly at finite order. For the inclusive production of neutral Higgs bosons with bottom quarks, $pp \to b\bar{b}H + X$, the four- and five-flavour scheme calculations numerically agree within their respective uncertainties, once higher-order QCD corrections are taken into account [191, 197, 198, 222], see Section 6 of this Report.

There has been considerable progress recently in improving the cross-section predictions for the associated production of charged Higgs bosons with heavy quarks by calculating NLO SUSY QCD and electroweak corrections in the four- and five-flavour schemes [223–230], and the matching of the NLO five-flavour scheme calculation with parton showers [231]. Below, we shall present state-of-the-art NLO QCD predictions in the 4FS (Section 7.2.1), in the 5FS (Section 7.2.2), and a first comparison of the two schemes at NLO (Section 7.2.3).

7.2.1 NLO QCD predictions for $pp \to tbH^\pm$ in the 4FS

In the 4FS the production of charged Higgs bosons in association with top and bottom quarks proceeds at LO through the parton processes $gg \to t\bar{b}H^-$ and $q\bar{q} \to t\bar{b}H^-$, and the charge-conjugate processes with the $\bar{t}bH^+$ final state [232–234]. Throughout this section we present results for the $t\bar{b}H^-$ channels. Generic Feynman diagrams that contribute at LO are displayed in Fig. 27.
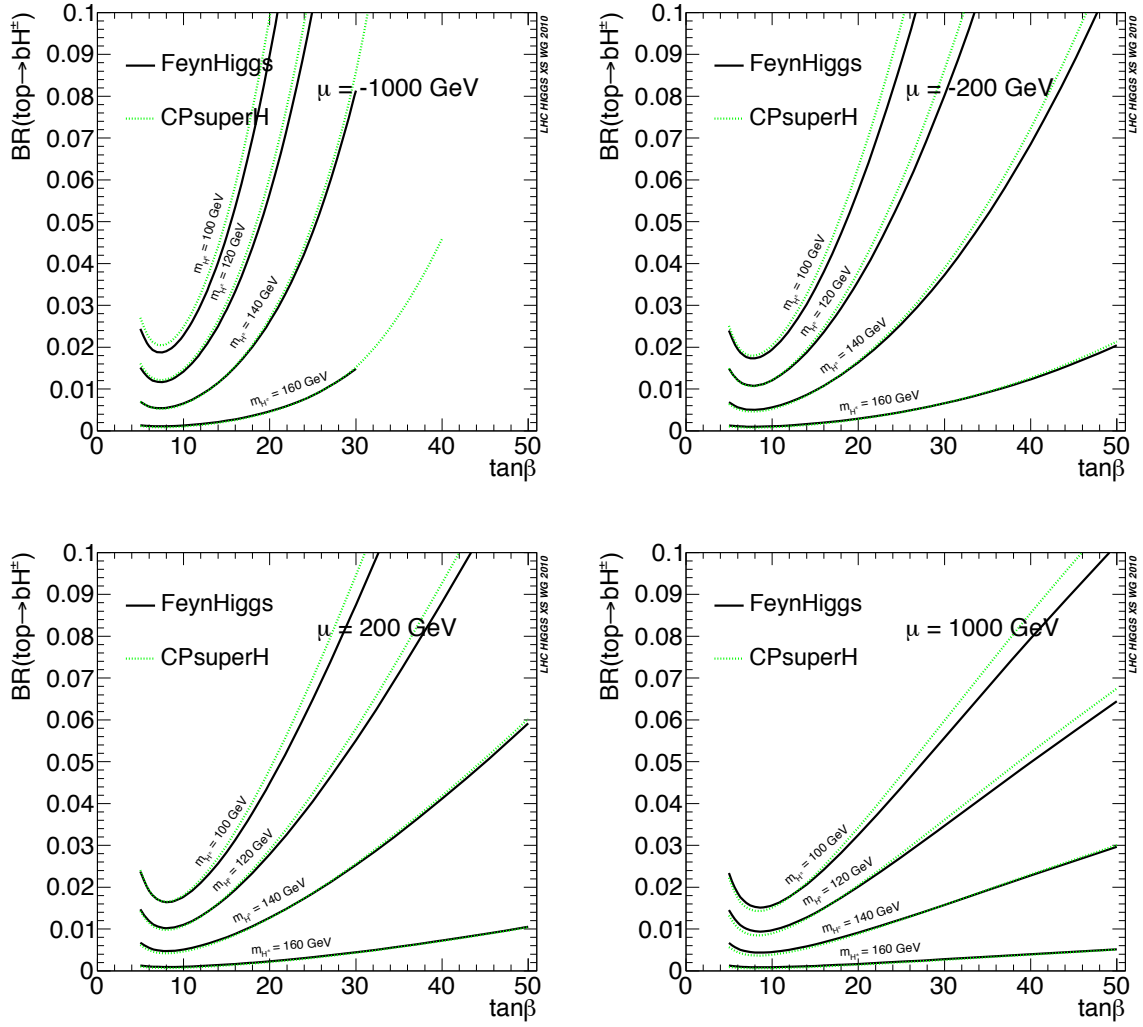
Fig. 25: The branching fraction of $t \to bH^{\pm}$ as a function of $\tan \beta$ for different values of μ and $M_{H^{\pm}}$. The lines in the upper left plot terminate when the specific code reaches a negative light Higgs mass squared. Depending on the code this happens for slightly smaller or larger $\tan \beta$ values (in this extreme scenario).

The calculation of the NLO QCD corrections to charged Higgs production in the 4FS has been discussed in detail in Ref. [235], both within a two-Higgs-doublet model with the SM particle content besides the extended Higgs sector, and within the MSSM. The NLO QCD effects considerably enhance the cross section and reduce the dependence on the renormalization and factorization scales. In the MSSM, additional loop corrections from squark and gluino exchange are sizable for large $\tan \beta$, but they can be taken into account through the Δ_b corrections to the bottom–Higgs-Yukawa coupling [cf. Eq. (7)], i.e. through a rescaling of the NLO QCD prediction according to $m_b \tan \beta / v \to m_b \tan \beta / v \, (1 - \Delta_b / \tan^2 \beta)/(1 + \Delta_b)$ [235].

In Tables 21 and 22 we present 4FS NLO QCD results for the production of heavy charged Higgs bosons in a two-Higgs-doublet model. Cross sections for MSSM scenarios with large $\tan \beta$ can be obtained from the NLO QCD cross sections by the rescaling defined above. Predictions are presented for LHC cross sections at 7 TeV and 14 TeV energy, with $\tan \beta = 30$ and the SM input parameters according to Table A.

For a consistent evaluation of the hadronic cross sections in the 4FS we adopt the recent MSTW
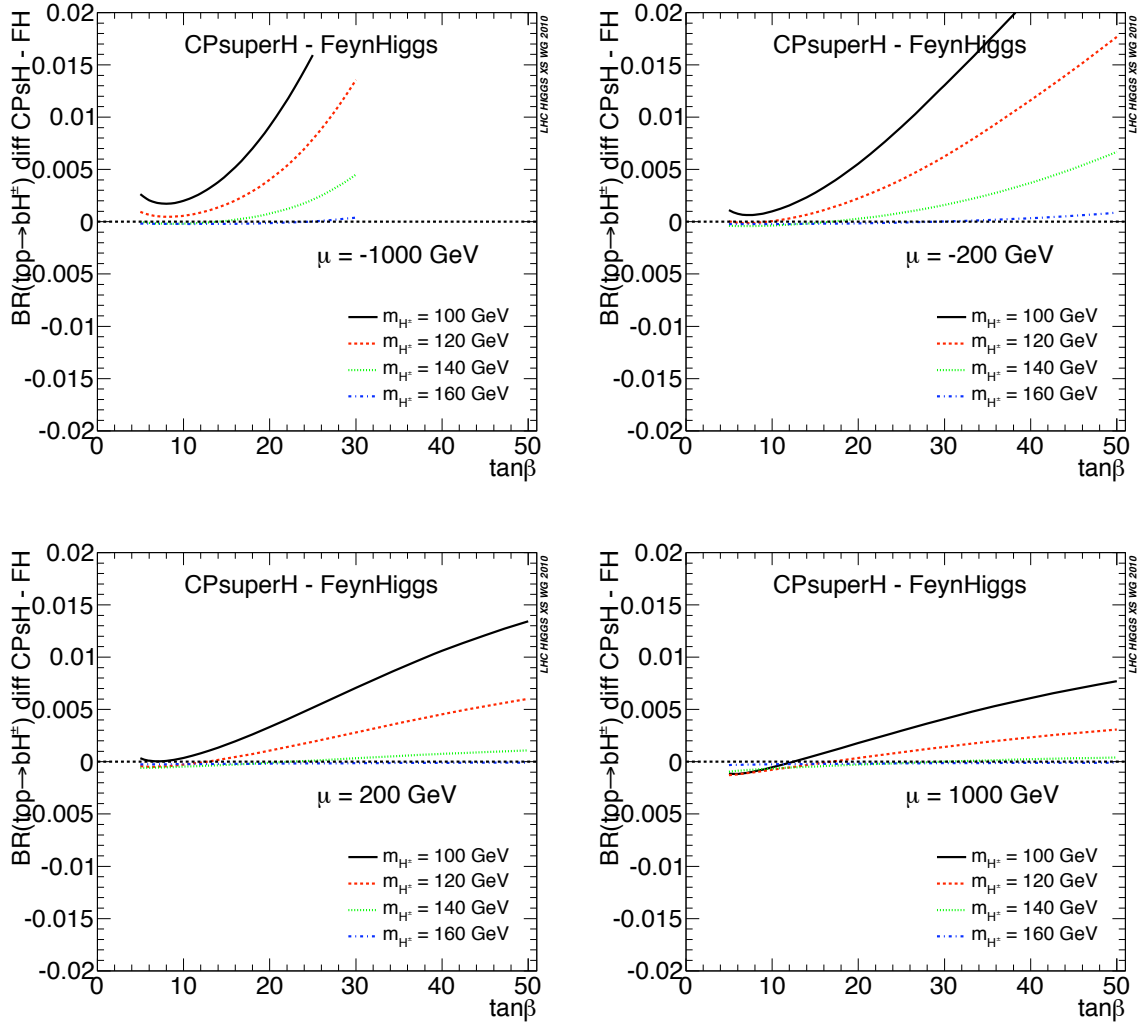
Fig. 26: The difference of BR(t $\rightarrow$ bH$^\pm$) calculated with CPSUPERH and FEYNHIGGS as a function of $\tan\beta$ for different values of μ and $M_{\mathrm{H}^\pm}$.

Table 21: NLO QCD cross sections for pp $\rightarrow$ t$\bar{\mathrm{b}}$H$^-$ in the 4FS at the LHC with 7 TeV, $\tan\beta = 30$.

$M_{\mathrm{H}^\pm}$ [GeV]	σ [fb]	Scale uncert. [%]	PDF + α_{s} [%]
200	130	$-33\ +27$	$-5.5\ +4.5$
300	45.9	$-33\ +34$	$-6.7\ +5.6$
400	18.0	$-34\ +30$	$-7.7\ +6.6$
500	7.59	$-35\ +32$	$-8.6\ +7.5$

Table 22: NLO QCD cross sections for pp $\rightarrow$ t$\bar{\mathrm{b}}$H$^-$ in the 4FS at the LHC with 14 TeV, $\tan\beta = 30$.

$M_{\mathrm{H}^\pm}$ [GeV]	σ [fb]	Scale uncert. [%]	PDF + α_{s} [%]
200	972	$-30\ +27$	$-3.4\ +2.7$
300	405	$-30\ +26$	$-4.0\ +3.2$
400	184	$-30\ +26$	$-4.7\ +3.7$
500	92.6	$-32\ +29$	$-5.1\ +4.1$

four-flavour PDF [205] and the corresponding four-flavour α_{s}. Note, however, that the evaluation of
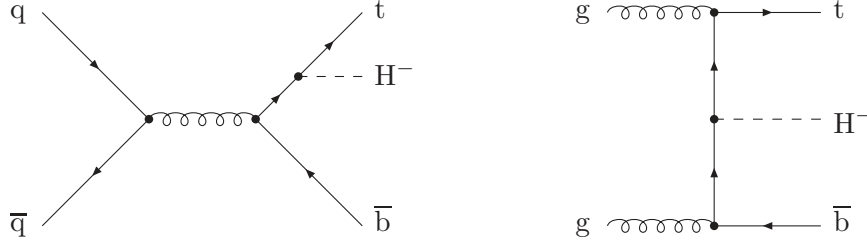
Fig. 27: Generic Feynman diagrams for $pp \to t\bar{b}H^- + X$ in the 4FS at LO.
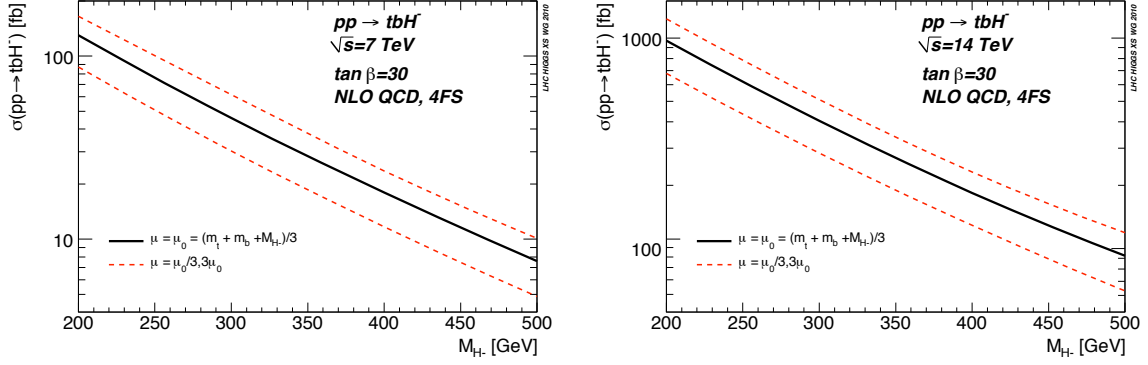
Fig. 28: NLO QCD cross sections for $pp \to t\bar{b}H^-$ in the 4FS at the LHC (7 TeV and 14 TeV) as a function of the Higgs-boson mass. The error band includes the NLO scale uncertainty. (Calculation from Ref. [235].)

the running b-quark mass in the bottom–Higgs-Yukawa coupling is based on a five-flavour α_s with $\alpha_s(M_Z) = 0.120$. The renormalization and factorization scales have been identified and are set to $\mu = (m_t + m_b + M_{H^-})/3$ as our default choice. The NLO scale uncertainty has been estimated from the variation of the renormalization and factorization scales by a factor of three about the central scale choice $\mu = (m_t + m_b + M_{H^-})/3$. As shown in Ref. [235], the variation of the QCD scales by a factor three about the central scale provides a more reliable estimate of the theory uncertainty than the usual variation by a factor two, as the variation by a factor three encompasses the maximum of the NLO prediction. The residual NLO scale uncertainty is then approximately $\pm 30\%$. While no four-flavour PDF parametrization exists that would allow to estimate the combined PDF and α_s error, the difference in the relative PDF error as obtained from the MSTW four- and five-flavour sets is marginal. We have thus adopted the five-flavour MSTW PDF [41] to estimate the combined PDF and α_s uncertainty shown in Tables 21 and 22. We find that the theoretical uncertainty of the 4FS NLO QCD prediction for $pp \to t\bar{b}H^-$ at the LHC is by far dominated by the scale uncertainty.

The NLO QCD cross section for $pp \to t\bar{b}H^-$ at the LHC with 7 TeV and 14 TeV is shown in Fig. 28 as a function of the Higgs-boson mass. The error band quantify the NLO scale uncertainty.

7.2.2 NLO QCD predictions for $pp \to tH^\pm$ in the 5FS

In the 5FS the LO process for the inclusive $H^\pm$ cross section is gluon–bottom fusion, $gb \to tH^\pm$. The NLO cross section includes $\mathcal{O}(\alpha_s)$ corrections to $gb \to tH^\pm$ and the tree-level processes $gg \to tbH^\pm$ and $q\bar{q} \to tbH^\pm$, and has been calculated in Refs. [225, 226, 231]. In Tables 23 and 24 we present NLO QCD results for the production of heavy charged Higgs bosons in the 5FS, with $\tan\beta = 30$ and the SM input parameters according to Table A. As in the 4FS calculation, cross sections for MSSM scenarios
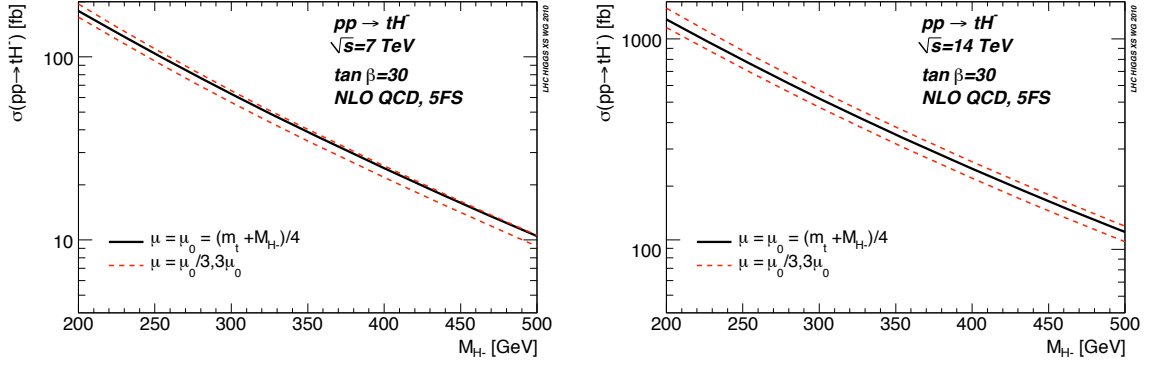
Fig. 29: NLO QCD cross sections for $pp \to tH^-$ in the 5FS at the LHC (7 TeV and 14 TeV) as a function of the Higgs-boson mass. The error band includes the NLO scale uncertainty. (Calculation from Ref. [231].)

with large $\tan\beta$ can be obtained from the NLO QCD cross sections by rescaling the bottom–Higgs-Yukawa coupling. The NLO cross section values have been obtained using MC@NLO 4.0 [236], with

Table 23: NLO QCD cross sections for $pp \to tH^-$ in the 5FS at the LHC with 7 TeV, $\tan\beta = 30$.

$M_{H^\pm}$ [GeV]	σ [fb]	Scale uncert. [%]
200	178	$-7.1 \ +9.4$
300	62.7	$-10.0 \ +4.7$
400	24.7	$-11.0 \ +2.7$
500	10.5	$-12.0 \ +1.1$

Table 24: NLO QCD cross sections for $pp \to tH^-$ in the 5FS at the LHC with 14 TeV, $\tan\beta = 30$.

$M_{H^\pm}$ [GeV]	σ [fb]	Scale uncert. [%]
200	1237	$-8.4 \ +13$
300	521	$-9.0 \ +9.5$
400	242	$-9.8 \ +7.7$
500	121	$-10.0 \ +6.5$

the option `rflag` switched to 0 (for MSbar Yukawa renormalization). The central scale has been set to $\mu_0 = (m_t + M_{H^-})/4$, and the five-flavour MSTW PDF [41] has been adopted. We find a residual NLO scale uncertainty of $10-20\%$. Since there are no direct experimental constraints on the bottom PDF, the PDF uncertainty of the $gb \to tH^\pm$ process is difficult to quantify. Thus, unfortunately, no reliable estimates of the PDF and α_s uncertainty of the 5FS calculation exist to date.

The total 5FS NLO QCD cross section for $pp \to tH^-$ at the LHC with 7 TeV and 14 TeV is shown in Fig. 29 as a function of the Higgs-boson mass. The error band includes the NLO scale uncertainty only.

Note that supersymmetric electroweak $\mathcal{O}(\alpha)$ corrections to charged Higgs-boson production in the five-flavour scheme have been studied in Ref. [229]. These corrections depend sensitively on the MSSM scenario and have thus not been included in the numbers presented here.

7.2.3 Comparison of the 4FS and 5FS calculations

The 4FS and 5FS calculations represent different ways of ordering the perturbative expansion, and the results will not match exactly at finite order. However, taking into account higher-order corrections, the
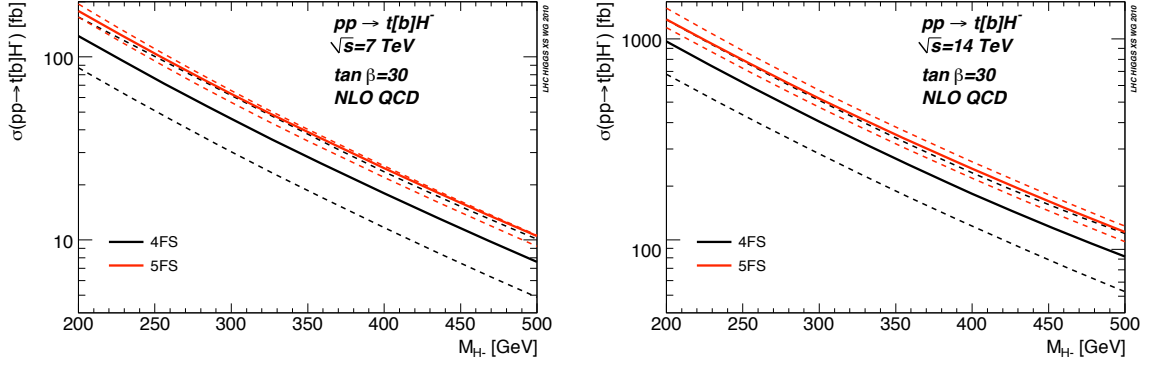
Fig. 30: NLO QCD cross sections for $pp \to tH^-(\bar{b})$ in the 4FS and 5FS at the LHC (7 TeV and 14 TeV) as a function of the Higgs-boson mass. The error band includes the NLO scale uncertainty. (Calculations from Refs. [231, 235].)

two predictions are expected to agree within their respective uncertainties, see Section 6 of this Report for a similar comparison for the inclusive production of neutral Higgs bosons with bottom quarks.

In Fig. 30 we present a comparison of the 4FS and 5FS calculations at NLO QCD for the inclusive $pp \to tH^-(\bar{b})$ cross section at the LHC. The error band indicates the theoretical uncertainty when the renormalization and factorization scales are varied between $\mu_0/3$ and $3\mu_0$, with $\mu_0 = (m_t + m_b + M_{H^-})/3$ and $\mu_0 = (m_t + M_{H^-})/4$ for the 4FS and 5FS calculations, respectively. Taking the scale uncertainty into account, the 4FS and 5FS cross sections at NLO are consistent, even though the predictions in the 5FS at our choice of the central scales are larger than those of the 4FS by approximately 30%, almost independently of the Higgs-boson mass. Qualitatively similar results have been obtained from a comparison of 4FS and 5FS NLO calculations for single-top production at the LHC [237]. Note that the bottom PDF of the recent five-flavour MSTW fit [41] is considerably smaller than that of previous fits [238] and has lead to a significant decrease in the 5FS cross section prediction.

8 Parton distribution functions[12]

8.1 Introduction

Parton distribution functions (PDFs) are crucial for the prediction of any physical process to be measured at the LHC, hence PDFs and their uncertainties have very important significance, in particular for discovery and exclusion limits. At present these PDFs are obtained from fits to data from deep-inelastic scattering, Drell–Yan, and jet production from a wide variety of different experiments. A number of groups have produced publicly available PDFs using different data sets and analysis frameworks. Here we summarise our level of understanding as the first LHC cross sections at 7 TeV are being determined. There are many differences between existing PDF analyses: different input data, different methodologies and criteria for determining uncertainties, different ways of parametrizing the PDFs, different number of parametrized PDFs, different treatments of heavy quarks, different perturbative orders, different ways of treating α_s (as an input or as a fit parameter), different values of physical parameters such as α_s and heavy-quark masses, and more. Hence, we begin by summarizing the main features of current PDF sets. We subsequently introduce various theoretical uncertainties on PDFs, focusing on the uncertainty related to the value of the strong coupling constant, and provide a presentation of choices made by different groups. We then briefly summarise the computation of physical processes using various PDF sets. As an outcome of this, we motivate and describe the PDF4LHC interim recommendation [45] to obtain current combined predictions and uncertainties based on several global PDF sets, and illustrate it by showing its application to the Higgs production cross section via gluon–gluon fusion, both at NLO and at NNLO.

We will discuss the following PDF sets (when several releases are available, the reference release for our discussion below is given parenthesis in each case): ABKM [46], CTEQ/CT (CTEQ6.6 [239]), GJR [240, 241], HERAPDF (HERAPDF1.0 [242]), MSTW (MSTW08 [41, 44, 205]) and NNPDF (NNPDF2.0 [134]). ABKM, JR [243] (for variable flavour see Ref. [47]), MSTW, and HERAPDF [48] are available with NNLO evolution [244, 245]. A CTEQ/CT update is already available (CT10 [246]), while preliminary updates of ABM [247], NNPDF [248], HERAPDF [48], and MSTW [249] have also been presented.

8.2 PDF determinations – experimental uncertainties

Experimental uncertainties on PDFs determined in global fits (usually called *PDF uncertainties*, for short) reflect the information available (or lack thereof) in the underlying data and the way it constrains PDFs; they should be interpreted as genuine statistical uncertainties, and indeed they are often given in the form of confidence levels (CL). They may differ because of different choices made in the analysis that extracts this information from the data, specifically in: (1) the choice of data sets; (2) the statistical treatment which is used to determine the uncertainties and which also determines the way in which PDFs are delivered to the user; (3) the form and size of parton parametrization.

8.2.1 Data sets

A wider data set contains more information, but data coming from different experiments may be inconsistent to some extent. The choices made by the various groups are the following:

- The data sets considered by CTEQ, MSTW, and NNPDF include data from both electroproduction and hadroproduction, in each case from both fixed-target and collider experiments. The electroproduction data include electron, muon and neutrino deep-inelastic scattering data (both inclusive and charm production). The hadroproduction data include Drell–Yan (fixed-target virtual photon and collider W and Z production) and jet productions (Tevatron jets requiring some approximation for the MSTW NNLO analysis). Details vary slightly among particular versions of CTEQ, MSTW, and NNPDF fits.

---

[12]S. Forte, J. Huston, K. Mazumdar, R.S. Thorne and A. Vicini.

– For GJR (and JR) the data set consists of electroproduction data which include electron- and muon-inclusive deep-inelastic scattering data, and deep-inelastic charm production from charged leptons and neutrinos from fixed-target and collider experiments, and a smaller set of hadroproduction data, i.e. fixed-target virtual photon Drell–Yan production and Tevatron jet production.

– The ABKM data set includes electroproduction from fixed-target and collider experiments, including electron, muon, and neutrino deep-inelastic scattering data (both inclusive and charm production), and fixed-target hadroproduction data, i.e. virtual photon Drell–Yan production[13].

– The HERAPDF input contains all HERA deep-inelastic inclusive data.

8.2.2 Statistical treatment

Available PDF determinations fall in two broad categories: those based on a Hessian approach and those which use a Monte Carlo approach. The output format for information on PDFs is different in each case. Here we outline only the basic features. The precise manner in which to implement the PDFs is explained in more detail in the appropriate references for each group.

Within the Hessian method, PDFs are determined by minimizing a χ^2 function defined as $\chi^2 = \frac{1}{N_{\text{dat}}} \sum_{i,j} (d_i - \bar{d}_i) \text{cov}_{ij} (d_j - \bar{d}_j)$, where $\bar{d}_i$ are data, d_i theoretical predictions, N_{dat} is the number of data points, and cov_{ij} is the covariance matrix[14]. The best fit is the point in parameter space at which χ^2 is minimum, while PDF uncertainties are found by evaluating, and often diagonalizing the (Hessian) matrix of second derivatives of the χ^2 at the minimum, and then determining the range of parameter variation corresponding to a prescribed increase of the χ^2 function with respect to the minimum. In principle, the increase in χ^2 which provides 68% CL (1σ) is $\Delta\chi^2 = 1$. However, a larger variation of $\Delta\chi^2 = T^2$, with $T > 1$ a suitable 'tolerance' parameter [43, 250, 251] may turn out to be necessary for a more realistic error estimate for fits containing a wide variety of input processes and data, and in particular, in order for each experiment which enters the global fit to be consistent with the global best fit within one sigma (or an alternative confidence level, e.g. 90%). Possible reasons why this is necessary could be data inconsistencies or incompatibilities, underestimated experimental systematics, insufficiently flexible parton parametrizations, theoretical uncertainties or approximations in the PDF extraction. At present, HERAPDF and ABKM use $\Delta\chi^2 = 1$, GJR uses $T \approx 4.7$, CTEQ6.6 uses $T = 10$ at 90% CL (corresponding to $T \approx 6$ at 68% CL), while MSTW08 uses a dynamical tolerance [41], i.e., a different value of T for each eigenvector, with values from $T \approx 1$ to $T \approx 6.5$ and most values being in the range of $2 < T < 5$.

Within a Monte Carlo method, PDFs are determined by first producing a Monte Carlo sample of N_{rep} pseudo-data replicas. Each replica contains a number of points equal to the number of original data points. The sample is constructed in such a way that, in the limit $N_{\text{rep}} \to \infty$, the central value of the i-th data point is equal to the mean over the N_{rep} values that the i-th point takes in each replica, the uncertainty of the same point is equal to the variance over the replicas, and the correlations between any two original data points is equal to their covariance over the replicas. From each pseudo-data replica, a PDF replica is constructed by minimizing a χ^2 function. The PDF central values, uncertainties and correlations are then computed by taking means, variances, and covariances over this replica sample. NNPDF uses a Monte Carlo method, with each PDF replica obtained as the minimum χ^2 which satisfies a cross-validation criterion [134, 252], and is thus larger than the absolute minimum of the χ^2. This method has been used in all NNPDF sets from NNPDF1.0 version onwards.

---

[13] An update is being prepared that includes the Tevatron jet data as well.

[14] Different groups use differing definitions of the covariance matrix – including entirely or only partially correlated uncertainties – see the papers for details. Hence the values of the χ^2 quoted are only roughly comparable.

8.2.3 Parton parametrization

Existing PDF sets differ in the number and choice of linear combinations of PDFs which are independently parametrized and the functional form and number of parameters used. For the functional form the most common choice is that each PDF at some reference scale Q_0 is parametrized as

$$f_i(x, Q_0) = N x^{\alpha_i} (1 - x)^{\beta_i} g_i(x) \tag{10}$$

where $g_i(x)$ is a function which tends to a constant for both $x \to 1$ and $x \to 0$, for example $g_i(x) = 1 + \epsilon_i \sqrt{x} + D_i x + E_i x^2$ (HERAPDF). The fit parameters are α_i, β_i, and the parameters in g_i. Some of these parameters may be chosen to take a fixed value (including zero). The general form (10) is adopted in all the PDF sets which we discuss here except for the case of NNPDF which, instead, defines

$$f_i(x, Q_0) = c_i(x) N N_i(x), \tag{11}$$

where $NN_i(x)$ is a neural network (a feed-forward neural network with two hidden layers, see Ref. [134] for details) and $c_i(x)$ is a *preprocessing* function. The fit parameters determine the shape of $NN_i(x)$. The function $c_i(x)$ is chosen randomly in a space of functions of the form $x^{\alpha_i}(1 - x)^{\beta_i}$, within some acceptable range of the parameters α_i and β_i. For each group the basis functions and number of parameters are the following.

- ABKM parametrizes the two lightest flavours, corresponding anti-flavours, the total strange-ness, and the gluon (six independent PDFs) with 21 free parameters.
- CTEQ6.6 and CT10 parametrize the two lightest flavours and anti-flavours, the total strangeness, and the gluon (six independent PDFs) with respectively 22 and 26 free parameters.
- GJR parametrizes the two lightest flavours, their anti-flavours, and the gluon with 20 free parameters (five independent PDFs); the strange distribution is assumed to be either proportional to the light sea or to vanish at a low scale $Q_0 < 1$ GeV at which PDFs become valence-like.
- HERAPDF parametrizes the two lightest flavours, $\overline{u}$, the combination $\overline{d} + \overline{s}$, and the gluon with 10 free parameters (five independent PDFs), strangeness is assumed to be proportional to the $\overline{d}$ distribution; the effect of varying the form of the parametrization and the size of the strange component is also studied.
- MSTW parametrizes the three lightest flavours and anti-flavours, and the gluon with 28 free parameters (seven independent PDFs) to find the best fit, but 8 are held fixed in the determination of the uncertainty eigenvectors.
- NNPDF parametrizes the three lightest flavours and anti-flavours, and the gluon with 259 free parameters (37 for each of the seven independent PDFs).

8.3 PDF determinations – theoretical uncertainties

The theoretical uncertainties of the PDFs reflect the approximations in the theory which is used in order to relate the PDFs to the measurable quantities. The study of theoretical PDF uncertainties is currently less advanced than that of experimental uncertainties, and only some of the theoretical uncertainties have been explored till now. One might expect that one of the main theoretical uncertainties in PDF determinations should be related to the treatment of the strong interaction: in particular, to the values of the strong coupling constant (α_s) and of the heavy-quark masses (m_c and m_b), and the uncertainties related to the truncation of the perturbative expansion (commonly estimated through the variation of renormalization and factorization scales). The uncertainty on α_s has been explored systematically by the PDF groups. The effect of varying m_b and m_c has been included by HERAPDF in model uncertainties, and these are parameters in the covariance matrix for ABKM [46]. Sets with varying quark masses and implications have been made available by MSTW [205], and preliminary studies of the effect of m_b

and m_c have also been presented by NNPDF [253]. Further uncertainties are related to the treatment of the heavy-quark thresholds, which are handled in various ways by different groups (see Section 22 of Ref. [131]), to numerical approximations, and to the treatment of electroweak effects (such as QED PDF evolution [254]).

8.3.1 The value of α_s and its uncertainty

The choice of value of α_s is clearly important because it is strongly correlated to PDFs, especially the gluon distribution: this correlation is studied in detail in Ref. [255] using CTEQ, MSTW, and NNPDF PDFs; α_s is a parameter in the covariance matrix for ABKM, GJR(JR). There are two separate issues related to the value of α_s in PDF fits: first, the choice of α_s for which PDFs are made available, and second the choice of the preferred value of α_s to be used when giving PDFs and their uncertainties. These are two separate though related issues, and for each of them two different basic philosophies may be adopted. In what concerns available values, for some groups PDF fits are performed for a number of different values of α_s. Though a PDF set corresponding to some reference value of α_s is given, the user is free to choose any of the given sets. This philosophy is adopted by CTEQ (0.118), HERAPDF (0.1177), MSTW (0.120), and NNPDF (0.119), where, in parenthesis, the reference (NLO) value of α_s for each set is indicated. For others, α_s is treated as a fit parameter, and PDFs are given only for the best-fit value. This philosophy is adopted by ABKM (0.11801) and GJR (0.1145). Concerning the preferred central value and uncertainty, for some groups the value of $\alpha_s(M_Z)$ is taken as an external parameter. This philosophy is adopted by CTEQ, HERAPDF1.0, and NNPDF. In this case, there is no a-priori central value of $\alpha_s(M_Z)$, and the uncertainty on $\alpha_s(M_Z)$ is included by repeating the PDF determination as α_s is varied in a suitable range. For others α_s is treated as a fit parameter, so its value and uncertainty are determined along with the PDFs. This philosophy is adopted by MSTW, ABKM, and GJR08.

When comparing results obtained using different PDF sets it should be borne in mind that if different values of α_s are used, predictions for cross sections change both due to their dependence on α_s (which for some LHC processes, such as top-pair production or Higgs production in gg fusion may be quite strong), as well as to the dependence of the PDFs on the value of α_s. Differences due to the PDFs alone can be isolated only while performing comparisons at a common value of α_s. The different groups have different ways of calculating the total uncertainty due to both the PDFs and α_s. This is explained in more detail in Ref. [255] and in publications from each of the groups, in particular, Refs. [44,46,256].

8.4 Comparison of results from different PDFs

To compare results from different PDF sets it is useful to introduce differential parton–parton luminosities, which, when multiplied by the dimensionless cross section $\hat{s}\hat{\sigma}$ for a process, provide an estimate of the size of an event cross section at the LHC. The differential parton–parton luminosity $dL_{ij}/d\hat{s}$ is

$$\frac{dL_{ij}}{d\hat{s}\,dy} \equiv \frac{1}{s}\frac{1}{1+\delta_{ij}}\left[f_i(x_1,\mu)f_j(x_2,\mu) + (1 \leftrightarrow 2)\right], \qquad (12)$$

where the prefactor avoids double-counting for identical partons. A generic cross section is written as

$$\sigma = \sum_{i,j}\int_0^1 dx_1\,dx_2\,f_i(x_1,\mu)\,f_j(x_2,\mu)\,\hat{\sigma}_{ij} \equiv \sum_{i,j}\int\left(\frac{d\hat{s}}{\hat{s}}\right)\left(\frac{dL_{ij}}{d\hat{s}}\right)(\hat{s}\,\hat{\sigma}_{ij})\ . \qquad (13)$$

The relative gg PDF luminosities at NLO, along with their 68% CL error bands, are shown in Fig. 31, normalized to the MSTW08 central value [257]. For HERAPDF1.0 the inner uncertainty bands (dashed lines) correspond to the experimental errors, and the outer uncertainty bands (shaded regions) include errors due to model and parametrization. The $q\overline{q}$ luminosity plots [257] look similar, but turn upwards at high $\hat{s}/s$ for HERAPDF1.0. The error bands for each of the PDF luminosities are of similar size. The luminosity for the range of $t\overline{t}$ and Higgs production are in good agreement for CTEQ, MSTW,
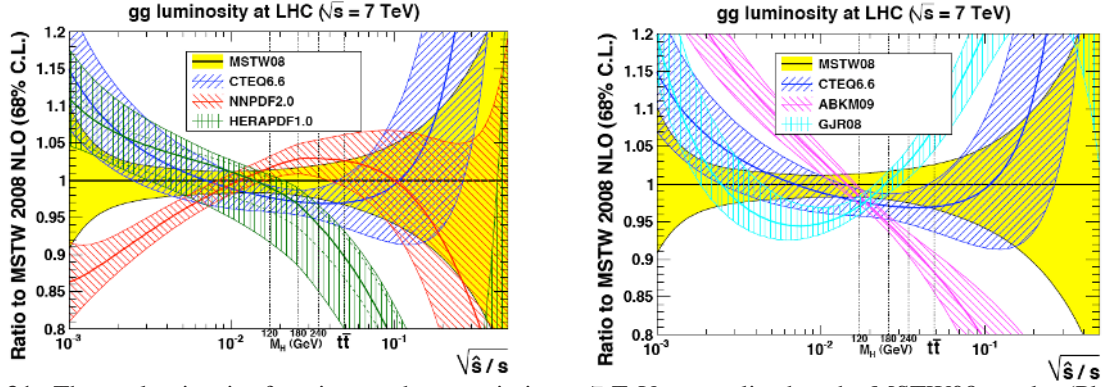
Fig. 31: The gg luminosity functions and uncertainties at 7 TeV, normalized to the MSTW08 result. (Plots by G. Watt [257].)

and NNPDF, while the agreement with ABKM, HERAPDF, and GJR is less good at higher masses. It is notable that the PDF luminosities tend to differ at low x and high x. The CTEQ6.6 distributions, for example, may be larger at low x than MSTW2008, due to the positive-definite parametrization of the gluon distribution; the MSTW gluon starts off as negative at low x and Q^2, and this results in an impact for both the gluon and sea-quark distributions at larger Q^2 values. The NNPDF2.0 $q\bar{q}$ luminosity tends to be somewhat lower, in the W, Z region for example. Part of this effect might come from the use of a zero-mass heavy-quark scheme, although other differences might be relevant. However, there are other discrepancies of more than 20% at high or low invariant masses.

At small x details of heavy-flavour treatment cause some deviation, and there is also an anticorrelation with the value of α_s which varies between groups (with the GJR value differing most). At high x Tevatron jet data gives a constraint on the gluon (though there is some variation depending on the data set) and this data is not used in ABKM09 (investigations by ABM may be found at Refs. [258, 259]) and HERAPDF1.0 fits. At high x, W production data (not used by ABKM, GJR, and HERAPDF) constrain the light-quark distributions, which are then correlated to the gluon by the momentum sum rule. The high and low-x gluon distributions are also anti-correlated by the momentum sum rule. All these factors, amongst others, may influence the forms of the gluon luminosities and be responsible for the discrepancies observed.

Benchmark computations of LHC total cross sections and rapidity distributions from various PDF groups can be found in Ref. [260] (see also Ref. [261]); the degree of agreement and discrepancy between the groups is commensurate with the luminosity plots shown here. Differences between the luminosities and predictions for those sets which exist at NNLO are similar to NLO, showing that they are most likely due to choices of data sets in the fit or other assumptions rather than theoretical procedures, such as different schemes for the treatment heavy flavours, for which differences should become smaller at higher orders.

It is also very useful to show the cross sections as a function of α_s. The predictions for Higgs production from gg fusion (shown for MSTW08 and NNPDF2.0 in the top left and right plots of Fig. 32, respectively) depend strongly on the value of α_s: the anticorrelation (or correlation for the Tevatron) between the gluon distribution and the value of α_s is not sufficient to offset the growth of the cross section as seen from the top-left plot. In the bottom plot one sees that CTEQ, MSTW, and NNPDF predictions are in moderate agreement but CTEQ lies somewhat lower, to some extent due to the lower choice of α_s. Compared at the common value of $\alpha_s(M_Z^2) = 0.119$, the CTEQ prediction and those from others have one-sigma PDF uncertainties which just about overlap for $M_H = 120$ GeV. This trend is similar up to about $M_H = 180$ GeV, and the agreement improves for higher masses, as seen in Fig. 33 below. Hence, both the difference in PDFs and in the dependence of the cross section on the value of
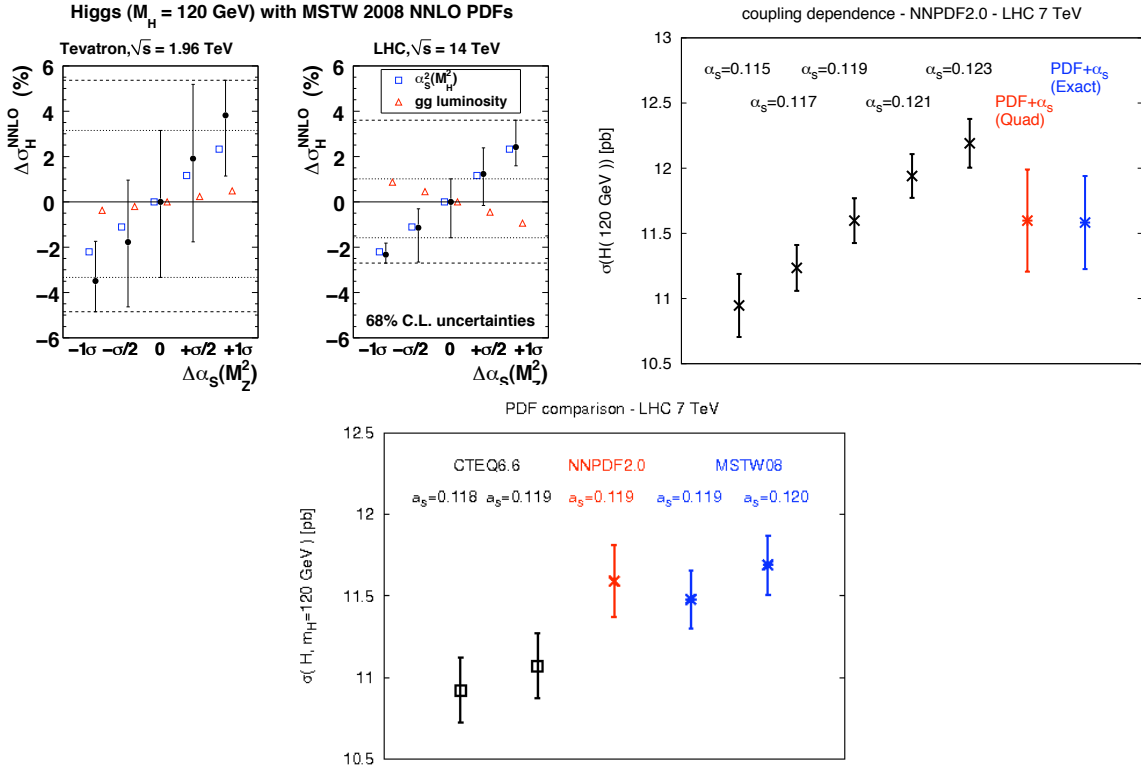
Fig. 32: Cross-section predictions as a function of α_s for a Higgs (gg fusion) for a Higgs mass of 120 GeV at NNLO for the Tevatron and LHC at 14 TeV [44] (top-left) and at NLO for the LHC at 7 TeV [262] (top-right) and for various groups all at NLO [262] (bottom).

α_s are responsible for the differences observed. A useful measure of this is to note that the difference in the central values of the MSTW and CTEQ predictions for a common value of $\alpha_s(M_Z^2) = 0.119$ and for a Higgs-boson mass of 120 GeV (a typical discrepancy) is equivalent to a change in $\alpha_s(M_Z^2)$ of about 0.0025. The worst discrepancy between CTEQ and either MSTW or NNPDF at any mass value of the Higgs is similar to a change in α_s of about 0.004. The predictions using some of the other PDF sets are rather lower [260], particularly at high masses, reflecting the behaviour of the gluon luminosity of Fig. 31.

8.5   The PDF4LHC recommendation

Before we present our recommendation, we would like to highlight the differences between two use cases: (1) cross sections which have not yet been measured (such as, for example, Higgs production) and (2) comparisons to existing cross sections. For the latter, the most useful comparisons should be to the predictions using individual PDFs (and their uncertainty bands) discussed above. Such cross sections have the potential, for example, to provide information useful for modification of those PDFs. For the former, in particular the cross-section predictions in this Report, we would like to provide a reliable estimate of the true uncertainty, taking into account possible differences between the central values of predictions using different PDFs. From the results seen it is clear that this uncertainty should be larger than that from any single PDF set; however in order for the probabilistic interpretation of PDF uncertainties to be preserved, it should not lose all connection to the individual PDF uncertainties, which would inevitably happen for many processes if the full spread of all PDFs were used. In order to do this, some compromise must be reached.

As seen at NLO there is always reasonable agreement between MSTW, CTEQ, and NNPDF, and potentially more deviation with the other sets. In some cases this deviation has at least one potential
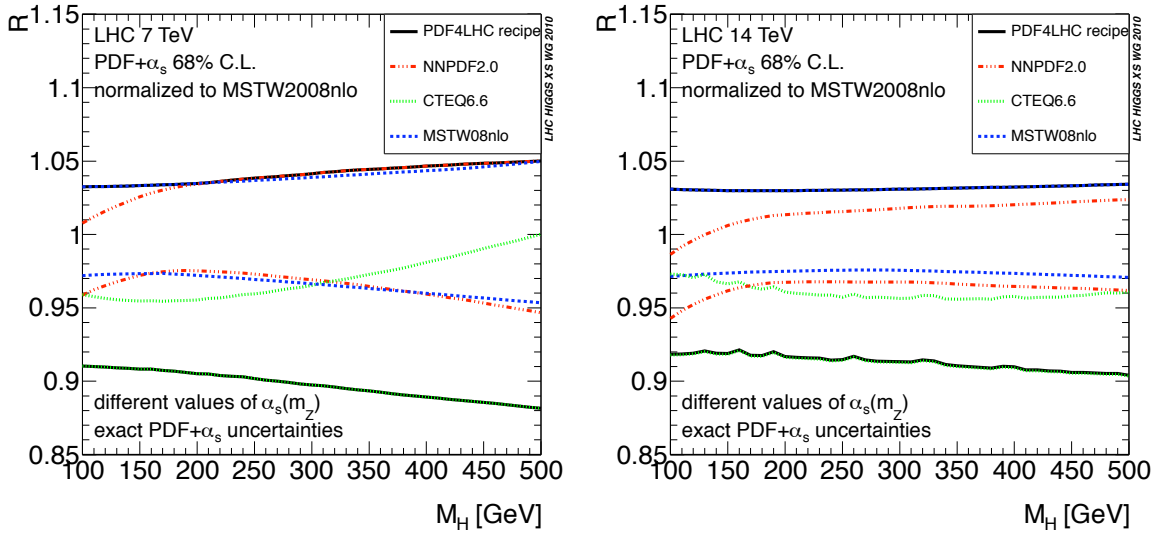
Fig. 33: Combined PDF+α_s uncertainty band for the total Higgs production cross section via gluon fusion, at NLO, evaluated according to the PDF4LHC recipe. The bands are normalized to the central MSTW2008 NLO result.

origin, e.g. the $t\bar{t}$ cross section at 7 TeV at the LHC probes similar PDFs as probed in the lower-p_T jet production at the Tevatron, which has neither been fit nor validated against quantitatively by some groups (preliminary results for ABM may be found at Refs. [258, 259]). As noted, large deviations in predictions between existing NNLO sets are similar to those between the same NLO sets. Discrepancies in MSTW, CTEQ, and NNPDF do not always have clear origin, or may be a matter of procedure (e.g. gluon parametrization) which is an ongoing debate between groups. Bearing this in mind and having been requested to provide a procedure to give a moderately conservative uncertainty, we adopt the following PDF4LHC recommendation [45].

8.5.1 NLO prescription

At NLO the recommendation is to use (at least) predictions from the PDF fits from CTEQ, MSTW, and NNPDF. These sets all use results from a hadron collider experiment, i.e., the Tevatron as well as fixed-target experiments and HERA, and they make available specific sets for a variety of values of α_s. The PDF versions to be used are: CTEQ6.6, MSTW2008, and NNPDF2.0. Neither the CTEQ6.6 nor the MSTW2008 use the new combined very accurate HERA data sets, whereas NNPDF2.0 does use this data (the CT10 [246] update of the CTEQ PDFs does include them and future updates of MSTW [249] will as well). It is to be noted that CTEQ6.6 and MSTW2008 are the PDF versions most commonly used by the LHC experiments currently, hence it is these versions that are suggested in the recommendation. The NNPDF2.0 set does not use a general-mass variable flavour number scheme (the NNPDF2.1 PDF set, which does use a general-mass variable flavour number scheme is currently being finalized [248]), but the alternative method which NNPDF use for determining PDF uncertainties provides important independent information. Other PDF sets, GJR08, ABKM09, and HERAPDF1.0 are useful for more conservative or extensive evaluations of the uncertainty. For example a study of the theoretical uncertainties related to the charm-mass treatment is possible using HERAPDF1.0 and ABKM.

The α_s uncertainties can be evaluated by taking a range of ± 0.0012 for 68% CL (or ± 0.002 for 90% CL) from the preferred central value for CTEQ and NNPDF. The total PDF+α_s uncertainty can then be evaluated by adding the variations in PDFs due to α_s uncertainty in quadrature with the fixed α_s PDF uncertainty (shown [256] to correctly incorporate correlations in the quadratic error approximation) or, for NNPDF, more efficiently taking a gaussian distribution of PDF replicas corresponding to different values of α_s. For MSTW the PDF+α_s uncertainties should be evaluated using their prescription which

better accounts for correlations between the PDF and α_s uncertainties when using the MSTW dynamical tolerance procedure for uncertainties. Adding the α_s uncertainty in quadrature for MSTW can be used as a simplification but generally gives slightly smaller uncertainties.

So the prescription for NLO is as follows:

– For the calculation of uncertainties at the LHC, use the envelope provided by the central values and PDF+α_s errors from the MSTW08, CTEQ6.6, and NNPDF2.0 PDFs, using each group's prescriptions for combining the two types of errors. We propose this definition of an envelope because the deviations between the predictions can sometimes be as large as their uncertainties. As a central value, use the midpoint of this envelope. We follow the PDF4LHC prescription and recommend that a 68% CL uncertainty envelope be calculated and the α_s variation suggested is consistent with this. Note that the CTEQ6.6 set has uncertainties and α_s variations provided only at 90% CL and thus their uncertainties should be reduced by a factor of 1.645 for 68% CL. Within the quadratic approximation, this procedure is exact.

8.5.2 NNLO prescription

For estimating uncertainties in cross section at NNLO, the recommendation is to use for base predictions the only NNLO set which currently includes a wide variety of hadron collider data sets, i.e., MSTW2008. There seems to be no reason to expect that the spread in predictions of the sets used in the NLO prescription, i.e., MSTW, CTEQ, and NNPDF, will diminish significantly at NNLO compared to NLO, where this spread was somewhat larger than the uncertainty from each single group. Hence, at NNLO the uncertainty obtained from MSTW alone should be expanded to some degree. It seems appropriate to do this by multiplying the MSTW uncertainty at NNLO by the factor obtained by dividing the full uncertainty obtained from the envelope of MSTW, CTEQ, and NNPDF results at NLO by the MSTW uncertainty at NLO. In all cases the α_s uncertainty should be included. We note that in several cases so far examined, for the LHC running at 7 TeV centre-of-mass energy, this factor of the envelope divided by the MSTW uncertainty is approximately constant, and quite close to 2 for Higgs production as shown below: this constant factor can be used as a short-hand prescription.

Since there are NNLO PDFs obtained from fits including fewer data sets by the ABKM, JR, and HERAPDF groups, these should ideally be compared with the above procedure, bearing in mind that it is possible there will be kinematic regions where the absence of data, or other reasons – e.g. in the JR case a theoretical constraint is imposed on the input by the choice of assuming the form Eq. (10) of PDFs at a very low, arguably non-perturbative, starting scale (though data are fit only at higher scales) – may lead to PDFs and predictions differing significantly from the central value and the extent of the uncertainty band.

So the prescription at NNLO is:

– As a central value, use the MSTW08 prediction. As an uncertainty, take the same percentage uncertainty on this NNLO prediction as found using the NLO uncertainty prescription given above.

8.5.3 Application to Higgs production via gluon fusion

In accordance with the recommendation, we have considered the CTEQ6.6 [239], MSTW2008 [41,44], and NNPDF2.0 [134] PDF sets. Combined PDF+α_s uncertainties for each of the three global sets are computed as discussed in Sections 8.2 and 8.3 (more details are in Ref. [255]). Computations have been performed using the code described in Refs. [32,33,163,164,263,264], improved with the NNLO corrections [11–16].

70
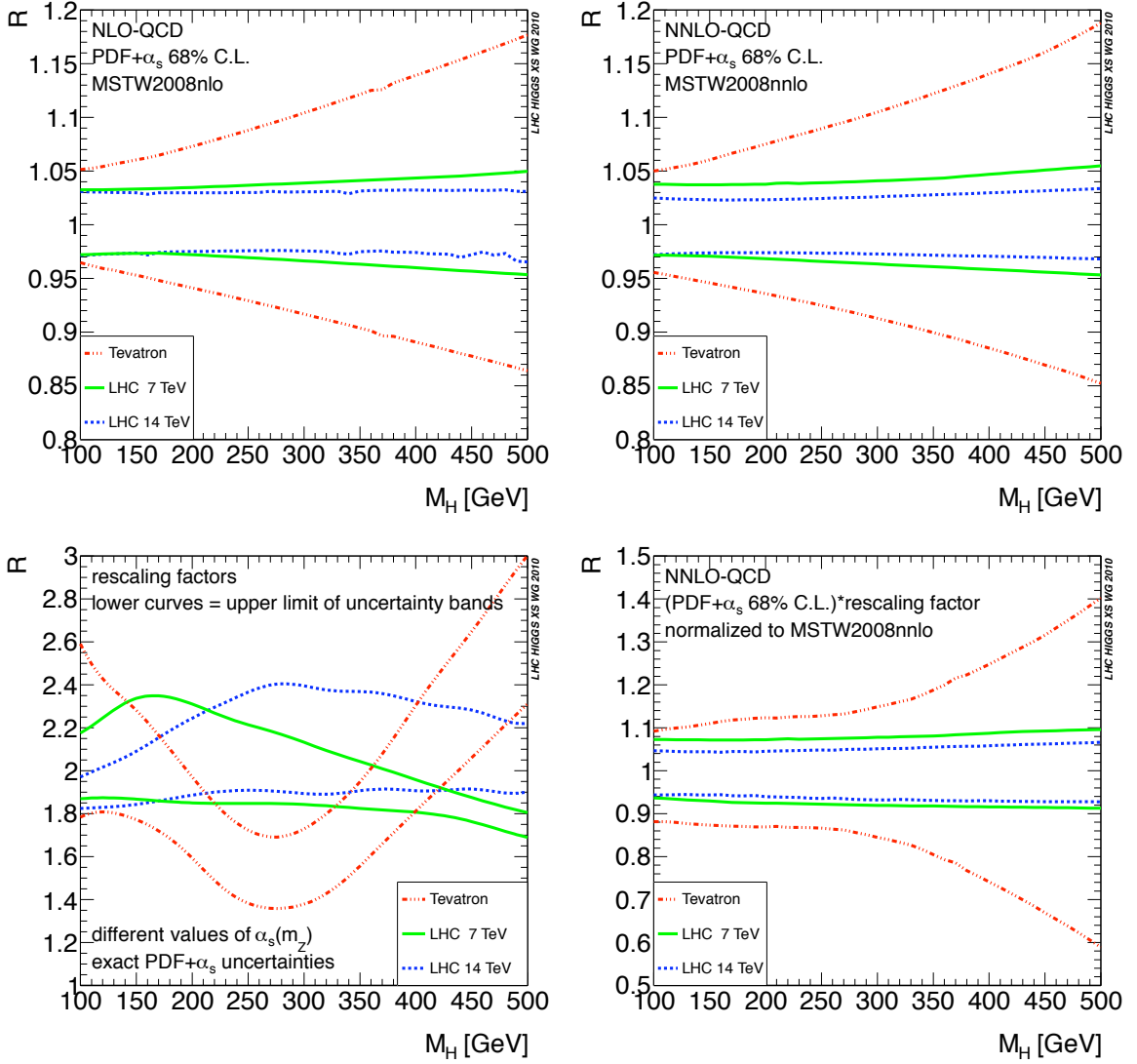
Fig. 34: Top: Combined relative PDF+$\alpha_{\rm s}$ uncertainty band for the total Higgs cross section from gluon fusion, at NLO (left) and at NNLO (right) obtained using MSTW2008. Bottom: rescaling factor for the NNLO uncertainty (left), obtained as the ratio of the percentage width of the NLO envelope with respect to its mid point to the percentage uncertainty of the MSTW2008 NLO band, and final NNLO uncertainty band obtained applying the rescaling to the MSTW08 NNLO result (right).

In order to obtain a meaningful comparison between different PDF sets it is crucial to adopt the same uncertainty range for the value of $\alpha_{\rm s}$. Here we assume the same range as for the PDF4LHC benchmarks of Ref. [45] namely

$$\delta^{(90)}\alpha_{\rm s} = 0.002 \quad \text{at} \quad 90\% \text{ CL}, \qquad \delta^{(68)}\alpha_{\rm s} = 0.0012 = 0.002/C_{90} \quad \text{at} \quad 68\% \text{ CL}, \qquad (14)$$

where $C_{90} = 1.64485$. In Fig. 33 we show the combined PDF+$\alpha_{\rm s}$ uncertainty bands obtained with CTEQ6.6, MSTW2008, NNPDF2.0, for LHC at 7 TeV and 14 TeV, all normalized to the central MSTW2008. For different Higgs mass values the predictions show partial agreement of different pairs of the three collaborations in such a way that only an envelope (the black line) of the three bands provides a conservative estimate of the uncertainty. This black line corresponds to the NLO PDF4LHC prescription.

At NNLO, the PDF4LHC prescription amounts to multiplying the MSTW08 NNLO percentage uncertainty by a factor obtained as the ratio of the MSTW08 NLO percentage uncertainty to the NLO envelope percentage uncertainty (all shown in Fig. 34 along with the final result). Note that in this case

the MSTW2008 NLO and NNLO PDF+α_s bands are very similar to each other. As can be observed in Fig. 34, the rescaling factor is of order 2: it is approximately constant for LHC at 7 TeV, but it displays a non-trivial Higgs mass dependence at the Tevatron. Use of the full range of NNLO PDF sets would provide significantly more variation, e.g. in the above example for a Higgs mass of 500 GeV the downwards error band for the LHC at 7 TeV would increase from 4.5% for MSTW2008 to 27%, as opposed to 4.5% to 8% using the PDF4LHC prescription. Some updates on various sets were seen at Ref. [258] with some signs of convergence evident.

8.6 Summary

We have summarized our understanding of PDFs and the associated experimental and theoretical uncertainties. The PDF4LHC recommendation is a pragmatic recommendation to be used when a prediction for the central value and a conservative estimate of the uncertainties is required, which acknowledges that the latter will be larger than that from an individual set, but is still representative of this uncertainty. It has the feature that the uncertainty bands are never too far from those PDF fits that include the largest number of data sets, in particular hadron collider data from the Tevatron which has the closest correlation to the measurements (particularly for high-mass final states) at the LHC. It is most likely expected to evolve when new experimental sets and new PDF determinations become available. In the near future some of the data used in the PDF determinations will be from the LHC, and this will help to improve the PDFs from all groups. Comparison of current predictions, together with uncertainties, will help to determine which of the different choices currently made by different groups are most successful.

9 Branching ratios[15]

9.1 Standard Model (SM) Higgs branching ratios

The branching ratios of the Higgs boson in the Standard Model have been determined using the programs HDECAY [64, 155, 156] and PROPHECY4F [265–267]. In a first step, all partial widths have been calculated as accurately as possible. Then the branching ratios have been derived from this full set of partial widths. Since the widths are calculated for on-shell Higgs bosons, the results have to be used with care for a heavy Higgs boson ($M_H \gtrsim 500$ GeV).

The code HDECAY calculates the decay widths and branching ratios of the Higgs boson(s) in the SM and the MSSM. For the SM it includes all kinematically allowed channels and all relevant higher-order QCD corrections to decays into quark pairs and into gluons. More details are given below. The electroweak next-to-leading order (NLO) corrections to the decays $H \to \gamma\gamma$ and $H \to gg$ have been calculated in Refs. [32, 33, 35, 263, 264, 268]. They are implemented in HDECAY in form of a grid based on the calculation of Ref. [35].

PROPHECY4F is a Monte Carlo event generator for $H \to WW/ZZ \to 4f$ (leptonic, semi-leptonic, and hadronic) final states. It provides the leading-order (LO) and NLO partial widths for any possible 4-fermion final state. It includes the complete NLO QCD and electroweak corrections and all interferences at LO and NLO. In other words, it takes into account both the corrections to the decays into intermediate WW and ZZ states as well as their interference for final states that allow for both. The dominant two-loop contributions in the heavy-Higgs-mass limit proportional to $G_\mu^2 M_H^4$ are included according to Refs. [76, 77]. Since the calculation is consistently performed with off-shell gauge bosons without any on-shell approximation, it is valid above, near, and below the gauge-boson pair thresholds. Like all other light quarks and leptons, bottom quarks are treated as massless. Using the LO/NLO gauge-boson widths in the LO/NLO calculation ensures that the effective branching ratios of the W and Z bosons obtained by summing over all decay channels add up to one.

The results presented below have been obtained as follows. The Higgs total width resulting from HDECAY has been modified according to the prescription

$$\Gamma_H = \Gamma^{HD} - \Gamma_{ZZ}^{HD} - \Gamma_{WW}^{HD} + \Gamma_{4f}^{Proph.}, \tag{15}$$

where Γ_H is the total Higgs width, Γ^{HD} the Higgs width obtained from HDECAY, Γ_{ZZ}^{HD} and Γ_{WW}^{HD} stand for the partial widths to ZZ and WW calculated with HDECAY, while $\Gamma_{4f}^{Proph.}$ represents the partial width of $H \to 4f$ calculated with PROPHECY4F. The latter can be split into the decays into ZZ, WW, and the interference,

$$\Gamma_{4f}^{Proph.} = \Gamma_{H \to W^*W^* \to 4f} + \Gamma_{H \to Z^*Z^* \to 4f} + \Gamma_{WW/ZZ-int.}. \tag{16}$$

The relative theoretical uncertainties of the calculation resulting from missing higher-order corrections are summarized in Table 25.

For QCD corrections the uncertainties have been estimated by the scale dependence of the widths resulting from a variation of the scale up and down by a factor 2 or from the size of known omitted corrections. For electroweak corrections the missing higher orders have been estimated based on the known structure and size of the NLO corrections. For cases where HDECAY takes into account the known NLO corrections only approximately the accuracy of these approximations has been used. These theoretical uncertainties from missing higher-order corrections will have to be combined with the parametric uncertainties (most notably from the bottom-quark mass and α_s) to arrive at the full theory uncertainties.

Specifically, the uncertainties of the results from HDECAY are obtained as follows: For the decays $H \to bb, cc$, HDECAY includes the complete massless QCD corrections up to and including

---

[15]A. Denner, S. Heinemeyer, I. Puljak, D. Rebuzzi (eds.); S. Dittmaier, A. Mück, M. Spira, M. Weber and G. Weiglein.

Table 25: Estimate of theoretical uncertainties from missing higher orders.

Partial width	QCD	Electroweak	Total
H → bb/cc	$\sim 0.1{-}0.2\%$	$\sim 1{-}2\%$ for $M_H \lesssim 135$ GeV	$\sim 1{-}2\%$
H → ττ		$\sim 1{-}2\%$ for $M_H \lesssim 135$ GeV	$\sim 1{-}2\%$
H → tt	$\sim 5\%$	$\lesssim 2{-}5\%$ for $M_H < 500$ GeV	$\sim 5\%$
		$\sim 0.1(M_H/1\text{ TeV})^4$ for $M_H > 500$ GeV	$\sim 5{-}10\%$
H → gg	$\sim 10\%$	$\sim 1\%$	$\sim 10\%$
H → γγ	$< 1\%$	$< 1\%$	$\sim 1\%$
H → WW/ZZ → 4f	$< 0.5\%$	$\sim 0.5\%$ for $M_H < 500$ GeV	$\sim 0.5\%$
		$\sim 0.17(M_H/1\text{ TeV})^4$ for $M_H > 500$ GeV	$\sim 0.5{-}15\%$

NNNLO, with a corresponding scale dependence of about $0.1{-}0.2\%$. The NLO electroweak corrections [269–272] are included in the approximation for small Higgs masses [273] which has an accuracy of about 1% for $M_H < 135$ GeV. The same applies to the electroweak corrections to H $\to \tau^+\tau^-$. For Higgs decays into top quarks HDECAY includes the complete NLO QCD corrections for small Higgs masses [274–280] interpolated to the large-Higgs-mass results at NNNLO far above the threshold [281–287]. The corresponding scale dependence is below 5%. Only the NLO electroweak corrections due to the self-interaction of the Higgs boson are included, and the neglected electroweak corrections amount to about $2{-}5\%$ for $M_H < 500$ GeV, where 5% refers to the region near the t$\bar{\text{t}}$ threshold and 2% to Higgs masses far above. For $M_H > 500$ GeV higher-order heavy-Higgs corrections [288–293] dominate the error, resulting in an uncertainty of $0.1 \times (M_H/1\text{ TeV})^4$ for $M_H > 500$ GeV. For H $\to$ gg, HDECAY uses the NLO [8,10,294] and NNLO [295] QCD corrections in the limit of heavy top quarks, while NNNLO QCD corrections [296] are neglected. The uncertainty from the scale dependence at NNLO is about 10% for $M_H < 135$ GeV. The NLO electroweak corrections are included via an interpolation based on a grid from Ref. [35]; the uncertainty from missing higher-order electroweak corrections is estimated to be 1%. For the decay H $\to \gamma\gamma$, HDECAY includes the full NLO QCD corrections [10,297–302] and a grid from Ref. [35] for the NLO electroweak corrections. Missing higher orders are estimated to be below 1%. The contribution of the H $\to \gamma e^+e^-$ decay via virtual photon conversion, evaluated in Ref. [303] is not taken into account in the following results. Its correct treatment and its inclusion in HDECAY are in progress.

The decays H $\to$ WW/ZZ $\to 4f$ are based on PROPHECY4F, which includes the complete NLO QCD and electroweak corrections with all interferences and leading two-loop heavy-Higgs corrections. For $M_H > 500$ GeV higher-order heavy-Higgs corrections dominate the error leading to an uncertainty of $0.17 \times (M_H/1\text{ TeV})^4$ for $M_H > 500$ GeV.

The assessment of parametric uncertainties of the Higgs branching ratios is still work in progress. A thorough, but very conservative estimation has recently been made in Ref. [40].

9.2 MSSM Higgs branching ratios: work in progress

The common issues of MSSM cross section and branching-ratio calculations have been outlined in Section 6.1. It was stressed that *before* any branching-ratio calculation can be performed in a first step the Higgs-boson masses, couplings, and mixings have to be determined from the underlying set of (soft SUSY-breaking) parameters. A brief comparison of the dedicated codes that provide this kind of calculations (FEYNHIGGS [148–151] and CPSUPERH [152, 153]) has been given, where in the case of real parameters more corrections are included into FEYNHIGGS.

After the calculation of Higgs-boson masses and mixings from the original SUSY input the branching-ratio calculation has to be performed. This can be done with the codes, CPSUPERH and FEYNHIGGS for real or complex parameters, or HDECAY [64, 155, 156] for real parameters. The higher-order corrections included in the calculation of the various decay channels differ in the three

codes. A detailed analysis of the accuracy of the different codes for certain decay widths is currently performed.

As for MSSM Higgs-boson production cross sections (see Section 6.1) due to the complexity of the MSSM parameter space, results can only be derived in representative benchmark scenarios. In accordance with Section 6 we show in Table 35 exemplary values for the $\mathrm{BR}(\phi \to \tau^+\tau^-)$ ($\phi = \mathrm{h}, \mathrm{H}, \mathrm{A}$), in the $m_\mathrm{h}^\mathrm{max}$ scenario [147] (see Eq. (4) for the definition of the SUSY parameters) consistently derived with FEYNHIGGS 2.7.4. In the further progress of this work a machinery will be set up to evaluate MSSM Higgs-boson branching ratios (consistent with the corresponding cross-section calculations) that will be valid for the full MSSM parameter space.

9.3 Results

Final SM Higgs-boson branching ratios[16] for 2-fermion final states, gauge-boson pair and the total decay width are listed in Tables 26–29. In Tables 30–34 we list branching ratios of the SM Higgs boson decaying into 4-fermion final states, where leptons $\mathrm{l} = \mathrm{e}, \mu, \tau, \nu_\mathrm{e}, \nu_\mu, \nu_\tau$, and quarks $\mathrm{q} = \mathrm{u}, \mathrm{d}, \mathrm{s}, \mathrm{c}, \mathrm{b}$. All fermion masses are neglected, the branching ratios are therefore identical for different flavours. We display results for 4-lepton final states ($\mathrm{H} \to \mathrm{llll}$) in Tables 30–32. We also provide results for final states with 2 arbitrary leptons and quarks ($\mathrm{H} \to \mathrm{llqq}$), 4 arbitrary quarks ($\mathrm{H} \to \mathrm{qqqq}$), and for all possible 4-fermion final states ($\mathrm{H} \to \mathrm{ffff}$) in Tables 33–34. For Higgs-boson masses below the ZZ threshold, interference contributions become relevant for 4-fermion decays with identical fermions like $\mathrm{H} \to \mathrm{ZZ} \to \mathrm{eeee}$ or $\mathrm{H} \to \mathrm{WW}/\mathrm{ZZ} \to \mathrm{e}\nu_\mathrm{e}\mathrm{e}\nu_\mathrm{e}$. These enhance the branching ratios for $\mathrm{H} \to \mathrm{eeee}, \mu\mu\mu\mu$ by more than 10% and decrease those for $\mathrm{H} \to \mathrm{e}\nu_\mathrm{e}\mathrm{e}\nu_\mathrm{e}, \mu\nu_\mu\mu\nu_\mu$ by more than 5% compared to those without identical fermions for $M_\mathrm{H} = 120$ GeV. All partial widths are listed in Appendix B. Branching ratios as a function of the SM Higgs-boson mass up to 200 GeV are shown in Fig. 35. The full mass range is displayed in Fig. 43. Figure 36 shows the SM Higgs-boson total decay width as a function of its mass.

MSSM Higgs-boson branching ratios to $\tau^+\tau^-$ final states in the $m_\mathrm{h}^\mathrm{max}$ scenario as a function of M_A [GeV] and $\tan\beta$ are given in Table 35 as an example of the MSSM results.

All results have been obtained using the values of the electroweak parameters as given in Appendix A. For the strong coupling constant we used $\alpha_\mathrm{s}(M_\mathrm{Z}^2) = 0.119$ with two-loop running.

---

[16]Full listings can be found at *https://twiki.cern.ch/twiki/bin/view/LHCPhysics/CERNYellowReportPageBR*

Table 26: SM Higgs branching ratios in fermionic final states in the low- and intermediate-mass range.

M_H [GeV]	$H \to b\bar{b}$	$H \to \tau\tau$	$H \to \mu\mu$	$H \to s\bar{s}$	$H \to c\bar{c}$	$H \to t\bar{t}$
90	$8.12 \cdot 10^{-1}$	$8.41 \cdot 10^{-2}$	$2.92 \cdot 10^{-4}$	$6.20 \cdot 10^{-4}$	$3.78 \cdot 10^{-2}$	0.00
95	$8.04 \cdot 10^{-1}$	$8.41 \cdot 10^{-2}$	$2.92 \cdot 10^{-4}$	$6.13 \cdot 10^{-4}$	$3.73 \cdot 10^{-2}$	0.00
100	$7.91 \cdot 10^{-1}$	$8.36 \cdot 10^{-2}$	$2.90 \cdot 10^{-4}$	$6.03 \cdot 10^{-4}$	$3.68 \cdot 10^{-2}$	0.00
105	$7.73 \cdot 10^{-1}$	$8.25 \cdot 10^{-2}$	$2.86 \cdot 10^{-4}$	$5.89 \cdot 10^{-4}$	$3.59 \cdot 10^{-2}$	0.00
110	$7.45 \cdot 10^{-1}$	$8.03 \cdot 10^{-2}$	$2.79 \cdot 10^{-4}$	$5.68 \cdot 10^{-4}$	$3.46 \cdot 10^{-2}$	0.00
115	$7.05 \cdot 10^{-1}$	$7.65 \cdot 10^{-2}$	$2.66 \cdot 10^{-4}$	$5.37 \cdot 10^{-4}$	$3.27 \cdot 10^{-2}$	0.00
120	$6.49 \cdot 10^{-1}$	$7.11 \cdot 10^{-2}$	$2.47 \cdot 10^{-4}$	$4.94 \cdot 10^{-4}$	$3.01 \cdot 10^{-2}$	0.00
125	$5.78 \cdot 10^{-1}$	$6.37 \cdot 10^{-2}$	$2.21 \cdot 10^{-4}$	$4.40 \cdot 10^{-4}$	$2.68 \cdot 10^{-2}$	0.00
130	$4.94 \cdot 10^{-1}$	$5.49 \cdot 10^{-2}$	$1.91 \cdot 10^{-4}$	$3.76 \cdot 10^{-4}$	$2.29 \cdot 10^{-2}$	0.00
135	$4.04 \cdot 10^{-1}$	$4.52 \cdot 10^{-2}$	$1.57 \cdot 10^{-4}$	$3.07 \cdot 10^{-4}$	$1.87 \cdot 10^{-2}$	0.00
140	$3.14 \cdot 10^{-1}$	$3.54 \cdot 10^{-2}$	$1.23 \cdot 10^{-4}$	$2.39 \cdot 10^{-4}$	$1.46 \cdot 10^{-2}$	0.00
145	$2.31 \cdot 10^{-1}$	$2.62 \cdot 10^{-2}$	$9.09 \cdot 10^{-5}$	$1.76 \cdot 10^{-4}$	$1.07 \cdot 10^{-2}$	0.00
150	$1.57 \cdot 10^{-1}$	$1.79 \cdot 10^{-2}$	$6.20 \cdot 10^{-5}$	$1.19 \cdot 10^{-4}$	$7.25 \cdot 10^{-3}$	0.00
155	$9.18 \cdot 10^{-2}$	$1.06 \cdot 10^{-2}$	$3.66 \cdot 10^{-5}$	$6.98 \cdot 10^{-5}$	$4.25 \cdot 10^{-3}$	0.00
160	$3.44 \cdot 10^{-2}$	$3.97 \cdot 10^{-3}$	$1.38 \cdot 10^{-5}$	$2.61 \cdot 10^{-5}$	$1.59 \cdot 10^{-3}$	0.00
165	$1.19 \cdot 10^{-2}$	$1.38 \cdot 10^{-3}$	$4.78 \cdot 10^{-6}$	$9.02 \cdot 10^{-6}$	$5.49 \cdot 10^{-4}$	0.00
170	$7.87 \cdot 10^{-3}$	$9.20 \cdot 10^{-4}$	$3.19 \cdot 10^{-6}$	$5.99 \cdot 10^{-6}$	$3.64 \cdot 10^{-4}$	0.00
175	$6.12 \cdot 10^{-3}$	$7.19 \cdot 10^{-4}$	$2.49 \cdot 10^{-6}$	$4.65 \cdot 10^{-6}$	$2.83 \cdot 10^{-4}$	0.00
180	$4.97 \cdot 10^{-3}$	$5.87 \cdot 10^{-4}$	$2.04 \cdot 10^{-6}$	$3.78 \cdot 10^{-6}$	$2.30 \cdot 10^{-4}$	0.00
185	$3.85 \cdot 10^{-3}$	$4.57 \cdot 10^{-4}$	$1.59 \cdot 10^{-6}$	$2.93 \cdot 10^{-6}$	$1.78 \cdot 10^{-4}$	0.00
190	$3.15 \cdot 10^{-3}$	$3.76 \cdot 10^{-4}$	$1.30 \cdot 10^{-6}$	$2.39 \cdot 10^{-6}$	$1.46 \cdot 10^{-4}$	0.00
195	$2.70 \cdot 10^{-3}$	$3.24 \cdot 10^{-4}$	$1.13 \cdot 10^{-6}$	$2.06 \cdot 10^{-6}$	$1.25 \cdot 10^{-4}$	0.00
200	$2.38 \cdot 10^{-3}$	$2.87 \cdot 10^{-4}$	$9.96 \cdot 10^{-7}$	$1.81 \cdot 10^{-6}$	$1.10 \cdot 10^{-4}$	0.00
210	$1.92 \cdot 10^{-3}$	$2.34 \cdot 10^{-4}$	$8.11 \cdot 10^{-7}$	$1.46 \cdot 10^{-6}$	$8.89 \cdot 10^{-5}$	0.00
220	$1.60 \cdot 10^{-3}$	$1.96 \cdot 10^{-4}$	$6.81 \cdot 10^{-7}$	$1.22 \cdot 10^{-6}$	$7.40 \cdot 10^{-5}$	0.00
230	$1.36 \cdot 10^{-3}$	$1.68 \cdot 10^{-4}$	$5.82 \cdot 10^{-7}$	$1.03 \cdot 10^{-6}$	$6.27 \cdot 10^{-5}$	0.00
240	$1.17 \cdot 10^{-3}$	$1.45 \cdot 10^{-4}$	$5.04 \cdot 10^{-7}$	$8.86 \cdot 10^{-7}$	$5.39 \cdot 10^{-5}$	0.00
250	$1.01 \cdot 10^{-3}$	$1.27 \cdot 10^{-4}$	$4.42 \cdot 10^{-7}$	$7.70 \cdot 10^{-7}$	$4.68 \cdot 10^{-5}$	0.00
260	$8.89 \cdot 10^{-4}$	$1.12 \cdot 10^{-4}$	$3.90 \cdot 10^{-7}$	$6.75 \cdot 10^{-7}$	$4.11 \cdot 10^{-5}$	$5.14 \cdot 10^{-8}$
270	$7.86 \cdot 10^{-4}$	$1.00 \cdot 10^{-4}$	$3.47 \cdot 10^{-7}$	$5.97 \cdot 10^{-7}$	$3.63 \cdot 10^{-5}$	$2.29 \cdot 10^{-6}$
280	$7.00 \cdot 10^{-4}$	$8.98 \cdot 10^{-5}$	$3.11 \cdot 10^{-7}$	$5.31 \cdot 10^{-7}$	$3.23 \cdot 10^{-5}$	$1.09 \cdot 10^{-5}$
290	$6.27 \cdot 10^{-4}$	$8.09 \cdot 10^{-5}$	$2.80 \cdot 10^{-7}$	$4.76 \cdot 10^{-7}$	$2.90 \cdot 10^{-5}$	$3.06 \cdot 10^{-5}$
300	$5.65 \cdot 10^{-4}$	$7.33 \cdot 10^{-5}$	$2.54 \cdot 10^{-7}$	$4.29 \cdot 10^{-7}$	$2.61 \cdot 10^{-5}$	$6.87 \cdot 10^{-5}$
310	$5.12 \cdot 10^{-4}$	$6.68 \cdot 10^{-5}$	$2.32 \cdot 10^{-7}$	$3.89 \cdot 10^{-7}$	$2.36 \cdot 10^{-5}$	$1.38 \cdot 10^{-4}$
320	$4.66 \cdot 10^{-4}$	$6.12 \cdot 10^{-5}$	$2.12 \cdot 10^{-7}$	$3.54 \cdot 10^{-7}$	$2.15 \cdot 10^{-5}$	$2.66 \cdot 10^{-4}$
330	$4.26 \cdot 10^{-4}$	$5.63 \cdot 10^{-5}$	$1.95 \cdot 10^{-7}$	$3.24 \cdot 10^{-7}$	$1.97 \cdot 10^{-5}$	$5.21 \cdot 10^{-4}$
340	$3.92 \cdot 10^{-4}$	$5.20 \cdot 10^{-5}$	$1.80 \cdot 10^{-7}$	$2.98 \cdot 10^{-7}$	$1.81 \cdot 10^{-5}$	$1.20 \cdot 10^{-3}$
350	$3.57 \cdot 10^{-4}$	$4.76 \cdot 10^{-5}$	$1.65 \cdot 10^{-7}$	$2.71 \cdot 10^{-7}$	$1.65 \cdot 10^{-5}$	$1.56 \cdot 10^{-2}$
360	$3.16 \cdot 10^{-4}$	$4.23 \cdot 10^{-5}$	$1.47 \cdot 10^{-7}$	$2.40 \cdot 10^{-7}$	$1.46 \cdot 10^{-5}$	$5.15 \cdot 10^{-2}$
370	$2.81 \cdot 10^{-4}$	$3.78 \cdot 10^{-5}$	$1.31 \cdot 10^{-7}$	$2.13 \cdot 10^{-7}$	$1.29 \cdot 10^{-5}$	$8.37 \cdot 10^{-2}$
380	$2.52 \cdot 10^{-4}$	$3.40 \cdot 10^{-5}$	$1.18 \cdot 10^{-7}$	$1.91 \cdot 10^{-7}$	$1.16 \cdot 10^{-5}$	$1.10 \cdot 10^{-1}$
390	$2.28 \cdot 10^{-4}$	$3.10 \cdot 10^{-5}$	$1.07 \cdot 10^{-7}$	$1.73 \cdot 10^{-7}$	$1.05 \cdot 10^{-5}$	$1.32 \cdot 10^{-1}$
400	$2.08 \cdot 10^{-4}$	$2.84 \cdot 10^{-5}$	$9.83 \cdot 10^{-8}$	$1.58 \cdot 10^{-7}$	$9.59 \cdot 10^{-6}$	$1.48 \cdot 10^{-1}$
410	$1.91 \cdot 10^{-4}$	$2.61 \cdot 10^{-5}$	$9.06 \cdot 10^{-8}$	$1.45 \cdot 10^{-7}$	$8.80 \cdot 10^{-6}$	$1.62 \cdot 10^{-1}$
420	$1.76 \cdot 10^{-4}$	$2.43 \cdot 10^{-5}$	$8.41 \cdot 10^{-8}$	$1.34 \cdot 10^{-7}$	$8.13 \cdot 10^{-6}$	$1.72 \cdot 10^{-1}$
430	$1.64 \cdot 10^{-4}$	$2.26 \cdot 10^{-5}$	$7.84 \cdot 10^{-8}$	$1.24 \cdot 10^{-7}$	$7.55 \cdot 10^{-6}$	$1.79 \cdot 10^{-1}$
440	$1.53 \cdot 10^{-4}$	$2.12 \cdot 10^{-5}$	$7.34 \cdot 10^{-8}$	$1.16 \cdot 10^{-7}$	$7.05 \cdot 10^{-6}$	$1.85 \cdot 10^{-1}$
450	$1.43 \cdot 10^{-4}$	$1.99 \cdot 10^{-5}$	$6.90 \cdot 10^{-8}$	$1.09 \cdot 10^{-7}$	$6.60 \cdot 10^{-6}$	$1.89 \cdot 10^{-1}$
460	$1.35 \cdot 10^{-4}$	$1.88 \cdot 10^{-5}$	$6.51 \cdot 10^{-8}$	$1.02 \cdot 10^{-7}$	$6.21 \cdot 10^{-6}$	$1.91 \cdot 10^{-1}$
470	$1.27 \cdot 10^{-4}$	$1.78 \cdot 10^{-5}$	$6.16 \cdot 10^{-8}$	$9.63 \cdot 10^{-8}$	$5.85 \cdot 10^{-6}$	$1.93 \cdot 10^{-1}$
480	$1.20 \cdot 10^{-4}$	$1.69 \cdot 10^{-5}$	$5.85 \cdot 10^{-8}$	$9.10 \cdot 10^{-8}$	$5.53 \cdot 10^{-6}$	$1.94 \cdot 10^{-1}$
490	$1.14 \cdot 10^{-4}$	$1.60 \cdot 10^{-5}$	$5.56 \cdot 10^{-8}$	$8.63 \cdot 10^{-8}$	$5.24 \cdot 10^{-6}$	$1.94 \cdot 10^{-1}$

Table 27: SM Higgs branching ratios in fermionic final states in the high-mass range.

M_H [GeV]	$H \to b\bar{b}$	$H \to \tau\tau$	$H \to \mu\mu$	$H \to s\bar{s}$	$H \to c\bar{c}$	$H \to t\bar{t}$
500	$1.08 \cdot 10^{-4}$	$1.53 \cdot 10^{-5}$	$5.30 \cdot 10^{-8}$	$8.19 \cdot 10^{-8}$	$4.98 \cdot 10^{-6}$	$1.93 \cdot 10^{-1}$
510	$1.03 \cdot 10^{-4}$	$1.46 \cdot 10^{-5}$	$5.06 \cdot 10^{-8}$	$7.80 \cdot 10^{-8}$	$4.74 \cdot 10^{-6}$	$1.92 \cdot 10^{-1}$
520	$9.80 \cdot 10^{-5}$	$1.40 \cdot 10^{-5}$	$4.84 \cdot 10^{-8}$	$7.44 \cdot 10^{-8}$	$4.52 \cdot 10^{-6}$	$1.90 \cdot 10^{-1}$
530	$9.36 \cdot 10^{-5}$	$1.34 \cdot 10^{-5}$	$4.64 \cdot 10^{-8}$	$7.10 \cdot 10^{-8}$	$4.31 \cdot 10^{-6}$	$1.88 \cdot 10^{-1}$
540	$8.95 \cdot 10^{-5}$	$1.28 \cdot 10^{-5}$	$4.45 \cdot 10^{-8}$	$6.79 \cdot 10^{-8}$	$4.12 \cdot 10^{-6}$	$1.86 \cdot 10^{-1}$
550	$8.57 \cdot 10^{-5}$	$1.23 \cdot 10^{-5}$	$4.27 \cdot 10^{-8}$	$6.50 \cdot 10^{-8}$	$3.95 \cdot 10^{-6}$	$1.84 \cdot 10^{-1}$
560	$8.21 \cdot 10^{-5}$	$1.18 \cdot 10^{-5}$	$4.10 \cdot 10^{-8}$	$6.23 \cdot 10^{-8}$	$3.79 \cdot 10^{-6}$	$1.81 \cdot 10^{-1}$
570	$7.88 \cdot 10^{-5}$	$1.14 \cdot 10^{-5}$	$3.95 \cdot 10^{-8}$	$5.98 \cdot 10^{-8}$	$3.63 \cdot 10^{-6}$	$1.78 \cdot 10^{-1}$
580	$7.57 \cdot 10^{-5}$	$1.10 \cdot 10^{-5}$	$3.80 \cdot 10^{-8}$	$5.74 \cdot 10^{-8}$	$3.49 \cdot 10^{-6}$	$1.75 \cdot 10^{-1}$
590	$7.28 \cdot 10^{-5}$	$1.06 \cdot 10^{-5}$	$3.67 \cdot 10^{-8}$	$5.52 \cdot 10^{-8}$	$3.35 \cdot 10^{-6}$	$1.72 \cdot 10^{-1}$
600	$7.00 \cdot 10^{-5}$	$1.02 \cdot 10^{-5}$	$3.54 \cdot 10^{-8}$	$5.31 \cdot 10^{-8}$	$3.23 \cdot 10^{-6}$	$1.69 \cdot 10^{-1}$
610	$6.74 \cdot 10^{-5}$	$9.86 \cdot 10^{-6}$	$3.42 \cdot 10^{-8}$	$5.12 \cdot 10^{-8}$	$3.11 \cdot 10^{-6}$	$1.66 \cdot 10^{-1}$
620	$6.50 \cdot 10^{-5}$	$9.53 \cdot 10^{-6}$	$3.30 \cdot 10^{-8}$	$4.93 \cdot 10^{-8}$	$2.99 \cdot 10^{-6}$	$1.63 \cdot 10^{-1}$
630	$6.27 \cdot 10^{-5}$	$9.21 \cdot 10^{-6}$	$3.19 \cdot 10^{-8}$	$4.76 \cdot 10^{-8}$	$2.89 \cdot 10^{-6}$	$1.60 \cdot 10^{-1}$
640	$6.05 \cdot 10^{-5}$	$8.91 \cdot 10^{-6}$	$3.09 \cdot 10^{-8}$	$4.59 \cdot 10^{-8}$	$2.79 \cdot 10^{-6}$	$1.57 \cdot 10^{-1}$
650	$5.84 \cdot 10^{-5}$	$8.63 \cdot 10^{-6}$	$2.99 \cdot 10^{-8}$	$4.43 \cdot 10^{-8}$	$2.69 \cdot 10^{-6}$	$1.54 \cdot 10^{-1}$
660	$5.64 \cdot 10^{-5}$	$8.35 \cdot 10^{-6}$	$2.89 \cdot 10^{-8}$	$4.28 \cdot 10^{-8}$	$2.60 \cdot 10^{-6}$	$1.50 \cdot 10^{-1}$
670	$5.45 \cdot 10^{-5}$	$8.09 \cdot 10^{-6}$	$2.80 \cdot 10^{-8}$	$4.14 \cdot 10^{-8}$	$2.51 \cdot 10^{-6}$	$1.47 \cdot 10^{-1}$
680	$5.27 \cdot 10^{-5}$	$7.84 \cdot 10^{-6}$	$2.72 \cdot 10^{-8}$	$4.00 \cdot 10^{-8}$	$2.43 \cdot 10^{-6}$	$1.44 \cdot 10^{-1}$
690	$5.10 \cdot 10^{-5}$	$7.60 \cdot 10^{-6}$	$2.64 \cdot 10^{-8}$	$3.87 \cdot 10^{-8}$	$2.35 \cdot 10^{-6}$	$1.41 \cdot 10^{-1}$
700	$4.94 \cdot 10^{-5}$	$7.37 \cdot 10^{-6}$	$2.56 \cdot 10^{-8}$	$3.74 \cdot 10^{-8}$	$2.27 \cdot 10^{-6}$	$1.38 \cdot 10^{-1}$
710	$4.78 \cdot 10^{-5}$	$7.16 \cdot 10^{-6}$	$2.48 \cdot 10^{-8}$	$3.62 \cdot 10^{-8}$	$2.20 \cdot 10^{-6}$	$1.35 \cdot 10^{-1}$
720	$4.63 \cdot 10^{-5}$	$6.94 \cdot 10^{-6}$	$2.41 \cdot 10^{-8}$	$3.51 \cdot 10^{-8}$	$2.13 \cdot 10^{-6}$	$1.32 \cdot 10^{-1}$
730	$4.48 \cdot 10^{-5}$	$6.74 \cdot 10^{-6}$	$2.34 \cdot 10^{-8}$	$3.40 \cdot 10^{-8}$	$2.07 \cdot 10^{-6}$	$1.29 \cdot 10^{-1}$
740	$4.34 \cdot 10^{-5}$	$6.55 \cdot 10^{-6}$	$2.27 \cdot 10^{-8}$	$3.30 \cdot 10^{-8}$	$2.00 \cdot 10^{-6}$	$1.26 \cdot 10^{-1}$
750	$4.21 \cdot 10^{-5}$	$6.36 \cdot 10^{-6}$	$2.20 \cdot 10^{-8}$	$3.19 \cdot 10^{-8}$	$1.94 \cdot 10^{-6}$	$1.23 \cdot 10^{-1}$
760	$4.08 \cdot 10^{-5}$	$6.18 \cdot 10^{-6}$	$2.14 \cdot 10^{-8}$	$3.10 \cdot 10^{-8}$	$1.88 \cdot 10^{-6}$	$1.21 \cdot 10^{-1}$
770	$3.96 \cdot 10^{-5}$	$6.00 \cdot 10^{-6}$	$2.08 \cdot 10^{-8}$	$3.00 \cdot 10^{-8}$	$1.82 \cdot 10^{-6}$	$1.18 \cdot 10^{-1}$
780	$3.84 \cdot 10^{-5}$	$5.83 \cdot 10^{-6}$	$2.02 \cdot 10^{-8}$	$2.91 \cdot 10^{-8}$	$1.77 \cdot 10^{-6}$	$1.15 \cdot 10^{-1}$
790	$3.73 \cdot 10^{-5}$	$5.67 \cdot 10^{-6}$	$1.97 \cdot 10^{-8}$	$2.83 \cdot 10^{-8}$	$1.72 \cdot 10^{-6}$	$1.13 \cdot 10^{-1}$
800	$3.62 \cdot 10^{-5}$	$5.52 \cdot 10^{-6}$	$1.91 \cdot 10^{-8}$	$2.74 \cdot 10^{-8}$	$1.67 \cdot 10^{-6}$	$1.10 \cdot 10^{-1}$
810	$3.51 \cdot 10^{-5}$	$5.36 \cdot 10^{-6}$	$1.86 \cdot 10^{-8}$	$2.66 \cdot 10^{-8}$	$1.62 \cdot 10^{-6}$	$1.07 \cdot 10^{-1}$
820	$3.41 \cdot 10^{-5}$	$5.22 \cdot 10^{-6}$	$1.81 \cdot 10^{-8}$	$2.58 \cdot 10^{-8}$	$1.57 \cdot 10^{-6}$	$1.05 \cdot 10^{-1}$
830	$3.31 \cdot 10^{-5}$	$5.07 \cdot 10^{-6}$	$1.76 \cdot 10^{-8}$	$2.51 \cdot 10^{-8}$	$1.52 \cdot 10^{-6}$	$1.02 \cdot 10^{-1}$
840	$3.21 \cdot 10^{-5}$	$4.93 \cdot 10^{-6}$	$1.71 \cdot 10^{-8}$	$2.44 \cdot 10^{-8}$	$1.48 \cdot 10^{-6}$	$1.00 \cdot 10^{-1}$
850	$3.12 \cdot 10^{-5}$	$4.80 \cdot 10^{-6}$	$1.66 \cdot 10^{-8}$	$2.37 \cdot 10^{-8}$	$1.44 \cdot 10^{-6}$	$9.77 \cdot 10^{-2}$
860	$3.03 \cdot 10^{-5}$	$4.67 \cdot 10^{-6}$	$1.62 \cdot 10^{-8}$	$2.30 \cdot 10^{-8}$	$1.40 \cdot 10^{-6}$	$9.54 \cdot 10^{-2}$
870	$2.94 \cdot 10^{-5}$	$4.55 \cdot 10^{-6}$	$1.58 \cdot 10^{-8}$	$2.23 \cdot 10^{-8}$	$1.36 \cdot 10^{-6}$	$9.31 \cdot 10^{-2}$
880	$2.86 \cdot 10^{-5}$	$4.42 \cdot 10^{-6}$	$1.53 \cdot 10^{-8}$	$2.17 \cdot 10^{-8}$	$1.32 \cdot 10^{-6}$	$9.09 \cdot 10^{-2}$
890	$2.78 \cdot 10^{-5}$	$4.31 \cdot 10^{-6}$	$1.49 \cdot 10^{-8}$	$2.11 \cdot 10^{-8}$	$1.28 \cdot 10^{-6}$	$8.87 \cdot 10^{-2}$
900	$2.70 \cdot 10^{-5}$	$4.19 \cdot 10^{-6}$	$1.45 \cdot 10^{-8}$	$2.05 \cdot 10^{-8}$	$1.24 \cdot 10^{-6}$	$8.66 \cdot 10^{-2}$
910	$2.62 \cdot 10^{-5}$	$4.08 \cdot 10^{-6}$	$1.41 \cdot 10^{-8}$	$1.99 \cdot 10^{-8}$	$1.21 \cdot 10^{-6}$	$8.45 \cdot 10^{-2}$
920	$2.55 \cdot 10^{-5}$	$3.97 \cdot 10^{-6}$	$1.38 \cdot 10^{-8}$	$1.93 \cdot 10^{-8}$	$1.17 \cdot 10^{-6}$	$8.24 \cdot 10^{-2}$
930	$2.48 \cdot 10^{-5}$	$3.86 \cdot 10^{-6}$	$1.34 \cdot 10^{-8}$	$1.88 \cdot 10^{-8}$	$1.14 \cdot 10^{-6}$	$8.04 \cdot 10^{-2}$
940	$2.41 \cdot 10^{-5}$	$3.76 \cdot 10^{-6}$	$1.30 \cdot 10^{-8}$	$1.83 \cdot 10^{-8}$	$1.11 \cdot 10^{-6}$	$7.84 \cdot 10^{-2}$
950	$2.34 \cdot 10^{-5}$	$3.66 \cdot 10^{-6}$	$1.27 \cdot 10^{-8}$	$1.77 \cdot 10^{-8}$	$1.08 \cdot 10^{-6}$	$7.65 \cdot 10^{-2}$
960	$2.27 \cdot 10^{-5}$	$3.56 \cdot 10^{-6}$	$1.23 \cdot 10^{-8}$	$1.72 \cdot 10^{-8}$	$1.05 \cdot 10^{-6}$	$7.46 \cdot 10^{-2}$
970	$2.21 \cdot 10^{-5}$	$3.47 \cdot 10^{-6}$	$1.20 \cdot 10^{-8}$	$1.68 \cdot 10^{-8}$	$1.02 \cdot 10^{-6}$	$7.27 \cdot 10^{-2}$
980	$2.15 \cdot 10^{-5}$	$3.38 \cdot 10^{-6}$	$1.17 \cdot 10^{-8}$	$1.63 \cdot 10^{-8}$	$9.88 \cdot 10^{-7}$	$7.09 \cdot 10^{-2}$
990	$2.09 \cdot 10^{-5}$	$3.29 \cdot 10^{-6}$	$1.14 \cdot 10^{-8}$	$1.58 \cdot 10^{-8}$	$9.61 \cdot 10^{-7}$	$6.91 \cdot 10^{-2}$
1000	$2.03 \cdot 10^{-5}$	$3.20 \cdot 10^{-6}$	$1.11 \cdot 10^{-8}$	$1.54 \cdot 10^{-8}$	$9.34 \cdot 10^{-7}$	$6.74 \cdot 10^{-2}$

Table 28: SM Higgs branching ratios in bosonic final states and Higgs total widths in the low- and intermediate-mass range.

M_H [GeV]	$H \to gg$	$H \to \gamma\gamma$	$H \to Z\gamma$	$H \to WW$	$H \to ZZ$	Total Γ_H [GeV]
90	$6.12 \cdot 10^{-2}$	$1.23 \cdot 10^{-3}$	0.00	$2.09 \cdot 10^{-3}$	$4.21 \cdot 10^{-4}$	$2.20 \cdot 10^{-3}$
95	$6.74 \cdot 10^{-2}$	$1.40 \cdot 10^{-3}$	$4.52 \cdot 10^{-6}$	$4.72 \cdot 10^{-3}$	$6.72 \cdot 10^{-4}$	$2.32 \cdot 10^{-3}$
100	$7.37 \cdot 10^{-2}$	$1.59 \cdot 10^{-3}$	$4.98 \cdot 10^{-5}$	$1.11 \cdot 10^{-2}$	$1.13 \cdot 10^{-3}$	$2.46 \cdot 10^{-3}$
105	$7.95 \cdot 10^{-2}$	$1.78 \cdot 10^{-3}$	$1.73 \cdot 10^{-4}$	$2.43 \cdot 10^{-2}$	$2.15 \cdot 10^{-3}$	$2.62 \cdot 10^{-3}$
110	$8.44 \cdot 10^{-2}$	$1.97 \cdot 10^{-3}$	$3.95 \cdot 10^{-4}$	$4.82 \cdot 10^{-2}$	$4.39 \cdot 10^{-3}$	$2.82 \cdot 10^{-3}$
115	$8.76 \cdot 10^{-2}$	$2.13 \cdot 10^{-3}$	$7.16 \cdot 10^{-4}$	$8.67 \cdot 10^{-2}$	$8.73 \cdot 10^{-3}$	$3.09 \cdot 10^{-3}$
120	$8.82 \cdot 10^{-2}$	$2.25 \cdot 10^{-3}$	$1.12 \cdot 10^{-3}$	$1.43 \cdot 10^{-1}$	$1.60 \cdot 10^{-2}$	$3.47 \cdot 10^{-3}$
125	$8.56 \cdot 10^{-2}$	$2.30 \cdot 10^{-3}$	$1.55 \cdot 10^{-3}$	$2.16 \cdot 10^{-1}$	$2.67 \cdot 10^{-2}$	$4.03 \cdot 10^{-3}$
130	$7.96 \cdot 10^{-2}$	$2.26 \cdot 10^{-3}$	$1.96 \cdot 10^{-3}$	$3.05 \cdot 10^{-1}$	$4.02 \cdot 10^{-2}$	$4.87 \cdot 10^{-3}$
135	$7.06 \cdot 10^{-2}$	$2.14 \cdot 10^{-3}$	$2.28 \cdot 10^{-3}$	$4.03 \cdot 10^{-1}$	$5.51 \cdot 10^{-2}$	$6.14 \cdot 10^{-3}$
140	$5.94 \cdot 10^{-2}$	$1.94 \cdot 10^{-3}$	$2.47 \cdot 10^{-3}$	$5.04 \cdot 10^{-1}$	$6.92 \cdot 10^{-2}$	$8.12 \cdot 10^{-3}$
145	$4.70 \cdot 10^{-2}$	$1.68 \cdot 10^{-3}$	$2.49 \cdot 10^{-3}$	$6.03 \cdot 10^{-1}$	$7.96 \cdot 10^{-2}$	$1.14 \cdot 10^{-2}$
150	$3.43 \cdot 10^{-2}$	$1.37 \cdot 10^{-3}$	$2.32 \cdot 10^{-3}$	$6.99 \cdot 10^{-1}$	$8.28 \cdot 10^{-2}$	$1.73 \cdot 10^{-2}$
155	$2.16 \cdot 10^{-2}$	$1.00 \cdot 10^{-3}$	$1.91 \cdot 10^{-3}$	$7.96 \cdot 10^{-1}$	$7.36 \cdot 10^{-2}$	$3.02 \cdot 10^{-2}$
160	$8.57 \cdot 10^{-3}$	$5.33 \cdot 10^{-4}$	$1.15 \cdot 10^{-3}$	$9.09 \cdot 10^{-1}$	$4.16 \cdot 10^{-2}$	$8.29 \cdot 10^{-2}$
165	$3.11 \cdot 10^{-3}$	$2.30 \cdot 10^{-4}$	$5.45 \cdot 10^{-4}$	$9.60 \cdot 10^{-1}$	$2.22 \cdot 10^{-2}$	$2.46 \cdot 10^{-1}$
170	$2.18 \cdot 10^{-3}$	$1.58 \cdot 10^{-4}$	$4.00 \cdot 10^{-4}$	$9.65 \cdot 10^{-1}$	$2.36 \cdot 10^{-2}$	$3.80 \cdot 10^{-1}$
175	$1.80 \cdot 10^{-3}$	$1.23 \cdot 10^{-4}$	$3.38 \cdot 10^{-4}$	$9.58 \cdot 10^{-1}$	$3.23 \cdot 10^{-2}$	$5.00 \cdot 10^{-1}$
180	$1.54 \cdot 10^{-3}$	$1.02 \cdot 10^{-4}$	$2.96 \cdot 10^{-4}$	$9.32 \cdot 10^{-1}$	$6.02 \cdot 10^{-2}$	$6.31 \cdot 10^{-1}$
185	$1.26 \cdot 10^{-3}$	$8.09 \cdot 10^{-5}$	$2.44 \cdot 10^{-4}$	$8.44 \cdot 10^{-1}$	$1.50 \cdot 10^{-1}$	$8.32 \cdot 10^{-1}$
190	$1.08 \cdot 10^{-3}$	$6.74 \cdot 10^{-5}$	$2.11 \cdot 10^{-4}$	$7.86 \cdot 10^{-1}$	$2.09 \cdot 10^{-1}$	1.04
195	$9.84 \cdot 10^{-4}$	$5.89 \cdot 10^{-5}$	$1.91 \cdot 10^{-4}$	$7.57 \cdot 10^{-1}$	$2.39 \cdot 10^{-1}$	1.24
200	$9.16 \cdot 10^{-4}$	$5.26 \cdot 10^{-5}$	$1.75 \cdot 10^{-4}$	$7.41 \cdot 10^{-1}$	$2.56 \cdot 10^{-1}$	1.43
210	$8.27 \cdot 10^{-4}$	$4.34 \cdot 10^{-5}$	$1.52 \cdot 10^{-4}$	$7.23 \cdot 10^{-1}$	$2.74 \cdot 10^{-1}$	1.85
220	$7.69 \cdot 10^{-4}$	$3.67 \cdot 10^{-5}$	$1.34 \cdot 10^{-4}$	$7.14 \cdot 10^{-1}$	$2.84 \cdot 10^{-1}$	2.31
230	$7.27 \cdot 10^{-4}$	$3.14 \cdot 10^{-5}$	$1.19 \cdot 10^{-4}$	$7.08 \cdot 10^{-1}$	$2.89 \cdot 10^{-1}$	2.82
240	$6.97 \cdot 10^{-4}$	$2.72 \cdot 10^{-5}$	$1.07 \cdot 10^{-4}$	$7.04 \cdot 10^{-1}$	$2.94 \cdot 10^{-1}$	3.40
250	$6.75 \cdot 10^{-4}$	$2.37 \cdot 10^{-5}$	$9.54 \cdot 10^{-5}$	$7.01 \cdot 10^{-1}$	$2.97 \cdot 10^{-1}$	4.04
260	$6.59 \cdot 10^{-4}$	$2.08 \cdot 10^{-5}$	$8.57 \cdot 10^{-5}$	$6.99 \cdot 10^{-1}$	$2.99 \cdot 10^{-1}$	4.76
270	$6.48 \cdot 10^{-4}$	$1.84 \cdot 10^{-5}$	$7.72 \cdot 10^{-5}$	$6.97 \cdot 10^{-1}$	$3.02 \cdot 10^{-1}$	5.55
280	$6.42 \cdot 10^{-4}$	$1.63 \cdot 10^{-5}$	$6.98 \cdot 10^{-5}$	$6.95 \cdot 10^{-1}$	$3.04 \cdot 10^{-1}$	6.43
290	$6.42 \cdot 10^{-4}$	$1.45 \cdot 10^{-5}$	$6.32 \cdot 10^{-5}$	$6.93 \cdot 10^{-1}$	$3.05 \cdot 10^{-1}$	7.39
300	$6.46 \cdot 10^{-4}$	$1.30 \cdot 10^{-5}$	$5.75 \cdot 10^{-5}$	$6.92 \cdot 10^{-1}$	$3.07 \cdot 10^{-1}$	8.43
310	$6.56 \cdot 10^{-4}$	$1.17 \cdot 10^{-5}$	$5.24 \cdot 10^{-5}$	$6.90 \cdot 10^{-1}$	$3.08 \cdot 10^{-1}$	9.57
320	$6.73 \cdot 10^{-4}$	$1.05 \cdot 10^{-5}$	$4.79 \cdot 10^{-5}$	$6.89 \cdot 10^{-1}$	$3.09 \cdot 10^{-1}$	10.8
330	$6.99 \cdot 10^{-4}$	$9.56 \cdot 10^{-6}$	$4.39 \cdot 10^{-5}$	$6.88 \cdot 10^{-1}$	$3.10 \cdot 10^{-1}$	12.1
340	$7.42 \cdot 10^{-4}$	$8.73 \cdot 10^{-6}$	$4.04 \cdot 10^{-5}$	$6.87 \cdot 10^{-1}$	$3.11 \cdot 10^{-1}$	13.5
350	$8.05 \cdot 10^{-4}$	$7.62 \cdot 10^{-6}$	$3.65 \cdot 10^{-5}$	$6.76 \cdot 10^{-1}$	$3.07 \cdot 10^{-1}$	15.2
360	$8.42 \cdot 10^{-4}$	$6.10 \cdot 10^{-6}$	$3.17 \cdot 10^{-5}$	$6.51 \cdot 10^{-1}$	$2.97 \cdot 10^{-1}$	17.6
370	$8.54 \cdot 10^{-4}$	$4.85 \cdot 10^{-6}$	$2.76 \cdot 10^{-5}$	$6.28 \cdot 10^{-1}$	$2.87 \cdot 10^{-1}$	20.2
380	$8.51 \cdot 10^{-4}$	$3.86 \cdot 10^{-6}$	$2.42 \cdot 10^{-5}$	$6.09 \cdot 10^{-1}$	$2.79 \cdot 10^{-1}$	23.1
390	$8.40 \cdot 10^{-4}$	$3.09 \cdot 10^{-6}$	$2.14 \cdot 10^{-5}$	$5.94 \cdot 10^{-1}$	$2.73 \cdot 10^{-1}$	26.1
400	$8.22 \cdot 10^{-4}$	$2.47 \cdot 10^{-6}$	$1.90 \cdot 10^{-5}$	$5.82 \cdot 10^{-1}$	$2.69 \cdot 10^{-1}$	29.2
410	$8.02 \cdot 10^{-4}$	$1.98 \cdot 10^{-6}$	$1.70 \cdot 10^{-5}$	$5.72 \cdot 10^{-1}$	$2.65 \cdot 10^{-1}$	32.5
420	$7.80 \cdot 10^{-4}$	$1.60 \cdot 10^{-6}$	$1.53 \cdot 10^{-5}$	$5.64 \cdot 10^{-1}$	$2.63 \cdot 10^{-1}$	35.9
430	$7.56 \cdot 10^{-4}$	$1.28 \cdot 10^{-6}$	$1.38 \cdot 10^{-5}$	$5.59 \cdot 10^{-1}$	$2.61 \cdot 10^{-1}$	39.4
440	$7.33 \cdot 10^{-4}$	$1.03 \cdot 10^{-6}$	$1.26 \cdot 10^{-5}$	$5.54 \cdot 10^{-1}$	$2.60 \cdot 10^{-1}$	43.1
450	$7.09 \cdot 10^{-4}$	$8.27 \cdot 10^{-7}$	$1.15 \cdot 10^{-5}$	$5.51 \cdot 10^{-1}$	$2.59 \cdot 10^{-1}$	46.9
460	$6.85 \cdot 10^{-4}$	$6.62 \cdot 10^{-7}$	$1.05 \cdot 10^{-5}$	$5.49 \cdot 10^{-1}$	$2.59 \cdot 10^{-1}$	50.8
470	$6.62 \cdot 10^{-4}$	$5.29 \cdot 10^{-7}$	$9.64 \cdot 10^{-6}$	$5.47 \cdot 10^{-1}$	$2.59 \cdot 10^{-1}$	54.9
480	$6.39 \cdot 10^{-4}$	$4.21 \cdot 10^{-7}$	$8.87 \cdot 10^{-6}$	$5.46 \cdot 10^{-1}$	$2.59 \cdot 10^{-1}$	59.1
490	$6.17 \cdot 10^{-4}$	$3.34 \cdot 10^{-7}$	$8.19 \cdot 10^{-6}$	$5.46 \cdot 10^{-1}$	$2.60 \cdot 10^{-1}$	63.5

Table 29: SM Higgs branching ratios in bosonic final states and Higgs total widths in the high-mass range.

| M_H [GeV]	H → gg	H → γγ	H → Zγ	H → WW	H → ZZ	Total Γ_H [GeV]
500	$5.96 \cdot 10^{-4}$	$2.64 \cdot 10^{-7}$	$7.58 \cdot 10^{-6}$	$5.46 \cdot 10^{-1}$	$2.61 \cdot 10^{-1}$	68.0
510	$5.75 \cdot 10^{-4}$	$2.09 \cdot 10^{-7}$	$7.03 \cdot 10^{-6}$	$5.46 \cdot 10^{-1}$	$2.61 \cdot 10^{-1}$	72.7
520	$5.55 \cdot 10^{-4}$	$1.65 \cdot 10^{-7}$	$6.53 \cdot 10^{-6}$	$5.47 \cdot 10^{-1}$	$2.62 \cdot 10^{-1}$	77.6
530	$5.36 \cdot 10^{-4}$	$1.30 \cdot 10^{-7}$	$6.08 \cdot 10^{-6}$	$5.48 \cdot 10^{-1}$	$2.63 \cdot 10^{-1}$	82.6
540	$5.17 \cdot 10^{-4}$	$1.04 \cdot 10^{-7}$	$5.67 \cdot 10^{-6}$	$5.49 \cdot 10^{-1}$	$2.65 \cdot 10^{-1}$	87.7
550	$4.99 \cdot 10^{-4}$	$8.52 \cdot 10^{-8}$	$5.30 \cdot 10^{-6}$	$5.50 \cdot 10^{-1}$	$2.66 \cdot 10^{-1}$	93.1
560	$4.82 \cdot 10^{-4}$	$7.16 \cdot 10^{-8}$	$4.95 \cdot 10^{-6}$	$5.51 \cdot 10^{-1}$	$2.67 \cdot 10^{-1}$	98.7
570	$4.65 \cdot 10^{-4}$	$6.28 \cdot 10^{-8}$	$4.64 \cdot 10^{-6}$	$5.53 \cdot 10^{-1}$	$2.68 \cdot 10^{-1}$	104
580	$4.49 \cdot 10^{-4}$	$5.80 \cdot 10^{-8}$	$4.35 \cdot 10^{-6}$	$5.55 \cdot 10^{-1}$	$2.70 \cdot 10^{-1}$	110
590	$4.34 \cdot 10^{-4}$	$5.64 \cdot 10^{-8}$	$4.08 \cdot 10^{-6}$	$5.56 \cdot 10^{-1}$	$2.71 \cdot 10^{-1}$	116
600	$4.19 \cdot 10^{-4}$	$5.77 \cdot 10^{-8}$	$3.84 \cdot 10^{-6}$	$5.58 \cdot 10^{-1}$	$2.72 \cdot 10^{-1}$	123
610	$4.04 \cdot 10^{-4}$	$6.12 \cdot 10^{-8}$	$3.61 \cdot 10^{-6}$	$5.60 \cdot 10^{-1}$	$2.73 \cdot 10^{-1}$	129
620	$3.90 \cdot 10^{-4}$	$6.66 \cdot 10^{-8}$	$3.40 \cdot 10^{-6}$	$5.62 \cdot 10^{-1}$	$2.75 \cdot 10^{-1}$	136
630	$3.77 \cdot 10^{-4}$	$7.36 \cdot 10^{-8}$	$3.21 \cdot 10^{-6}$	$5.64 \cdot 10^{-1}$	$2.76 \cdot 10^{-1}$	143
640	$3.65 \cdot 10^{-4}$	$8.19 \cdot 10^{-8}$	$3.03 \cdot 10^{-6}$	$5.66 \cdot 10^{-1}$	$2.77 \cdot 10^{-1}$	150
650	$3.52 \cdot 10^{-4}$	$9.12 \cdot 10^{-8}$	$2.86 \cdot 10^{-6}$	$5.67 \cdot 10^{-1}$	$2.79 \cdot 10^{-1}$	158
660	$3.40 \cdot 10^{-4}$	$1.01 \cdot 10^{-7}$	$2.70 \cdot 10^{-6}$	$5.69 \cdot 10^{-1}$	$2.80 \cdot 10^{-1}$	166
670	$3.29 \cdot 10^{-4}$	$1.12 \cdot 10^{-7}$	$2.56 \cdot 10^{-6}$	$5.71 \cdot 10^{-1}$	$2.81 \cdot 10^{-1}$	174
680	$3.18 \cdot 10^{-4}$	$1.23 \cdot 10^{-7}$	$2.42 \cdot 10^{-6}$	$5.73 \cdot 10^{-1}$	$2.82 \cdot 10^{-1}$	182
690	$3.07 \cdot 10^{-4}$	$1.35 \cdot 10^{-7}$	$2.29 \cdot 10^{-6}$	$5.75 \cdot 10^{-1}$	$2.83 \cdot 10^{-1}$	190
700	$2.97 \cdot 10^{-4}$	$1.47 \cdot 10^{-7}$	$2.18 \cdot 10^{-6}$	$5.77 \cdot 10^{-1}$	$2.85 \cdot 10^{-1}$	199
710	$2.87 \cdot 10^{-4}$	$1.59 \cdot 10^{-7}$	$2.06 \cdot 10^{-6}$	$5.79 \cdot 10^{-1}$	$2.86 \cdot 10^{-1}$	208
720	$2.78 \cdot 10^{-4}$	$1.71 \cdot 10^{-7}$	$1.96 \cdot 10^{-6}$	$5.81 \cdot 10^{-1}$	$2.87 \cdot 10^{-1}$	218
730	$2.69 \cdot 10^{-4}$	$1.83 \cdot 10^{-7}$	$1.86 \cdot 10^{-6}$	$5.82 \cdot 10^{-1}$	$2.88 \cdot 10^{-1}$	227
740	$2.60 \cdot 10^{-4}$	$1.95 \cdot 10^{-7}$	$1.77 \cdot 10^{-6}$	$5.84 \cdot 10^{-1}$	$2.89 \cdot 10^{-1}$	237
750	$2.51 \cdot 10^{-4}$	$2.07 \cdot 10^{-7}$	$1.69 \cdot 10^{-6}$	$5.86 \cdot 10^{-1}$	$2.90 \cdot 10^{-1}$	248
760	$2.43 \cdot 10^{-4}$	$2.19 \cdot 10^{-7}$	$1.61 \cdot 10^{-6}$	$5.88 \cdot 10^{-1}$	$2.91 \cdot 10^{-1}$	258
770	$2.36 \cdot 10^{-4}$	$2.30 \cdot 10^{-7}$	$1.53 \cdot 10^{-6}$	$5.89 \cdot 10^{-1}$	$2.92 \cdot 10^{-1}$	269
780	$2.28 \cdot 10^{-4}$	$2.41 \cdot 10^{-7}$	$1.46 \cdot 10^{-6}$	$5.91 \cdot 10^{-1}$	$2.93 \cdot 10^{-1}$	281
790	$2.21 \cdot 10^{-4}$	$2.53 \cdot 10^{-7}$	$1.40 \cdot 10^{-6}$	$5.93 \cdot 10^{-1}$	$2.94 \cdot 10^{-1}$	292
800	$2.14 \cdot 10^{-4}$	$2.63 \cdot 10^{-7}$	$1.33 \cdot 10^{-6}$	$5.94 \cdot 10^{-1}$	$2.95 \cdot 10^{-1}$	304
810	$2.07 \cdot 10^{-4}$	$2.74 \cdot 10^{-7}$	$1.27 \cdot 10^{-6}$	$5.96 \cdot 10^{-1}$	$2.96 \cdot 10^{-1}$	317
820	$2.00 \cdot 10^{-4}$	$2.84 \cdot 10^{-7}$	$1.22 \cdot 10^{-6}$	$5.97 \cdot 10^{-1}$	$2.97 \cdot 10^{-1}$	330
830	$1.94 \cdot 10^{-4}$	$2.94 \cdot 10^{-7}$	$1.16 \cdot 10^{-6}$	$5.99 \cdot 10^{-1}$	$2.98 \cdot 10^{-1}$	343
840	$1.88 \cdot 10^{-4}$	$3.04 \cdot 10^{-7}$	$1.12 \cdot 10^{-6}$	$6.01 \cdot 10^{-1}$	$2.99 \cdot 10^{-1}$	357
850	$1.82 \cdot 10^{-4}$	$3.13 \cdot 10^{-7}$	$1.07 \cdot 10^{-6}$	$6.02 \cdot 10^{-1}$	$3.00 \cdot 10^{-1}$	371
860	$1.76 \cdot 10^{-4}$	$3.22 \cdot 10^{-7}$	$1.02 \cdot 10^{-6}$	$6.03 \cdot 10^{-1}$	$3.01 \cdot 10^{-1}$	386
870	$1.71 \cdot 10^{-4}$	$3.30 \cdot 10^{-7}$	$9.83 \cdot 10^{-7}$	$6.05 \cdot 10^{-1}$	$3.02 \cdot 10^{-1}$	401
880	$1.65 \cdot 10^{-4}$	$3.39 \cdot 10^{-7}$	$9.44 \cdot 10^{-7}$	$6.06 \cdot 10^{-1}$	$3.03 \cdot 10^{-1}$	416
890	$1.60 \cdot 10^{-4}$	$3.47 \cdot 10^{-7}$	$9.07 \cdot 10^{-7}$	$6.08 \cdot 10^{-1}$	$3.03 \cdot 10^{-1}$	432
900	$1.55 \cdot 10^{-4}$	$3.54 \cdot 10^{-7}$	$8.72 \cdot 10^{-7}$	$6.09 \cdot 10^{-1}$	$3.04 \cdot 10^{-1}$	449
910	$1.50 \cdot 10^{-4}$	$3.61 \cdot 10^{-7}$	$8.38 \cdot 10^{-7}$	$6.10 \cdot 10^{-1}$	$3.05 \cdot 10^{-1}$	466
920	$1.46 \cdot 10^{-4}$	$3.67 \cdot 10^{-7}$	$8.07 \cdot 10^{-7}$	$6.12 \cdot 10^{-1}$	$3.06 \cdot 10^{-1}$	484
930	$1.41 \cdot 10^{-4}$	$3.75 \cdot 10^{-7}$	$7.77 \cdot 10^{-7}$	$6.13 \cdot 10^{-1}$	$3.06 \cdot 10^{-1}$	502
940	$1.37 \cdot 10^{-4}$	$3.81 \cdot 10^{-7}$	$7.49 \cdot 10^{-7}$	$6.14 \cdot 10^{-1}$	$3.07 \cdot 10^{-1}$	521
950	$1.33 \cdot 10^{-4}$	$3.87 \cdot 10^{-7}$	$7.22 \cdot 10^{-7}$	$6.16 \cdot 10^{-1}$	$3.08 \cdot 10^{-1}$	540
960	$1.29 \cdot 10^{-4}$	$3.93 \cdot 10^{-7}$	$6.97 \cdot 10^{-7}$	$6.17 \cdot 10^{-1}$	$3.08 \cdot 10^{-1}$	560
970	$1.25 \cdot 10^{-4}$	$3.98 \cdot 10^{-7}$	$6.73 \cdot 10^{-7}$	$6.18 \cdot 10^{-1}$	$3.09 \cdot 10^{-1}$	581
980	$1.21 \cdot 10^{-4}$	$4.03 \cdot 10^{-7}$	$6.50 \cdot 10^{-7}$	$6.19 \cdot 10^{-1}$	$3.10 \cdot 10^{-1}$	602
990	$1.17 \cdot 10^{-4}$	$4.07 \cdot 10^{-7}$	$6.29 \cdot 10^{-7}$	$6.20 \cdot 10^{-1}$	$3.10 \cdot 10^{-1}$	624
1000	$1.14 \cdot 10^{-4}$	$4.12 \cdot 10^{-7}$	$6.08 \cdot 10^{-7}$	$6.21 \cdot 10^{-1}$	$3.11 \cdot 10^{-1}$	647
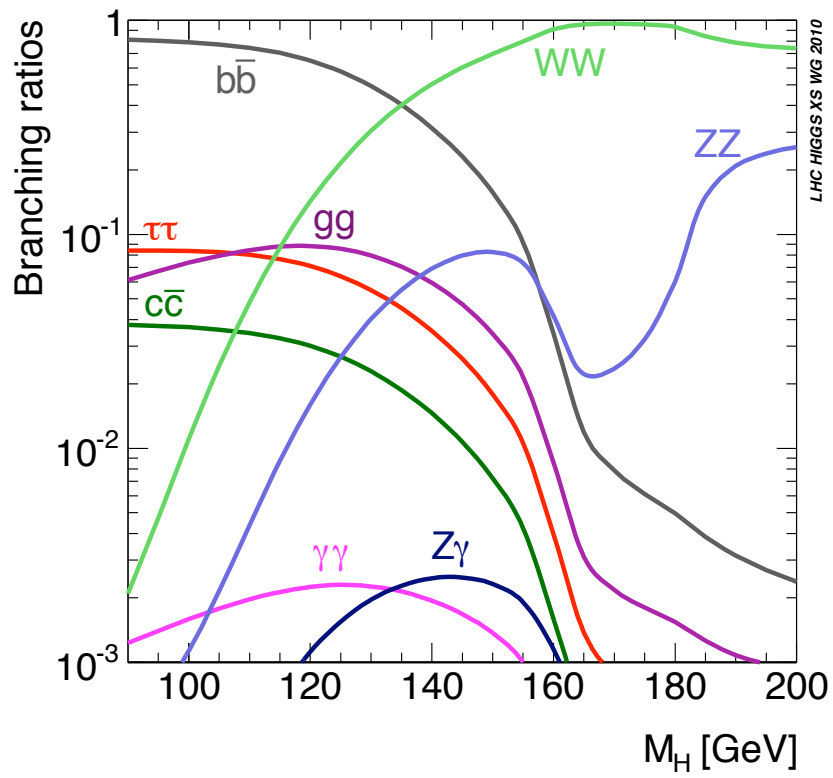
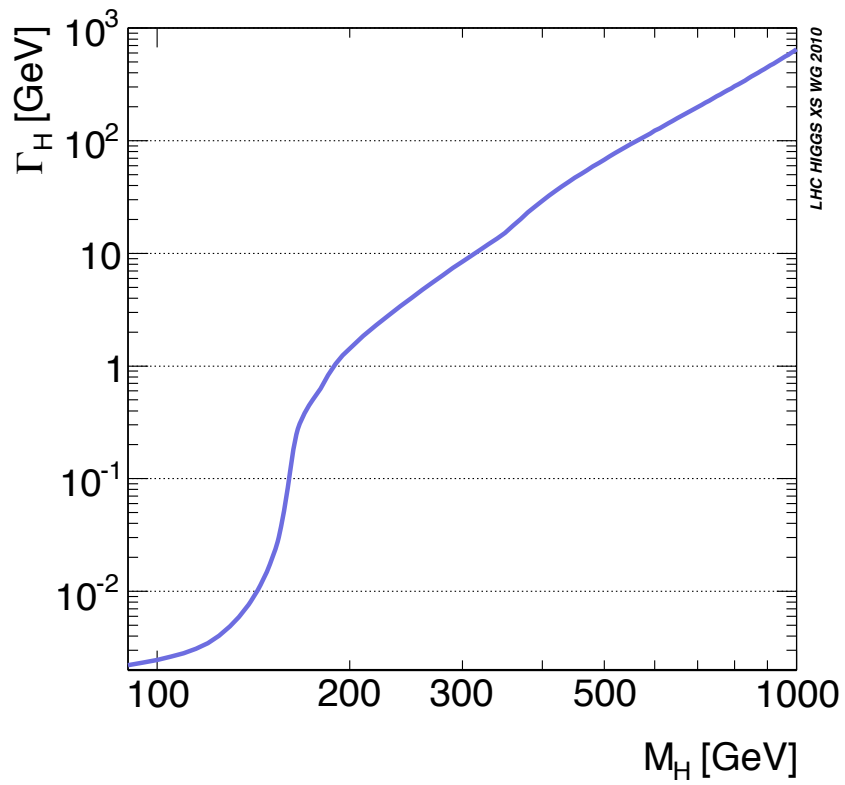**Fig. 35:** SM Higgs branching ratios as a function of the Higgs-boson mass.

Fig. 36: SM Higgs total width as a function of the Higgs-boson mass.

Table 30: SM Higgs branching ratios for 4-fermion final states in the low-mass range. We list results for the specific final states $e^+e^-e^+e^-$ and $e^+e^-\mu^+\mu^-$, for final states with 4 arbitrary charged leptons, $e^+\nu_e e^-\bar\nu_e$ and $e^+\nu_e\mu^-\bar\nu_\mu$, and for final states $l^+l^-\nu_l\bar\nu_l$ with 2 charged leptons plus 2 neutrinos (ν_l represents any type of neutrinos).

M_H [GeV]	$H \to e^+e^-e^+e^-$	$H \to e^+e^-\mu^+\mu^-$	$H \to l^+l^-l^+l^-$ (l = e or μ)	$H \to l^+l^-l^+l^-$ (l = e, μ or τ)	$H \to e^+\nu_e e^-\bar\nu_e$	$H \to e^+\nu_e\mu^-\bar\nu_\mu$	$H \to l^+l^-\nu_l\bar\nu_l$ (l = e or μ)	$H \to l^+l^-\nu_l\bar\nu_l$ (l = e, μ or τ)
90	$7.08 \cdot 10^{-7}$	$9.39 \cdot 10^{-7}$	$2.35 \cdot 10^{-6}$	$4.94 \cdot 10^{-6}$	$1.77 \cdot 10^{-5}$	$2.45 \cdot 10^{-5}$	$9.20 \cdot 10^{-5}$	$2.12 \cdot 10^{-4}$
95	$1.11 \cdot 10^{-6}$	$1.49 \cdot 10^{-6}$	$3.71 \cdot 10^{-6}$	$7.80 \cdot 10^{-6}$	$4.46 \cdot 10^{-5}$	$5.54 \cdot 10^{-5}$	$2.12 \cdot 10^{-4}$	$4.85 \cdot 10^{-4}$
100	$1.80 \cdot 10^{-6}$	$2.51 \cdot 10^{-6}$	$6.12 \cdot 10^{-6}$	$1.30 \cdot 10^{-5}$	$1.14 \cdot 10^{-4}$	$1.30 \cdot 10^{-4}$	$5.08 \cdot 10^{-4}$	$1.15 \cdot 10^{-3}$
105	$3.21 \cdot 10^{-6}$	$4.78 \cdot 10^{-6}$	$1.12 \cdot 10^{-5}$	$2.40 \cdot 10^{-5}$	$2.62 \cdot 10^{-4}$	$2.85 \cdot 10^{-4}$	$1.13 \cdot 10^{-3}$	$2.56 \cdot 10^{-3}$
110	$6.10 \cdot 10^{-6}$	$9.78 \cdot 10^{-6}$	$2.20 \cdot 10^{-5}$	$4.77 \cdot 10^{-5}$	$5.37 \cdot 10^{-4}$	$5.66 \cdot 10^{-4}$	$2.28 \cdot 10^{-3}$	$5.13 \cdot 10^{-3}$
115	$1.15 \cdot 10^{-5}$	$1.95 \cdot 10^{-5}$	$4.25 \cdot 10^{-5}$	$9.31 \cdot 10^{-5}$	$9.88 \cdot 10^{-4}$	$1.02 \cdot 10^{-3}$	$4.17 \cdot 10^{-3}$	$9.31 \cdot 10^{-3}$
120	$2.03 \cdot 10^{-5}$	$3.60 \cdot 10^{-5}$	$7.66 \cdot 10^{-5}$	$1.69 \cdot 10^{-4}$	$1.65 \cdot 10^{-3}$	$1.68 \cdot 10^{-3}$	$6.95 \cdot 10^{-3}$	$1.55 \cdot 10^{-2}$
125	$3.30 \cdot 10^{-5}$	$5.98 \cdot 10^{-5}$	$1.26 \cdot 10^{-4}$	$2.79 \cdot 10^{-4}$	$2.54 \cdot 10^{-3}$	$2.55 \cdot 10^{-3}$	$1.07 \cdot 10^{-2}$	$2.36 \cdot 10^{-2}$
130	$4.89 \cdot 10^{-5}$	$9.03 \cdot 10^{-5}$	$1.88 \cdot 10^{-4}$	$4.18 \cdot 10^{-4}$	$3.62 \cdot 10^{-3}$	$3.59 \cdot 10^{-3}$	$1.52 \cdot 10^{-2}$	$3.35 \cdot 10^{-2}$
135	$6.63 \cdot 10^{-5}$	$1.24 \cdot 10^{-4}$	$2.57 \cdot 10^{-4}$	$5.71 \cdot 10^{-4}$	$4.83 \cdot 10^{-3}$	$4.75 \cdot 10^{-3}$	$2.01 \cdot 10^{-2}$	$4.44 \cdot 10^{-2}$
140	$8.25 \cdot 10^{-5}$	$1.56 \cdot 10^{-4}$	$3.21 \cdot 10^{-4}$	$7.15 \cdot 10^{-4}$	$6.07 \cdot 10^{-3}$	$5.94 \cdot 10^{-3}$	$2.52 \cdot 10^{-2}$	$5.57 \cdot 10^{-2}$
145	$9.43 \cdot 10^{-5}$	$1.79 \cdot 10^{-4}$	$3.68 \cdot 10^{-4}$	$8.21 \cdot 10^{-4}$	$7.28 \cdot 10^{-3}$	$7.11 \cdot 10^{-3}$	$3.02 \cdot 10^{-2}$	$6.66 \cdot 10^{-2}$
150	$9.76 \cdot 10^{-5}$	$1.87 \cdot 10^{-4}$	$3.82 \cdot 10^{-4}$	$8.53 \cdot 10^{-4}$	$8.44 \cdot 10^{-3}$	$8.23 \cdot 10^{-3}$	$3.48 \cdot 10^{-2}$	$7.70 \cdot 10^{-2}$
155	$8.63 \cdot 10^{-5}$	$1.66 \cdot 10^{-4}$	$3.38 \cdot 10^{-4}$	$7.57 \cdot 10^{-4}$	$9.59 \cdot 10^{-3}$	$9.39 \cdot 10^{-3}$	$3.93 \cdot 10^{-2}$	$8.71 \cdot 10^{-2}$
160	$4.85 \cdot 10^{-5}$	$9.36 \cdot 10^{-5}$	$1.91 \cdot 10^{-4}$	$4.26 \cdot 10^{-4}$	$1.08 \cdot 10^{-2}$	$1.07 \cdot 10^{-2}$	$4.39 \cdot 10^{-2}$	$9.80 \cdot 10^{-2}$
165	$2.58 \cdot 10^{-5}$	$5.00 \cdot 10^{-5}$	$1.02 \cdot 10^{-4}$	$2.27 \cdot 10^{-4}$	$1.14 \cdot 10^{-2}$	$1.13 \cdot 10^{-2}$	$4.59 \cdot 10^{-2}$	$1.03 \cdot 10^{-1}$
170	$2.73 \cdot 10^{-5}$	$5.32 \cdot 10^{-5}$	$1.08 \cdot 10^{-4}$	$2.42 \cdot 10^{-4}$	$1.15 \cdot 10^{-2}$	$1.14 \cdot 10^{-2}$	$4.61 \cdot 10^{-2}$	$1.03 \cdot 10^{-1}$
175	$3.71 \cdot 10^{-5}$	$7.28 \cdot 10^{-5}$	$1.47 \cdot 10^{-4}$	$3.30 \cdot 10^{-4}$	$1.14 \cdot 10^{-2}$	$1.13 \cdot 10^{-2}$	$4.60 \cdot 10^{-2}$	$1.03 \cdot 10^{-1}$
180	$6.85 \cdot 10^{-5}$	$1.36 \cdot 10^{-4}$	$2.73 \cdot 10^{-4}$	$6.12 \cdot 10^{-4}$	$1.12 \cdot 10^{-2}$	$1.10 \cdot 10^{-2}$	$4.55 \cdot 10^{-2}$	$1.01 \cdot 10^{-1}$
185	$1.70 \cdot 10^{-4}$	$3.38 \cdot 10^{-4}$	$6.78 \cdot 10^{-4}$	$1.52 \cdot 10^{-3}$	$1.06 \cdot 10^{-2}$	$9.95 \cdot 10^{-3}$	$4.38 \cdot 10^{-2}$	$9.56 \cdot 10^{-2}$
190	$2.36 \cdot 10^{-4}$	$4.72 \cdot 10^{-4}$	$9.44 \cdot 10^{-4}$	$2.12 \cdot 10^{-3}$	$1.02 \cdot 10^{-2}$	$9.26 \cdot 10^{-3}$	$4.27 \cdot 10^{-2}$	$9.18 \cdot 10^{-2}$
195	$2.69 \cdot 10^{-4}$	$5.37 \cdot 10^{-4}$	$1.08 \cdot 10^{-3}$	$2.42 \cdot 10^{-3}$	$9.99 \cdot 10^{-3}$	$8.92 \cdot 10^{-3}$	$4.21 \cdot 10^{-2}$	$8.99 \cdot 10^{-2}$
200	$2.88 \cdot 10^{-4}$	$5.75 \cdot 10^{-4}$	$1.15 \cdot 10^{-3}$	$2.59 \cdot 10^{-3}$	$9.87 \cdot 10^{-3}$	$8.73 \cdot 10^{-3}$	$4.18 \cdot 10^{-2}$	$8.89 \cdot 10^{-2}$
210	$3.08 \cdot 10^{-4}$	$6.17 \cdot 10^{-4}$	$1.23 \cdot 10^{-3}$	$2.78 \cdot 10^{-3}$	$9.74 \cdot 10^{-3}$	$8.52 \cdot 10^{-3}$	$4.14 \cdot 10^{-2}$	$8.77 \cdot 10^{-2}$
220	$3.19 \cdot 10^{-4}$	$6.38 \cdot 10^{-4}$	$1.28 \cdot 10^{-3}$	$2.87 \cdot 10^{-3}$	$9.68 \cdot 10^{-3}$	$8.41 \cdot 10^{-3}$	$4.13 \cdot 10^{-2}$	$8.71 \cdot 10^{-2}$
230	$3.26 \cdot 10^{-4}$	$6.52 \cdot 10^{-4}$	$1.30 \cdot 10^{-3}$	$2.93 \cdot 10^{-3}$	$9.64 \cdot 10^{-3}$	$8.34 \cdot 10^{-3}$	$4.12 \cdot 10^{-2}$	$8.68 \cdot 10^{-2}$
240	$3.31 \cdot 10^{-4}$	$6.61 \cdot 10^{-4}$	$1.32 \cdot 10^{-3}$	$2.97 \cdot 10^{-3}$	$9.61 \cdot 10^{-3}$	$8.29 \cdot 10^{-3}$	$4.11 \cdot 10^{-2}$	$8.65 \cdot 10^{-2}$
250	$3.34 \cdot 10^{-4}$	$6.68 \cdot 10^{-4}$	$1.34 \cdot 10^{-3}$	$3.01 \cdot 10^{-3}$	$9.59 \cdot 10^{-3}$	$8.26 \cdot 10^{-3}$	$4.10 \cdot 10^{-2}$	$8.63 \cdot 10^{-2}$
260	$3.37 \cdot 10^{-4}$	$6.74 \cdot 10^{-4}$	$1.35 \cdot 10^{-3}$	$3.03 \cdot 10^{-3}$	$9.57 \cdot 10^{-3}$	$8.23 \cdot 10^{-3}$	$4.10 \cdot 10^{-2}$	$8.62 \cdot 10^{-2}$
270	$3.40 \cdot 10^{-4}$	$6.79 \cdot 10^{-4}$	$1.36 \cdot 10^{-3}$	$3.06 \cdot 10^{-3}$	$9.56 \cdot 10^{-3}$	$8.21 \cdot 10^{-3}$	$4.09 \cdot 10^{-2}$	$8.60 \cdot 10^{-2}$
280	$3.42 \cdot 10^{-4}$	$6.83 \cdot 10^{-4}$	$1.37 \cdot 10^{-3}$	$3.07 \cdot 10^{-3}$	$9.54 \cdot 10^{-3}$	$8.18 \cdot 10^{-3}$	$4.09 \cdot 10^{-2}$	$8.59 \cdot 10^{-2}$
290	$3.44 \cdot 10^{-4}$	$6.87 \cdot 10^{-4}$	$1.37 \cdot 10^{-3}$	$3.09 \cdot 10^{-3}$	$9.53 \cdot 10^{-3}$	$8.16 \cdot 10^{-3}$	$4.09 \cdot 10^{-2}$	$8.58 \cdot 10^{-2}$
300	$3.45 \cdot 10^{-4}$	$6.90 \cdot 10^{-4}$	$1.38 \cdot 10^{-3}$	$3.11 \cdot 10^{-3}$	$9.52 \cdot 10^{-3}$	$8.15 \cdot 10^{-3}$	$4.08 \cdot 10^{-2}$	$8.57 \cdot 10^{-2}$

Table 31: SM Higgs branching ratios for 4-fermion final states in the intermediate-mass range. We list results for the specific final states $e^+e^-e^+e^-$ and $e^+e^-\mu^+\mu^-$, for final states with 4 arbitrary charged leptons, $e^+\nu_e e^-\bar{\nu}_e$ and $e^+\nu_e\mu^-\bar{\nu}_\mu$, and for final states $l^+l^-\nu_l\bar{\nu}_l$ with 2 charged leptons plus 2 neutrinos (ν_l represents any type of neutrinos).

M_H [GeV]	$H \to e^+e^-e^+e^-$	$H \to e^+e^-\mu^+\mu^-$	$H \to l^+l^-l^+l^-$ ($l=e$ or μ)	$H \to l^+l^-l^+l^-$ ($l=e,\mu$ or τ)	$H \to e^+\nu_e e^-\bar{\nu}_e$	$H \to e^+\nu_e\mu^-\bar{\nu}_\mu$	$H \to l^+l^-\nu_l\bar{\nu}_l$ ($l=e$ or μ)	$H \to l^+l^-\nu_l\bar{\nu}_l$ ($l=e,\mu$ or τ)
310	$3.47 \cdot 10^{-4}$	$6.93 \cdot 10^{-4}$	$1.39 \cdot 10^{-3}$	$3.12 \cdot 10^{-3}$	$9.51 \cdot 10^{-3}$	$8.13 \cdot 10^{-3}$	$4.08 \cdot 10^{-2}$	$8.56 \cdot 10^{-2}$
320	$3.48 \cdot 10^{-4}$	$6.96 \cdot 10^{-4}$	$1.39 \cdot 10^{-3}$	$3.13 \cdot 10^{-3}$	$9.50 \cdot 10^{-3}$	$8.11 \cdot 10^{-3}$	$4.08 \cdot 10^{-2}$	$8.55 \cdot 10^{-2}$
330	$3.49 \cdot 10^{-4}$	$6.98 \cdot 10^{-4}$	$1.40 \cdot 10^{-3}$	$3.14 \cdot 10^{-3}$	$9.49 \cdot 10^{-3}$	$8.10 \cdot 10^{-3}$	$4.07 \cdot 10^{-2}$	$8.54 \cdot 10^{-2}$
340	$3.50 \cdot 10^{-4}$	$6.99 \cdot 10^{-4}$	$1.40 \cdot 10^{-3}$	$3.15 \cdot 10^{-3}$	$9.47 \cdot 10^{-3}$	$8.08 \cdot 10^{-3}$	$4.07 \cdot 10^{-2}$	$8.53 \cdot 10^{-2}$
350	$3.45 \cdot 10^{-4}$	$6.90 \cdot 10^{-4}$	$1.38 \cdot 10^{-3}$	$3.11 \cdot 10^{-3}$	$9.33 \cdot 10^{-3}$	$7.96 \cdot 10^{-3}$	$4.01 \cdot 10^{-2}$	$8.40 \cdot 10^{-2}$
360	$3.34 \cdot 10^{-4}$	$6.67 \cdot 10^{-4}$	$1.33 \cdot 10^{-3}$	$3.00 \cdot 10^{-3}$	$8.99 \cdot 10^{-3}$	$7.66 \cdot 10^{-3}$	$3.86 \cdot 10^{-2}$	$8.09 \cdot 10^{-2}$
370	$3.23 \cdot 10^{-4}$	$6.46 \cdot 10^{-4}$	$1.29 \cdot 10^{-3}$	$2.91 \cdot 10^{-3}$	$8.68 \cdot 10^{-3}$	$7.39 \cdot 10^{-3}$	$3.73 \cdot 10^{-2}$	$7.81 \cdot 10^{-2}$
380	$3.15 \cdot 10^{-4}$	$6.29 \cdot 10^{-4}$	$1.26 \cdot 10^{-3}$	$2.83 \cdot 10^{-3}$	$8.43 \cdot 10^{-3}$	$7.17 \cdot 10^{-3}$	$3.62 \cdot 10^{-2}$	$7.58 \cdot 10^{-2}$
390	$3.08 \cdot 10^{-4}$	$6.15 \cdot 10^{-4}$	$1.23 \cdot 10^{-3}$	$2.77 \cdot 10^{-3}$	$8.22 \cdot 10^{-3}$	$7.00 \cdot 10^{-3}$	$3.53 \cdot 10^{-2}$	$7.40 \cdot 10^{-2}$
400	$3.03 \cdot 10^{-4}$	$6.05 \cdot 10^{-4}$	$1.21 \cdot 10^{-3}$	$2.72 \cdot 10^{-3}$	$8.06 \cdot 10^{-3}$	$6.85 \cdot 10^{-3}$	$3.46 \cdot 10^{-2}$	$7.25 \cdot 10^{-2}$
410	$2.99 \cdot 10^{-4}$	$5.98 \cdot 10^{-4}$	$1.20 \cdot 10^{-3}$	$2.69 \cdot 10^{-3}$	$7.93 \cdot 10^{-3}$	$6.74 \cdot 10^{-3}$	$3.41 \cdot 10^{-2}$	$7.14 \cdot 10^{-2}$
420	$2.96 \cdot 10^{-4}$	$5.92 \cdot 10^{-4}$	$1.18 \cdot 10^{-3}$	$2.67 \cdot 10^{-3}$	$7.83 \cdot 10^{-3}$	$6.65 \cdot 10^{-3}$	$3.37 \cdot 10^{-2}$	$7.05 \cdot 10^{-2}$
430	$2.94 \cdot 10^{-4}$	$5.88 \cdot 10^{-4}$	$1.18 \cdot 10^{-3}$	$2.65 \cdot 10^{-3}$	$7.76 \cdot 10^{-3}$	$6.59 \cdot 10^{-3}$	$3.34 \cdot 10^{-2}$	$6.98 \cdot 10^{-2}$
440	$2.93 \cdot 10^{-4}$	$5.86 \cdot 10^{-4}$	$1.17 \cdot 10^{-3}$	$2.64 \cdot 10^{-3}$	$7.70 \cdot 10^{-3}$	$6.53 \cdot 10^{-3}$	$3.31 \cdot 10^{-2}$	$6.93 \cdot 10^{-2}$
450	$2.92 \cdot 10^{-4}$	$5.84 \cdot 10^{-4}$	$1.17 \cdot 10^{-3}$	$2.63 \cdot 10^{-3}$	$7.66 \cdot 10^{-3}$	$6.50 \cdot 10^{-3}$	$3.30 \cdot 10^{-2}$	$6.89 \cdot 10^{-2}$
460	$2.92 \cdot 10^{-4}$	$5.84 \cdot 10^{-4}$	$1.17 \cdot 10^{-3}$	$2.63 \cdot 10^{-3}$	$7.63 \cdot 10^{-3}$	$6.47 \cdot 10^{-3}$	$3.29 \cdot 10^{-2}$	$6.87 \cdot 10^{-2}$
470	$2.92 \cdot 10^{-4}$	$5.84 \cdot 10^{-4}$	$1.17 \cdot 10^{-3}$	$2.63 \cdot 10^{-3}$	$7.62 \cdot 10^{-3}$	$6.45 \cdot 10^{-3}$	$3.28 \cdot 10^{-2}$	$6.85 \cdot 10^{-2}$
480	$2.92 \cdot 10^{-4}$	$5.85 \cdot 10^{-4}$	$1.17 \cdot 10^{-3}$	$2.63 \cdot 10^{-3}$	$7.61 \cdot 10^{-3}$	$6.44 \cdot 10^{-3}$	$3.28 \cdot 10^{-2}$	$6.85 \cdot 10^{-2}$
490	$2.93 \cdot 10^{-4}$	$5.86 \cdot 10^{-4}$	$1.17 \cdot 10^{-3}$	$2.64 \cdot 10^{-3}$	$7.60 \cdot 10^{-3}$	$6.44 \cdot 10^{-3}$	$3.28 \cdot 10^{-2}$	$6.84 \cdot 10^{-2}$
500	$2.94 \cdot 10^{-4}$	$5.88 \cdot 10^{-4}$	$1.18 \cdot 10^{-3}$	$2.64 \cdot 10^{-3}$	$7.61 \cdot 10^{-3}$	$6.44 \cdot 10^{-3}$	$3.28 \cdot 10^{-2}$	$6.85 \cdot 10^{-2}$
510	$2.95 \cdot 10^{-4}$	$5.90 \cdot 10^{-4}$	$1.18 \cdot 10^{-3}$	$2.65 \cdot 10^{-3}$	$7.62 \cdot 10^{-3}$	$6.44 \cdot 10^{-3}$	$3.28 \cdot 10^{-2}$	$6.86 \cdot 10^{-2}$
520	$2.96 \cdot 10^{-4}$	$5.92 \cdot 10^{-4}$	$1.18 \cdot 10^{-3}$	$2.66 \cdot 10^{-3}$	$7.63 \cdot 10^{-3}$	$6.45 \cdot 10^{-3}$	$3.29 \cdot 10^{-2}$	$6.87 \cdot 10^{-2}$
530	$2.97 \cdot 10^{-4}$	$5.94 \cdot 10^{-4}$	$1.19 \cdot 10^{-3}$	$2.67 \cdot 10^{-3}$	$7.65 \cdot 10^{-3}$	$6.46 \cdot 10^{-3}$	$3.30 \cdot 10^{-2}$	$6.88 \cdot 10^{-2}$
540	$2.98 \cdot 10^{-4}$	$5.97 \cdot 10^{-4}$	$1.19 \cdot 10^{-3}$	$2.69 \cdot 10^{-3}$	$7.67 \cdot 10^{-3}$	$6.48 \cdot 10^{-3}$	$3.30 \cdot 10^{-2}$	$6.90 \cdot 10^{-2}$
550	$3.00 \cdot 10^{-4}$	$6.00 \cdot 10^{-4}$	$1.20 \cdot 10^{-3}$	$2.70 \cdot 10^{-3}$	$7.69 \cdot 10^{-3}$	$6.49 \cdot 10^{-3}$	$3.31 \cdot 10^{-2}$	$6.92 \cdot 10^{-2}$
560	$3.01 \cdot 10^{-4}$	$6.03 \cdot 10^{-4}$	$1.20 \cdot 10^{-3}$	$2.71 \cdot 10^{-3}$	$7.71 \cdot 10^{-3}$	$6.51 \cdot 10^{-3}$	$3.32 \cdot 10^{-2}$	$6.94 \cdot 10^{-2}$
570	$3.03 \cdot 10^{-4}$	$6.05 \cdot 10^{-4}$	$1.21 \cdot 10^{-3}$	$2.72 \cdot 10^{-3}$	$7.73 \cdot 10^{-3}$	$6.53 \cdot 10^{-3}$	$3.33 \cdot 10^{-2}$	$6.96 \cdot 10^{-2}$
580	$3.04 \cdot 10^{-4}$	$6.08 \cdot 10^{-4}$	$1.22 \cdot 10^{-3}$	$2.74 \cdot 10^{-3}$	$7.76 \cdot 10^{-3}$	$6.55 \cdot 10^{-3}$	$3.35 \cdot 10^{-2}$	$6.98 \cdot 10^{-2}$
590	$3.06 \cdot 10^{-4}$	$6.11 \cdot 10^{-4}$	$1.22 \cdot 10^{-3}$	$2.75 \cdot 10^{-3}$	$7.79 \cdot 10^{-3}$	$6.57 \cdot 10^{-3}$	$3.36 \cdot 10^{-2}$	$7.01 \cdot 10^{-2}$
600	$3.07 \cdot 10^{-4}$	$6.14 \cdot 10^{-4}$	$1.23 \cdot 10^{-3}$	$2.76 \cdot 10^{-3}$	$7.81 \cdot 10^{-3}$	$6.59 \cdot 10^{-3}$	$3.37 \cdot 10^{-2}$	$7.03 \cdot 10^{-2}$
610	$3.09 \cdot 10^{-4}$	$6.17 \cdot 10^{-4}$	$1.23 \cdot 10^{-3}$	$2.78 \cdot 10^{-3}$	$7.84 \cdot 10^{-3}$	$6.61 \cdot 10^{-3}$	$3.38 \cdot 10^{-2}$	$7.06 \cdot 10^{-2}$
620	$3.10 \cdot 10^{-4}$	$6.20 \cdot 10^{-4}$	$1.24 \cdot 10^{-3}$	$2.79 \cdot 10^{-3}$	$7.87 \cdot 10^{-3}$	$6.63 \cdot 10^{-3}$	$3.39 \cdot 10^{-2}$	$7.08 \cdot 10^{-2}$
630	$3.12 \cdot 10^{-4}$	$6.23 \cdot 10^{-4}$	$1.25 \cdot 10^{-3}$	$2.80 \cdot 10^{-3}$	$7.90 \cdot 10^{-3}$	$6.66 \cdot 10^{-3}$	$3.41 \cdot 10^{-2}$	$7.11 \cdot 10^{-2}$
640	$3.13 \cdot 10^{-4}$	$6.26 \cdot 10^{-4}$	$1.25 \cdot 10^{-3}$	$2.82 \cdot 10^{-3}$	$7.93 \cdot 10^{-3}$	$6.68 \cdot 10^{-3}$	$3.42 \cdot 10^{-2}$	$7.13 \cdot 10^{-2}$
650	$3.15 \cdot 10^{-4}$	$6.29 \cdot 10^{-4}$	$1.26 \cdot 10^{-3}$	$2.83 \cdot 10^{-3}$	$7.96 \cdot 10^{-3}$	$6.70 \cdot 10^{-3}$	$3.43 \cdot 10^{-2}$	$7.16 \cdot 10^{-2}$

Table 32: SM Higgs branching ratios for 4-fermion final states in the high-mass range. We list results for the specific final states $e^+e^-e^+e^-$ and $e^+e^-\mu^+\mu^-$, for final states with 4 arbitrary charged leptons, $e^+\nu_e e^-\bar{\nu}_e$ and $e^+\nu_e\mu^-\bar{\nu}_\mu$, and for final states $l^+l^-\nu_l\bar{\nu}_l$ with 2 charged leptons plus 2 neutrinos (ν_l represents any type of neutrinos).

M_H [GeV]	$H \to e^+e^-e^+e^-$	$H \to e^+e^-\mu^+\mu^-$	$H \to l^+l^-l^+l^-$ (l = e or μ)	$H \to l^+l^-l^+l^-$ (l = e, μ or τ)	$H \to e^+\nu_e e^-\bar{\nu}_e$	$H \to e^+\nu_e\mu^-\bar{\nu}_\mu$	$H \to l^+l^-\nu_l\bar{\nu}_l$ (l = e or μ)	$H \to l^+l^-\nu_l\bar{\nu}_l$ (l = e, μ or τ)
660	$3.16 \cdot 10^{-4}$	$6.32 \cdot 10^{-4}$	$1.26 \cdot 10^{-3}$	$2.84 \cdot 10^{-3}$	$7.98 \cdot 10^{-3}$	$6.73 \cdot 10^{-3}$	$3.44 \cdot 10^{-2}$	$7.18 \cdot 10^{-2}$
670	$3.17 \cdot 10^{-4}$	$6.35 \cdot 10^{-4}$	$1.27 \cdot 10^{-3}$	$2.86 \cdot 10^{-3}$	$8.01 \cdot 10^{-3}$	$6.75 \cdot 10^{-3}$	$3.46 \cdot 10^{-2}$	$7.21 \cdot 10^{-2}$
680	$3.19 \cdot 10^{-4}$	$6.38 \cdot 10^{-4}$	$1.28 \cdot 10^{-3}$	$2.87 \cdot 10^{-3}$	$8.04 \cdot 10^{-3}$	$6.77 \cdot 10^{-3}$	$3.47 \cdot 10^{-2}$	$7.24 \cdot 10^{-2}$
690	$3.20 \cdot 10^{-4}$	$6.41 \cdot 10^{-4}$	$1.28 \cdot 10^{-3}$	$2.88 \cdot 10^{-3}$	$8.07 \cdot 10^{-3}$	$6.80 \cdot 10^{-3}$	$3.48 \cdot 10^{-2}$	$7.26 \cdot 10^{-2}$
700	$3.22 \cdot 10^{-4}$	$6.43 \cdot 10^{-4}$	$1.29 \cdot 10^{-3}$	$2.90 \cdot 10^{-3}$	$8.10 \cdot 10^{-3}$	$6.82 \cdot 10^{-3}$	$3.50 \cdot 10^{-2}$	$7.29 \cdot 10^{-2}$
710	$3.23 \cdot 10^{-4}$	$6.46 \cdot 10^{-4}$	$1.29 \cdot 10^{-3}$	$2.91 \cdot 10^{-3}$	$8.13 \cdot 10^{-3}$	$6.84 \cdot 10^{-3}$	$3.51 \cdot 10^{-2}$	$7.31 \cdot 10^{-2}$
720	$3.24 \cdot 10^{-4}$	$6.49 \cdot 10^{-4}$	$1.30 \cdot 10^{-3}$	$2.92 \cdot 10^{-3}$	$8.15 \cdot 10^{-3}$	$6.86 \cdot 10^{-3}$	$3.52 \cdot 10^{-2}$	$7.34 \cdot 10^{-2}$
730	$3.26 \cdot 10^{-4}$	$6.51 \cdot 10^{-4}$	$1.30 \cdot 10^{-3}$	$2.93 \cdot 10^{-3}$	$8.18 \cdot 10^{-3}$	$6.88 \cdot 10^{-3}$	$3.53 \cdot 10^{-2}$	$7.36 \cdot 10^{-2}$
740	$3.27 \cdot 10^{-4}$	$6.54 \cdot 10^{-4}$	$1.31 \cdot 10^{-3}$	$2.94 \cdot 10^{-3}$	$8.21 \cdot 10^{-3}$	$6.91 \cdot 10^{-3}$	$3.54 \cdot 10^{-2}$	$7.39 \cdot 10^{-2}$
750	$3.28 \cdot 10^{-4}$	$6.57 \cdot 10^{-4}$	$1.31 \cdot 10^{-3}$	$2.95 \cdot 10^{-3}$	$8.24 \cdot 10^{-3}$	$6.93 \cdot 10^{-3}$	$3.56 \cdot 10^{-2}$	$7.41 \cdot 10^{-2}$
760	$3.29 \cdot 10^{-4}$	$6.59 \cdot 10^{-4}$	$1.32 \cdot 10^{-3}$	$2.97 \cdot 10^{-3}$	$8.26 \cdot 10^{-3}$	$6.95 \cdot 10^{-3}$	$3.57 \cdot 10^{-2}$	$7.44 \cdot 10^{-2}$
770	$3.31 \cdot 10^{-4}$	$6.62 \cdot 10^{-4}$	$1.32 \cdot 10^{-3}$	$2.98 \cdot 10^{-3}$	$8.29 \cdot 10^{-3}$	$6.97 \cdot 10^{-3}$	$3.58 \cdot 10^{-2}$	$7.46 \cdot 10^{-2}$
780	$3.32 \cdot 10^{-4}$	$6.64 \cdot 10^{-4}$	$1.33 \cdot 10^{-3}$	$2.99 \cdot 10^{-3}$	$8.32 \cdot 10^{-3}$	$6.99 \cdot 10^{-3}$	$3.59 \cdot 10^{-2}$	$7.48 \cdot 10^{-2}$
790	$3.33 \cdot 10^{-4}$	$6.66 \cdot 10^{-4}$	$1.33 \cdot 10^{-3}$	$3.00 \cdot 10^{-3}$	$8.34 \cdot 10^{-3}$	$7.01 \cdot 10^{-3}$	$3.60 \cdot 10^{-2}$	$7.51 \cdot 10^{-2}$
800	$3.34 \cdot 10^{-4}$	$6.69 \cdot 10^{-4}$	$1.34 \cdot 10^{-3}$	$3.01 \cdot 10^{-3}$	$8.36 \cdot 10^{-3}$	$7.03 \cdot 10^{-3}$	$3.61 \cdot 10^{-2}$	$7.53 \cdot 10^{-2}$
810	$3.35 \cdot 10^{-4}$	$6.71 \cdot 10^{-4}$	$1.34 \cdot 10^{-3}$	$3.02 \cdot 10^{-3}$	$8.39 \cdot 10^{-3}$	$7.05 \cdot 10^{-3}$	$3.62 \cdot 10^{-2}$	$7.55 \cdot 10^{-2}$
820	$3.36 \cdot 10^{-4}$	$6.73 \cdot 10^{-4}$	$1.35 \cdot 10^{-3}$	$3.03 \cdot 10^{-3}$	$8.41 \cdot 10^{-3}$	$7.07 \cdot 10^{-3}$	$3.63 \cdot 10^{-2}$	$7.57 \cdot 10^{-2}$
830	$3.38 \cdot 10^{-4}$	$6.75 \cdot 10^{-4}$	$1.35 \cdot 10^{-3}$	$3.04 \cdot 10^{-3}$	$8.44 \cdot 10^{-3}$	$7.09 \cdot 10^{-3}$	$3.64 \cdot 10^{-2}$	$7.59 \cdot 10^{-2}$
840	$3.39 \cdot 10^{-4}$	$6.77 \cdot 10^{-4}$	$1.35 \cdot 10^{-3}$	$3.05 \cdot 10^{-3}$	$8.46 \cdot 10^{-3}$	$7.11 \cdot 10^{-3}$	$3.65 \cdot 10^{-2}$	$7.61 \cdot 10^{-2}$
850	$3.40 \cdot 10^{-4}$	$6.79 \cdot 10^{-4}$	$1.36 \cdot 10^{-3}$	$3.06 \cdot 10^{-3}$	$8.49 \cdot 10^{-3}$	$7.13 \cdot 10^{-3}$	$3.66 \cdot 10^{-2}$	$7.64 \cdot 10^{-2}$
860	$3.41 \cdot 10^{-4}$	$6.81 \cdot 10^{-4}$	$1.36 \cdot 10^{-3}$	$3.07 \cdot 10^{-3}$	$8.51 \cdot 10^{-3}$	$7.15 \cdot 10^{-3}$	$3.67 \cdot 10^{-2}$	$7.66 \cdot 10^{-2}$
870	$3.42 \cdot 10^{-4}$	$6.83 \cdot 10^{-4}$	$1.37 \cdot 10^{-3}$	$3.08 \cdot 10^{-3}$	$8.53 \cdot 10^{-3}$	$7.17 \cdot 10^{-3}$	$3.68 \cdot 10^{-2}$	$7.68 \cdot 10^{-2}$
880	$3.43 \cdot 10^{-4}$	$6.85 \cdot 10^{-4}$	$1.37 \cdot 10^{-3}$	$3.08 \cdot 10^{-3}$	$8.55 \cdot 10^{-3}$	$7.19 \cdot 10^{-3}$	$3.69 \cdot 10^{-2}$	$7.70 \cdot 10^{-2}$
890	$3.44 \cdot 10^{-4}$	$6.87 \cdot 10^{-4}$	$1.37 \cdot 10^{-3}$	$3.09 \cdot 10^{-3}$	$8.57 \cdot 10^{-3}$	$7.20 \cdot 10^{-3}$	$3.70 \cdot 10^{-2}$	$7.72 \cdot 10^{-2}$
900	$3.45 \cdot 10^{-4}$	$6.89 \cdot 10^{-4}$	$1.38 \cdot 10^{-3}$	$3.10 \cdot 10^{-3}$	$8.60 \cdot 10^{-3}$	$7.22 \cdot 10^{-3}$	$3.71 \cdot 10^{-2}$	$7.74 \cdot 10^{-2}$
910	$3.46 \cdot 10^{-4}$	$6.91 \cdot 10^{-4}$	$1.38 \cdot 10^{-3}$	$3.11 \cdot 10^{-3}$	$8.62 \cdot 10^{-3}$	$7.24 \cdot 10^{-3}$	$3.72 \cdot 10^{-2}$	$7.76 \cdot 10^{-2}$
920	$3.47 \cdot 10^{-4}$	$6.93 \cdot 10^{-4}$	$1.39 \cdot 10^{-3}$	$3.12 \cdot 10^{-3}$	$8.64 \cdot 10^{-3}$	$7.26 \cdot 10^{-3}$	$3.73 \cdot 10^{-2}$	$7.77 \cdot 10^{-2}$
930	$3.47 \cdot 10^{-4}$	$6.95 \cdot 10^{-4}$	$1.39 \cdot 10^{-3}$	$3.13 \cdot 10^{-3}$	$8.66 \cdot 10^{-3}$	$7.28 \cdot 10^{-3}$	$3.74 \cdot 10^{-2}$	$7.79 \cdot 10^{-2}$
940	$3.48 \cdot 10^{-4}$	$6.97 \cdot 10^{-4}$	$1.39 \cdot 10^{-3}$	$3.13 \cdot 10^{-3}$	$8.68 \cdot 10^{-3}$	$7.29 \cdot 10^{-3}$	$3.75 \cdot 10^{-2}$	$7.81 \cdot 10^{-2}$
950	$3.49 \cdot 10^{-4}$	$6.98 \cdot 10^{-4}$	$1.40 \cdot 10^{-3}$	$3.14 \cdot 10^{-3}$	$8.70 \cdot 10^{-3}$	$7.31 \cdot 10^{-3}$	$3.76 \cdot 10^{-2}$	$7.83 \cdot 10^{-2}$
960	$3.50 \cdot 10^{-4}$	$7.00 \cdot 10^{-4}$	$1.40 \cdot 10^{-3}$	$3.15 \cdot 10^{-3}$	$8.72 \cdot 10^{-3}$	$7.32 \cdot 10^{-3}$	$3.77 \cdot 10^{-2}$	$7.85 \cdot 10^{-2}$
970	$3.51 \cdot 10^{-4}$	$7.02 \cdot 10^{-4}$	$1.40 \cdot 10^{-3}$	$3.16 \cdot 10^{-3}$	$8.74 \cdot 10^{-3}$	$7.34 \cdot 10^{-3}$	$3.77 \cdot 10^{-2}$	$7.86 \cdot 10^{-2}$
980	$3.52 \cdot 10^{-4}$	$7.03 \cdot 10^{-4}$	$1.41 \cdot 10^{-3}$	$3.17 \cdot 10^{-3}$	$8.76 \cdot 10^{-3}$	$7.35 \cdot 10^{-3}$	$3.78 \cdot 10^{-2}$	$7.88 \cdot 10^{-2}$
990	$3.53 \cdot 10^{-4}$	$7.05 \cdot 10^{-4}$	$1.41 \cdot 10^{-3}$	$3.17 \cdot 10^{-3}$	$8.78 \cdot 10^{-3}$	$7.37 \cdot 10^{-3}$	$3.79 \cdot 10^{-2}$	$7.90 \cdot 10^{-2}$
1000	$3.53 \cdot 10^{-4}$	$7.07 \cdot 10^{-4}$	$1.41 \cdot 10^{-3}$	$3.18 \cdot 10^{-3}$	$8.80 \cdot 10^{-3}$	$7.39 \cdot 10^{-3}$	$3.80 \cdot 10^{-2}$	$7.91 \cdot 10^{-2}$

Table 33: SM Higgs branching ratios for 4-fermion final states in the low- and intermediate-mass range. We list results for the specific final states for 2 charged leptons plus 2 quarks, $l^+ l^- q\bar{q}'$ (not including charge conjugate state), 2 neutrinos plus 2 quarks, 4 quarks, as well as the result for arbitrary 4 fermions, where q = udscb and ν_l represents any type of neutrinos.

M_H [GeV]	$H \to l^+ l^- q\bar{q}$ (l = e or μ)	$H \to l^+ l^- q\bar{q}$ (l = e, μ or τ)	$H \to l^+ \nu_l q\bar{q}'$ (l = e or μ)	$H \to \nu_l \bar{\nu}_l q\bar{q}$	$H \to qqqq$	$H \to ffff$
90	$3.95 \cdot 10^{-5}$	$5.92 \cdot 10^{-5}$	$3.06 \cdot 10^{-4}$	$1.19 \cdot 10^{-4}$	$1.06 \cdot 10^{-3}$	$2.40 \cdot 10^{-3}$
95	$6.27 \cdot 10^{-5}$	$9.41 \cdot 10^{-5}$	$6.92 \cdot 10^{-4}$	$1.89 \cdot 10^{-4}$	$2.34 \cdot 10^{-3}$	$5.22 \cdot 10^{-3}$
100	$1.05 \cdot 10^{-4}$	$1.58 \cdot 10^{-4}$	$1.62 \cdot 10^{-3}$	$3.17 \cdot 10^{-4}$	$5.39 \cdot 10^{-3}$	$1.20 \cdot 10^{-2}$
105	$2.00 \cdot 10^{-4}$	$3.00 \cdot 10^{-4}$	$3.56 \cdot 10^{-3}$	$6.01 \cdot 10^{-4}$	$1.18 \cdot 10^{-2}$	$2.61 \cdot 10^{-2}$
110	$4.08 \cdot 10^{-4}$	$6.12 \cdot 10^{-4}$	$7.06 \cdot 10^{-3}$	$1.22 \cdot 10^{-3}$	$2.36 \cdot 10^{-2}$	$5.20 \cdot 10^{-2}$
115	$8.13 \cdot 10^{-4}$	$1.22 \cdot 10^{-3}$	$1.27 \cdot 10^{-2}$	$2.44 \cdot 10^{-3}$	$4.31 \cdot 10^{-2}$	$9.46 \cdot 10^{-2}$
120	$1.50 \cdot 10^{-3}$	$2.24 \cdot 10^{-3}$	$2.09 \cdot 10^{-2}$	$4.48 \cdot 10^{-3}$	$7.19 \cdot 10^{-2}$	$1.58 \cdot 10^{-1}$
125	$2.49 \cdot 10^{-3}$	$3.73 \cdot 10^{-3}$	$3.17 \cdot 10^{-2}$	$7.45 \cdot 10^{-3}$	$1.10 \cdot 10^{-1}$	$2.42 \cdot 10^{-1}$
130	$3.75 \cdot 10^{-3}$	$5.63 \cdot 10^{-3}$	$4.47 \cdot 10^{-2}$	$1.12 \cdot 10^{-2}$	$1.57 \cdot 10^{-1}$	$3.44 \cdot 10^{-1}$
135	$5.15 \cdot 10^{-3}$	$7.73 \cdot 10^{-3}$	$5.90 \cdot 10^{-2}$	$1.54 \cdot 10^{-2}$	$2.09 \cdot 10^{-1}$	$4.57 \cdot 10^{-1}$
140	$6.48 \cdot 10^{-3}$	$9.71 \cdot 10^{-3}$	$7.38 \cdot 10^{-2}$	$1.93 \cdot 10^{-2}$	$2.62 \cdot 10^{-1}$	$5.72 \cdot 10^{-1}$
145	$7.46 \cdot 10^{-3}$	$1.12 \cdot 10^{-2}$	$8.83 \cdot 10^{-2}$	$2.22 \cdot 10^{-2}$	$3.12 \cdot 10^{-1}$	$6.81 \cdot 10^{-1}$
150	$7.76 \cdot 10^{-3}$	$1.16 \cdot 10^{-2}$	$1.02 \cdot 10^{-1}$	$2.32 \cdot 10^{-2}$	$3.57 \cdot 10^{-1}$	$7.80 \cdot 10^{-1}$
155	$6.90 \cdot 10^{-3}$	$1.03 \cdot 10^{-2}$	$1.17 \cdot 10^{-1}$	$2.06 \cdot 10^{-2}$	$3.97 \cdot 10^{-1}$	$8.69 \cdot 10^{-1}$
160	$3.89 \cdot 10^{-3}$	$5.84 \cdot 10^{-3}$	$1.33 \cdot 10^{-1}$	$1.16 \cdot 10^{-2}$	$4.33 \cdot 10^{-1}$	$9.50 \cdot 10^{-1}$
165	$2.08 \cdot 10^{-3}$	$3.12 \cdot 10^{-3}$	$1.41 \cdot 10^{-1}$	$6.21 \cdot 10^{-3}$	$4.47 \cdot 10^{-1}$	$9.82 \cdot 10^{-1}$
170	$2.21 \cdot 10^{-3}$	$3.32 \cdot 10^{-3}$	$1.41 \cdot 10^{-1}$	$6.61 \cdot 10^{-3}$	$4.50 \cdot 10^{-1}$	$9.88 \cdot 10^{-1}$
175	$3.03 \cdot 10^{-3}$	$4.54 \cdot 10^{-3}$	$1.40 \cdot 10^{-1}$	$9.05 \cdot 10^{-3}$	$4.51 \cdot 10^{-1}$	$9.91 \cdot 10^{-1}$
180	$5.65 \cdot 10^{-3}$	$8.47 \cdot 10^{-3}$	$1.37 \cdot 10^{-1}$	$1.69 \cdot 10^{-2}$	$4.53 \cdot 10^{-1}$	$9.92 \cdot 10^{-1}$
185	$1.41 \cdot 10^{-2}$	$2.11 \cdot 10^{-2}$	$1.24 \cdot 10^{-1}$	$4.21 \cdot 10^{-2}$	$4.57 \cdot 10^{-1}$	$9.94 \cdot 10^{-1}$
190	$1.97 \cdot 10^{-2}$	$2.95 \cdot 10^{-2}$	$1.15 \cdot 10^{-1}$	$5.87 \cdot 10^{-2}$	$4.59 \cdot 10^{-1}$	$9.95 \cdot 10^{-1}$
195	$2.24 \cdot 10^{-2}$	$3.36 \cdot 10^{-2}$	$1.11 \cdot 10^{-1}$	$6.69 \cdot 10^{-2}$	$4.60 \cdot 10^{-1}$	$9.96 \cdot 10^{-1}$
200	$2.40 \cdot 10^{-2}$	$3.60 \cdot 10^{-2}$	$1.08 \cdot 10^{-1}$	$7.16 \cdot 10^{-2}$	$4.61 \cdot 10^{-1}$	$9.96 \cdot 10^{-1}$
210	$2.57 \cdot 10^{-2}$	$3.86 \cdot 10^{-2}$	$1.06 \cdot 10^{-1}$	$7.68 \cdot 10^{-2}$	$4.62 \cdot 10^{-1}$	$9.97 \cdot 10^{-1}$
220	$2.66 \cdot 10^{-2}$	$3.99 \cdot 10^{-2}$	$1.05 \cdot 10^{-1}$	$7.95 \cdot 10^{-2}$	$4.63 \cdot 10^{-1}$	$9.97 \cdot 10^{-1}$
230	$2.72 \cdot 10^{-2}$	$4.07 \cdot 10^{-2}$	$1.04 \cdot 10^{-1}$	$8.12 \cdot 10^{-2}$	$4.63 \cdot 10^{-1}$	$9.98 \cdot 10^{-1}$
240	$2.76 \cdot 10^{-2}$	$4.13 \cdot 10^{-2}$	$1.03 \cdot 10^{-1}$	$8.23 \cdot 10^{-2}$	$4.63 \cdot 10^{-1}$	$9.98 \cdot 10^{-1}$
250	$2.78 \cdot 10^{-2}$	$4.18 \cdot 10^{-2}$	$1.03 \cdot 10^{-1}$	$8.32 \cdot 10^{-2}$	$4.64 \cdot 10^{-1}$	$9.98 \cdot 10^{-1}$
260	$2.81 \cdot 10^{-2}$	$4.21 \cdot 10^{-2}$	$1.02 \cdot 10^{-1}$	$8.39 \cdot 10^{-2}$	$4.64 \cdot 10^{-1}$	$9.98 \cdot 10^{-1}$
270	$2.83 \cdot 10^{-2}$	$4.24 \cdot 10^{-2}$	$1.02 \cdot 10^{-1}$	$8.45 \cdot 10^{-2}$	$4.64 \cdot 10^{-1}$	$9.98 \cdot 10^{-1}$
280	$2.85 \cdot 10^{-2}$	$4.27 \cdot 10^{-2}$	$1.02 \cdot 10^{-1}$	$8.51 \cdot 10^{-2}$	$4.64 \cdot 10^{-1}$	$9.98 \cdot 10^{-1}$
290	$2.86 \cdot 10^{-2}$	$4.30 \cdot 10^{-2}$	$1.02 \cdot 10^{-1}$	$8.56 \cdot 10^{-2}$	$4.64 \cdot 10^{-1}$	$9.99 \cdot 10^{-1}$
300	$2.88 \cdot 10^{-2}$	$4.32 \cdot 10^{-2}$	$1.01 \cdot 10^{-1}$	$8.60 \cdot 10^{-2}$	$4.64 \cdot 10^{-1}$	$9.99 \cdot 10^{-1}$
310	$2.89 \cdot 10^{-2}$	$4.34 \cdot 10^{-2}$	$1.01 \cdot 10^{-1}$	$8.64 \cdot 10^{-2}$	$4.64 \cdot 10^{-1}$	$9.99 \cdot 10^{-1}$
320	$2.90 \cdot 10^{-2}$	$4.35 \cdot 10^{-2}$	$1.01 \cdot 10^{-1}$	$8.67 \cdot 10^{-2}$	$4.64 \cdot 10^{-1}$	$9.98 \cdot 10^{-1}$
330	$2.91 \cdot 10^{-2}$	$4.37 \cdot 10^{-2}$	$1.01 \cdot 10^{-1}$	$8.70 \cdot 10^{-2}$	$4.64 \cdot 10^{-1}$	$9.98 \cdot 10^{-1}$
340	$2.92 \cdot 10^{-2}$	$4.37 \cdot 10^{-2}$	$1.01 \cdot 10^{-1}$	$8.72 \cdot 10^{-2}$	$4.64 \cdot 10^{-1}$	$9.98 \cdot 10^{-1}$
350	$2.88 \cdot 10^{-2}$	$4.32 \cdot 10^{-2}$	$9.90 \cdot 10^{-2}$	$8.61 \cdot 10^{-2}$	$4.57 \cdot 10^{-1}$	$9.83 \cdot 10^{-1}$
360	$2.78 \cdot 10^{-2}$	$4.17 \cdot 10^{-2}$	$9.53 \cdot 10^{-2}$	$8.31 \cdot 10^{-2}$	$4.41 \cdot 10^{-1}$	$9.47 \cdot 10^{-1}$
370	$2.69 \cdot 10^{-2}$	$4.04 \cdot 10^{-2}$	$9.20 \cdot 10^{-2}$	$8.05 \cdot 10^{-2}$	$4.26 \cdot 10^{-1}$	$9.15 \cdot 10^{-1}$
380	$2.62 \cdot 10^{-2}$	$3.93 \cdot 10^{-2}$	$8.92 \cdot 10^{-2}$	$7.83 \cdot 10^{-2}$	$4.13 \cdot 10^{-1}$	$8.89 \cdot 10^{-1}$
390	$2.57 \cdot 10^{-2}$	$3.85 \cdot 10^{-2}$	$8.70 \cdot 10^{-2}$	$7.66 \cdot 10^{-2}$	$4.03 \cdot 10^{-1}$	$8.67 \cdot 10^{-1}$
400	$2.52 \cdot 10^{-2}$	$3.78 \cdot 10^{-2}$	$8.52 \cdot 10^{-2}$	$7.54 \cdot 10^{-2}$	$3.96 \cdot 10^{-1}$	$8.50 \cdot 10^{-1}$
410	$2.49 \cdot 10^{-2}$	$3.74 \cdot 10^{-2}$	$8.38 \cdot 10^{-2}$	$7.44 \cdot 10^{-2}$	$3.90 \cdot 10^{-1}$	$8.37 \cdot 10^{-1}$
420	$2.47 \cdot 10^{-2}$	$3.70 \cdot 10^{-2}$	$8.27 \cdot 10^{-2}$	$7.37 \cdot 10^{-2}$	$3.85 \cdot 10^{-1}$	$8.27 \cdot 10^{-1}$
430	$2.45 \cdot 10^{-2}$	$3.68 \cdot 10^{-2}$	$8.18 \cdot 10^{-2}$	$7.32 \cdot 10^{-2}$	$3.81 \cdot 10^{-1}$	$8.20 \cdot 10^{-1}$
440	$2.44 \cdot 10^{-2}$	$3.66 \cdot 10^{-2}$	$8.12 \cdot 10^{-2}$	$7.29 \cdot 10^{-2}$	$3.79 \cdot 10^{-1}$	$8.14 \cdot 10^{-1}$
450	$2.43 \cdot 10^{-2}$	$3.65 \cdot 10^{-2}$	$8.07 \cdot 10^{-2}$	$7.27 \cdot 10^{-2}$	$3.77 \cdot 10^{-1}$	$8.10 \cdot 10^{-1}$
460	$2.43 \cdot 10^{-2}$	$3.65 \cdot 10^{-2}$	$8.04 \cdot 10^{-2}$	$7.26 \cdot 10^{-2}$	$3.76 \cdot 10^{-1}$	$8.08 \cdot 10^{-1}$
470	$2.43 \cdot 10^{-2}$	$3.65 \cdot 10^{-2}$	$8.01 \cdot 10^{-2}$	$7.26 \cdot 10^{-2}$	$3.75 \cdot 10^{-1}$	$8.06 \cdot 10^{-1}$
480	$2.43 \cdot 10^{-2}$	$3.65 \cdot 10^{-2}$	$8.00 \cdot 10^{-2}$	$7.27 \cdot 10^{-2}$	$3.75 \cdot 10^{-1}$	$8.06 \cdot 10^{-1}$
490	$2.44 \cdot 10^{-2}$	$3.66 \cdot 10^{-2}$	$7.99 \cdot 10^{-2}$	$7.29 \cdot 10^{-2}$	$3.75 \cdot 10^{-1}$	$8.06 \cdot 10^{-1}$

Table 34: SM Higgs branching ratios for 4-fermion final states in the high-mass range. We list results for the specific final states for 2 charged leptons plus 2 quarks, $l^+\nu_1 q\overline{q}'$ (not including charge conjugate state), 2 neutrinos plus 2 quarks, 4 quarks, as well as the result for arbitrary 4 fermions, where q = udscb and ν_1 represents any type of neutrinos.

M_H [GeV]	$H \to l^+l^- q\overline{q}$ ($l = e$ or μ)	$H \to l^+l^- q\overline{q}$ ($l = e, \mu$ or τ)	$H \to l^+\nu_1 q\overline{q}'$ ($l = e$ or μ)	$H \to \nu_1\overline{\nu}_1 q\overline{q}$	$H \to qqqq$	$H \to ffff$
500	$2.45 \cdot 10^{-2}$	$3.67 \cdot 10^{-2}$	$7.99 \cdot 10^{-2}$	$7.31 \cdot 10^{-2}$	$3.75 \cdot 10^{-1}$	$8.06 \cdot 10^{-1}$
510	$2.45 \cdot 10^{-2}$	$3.68 \cdot 10^{-2}$	$8.00 \cdot 10^{-2}$	$7.33 \cdot 10^{-2}$	$3.76 \cdot 10^{-1}$	$8.08 \cdot 10^{-1}$
520	$2.46 \cdot 10^{-2}$	$3.70 \cdot 10^{-2}$	$8.01 \cdot 10^{-2}$	$7.36 \cdot 10^{-2}$	$3.76 \cdot 10^{-1}$	$8.09 \cdot 10^{-1}$
530	$2.47 \cdot 10^{-2}$	$3.71 \cdot 10^{-2}$	$8.02 \cdot 10^{-2}$	$7.39 \cdot 10^{-2}$	$3.77 \cdot 10^{-1}$	$8.11 \cdot 10^{-1}$
540	$2.48 \cdot 10^{-2}$	$3.73 \cdot 10^{-2}$	$8.04 \cdot 10^{-2}$	$7.42 \cdot 10^{-2}$	$3.78 \cdot 10^{-1}$	$8.13 \cdot 10^{-1}$
550	$2.50 \cdot 10^{-2}$	$3.74 \cdot 10^{-2}$	$8.06 \cdot 10^{-2}$	$7.45 \cdot 10^{-2}$	$3.80 \cdot 10^{-1}$	$8.16 \cdot 10^{-1}$
560	$2.51 \cdot 10^{-2}$	$3.76 \cdot 10^{-2}$	$8.08 \cdot 10^{-2}$	$7.48 \cdot 10^{-2}$	$3.81 \cdot 10^{-1}$	$8.18 \cdot 10^{-1}$
570	$2.52 \cdot 10^{-2}$	$3.78 \cdot 10^{-2}$	$8.10 \cdot 10^{-2}$	$7.52 \cdot 10^{-2}$	$3.82 \cdot 10^{-1}$	$8.21 \cdot 10^{-1}$
580	$2.53 \cdot 10^{-2}$	$3.80 \cdot 10^{-2}$	$8.13 \cdot 10^{-2}$	$7.55 \cdot 10^{-2}$	$3.83 \cdot 10^{-1}$	$8.24 \cdot 10^{-1}$
590	$2.54 \cdot 10^{-2}$	$3.81 \cdot 10^{-2}$	$8.15 \cdot 10^{-2}$	$7.59 \cdot 10^{-2}$	$3.85 \cdot 10^{-1}$	$8.27 \cdot 10^{-1}$
600	$2.55 \cdot 10^{-2}$	$3.83 \cdot 10^{-2}$	$8.18 \cdot 10^{-2}$	$7.63 \cdot 10^{-2}$	$3.86 \cdot 10^{-1}$	$8.30 \cdot 10^{-1}$
610	$2.57 \cdot 10^{-2}$	$3.85 \cdot 10^{-2}$	$8.21 \cdot 10^{-2}$	$7.66 \cdot 10^{-2}$	$3.88 \cdot 10^{-1}$	$8.33 \cdot 10^{-1}$
620	$2.58 \cdot 10^{-2}$	$3.87 \cdot 10^{-2}$	$8.23 \cdot 10^{-2}$	$7.70 \cdot 10^{-2}$	$3.89 \cdot 10^{-1}$	$8.37 \cdot 10^{-1}$
630	$2.59 \cdot 10^{-2}$	$3.89 \cdot 10^{-2}$	$8.26 \cdot 10^{-2}$	$7.74 \cdot 10^{-2}$	$3.91 \cdot 10^{-1}$	$8.40 \cdot 10^{-1}$
640	$2.60 \cdot 10^{-2}$	$3.91 \cdot 10^{-2}$	$8.29 \cdot 10^{-2}$	$7.77 \cdot 10^{-2}$	$3.92 \cdot 10^{-1}$	$8.43 \cdot 10^{-1}$
650	$2.62 \cdot 10^{-2}$	$3.92 \cdot 10^{-2}$	$8.32 \cdot 10^{-2}$	$7.81 \cdot 10^{-2}$	$3.94 \cdot 10^{-1}$	$8.46 \cdot 10^{-1}$
660	$2.63 \cdot 10^{-2}$	$3.94 \cdot 10^{-2}$	$8.35 \cdot 10^{-2}$	$7.84 \cdot 10^{-2}$	$3.95 \cdot 10^{-1}$	$8.49 \cdot 10^{-1}$
670	$2.64 \cdot 10^{-2}$	$3.96 \cdot 10^{-2}$	$8.37 \cdot 10^{-2}$	$7.88 \cdot 10^{-2}$	$3.96 \cdot 10^{-1}$	$8.52 \cdot 10^{-1}$
680	$2.65 \cdot 10^{-2}$	$3.98 \cdot 10^{-2}$	$8.40 \cdot 10^{-2}$	$7.91 \cdot 10^{-2}$	$3.98 \cdot 10^{-1}$	$8.55 \cdot 10^{-1}$
690	$2.66 \cdot 10^{-2}$	$3.99 \cdot 10^{-2}$	$8.43 \cdot 10^{-2}$	$7.95 \cdot 10^{-2}$	$3.99 \cdot 10^{-1}$	$8.59 \cdot 10^{-1}$
700	$2.67 \cdot 10^{-2}$	$4.01 \cdot 10^{-2}$	$8.46 \cdot 10^{-2}$	$7.98 \cdot 10^{-2}$	$4.01 \cdot 10^{-1}$	$8.62 \cdot 10^{-1}$
710	$2.69 \cdot 10^{-2}$	$4.03 \cdot 10^{-2}$	$8.48 \cdot 10^{-2}$	$8.01 \cdot 10^{-2}$	$4.02 \cdot 10^{-1}$	$8.65 \cdot 10^{-1}$
720	$2.70 \cdot 10^{-2}$	$4.04 \cdot 10^{-2}$	$8.51 \cdot 10^{-2}$	$8.05 \cdot 10^{-2}$	$4.04 \cdot 10^{-1}$	$8.68 \cdot 10^{-1}$
730	$2.71 \cdot 10^{-2}$	$4.06 \cdot 10^{-2}$	$8.54 \cdot 10^{-2}$	$8.08 \cdot 10^{-2}$	$4.05 \cdot 10^{-1}$	$8.70 \cdot 10^{-1}$
740	$2.72 \cdot 10^{-2}$	$4.08 \cdot 10^{-2}$	$8.56 \cdot 10^{-2}$	$8.11 \cdot 10^{-2}$	$4.06 \cdot 10^{-1}$	$8.73 \cdot 10^{-1}$
750	$2.73 \cdot 10^{-2}$	$4.09 \cdot 10^{-2}$	$8.59 \cdot 10^{-2}$	$8.14 \cdot 10^{-2}$	$4.08 \cdot 10^{-1}$	$8.76 \cdot 10^{-1}$
760	$2.74 \cdot 10^{-2}$	$4.11 \cdot 10^{-2}$	$8.61 \cdot 10^{-2}$	$8.17 \cdot 10^{-2}$	$4.09 \cdot 10^{-1}$	$8.79 \cdot 10^{-1}$
770	$2.75 \cdot 10^{-2}$	$4.12 \cdot 10^{-2}$	$8.64 \cdot 10^{-2}$	$8.20 \cdot 10^{-2}$	$4.10 \cdot 10^{-1}$	$8.82 \cdot 10^{-1}$
780	$2.76 \cdot 10^{-2}$	$4.14 \cdot 10^{-2}$	$8.66 \cdot 10^{-2}$	$8.23 \cdot 10^{-2}$	$4.11 \cdot 10^{-1}$	$8.85 \cdot 10^{-1}$
790	$2.77 \cdot 10^{-2}$	$4.15 \cdot 10^{-2}$	$8.69 \cdot 10^{-2}$	$8.26 \cdot 10^{-2}$	$4.12 \cdot 10^{-1}$	$8.87 \cdot 10^{-1}$
800	$2.78 \cdot 10^{-2}$	$4.17 \cdot 10^{-2}$	$8.71 \cdot 10^{-2}$	$8.28 \cdot 10^{-2}$	$4.14 \cdot 10^{-1}$	$8.90 \cdot 10^{-1}$
810	$2.79 \cdot 10^{-2}$	$4.18 \cdot 10^{-2}$	$8.74 \cdot 10^{-2}$	$8.31 \cdot 10^{-2}$	$4.15 \cdot 10^{-1}$	$8.92 \cdot 10^{-1}$
820	$2.79 \cdot 10^{-2}$	$4.19 \cdot 10^{-2}$	$8.76 \cdot 10^{-2}$	$8.34 \cdot 10^{-2}$	$4.16 \cdot 10^{-1}$	$8.95 \cdot 10^{-1}$
830	$2.80 \cdot 10^{-2}$	$4.21 \cdot 10^{-2}$	$8.78 \cdot 10^{-2}$	$8.36 \cdot 10^{-2}$	$4.17 \cdot 10^{-1}$	$8.97 \cdot 10^{-1}$
840	$2.81 \cdot 10^{-2}$	$4.22 \cdot 10^{-2}$	$8.81 \cdot 10^{-2}$	$8.39 \cdot 10^{-2}$	$4.18 \cdot 10^{-1}$	$9.00 \cdot 10^{-1}$
850	$2.82 \cdot 10^{-2}$	$4.23 \cdot 10^{-2}$	$8.83 \cdot 10^{-2}$	$8.41 \cdot 10^{-2}$	$4.19 \cdot 10^{-1}$	$9.02 \cdot 10^{-1}$
860	$2.83 \cdot 10^{-2}$	$4.24 \cdot 10^{-2}$	$8.85 \cdot 10^{-2}$	$8.44 \cdot 10^{-2}$	$4.20 \cdot 10^{-1}$	$9.04 \cdot 10^{-1}$
870	$2.84 \cdot 10^{-2}$	$4.26 \cdot 10^{-2}$	$8.87 \cdot 10^{-2}$	$8.46 \cdot 10^{-2}$	$4.21 \cdot 10^{-1}$	$9.07 \cdot 10^{-1}$
880	$2.84 \cdot 10^{-2}$	$4.27 \cdot 10^{-2}$	$8.89 \cdot 10^{-2}$	$8.48 \cdot 10^{-2}$	$4.22 \cdot 10^{-1}$	$9.09 \cdot 10^{-1}$
890	$2.85 \cdot 10^{-2}$	$4.28 \cdot 10^{-2}$	$8.91 \cdot 10^{-2}$	$8.51 \cdot 10^{-2}$	$4.23 \cdot 10^{-1}$	$9.11 \cdot 10^{-1}$
900	$2.86 \cdot 10^{-2}$	$4.29 \cdot 10^{-2}$	$8.94 \cdot 10^{-2}$	$8.53 \cdot 10^{-2}$	$4.24 \cdot 10^{-1}$	$9.13 \cdot 10^{-1}$
910	$2.87 \cdot 10^{-2}$	$4.30 \cdot 10^{-2}$	$8.96 \cdot 10^{-2}$	$8.55 \cdot 10^{-2}$	$4.25 \cdot 10^{-1}$	$9.15 \cdot 10^{-1}$
920	$2.87 \cdot 10^{-2}$	$4.31 \cdot 10^{-2}$	$8.97 \cdot 10^{-2}$	$8.57 \cdot 10^{-2}$	$4.26 \cdot 10^{-1}$	$9.17 \cdot 10^{-1}$
930	$2.88 \cdot 10^{-2}$	$4.32 \cdot 10^{-2}$	$8.99 \cdot 10^{-2}$	$8.59 \cdot 10^{-2}$	$4.27 \cdot 10^{-1}$	$9.19 \cdot 10^{-1}$
940	$2.89 \cdot 10^{-2}$	$4.33 \cdot 10^{-2}$	$9.01 \cdot 10^{-2}$	$8.61 \cdot 10^{-2}$	$4.28 \cdot 10^{-1}$	$9.21 \cdot 10^{-1}$
950	$2.90 \cdot 10^{-2}$	$4.34 \cdot 10^{-2}$	$9.03 \cdot 10^{-2}$	$8.63 \cdot 10^{-2}$	$4.29 \cdot 10^{-1}$	$9.23 \cdot 10^{-1}$
960	$2.90 \cdot 10^{-2}$	$4.35 \cdot 10^{-2}$	$9.05 \cdot 10^{-2}$	$8.65 \cdot 10^{-2}$	$4.30 \cdot 10^{-1}$	$9.25 \cdot 10^{-1}$
970	$2.91 \cdot 10^{-2}$	$4.36 \cdot 10^{-2}$	$9.07 \cdot 10^{-2}$	$8.67 \cdot 10^{-2}$	$4.30 \cdot 10^{-1}$	$9.27 \cdot 10^{-1}$
980	$2.92 \cdot 10^{-2}$	$4.37 \cdot 10^{-2}$	$9.09 \cdot 10^{-2}$	$8.69 \cdot 10^{-2}$	$4.31 \cdot 10^{-1}$	$9.29 \cdot 10^{-1}$
990	$2.92 \cdot 10^{-2}$	$4.38 \cdot 10^{-2}$	$9.10 \cdot 10^{-2}$	$8.71 \cdot 10^{-2}$	$4.32 \cdot 10^{-1}$	$9.31 \cdot 10^{-1}$
1000	$2.93 \cdot 10^{-2}$	$4.39 \cdot 10^{-2}$	$9.12 \cdot 10^{-2}$	$8.73 \cdot 10^{-2}$	$4.33 \cdot 10^{-1}$	$9.32 \cdot 10^{-1}$

Table 35: MSSM Higgs branching ratio to $\tau^+\tau^-$ final states in the $m_h^{\max}$ scenario as a function of M_A [GeV] and $\tan\beta$. The format in each cell is M_h [GeV], BR(h $\to \tau^+\tau^-$) (upper line), M_H [GeV], BR(H $\to \tau^+\tau^-$) (middle line), M_A [GeV], BR(A $\to \tau^+\tau^-$) (lower line).

M_A	$\tan\beta=20$	$\tan\beta=30$	$\tan\beta=40$	$\tan\beta=50$	$\tan\beta=60$
90	89.6 $1.09\cdot10^{-1}$	89.8 $1.17\cdot10^{-1}$	89.9 $1.25\cdot10^{-1}$	89.9 $1.34\cdot10^{-1}$	89.9 $1.44\cdot10^{-1}$
	130.6 $9.63\cdot10^{-2}$	130.9 $1.05\cdot10^{-1}$	130.6 $1.15\cdot10^{-1}$	130.7 $1.20\cdot10^{-1}$	130.9 $1.36\cdot10^{-1}$
	90.0 $1.09\cdot10^{-1}$	90.0 $1.16\cdot10^{-1}$	90.0 $1.25\cdot10^{-1}$	90.0 $1.33\cdot10^{-1}$	90.0 $1.43\cdot10^{-1}$
100	99.4 $1.11\cdot10^{-1}$	99.7 $1.19\cdot10^{-1}$	99.9 $1.28\cdot10^{-1}$	99.9 $1.37\cdot10^{-1}$	99.9 $1.47\cdot10^{-1}$
	130.8 $1.06\cdot10^{-1}$	130.6 $1.16\cdot10^{-1}$	130.6 $1.27\cdot10^{-1}$	130.7 $1.38\cdot10^{-1}$	130.9 $1.50\cdot10^{-1}$
	100.0 $1.11\cdot10^{-1}$	100.0 $1.18\cdot10^{-1}$	100.0 $1.27\cdot10^{-1}$	100.0 $1.36\cdot10^{-1}$	100.0 $1.45\cdot10^{-1}$
110	109.0 $1.13\cdot10^{-1}$	109.6 $1.21\cdot10^{-1}$	109.8 $1.30\cdot10^{-1}$	109.8 $1.39\cdot10^{-1}$	109.9 $1.50\cdot10^{-1}$
	131.1 $1.13\cdot10^{-1}$	130.7 $1.23\cdot10^{-1}$	130.7 $1.33\cdot10^{-1}$	130.8 $1.45\cdot10^{-1}$	130.9 $1.57\cdot10^{-1}$
	110.0 $1.12\cdot10^{-1}$	110.0 $1.20\cdot10^{-1}$	110.0 $1.29\cdot10^{-1}$	110.0 $1.37\cdot10^{-1}$	110.0 $1.47\cdot10^{-1}$
120	118.2 $1.14\cdot10^{-1}$	119.1 $1.23\cdot10^{-1}$	119.5 $1.32\cdot10^{-1}$	119.7 $1.42\cdot10^{-1}$	119.7 $1.52\cdot10^{-1}$
	132.0 $1.16\cdot10^{-1}$	131.2 $1.25\cdot10^{-1}$	131.0 $1.35\cdot10^{-1}$	130.9 $1.45\cdot10^{-1}$	131.0 $1.57\cdot10^{-1}$
	120.0 $1.14\cdot10^{-1}$	120.0 $1.22\cdot10^{-1}$	120.0 $1.30\cdot10^{-1}$	120.0 $1.39\cdot10^{-1}$	120.0 $1.49\cdot10^{-1}$
130	125.2 $1.15\cdot10^{-1}$	126.9 $1.23\cdot10^{-1}$	127.8 $1.33\cdot10^{-1}$	128.4 $1.43\cdot10^{-1}$	128.9 $1.54\cdot10^{-1}$
	134.9 $1.17\cdot10^{-1}$	133.4 $1.25\cdot10^{-1}$	132.6 $1.34\cdot10^{-1}$	132.2 $1.43\cdot10^{-1}$	131.8 $1.53\cdot10^{-1}$
	130.0 $1.16\cdot10^{-1}$	130.0 $1.23\cdot10^{-1}$	130.0 $1.32\cdot10^{-1}$	130.0 $1.41\cdot10^{-1}$	130.0 $1.51\cdot10^{-1}$
140	128.1 $1.13\cdot10^{-1}$	129.3 $1.21\cdot10^{-1}$	129.8 $1.29\cdot10^{-1}$	130.2 $1.38\cdot10^{-1}$	130.5 $1.48\cdot10^{-1}$
	142.1 $1.18\cdot10^{-1}$	141.1 $1.26\cdot10^{-1}$	140.6 $1.34\cdot10^{-1}$	140.4 $1.43\cdot10^{-1}$	140.3 $1.53\cdot10^{-1}$
	140.0 $1.17\cdot10^{-1}$	140.0 $1.25\cdot10^{-1}$	140.0 $1.33\cdot10^{-1}$	140.0 $1.42\cdot10^{-1}$	140.0 $1.52\cdot10^{-1}$
150	128.9 $1.10\cdot10^{-1}$	129.7 $1.17\cdot10^{-1}$	130.1 $1.24\cdot10^{-1}$	130.4 $1.31\cdot10^{-1}$	130.6 $1.39\cdot10^{-1}$
	151.2 $1.19\cdot10^{-1}$	150.6 $1.27\cdot10^{-1}$	150.4 $1.35\cdot10^{-1}$	150.2 $1.44\cdot10^{-1}$	150.1 $1.54\cdot10^{-1}$
	150.0 $1.18\cdot10^{-1}$	150.0 $1.26\cdot10^{-1}$	150.0 $1.35\cdot10^{-1}$	150.0 $1.44\cdot10^{-1}$	150.0 $1.54\cdot10^{-1}$
160	129.2 $1.07\cdot10^{-1}$	129.9 $1.12\cdot10^{-1}$	130.2 $1.18\cdot10^{-1}$	130.4 $1.24\cdot10^{-1}$	130.6 $1.30\cdot10^{-1}$
	160.9 $1.20\cdot10^{-1}$	160.4 $1.28\cdot10^{-1}$	160.3 $1.36\cdot10^{-1}$	160.2 $1.46\cdot10^{-1}$	160.1 $1.55\cdot10^{-1}$
	160.0 $1.19\cdot10^{-1}$	160.0 $1.27\cdot10^{-1}$	160.0 $1.36\cdot10^{-1}$	160.0 $1.45\cdot10^{-1}$	160.0 $1.55\cdot10^{-1}$
170	129.4 $1.03\cdot10^{-1}$	123.0 $1.07\cdot10^{-1}$	130.2 $1.12\cdot10^{-1}$	130.4 $1.17\cdot10^{-1}$	130.6 $1.23\cdot10^{-1}$
	170.7 $1.21\cdot10^{-1}$	170.4 $1.29\cdot10^{-1}$	170.2 $1.38\cdot10^{-1}$	170.1 $1.47\cdot10^{-1}$	170.1 $1.57\cdot10^{-1}$
	170.0 $1.21\cdot10^{-1}$	170.0 $1.29\cdot10^{-1}$	170.0 $1.37\cdot10^{-1}$	170.0 $1.46\cdot10^{-1}$	170.0 $1.56\cdot10^{-1}$
180	129.5 $9.90\cdot10^{-2}$	130.0 $1.03\cdot10^{-1}$	130.2 $1.07\cdot10^{-1}$	130.4 $1.11\cdot10^{-1}$	130.6 $1.15\cdot10^{-1}$
	180.6 $1.22\cdot10^{-1}$	180.3 $1.30\cdot10^{-1}$	180.2 $1.39\cdot10^{-1}$	180.1 $1.48\cdot10^{-1}$	180.1 $1.58\cdot10^{-1}$
	180.0 $1.20\cdot10^{-1}$	180.0 $1.29\cdot10^{-1}$	180.0 $1.38\cdot10^{-1}$	180.0 $1.47\cdot10^{-1}$	180.0 $1.57\cdot10^{-1}$
190	129.6 $9.55\cdot10^{-2}$	130.0 $9.87\cdot10^{-2}$	130.3 $1.02\cdot10^{-1}$	130.4 $1.06\cdot10^{-1}$	130.6 $1.09\cdot10^{-1}$
	190.5 $1.22\cdot10^{-1}$	190.3 $1.31\cdot10^{-1}$	190.2 $1.40\cdot10^{-1}$	190.1 $1.49\cdot10^{-1}$	190.0 $1.59\cdot10^{-1}$
	190.0 $1.20\cdot10^{-1}$	190.0 $1.30\cdot10^{-1}$	190.0 $1.39\cdot10^{-1}$	190.0 $1.48\cdot10^{-1}$	190.0 $1.58\cdot10^{-1}$
200	129.7 $9.23\cdot10^{-2}$	130.1 $9.50\cdot10^{-2}$	130.3 $9.78\cdot10^{-2}$	130.4 $1.01\cdot10^{-1}$	130.6 $1.04\cdot10^{-1}$
	200.5 $1.23\cdot10^{-1}$	200.3 $1.32\cdot10^{-1}$	200.2 $1.40\cdot10^{-1}$	200.1 $1.50\cdot10^{-1}$	200.0 $1.60\cdot10^{-1}$
	200.0 $1.21\cdot10^{-1}$	200.0 $1.30\cdot10^{-1}$	200.0 $1.40\cdot10^{-1}$	200.0 $1.49\cdot10^{-1}$	200.0 $1.59\cdot10^{-1}$
220	129.7 $8.68\cdot10^{-2}$	130.1 $8.87\cdot10^{-2}$	130.3 $9.08\cdot10^{-2}$	130.4 $9.29\cdot10^{-2}$	130.6 $9.51\cdot10^{-2}$
	220.4 $1.24\cdot10^{-1}$	220.2 $1.33\cdot10^{-1}$	220.1 $1.42\cdot10^{-1}$	220.1 $1.52\cdot10^{-1}$	220.0 $1.62\cdot10^{-1}$
	220.0 $1.22\cdot10^{-1}$	220.0 $1.32\cdot10^{-1}$	220.0 $1.41\cdot10^{-1}$	220.0 $1.51\cdot10^{-1}$	220.0 $1.61\cdot10^{-1}$
240	129.8 $8.24\cdot10^{-2}$	130.1 $8.37\cdot10^{-2}$	130.3 $8.53\cdot10^{-2}$	130.4 $8.69\cdot10^{-2}$	130.6 $8.85\cdot10^{-2}$
	240.4 $1.25\cdot10^{-1}$	240.2 $1.35\cdot10^{-1}$	240.2 $1.44\cdot10^{-1}$	240.1 $1.53\cdot10^{-1}$	240.0 $1.63\cdot10^{-1}$
	240.0 $1.21\cdot10^{-1}$	240.0 $1.33\cdot10^{-1}$	240.0 $1.43\cdot10^{-1}$	240.0 $1.53\cdot10^{-1}$	240.0 $1.63\cdot10^{-1}$
260	129.8 $7.88\cdot10^{-2}$	130.1 $7.98\cdot10^{-2}$	130.3 $8.10\cdot10^{-2}$	130.4 $8.22\cdot10^{-2}$	130.6 $8.35\cdot10^{-2}$
	260.4 $1.25\cdot10^{-1}$	260.2 $1.35\cdot10^{-1}$	260.2 $1.45\cdot10^{-1}$	260.1 $1.55\cdot10^{-1}$	260.0 $1.65\cdot10^{-1}$
	260.0 $1.17\cdot10^{-1}$	260.0 $1.31\cdot10^{-1}$	260.0 $1.42\cdot10^{-1}$	260.0 $1.53\cdot10^{-1}$	260.0 $1.63\cdot10^{-1}$
280	129.8 $7.60\cdot10^{-2}$	130.1 $7.67\cdot10^{-2}$	130.3 $7.76\cdot10^{-2}$	130.4 $7.85\cdot10^{-2}$	130.6 $7.95\cdot10^{-2}$
	280.4 $1.24\cdot10^{-1}$	280.2 $1.36\cdot10^{-1}$	280.2 $1.46\cdot10^{-1}$	280.1 $1.56\cdot10^{-1}$	280.0 $1.66\cdot10^{-1}$
	280.0 $1.16\cdot10^{-1}$	280.0 $1.31\cdot10^{-1}$	280.0 $1.43\cdot10^{-1}$	280.0 $1.54\cdot10^{-1}$	280.0 $1.64\cdot10^{-1}$
300	129.8 $7.36\cdot10^{-2}$	130.1 $7.41\cdot10^{-2}$	130.3 $7.48\cdot10^{-2}$	130.4 $7.56\cdot10^{-2}$	130.6 $7.64\cdot10^{-2}$
	300.4 $1.22\cdot10^{-1}$	300.3 $1.36\cdot10^{-1}$	300.3 $1.46\cdot10^{-1}$	300.2 $1.56\cdot10^{-1}$	300.1 $1.67\cdot10^{-1}$
	300.0 $1.06\cdot10^{-1}$	300.0 $1.27\cdot10^{-1}$	300.0 $1.41\cdot10^{-1}$	300.0 $1.53\cdot10^{-1}$	300.0 $1.65\cdot10^{-1}$

10 NLO Monte Carlo event generators[17]

10.1 Introduction

In recent years Monte Carlo event generators have been the subject of great theoretical and practical developments, most significantly in the extension of existing parton-shower simulations to consistently include exact next-to-leading order (NLO) corrections [304–322] and, separately, in the consistent combination of parton-shower simulations and high-multiplicity tree-level matrix-element generators [323–331].

In this note we aim at concisely reviewing the basic principles of the new generation of tools which are now available, underlying the most important improvements with respect to a more standard parton-shower approach. We provide also guidelines for experimentalists on which tools to use for a given Higgs production channel, on the possible improvements/limitations and on how to perform a meaningful cross validation of the MC tools used in an experimental analysis vis-a-vis the best theoretical predictions available at a given moment (for example, at NNLO level). As a result, we provide enough motivation for the new MC tools to be used as *default* analysis tools, both to better tune Higgs-boson searches and to perform precise measurements of its properties. We also aim at providing guidelines for how and when to use these tools. We conclude by summarising the results and by commenting on the readiness of these theoretical tools for anticipated Higgs analyses, and by adding a wish-list for tools from the experimentalist point of view.

10.2 Embedding higher-order corrections into parton-shower Monte Carlo event generators

10.2.1 NLO cross sections

Let us start by reminding the equation describing the calculation of next-to-leading order corrections in QCD for a $2 \rightarrow n$ process; schematically it reads

$$\mathrm{d}\sigma^{(\mathrm{NLO})} = \mathrm{d}\Phi_B \left[B(\Phi_B) + V(\Phi_B) \right] + \mathrm{d}\Phi_R R(\Phi_R) , \tag{17}$$

where Φ_B and Φ_R denote the phase-space elements related to the $2 \rightarrow n$ (Born level) and $2 \rightarrow n+1$ (real-emission correction) kinematics; $B(\Phi_B), V(\Phi_B)$ denote the Born-level and the virtual contribution, while $R(\Phi_R)$ is the real-emission correction.

In this equation the virtual term contains soft and collinear divergences. When integrated over the full real phase space, the real term generates soft and collinear divergences, too, and only when *infrared(IR)-safe* quantities are computed, these divergences cancel to yield a finite result. IR-safe observables $O(\Phi)$ can be best understood by considering the soft or collinear limit of Φ_R, i.e. when the additional parton has low energy or is parallel to another parton. In this limit, an IR-safe observable yields $\lim O(\Phi_R) = O(\Phi_B)$, where the Born-level configuration Φ_B is obtained from Φ_R by eliminating the soft particle (in case of soft singularities) or by merging the collinear particles (in case of collinear singularities).

Technically, singularities are often handled with the subtraction method, where the real phase space is parametrized in terms of an underlying Born phase space Φ_B and a radiation phase space $\Phi_{R|B}$. The only requirement upon this parametrization is that, in the singular limits, by merging collinear partons, or eliminating the soft parton, the real phase becomes equal to the underlying Born one. Then the expectation value of an IR-safe observable reads

$$
\begin{aligned}
\int \mathrm{d}\sigma^{(\mathrm{NLO})} O(\Phi) &= \int \mathrm{d}\Phi_B \left[B(\Phi_B) + V(\Phi_B) \right] O(\Phi_B) + \int \mathrm{d}\Phi_R R(\Phi_R)\, O(\Phi_R) \\
&= \int \mathrm{d}\Phi_B \left[B(\Phi_B) + V(\Phi_B) + \int \mathrm{d}\Phi_{R|B} S(\Phi_R) \right] O(\Phi_B)
\end{aligned}
$$

---

[17]M. Felcini, F. Krauss, F. Maltoni, P. Nason and J. Yu.

$$+ \quad \int \mathrm{d}\Phi_R \left[R(\Phi_R)\, O(\Phi_R) - S(\Phi_R) O(\Phi_B) \right] \,. \tag{18}$$

The third member of the above equation is obtained by adding and subtracting the same quantity from the two terms of the second member. The terms $S(\Phi_{R|B})$ are the subtraction terms, which contain all soft and collinear singularities of the real-emission term. Typically, using the universality of soft and collinear divergences, they are written in a factorised form as

$$S(\Phi_R) = B(\Phi_B) \otimes \tilde{S}(\Phi_{R|B})\,, \tag{19}$$

where the $\tilde{S}(\Phi_{R|B})$ can be composed from universal, process-independent subtraction kernels with analytically known (divergent) integrals. These integral, when summed and added to the virtual term, yield a finite result. The second term of the last member of Eq. (18) is also finite if O is an IR-safe observable, since by construction S cancels all singularities in R in the soft and collinear regions.

In the following we will always write the NLO corrections in the form of Eq. (17), assuming that a subtraction procedure is carried out in order to evaluate it explicitly.

10.2.2 Parton shower (PS)

Parton showers are able to dress a given Born process with all the dominant (i.e. enhanced by collinear logarithms, and to some extent also soft ones) QCD radiation processes at all orders in perturbation theory. In particular, also the hardest radiation includes next-to-leading order corrections, but only the dominant ones, i.e. those given by the leading logarithms. The cross section for the hardest emission in a shower – often this is the first emission – reads:

$$\mathrm{d}\sigma^{\mathrm{PS}} = \mathrm{d}\Phi_B B(\Phi_B) \left[\Delta(p_\perp^{\mathrm{min}}) + \mathrm{d}\Phi_{R|B} \Delta(p_{\mathrm{T}}(\Phi_{R|B})) \frac{R^{\mathrm{PS}}(\Phi_R)}{B(\Phi_B)} \right] \,, \tag{20}$$

where $\Delta(p_{\mathrm{T}})$ denotes the Sudakov form factor

$$\Delta(p_{\mathrm{T}}) = \exp\left[- \int \mathrm{d}\Phi_{R|B} \frac{R^{\mathrm{PS}}(\Phi_R)}{B(\Phi_B)} \Theta(p_{\mathrm{T}}(\Phi_R) - p_{\mathrm{T}}) \right] \,. \tag{21}$$

This Sudakov form factor can be understood as a no-emission probability of secondary partons down to a resolution scale of p_{T}. Here R^{PS} represents the PS approximation to the real cross section, typically given schematically by a product of the underlying Born-level term folded with a process-independent universal splitting function P:

$$R^{\mathrm{PS}}(\Phi) = P(\Phi_{R|B})\, B(\Phi_B). \tag{22}$$

In this framework, $\Phi_{R|B}$ is often expressed in terms of three showering variables, like the virtuality t in the splitting process[18], the energy fraction of the splitting z and the azimuth ϕ. The above definition of the Sudakov form factor, guarantees that the square bracket in Eq. (20) integrates to unity, a manifestation of the probabilistic nature of the parton shower. Thus, integrating the shower cross section over the radiation variables yields the total cross section, given at LO by the Born amplitude. The corresponding radiation pattern consists of two parts: one given by the first term in the square bracket, where no further resolvable emission above the parton-shower cut-off $p_\perp^{\mathrm{min}}$ – typically of the order of 1 GeV – emerges, and the other given by the second term in the square bracket describing the first emission, as determined by the splitting kernel.

It is important to stress that the real-emission cross section in a PS generator is only correct in the small angle and/or soft limit, where R^{PS} is a reliable approximation of the complete matrix element.

---

[18]In more modern parton showers the transverse momentum of the splitting or the (scaled) opening angle serve as ordering variables instead of the virtuality, such a choice usually allows to catch more of the leading logarithmic terms.

While rather crude, the PS approximation is a very powerful one, due mainly to the great flexibility and simplicity in the implementation of $2 \to 1$ and $2 \to 2$ high-Q^2 processes. In addition, once augmented with a hadronisation model the simulation can easily provide a full description of a collision in terms of physical final states, i.e., hadrons, leptons and photons. In the current terminology a generic Monte Carlo generator mainly refers to such tools, the most relevant examples of are PYTHIA 6 and PYTHIA 8 [332,333], HERWIG [334], HERWIG++ [335], and SHERPA [336].

It should be noted here, however, that each of these tools employs a variety of the more advanced methods listed below, to enhance its accuracy in the description of the radiation pattern or the total cross sections, thus going in some cases beyond the simple PS approach.

10.2.3 Matrix-element correction (MEC)

A first improvement of the parton-shower approximation is to correct the hardest emission with the *exact first-order real-emission matrix element*. This has traditionally been achieved by matrix-element corrections [337–342]. These are provided by either replacing the approximate expression for the real-emission cross section R^{PS} with the exact one R, or by adding real-emission events with a cross section $R - R^{\mathrm{PS}}$, in order to compensate for the PS inaccuracies (including lack of complete coverage of phase space) in large-angle emissions. Matrix-element corrections in PS have only been introduced for the most simple processes, such as Drell–Yan or W production, Higgs production in gluon fusion, or top decay, all present in PYTHIA 6, PYTHIA 8, HERWIG, and HERWIG++.

Decomposing the real-emission cross section into a singular and non-singular part, $R = R^s + R^f$ (both being non-negative), the first-emission cross section in this method can be written as

$$\mathrm{d}\sigma^{\mathrm{MEC}} = \mathrm{d}\Phi_B B(\Phi_B) \left[\bar{\Delta}(p_\perp^{\min}) + \int_{p_\perp^{\min}} \mathrm{d}\Phi_{R|B} \frac{R^s(\Phi_R)}{B(\Phi_B)} \bar{\Delta}(p_\mathrm{T}(\Phi_{R|B})) \right] + \mathrm{d}\Phi_R R^f(\Phi_R), \qquad (23)$$

where the modified Sudakov form factor is given by replacing the splitting function with the ratio of real-emission and Born-level matrix elements,

$$\bar{\Delta}(p_\mathrm{T}) = \exp \left[- \int_{p_\perp^{\min}} \mathrm{d}\Phi_{R|B} \frac{R^s(\Phi_R)}{B(\Phi_B)} \right] . \qquad (24)$$

Note that the term in the square bracket integrates to unity, as in the usual PS case. In the PYTHIA implementation $R^f = 0$, while in HERWIG, due to the lack of full phase-space coverage the term R^f is introduced, with support only in the region of phase space that the parton shower cannot fill. In the latter the hardest emission is not necessarily the first one, since the ordering parameter is the splitting angle. The correction is thus applied to all branchings that are the hardest so far in the shower development.

While this method correctly reproduces the first-emission kinematics (formally this is a next-to-leading order effect with respect to the Born-level cross section), it does not include the full next-to-leading order accuracy to the total cross section.

10.2.4 NLO+PS

Several proposals have been made for the full inclusion of complete NLO effects in PS generators. At this moment, only two of them have reached a mature enough stage to be used in practice: MC@NLO [304] and POWHEG [311]. Both methods correct – in different ways – the real-emission matrix element to achieve an exact tree-level emission matrix element, even at large angle. As we have seen in the previous subsection, this is what is also achieved with matrix-element corrections in parton showers, at least for the simplest processes listed earlier. This, however, is not sufficient for the NLO accuracy, since the

effect of virtual corrections also needs to be included. In both methods, the real-emission cross section is split into a singular and non-singular part, $R = R^s + R^f$. One then computes the total NLO inclusive cross section, excluding the finite contribution, at fixed underlying Born kinematics, defined as

$$\bar{B}^s = B(\Phi_B) + \left[V(\Phi_B) + \int d\Phi_{R|B} R^s(\Phi_{R|B}) \right] , \tag{25}$$

and uses the formula

$$d\sigma^{\mathrm{NLO+PS}} = d\Phi_B \bar{B}^s(\Phi_B) \left[\Delta^s(p_\perp^{\mathrm{min}}) + d\Phi_{R|B} \frac{R^s(\Phi_R)}{B(\Phi_B)} \Delta^s(p_{\mathrm{T}}(\Phi)) \right] + d\Phi_R R^f(\Phi_R) \tag{26}$$

for the generation of the events. In this formula, the term $\bar{B}$ can be understood as a local K-factor reweighting the soft matrix-element correction part of the simulation. Clearly, employing the fact that the term in the first square bracket integrates to unity, as before, the cross section integrates to the full NLO cross section.

10.2.5   MC@NLO

In MC@NLO one chooses R^s to be identically equal to the term $B \otimes P$ that the PS generator employs to generate emissions. Within MC@NLO, n-body events are obtained using the $\bar{B}^s$ function, and then fed to the PS, which will generate the hardest emission according to Eq. (25). These are called $\mathcal{S}$ events in the MC@NLO language. An appropriate number of events are also generated according to the R^f cross section, and are directly passed to the PS generator. These are called $\mathcal{H}$ events.

In MC@NLO, $R^f = R - R^s$ is not positive definite, and it is thus necessary to generate negative weighted events in this framework.

A library of MC@NLO Higgs processes (gluon fusion, vector-boson associated production, and charged Higgs associated with top) is available at Ref. [236], which is interfaced to HERWIG and HERWIG++. A MC@NLO interface to the virtuality-ordered PYTHIA shower for the W-production process has been recently achieved [343].

10.2.6   POWHEG

In POWHEG, one chooses $R^s \leq R$, and in many cases even $R^s = R$, so that the finite cross section R^f vanishes. In this case, the hardest emission is generated within POWHEG itself, and the process is passed to the parton shower only after the hardest radiation is generated. Positive weighted events are obtained, since R^f can always be chosen to be positive definite. In all cases the chosen R^s has exactly the same singularity structure as R, so that R^f always yield a finite contribution to the cross section.

In angular-ordered parton showers, the hardest emission is not necessarily the first, so that, when interfacing POWHEG to an angular order shower (HERWIG and HERWIG++) soft coherence is spoiled unless truncated showers are introduced. These are in fact generally needed when interfacing angular-ordered parton showers to matrix-element generators. The effect of truncated showers has been studied in the HERWIG++ implementations of POWHEG processes. Implementations of Higgs production processes with the POWHEG method are available in HERWIG++ [318], in the POWHEG BOX [344] (interfaced to both HERWIG and PYTHIA) and recently in SHERPA [345].

10.2.7   Matrix-element merging (ME+PS)

Matrix-element merging [324] aims at correcting as many large-angle emissions as possible with the corresponding tree-level accurate prediction, rather than only *small-angle* accurate. This is achieved by generating events up to a given (high) multiplicity using a matrix-element generator, with some internal jet-resolution parameter Q_{cut} on the jet separation, such that practically all emissions above this scale

are described by corresponding tree-level matrix elements. Their contributions are corrected for running-coupling effects and by Sudakov form factors. Radiation below Q_{cut} on the other hand is generated by a parton-shower program, which is required to veto radiation with separation larger than Q_{cut}. As far as the hardest emission is concerned, matrix-element merging is as accurate as matrix-element corrections (when these are available) or NLO+PS. Since they lack NLO virtual corrections, however, they do not reach NLO accuracy for inclusive quantities. Nevertheless, they are capable to achieve leading-order accuracy for multiple hard radiation, beyond the hardest only, while NLO+PS programs, relying on the parton shower there are only accurate in the collinear and/or soft limit for these quantities.

Several merging schemes have been proposed, which include the CKKW scheme [324–326] and its improvements [330, 331], the MLM matching [323], and the k_{T}-MLM variation [346]. The MLM schemes have been implemented in several matrix element codes such as ALPGEN, HELAC, and MADGRAPH/MADEVENT, through interfaces to PYTHIA/HERWIG, while SHERPA/HERWIG++ have adopted the CKKW schemes and rely on their own parton showers. In Ref. [329] a detailed, although somewhat outdated description of each method has been given and a comparative study has been performed.

Basically all Higgs-boson production processes and their backgrounds are available in this method.

10.2.8 MENLOPS

The MENLOPS method [347, 348] aims at combining matrix-element merging and POWHEG, in such a way that, besides having accurate LO matrix element for multi-jet generation, inclusive observables are also accurate at the NLO level. In essence, one introduces a MENLOPS separation scale, similar to the merging scale above. Events with one extra jet (with respect to the basic process) above the hardest scale are generated by POWHEG, and events with more than one jet are generated by the matrix-element merging method. The method works as long as the fraction of events with more than one extra jet is of the order of an NNLO correction.

10.3 Higgs production channels

In this section we list and briefly discuss, channel by channel, the tools available for the simulation of Higgs production.

10.3.1 Gluon fusion

The gluon-fusion production process is implemented with all methods listed in the previous section. Parton-shower codes based on the $2 \rightarrow 1$ process with the exact m_{t} dependence or in the large-m_{t} limit, and with matrix-element corrections, are available for this process. Furthermore, ME+PS is available in the large-m_{t} limit in several matrix-element-based generators, such as ALPGEN, SHERPA and MADGRAPH/MADEVENT. The MC@NLO and POWHEG (POWHEG BOX, HERWIG++ and SHERPA) implementations use the large-m_{t} limit, but the Born term in the expression for the $\bar{B}$ function is computed with the full m_{t} dependence. Several variations of this approach are also available, the most realistic one being the reweighting of the full $\bar{B}$ function with the ratio of the Born term with exact top mass dependence, with respect to its value in the large-m_{t} limit. Since the full NLO calculation with finite m_{t} is available [8, 10], comparison studies between Monte Carlos and this NLO result can and should be carried out.

A comparison of several available Monte Carlo methods, together with the bare NNLO calculation [349], was performed in the context of Les Houches 2009 [350], page 58. Details of the generation (parameters, inputs, cuts) of some key observables can be found there as well, allowing for a careful further validation and experimental work. The analysis there was performed on the generated final states and, with the exception of HNNLO, after parton showering. Hadronisation effects were included for the MC@NLO and POWHEG results only. MADGRAPH/MADEVENT and SHERPA results have been

rescaled to the HNNLO result, while HERWIG++, MC@NLO, and POWHEG have not been rescaled. In this study it was found that all methods gave a rather consistent behaviour, with only few marginally problematic areas, displayed in Fig. 37. In particular, the MC@NLO result exhibits a much softer p_T
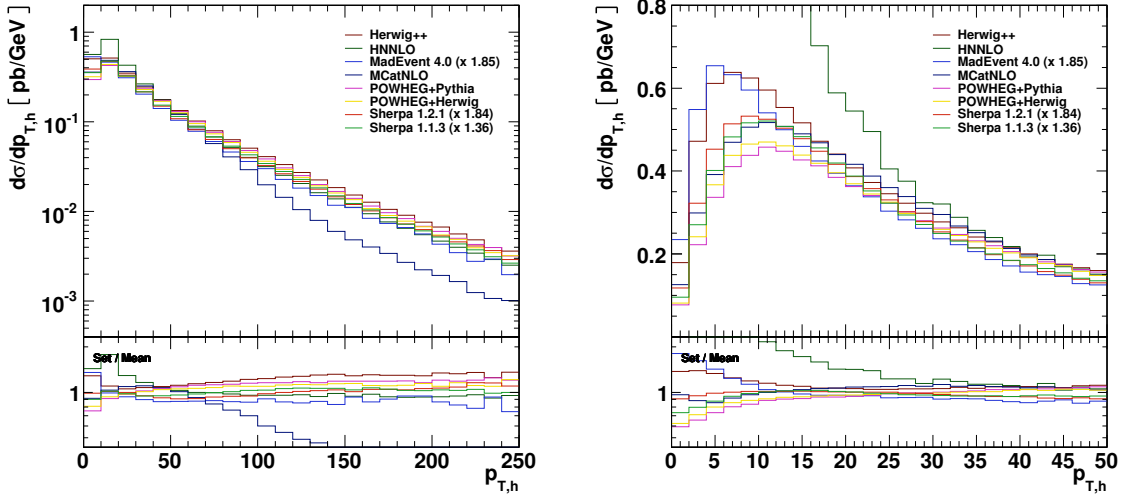

Fig. 37: Comparison of the p_T spectrum of the Higgs in various approaches, from Ref. [350].

spectrum, for transverse momenta above roughly one half of the Higgs-boson mass. The transverse momentum region below 15 GeV (i.e. the Sudakov region) also displayed a somewhat different behaviour, being peaked around $5-6$ GeV for HERWIG++ and MADGRAPH/MADEVENT+PYTHIA while for all the others the peak is slightly above 10 GeV. On the other hand, this discrepancy cannot be considered fully conclusive, since hadronisation effects – although expected to be small – were only included in the MC@NLO and POWHEG output.

In Ref. [320], a further detailed study was carried out comparing results from PYTHIA, POWHEG, and MC@NLO with the fixed-order NNLO calculation, and with the NNLL resummed transverse-momentum distribution of the Higgs boson. The findings of the study can be summarised in few points:

- First of all, the PYTHIA (including MEC) distributions differ from the POWHEG ones by a K-factor that depends only mildly upon the Higgs rapidity. This is explained by the fact that the first radiation in both is of the same accuracy, the only difference being that in PYTHIA it is B rather than $\bar{B}$ that appears in front of this formula.

- This observation also clarifies why all methods but MC@NLO yield very similar transverse-momentum spectra. We can understand the reason for this behaviour from Eq. (25). We see the reason for this: here the K-factor is applied to $\mathcal{S}$ events only, but not to $\mathcal{H}$ events. These last ones populate the region of p_T above roughly 60 GeV, and they are not amplified by the large K-factor present in Higgs production.

- The Higgs transverse-momentum distribution in POWHEG shows very good agreement with the NNLO calculation. Again we should state that the transverse-momentum spectrum of the Higgs is only computed at leading order in POWHEG (being in fact part of the NLO correction to inclusive Higgs production). The presence of the full K-factor in front of this distribution should thus be seen as an arbitrary correction, trying to catch the true NNLO one.

- Similar observations also apply to ME+PS and PYTHIA results rescaled to the full NLO cross section. It turns out, in this case, that the NNLO calculation is in better agreement with these results. It is not clear whether this is a general pattern of NNLO corrections; however, while

the same pattern is observed also in W and Z production it should be noted that these processes, being s-channel production as well are very similar to Higgs production. It would be interesting to investigate whether this is also the case in processes for which the NLO corrections to the production of an associated jet is also known, like, for example, $t\bar{t}$ production.

– In the Sudakov region the transverse-momentum distribution of POWHEG agrees well with the analytic NLL calculation of Ref. [351], while the also available NNLL result is above POWHEG, but with a very similar shape (see Fig. 38). This can be understood as being mostly an effect due
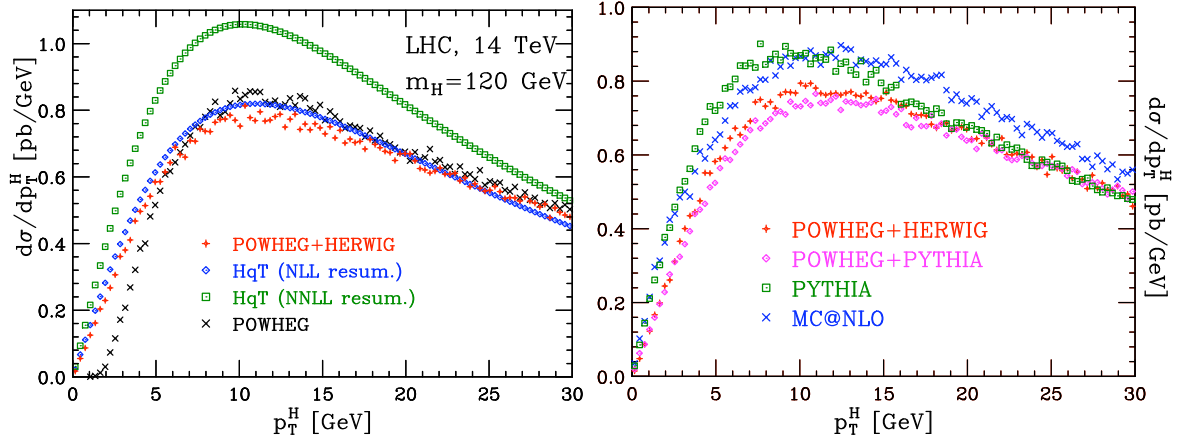

Fig. 38: Comparison of the Higgs p_T spectrum of POWHEG compared with the analytical resummed results of Ref. [351] (on the left), and comparison of POWHEG interfaced with PYTHIA, POWHEG interfaced with HERWIG, MC@NLO and PYTHIA standalone (on the right).

to the inclusion of NNLO terms in the analytic calculation, which globally increases the cross section. In the same region, MC@NLO and POWHEG, when both interfaced to HERWIG, give very similar results. This region is the most likely to be important when a jet veto is applied, and is affected by several physical effects of perturbative and non-perturbative origin. These should be studied, for example, using the POWHEG and ME+PS methods, preferably interfaced to different shower programs.

Detailed studies comparing MC@NLO, the NNLO, and the NNLL results for specific Higgs decay modes have been performed in Ref. [352] for the $\gamma\gamma$ channel, and in Ref. [353] for the W^+W^- channel. In both cases, a good agreement is found for the acceptance correction found using the parton-level NNLO calculation and MC@NLO. This is quite remarkable, especially for the W^+W^-, where a jet veto is an essential ingredient to suppress the large $t\bar{t}$ background. Since the NNLL result only predict the inclusive transverse-momentum distribution of the Higgs, it is used to validate the shower Monte Carlo results. It is found that the NLL and also the NNLL results for the Higgs cross section below a given transverse-momentum cut match well with the shower results (consistently with what is displayed in Fig. 38), and also with the NNLO result. This is understandable, since apparently large Sudakov logarithms are important for this distribution. The shower Monte Carlo's (MC@NLO and HERWIG) both resum these logarithms at the NLL level, and in the NNLO result one more logarithmic term is included in the cross section with respect to the NLO one.

Hadronization and the underlying event are both likely to affect the efficiency of the jet veto, by adding more activity to the event. In Ref. [353] these effects are also studied using HERWIG and JIMMY [354], for both a cone and a k_T algorithm. The results are reported here in Fig. 39. Effects of the order of 10% are found for a jet veto of 25 GeV, with the hadronization and the underlying event acting in opposite directions. It would be desirable to extend these studies using other shower and underlying event models.
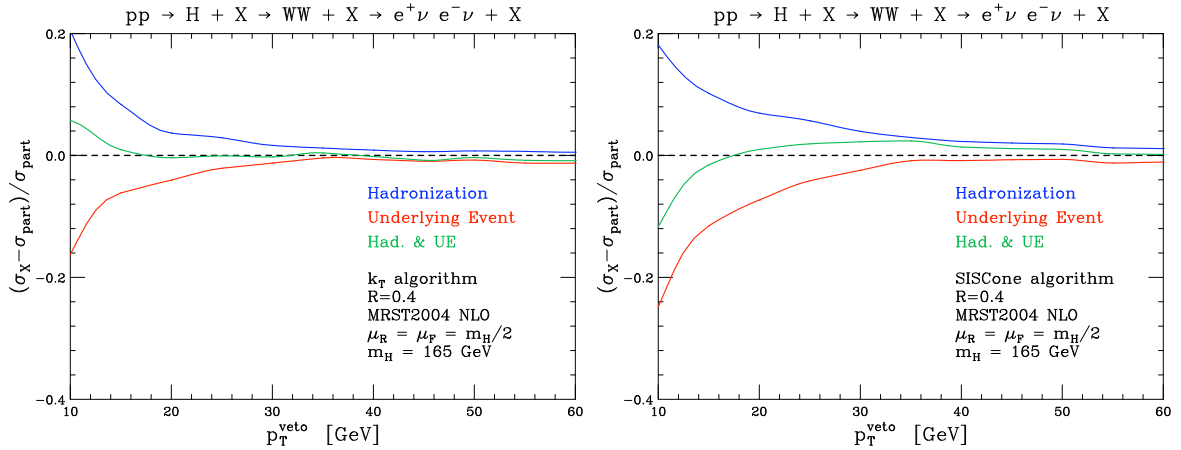
Fig. 39: Difference of the cross section after signal cuts including the underlying event and the hadronization model, with respect to the partonic cross section, from Ref. [353]. The cross section is shown as a function of the jet veto for both the SISCone and the k_T clustering algorithm.

10.3.2 VBF

Vector-boson fusion is available in the ME+PS approach in several matrix-element-based generators, such as ALPGEN, MADGRAPH/MADEVENT and SHERPA as well as in the POWHEG BOX implementation [355]. Another POWHEG implementation will be available soon also in the HERWIG++ event generator.

At variance with the gluon-fusion process, in VBF, NLO corrections are very small and extra QCD radiation in general is rather suppressed[19]. This feature is exploited experimentally to enhance the signal over the background by requiring a jet veto in the central region. Due to angular ordering a simple PS approach is expected to work well for VBF; in order to estimate uncertainties related to details of the parton shower, a careful study invoking ME+PS and NLO+PS could be important. A first study along these lines, using ME+PS, was presented in Ref. [62], where indeed substantial agreement between parton-level predictions and those merged with the PS on the key observables were found.

A more recent study compared the NLO fixed-order computation with the POWHEG implementation interfaced to both PYTHIA and HERWIG [355]. All the most relevant distributions are compared, from the most inclusive to the more exclusive. On the former, good agreement with fixed-order computations and only mild sensitivity to shower effects is found, confirming the small effects due to extra radiation. However, for the more exclusive observables, some discrepancies showed up. As the probably most prominent example for such a discrepancy consider the efficiency of the central jet veto compared to fixed-order LO and NLO computations. At low transverse momentum, where soft-resummation effects are important, fixed-order calculations cannot be reliable and resummation, realised by a parton-shower approach, becomes mandatory. Thus, in this case sizable differences between fixed-order calculations and the parton shower are expected and indeed found. All in all, jet-veto effects show some appreciable dependence on resummation and therefore on the shower algorithm, at least for low p_T veto, see Fig. 10 of Ref. [355].

This may deserve a further, more careful study, also including the impact of e.g. PDFs and the underlying event. On the same footing, it would be interesting to further compare the effect of jet vetoes or jet azimuthal correlations to fixed-order calculations that include one extra jet at NLO [90] and to top-loop-induced H + 2 jets [356].

---

[19]It should be noted that for VBF the electroweak corrections are roughly as large as the QCD ones, but there is currently no attempt to include them into a full simulation.

10.3.3 VH

Due to its comparably simple structure, Higgs associated production with a vector boson is available at the NLO and NNLO level; while the former is fully worked out, including spin correlations in the decays, such differential distributions in general are lacking for the latter. In addition, this process is also implemented in both the MC@NLO and the POWHEG approach. A detailed discussion of these implementations, together with a tuned comparison with fixed-order results at NLO accuracy is available in Ref. [318].

In addition, standard ME+PS tools such as ALPGEN, MADGRAPH/MADEVENT, and SHERPA are also capable to simulate this process. It should be stressed, however, that for searches based on the boosted-Higgs idea of [99] the impact of higher-order corrections to the Higgs decay into b quarks and especially the impact of hard gluon radiation off the b's is a crucial ingredient. Therefore further studies on all possible levels would be certainly most welcome.

10.3.4 ttH

As of today, no public code including either, at the parton-level NLO, or a full simulation in the MC@NLO or POWHEG frameworks, is available for Higgs production in association with top quarks. However, ME+PS matching is available in several matrix-element-based generators, such as ALPGEN, SHERPA, and MADGRAPH/MADEVENT.

However, as in VH, an accurate simulation of the Higgs decay to $b\bar{b}$, which includes extra hard radiation at the matrix element level, is recommended.

10.4 Modelling the Higgs boson in scenarios beyond the Standard Model

Accurate simulations of Higgs production in scenarios beyond the Standard Model will be needed both in the identification of the interesting signatures and also in the extraction of key information, such as masses, couplings strengths, and CP structure. As a template one can consider a general two-Higgs doublet model, which encompasses the much more studied SUSY cases and displays five scalar particles, three neutrals and one charged pair. Other extensions to higher representations, such as triplets, are also often considered.

The status of the MC tools in such models is quite different from that outlined above for the Standard Model (SM) Higgs. As many new physics models are now easily implementable in matrix-element generators such as MADGRAPH/MADEVENT or in SHERPA, ME+PS predictions are de facto available for many interesting scenarios, including the minimal supersymmetric SM (MSSM) or extensions such as the next-to-MSSM. To our knowledge, however, no systematic comparisons with standard PS or fixed-order NLO calculations have been performed.

Regarding NLO+PS the availability for cenarios beyond the Standard Model is much more limited. There are, however, notable exceptions. All processes in the new physics scenarios that can be obtained from those in the SM by simply rescaling the coupling strength and masses can be easily simulated. As an example, consider VBF and VH for SUSY neutral Higgs production, where the cross sections for the MSSM Higgs bosons h and H can be obtained by such a simple rescaling.

An example where simple rescaling will not work is the case of gluon fusion where a b-quark loop could give a sizable contribution in the large-$\tan\beta$ scenarios. In this case, the usual approach of using the Higgs-effective theory cannot be applied, and more work is needed (and would be welcome). In addition, in SUSY scenario, effects from heavy coloured states would also play a role.

On a similar level, new calculations may be recycled for other channels. For example, when a $t\bar{t}H$ calculation will be available in the NLO+PS framework, with a few replacements this could be easily recycled for $b\bar{b}H$. Extension to include the pseudo scalar $t\bar{t}A$ and $b\bar{b}A$ would also be straightforward.

Charged Higgs production is another example where a dedicated calculation was necessary. Cur-

Table 36: Combined set of Monte Carlo event generator tools currently used for mass production by the ATLAS and CMS collaborations. Most of these tools are used by both the collaborations, few are used in one collaboration only. The version numbers in the table represent the latest versions used but lower versions are also used in experiments due to validation and coordinated production schedules.

Type	Physics processes	Generator	Version	Comments
Multi-purpose LO generators	EW, QCD, SM Higgs, MSSM Higgs SUSY, exotica	PYTHIA6	6.423	Standard tune D6T with Q2 PS, PS hadronization for MADGRAPH, ALPGEN, and TopRex
	QCD di-jet	PYTHIA8	8.145	
	QCD studies	HERWIG6 HERWIG++	6.510 2.4.2	PS hadronization for MADGRAPH, ALPGEN, MC@NLO and POWHEG interfaced to JIMMY (V4.31) for UE/MI
Dedicated LO generators	$gg \rightarrow VV$ $t\bar{t}$	gg2ZZ, gg2WW TopRex	1.0.0 4.11	
Multi-leg matrix-element LO generators	QCD, Q+jets, QQ+jets, γ+jets, $\gamma\gamma$+jets, V+jets, VV+jets, $t\bar{t}$, single top, Z′	MADGRAPH	4.4.13	
		SHERPA	1.2.2	
	V+jets, $V b\bar{b}$, QCD, $t\bar{t}$	ALPGEN	2.13	
NLO event generators	DY, WW, $t\bar{t}$, single top, ggF Higgs	MC@NLO	3.41/3.42	
	Drell–Yan, Higgs	POWHEG		

rently, the most promising mechanism is via the excitation of a top quark, either in association (tH^+, heavy H^+) or via its decay ($t \rightarrow H + b$, light H^+). The first processes is available in MC@NLO [231]. For the second one, $t\bar{t}$ production is available both in MC@NLO and in POWHEG. However, the subsequent decay $t \rightarrow H + b$ can only be simulated without spin correlations and NLO corrections at present.

10.5 Currently used tools and wish list by the experimentalists

The experimental collaborations use a collection of publicly available tools, which are properly versioned, maintained, well described, and referenced. Typically all multi-purpose or parton-level event generators fall into this category. A list of currently used Monte Carlo generator tools for mass production of fully simulated and reconstructed events is presented in Table 36.

For some of the inclusive-cross-section calculators, however, are just privately communicated and,

thus, are not as systematically maintained as many of the event generators tools above. This issue needs to be addressed to achieve a more uniform prescription on how to incorporate and reference these calculations properly and make the results reproducible. On a somewhat similar footing, it is important to reference also the standard tools in a proper manner, by indicating both version number and tune identifier, and by making clear which tools have been interfaced with each other[20].

At the same time, flexibility of cross-section calculator tools that allow detailed experimental cut and efficiency analyses and the inclusion of fully exclusive final states into their results are critical. It would therefore be highly desirable to turn as many NLO calculations as possible into hadron-level event simulations. A possible avenue, of course, would be to ask the authors of the respective NLO codes to facilitate turning their calculations into a full-fledged simulation, through either POWHEG or MC@NLO techniques. Automation of the whole process (NLO computation and interface to the parton showering) is also possible.

It should be stressed, however, that it is necessary for all theoretical tools to be maintained and remain accessible at all times. A commonly agreed central code repository, such as the Hepforge database (http://www.hepforge.org/) would be highly useful for improved accessibility and maintenance.

Based on the most immediate needs for the Higgs searches in the experiments, a wish list for theorists is also proposed as follows for the Higgs-signal MC and for background studies. For Higgs signal MC generators, main processes that need urgent implementation are:

- NLO corrections to $H \to b\bar{b}$ decay[21],
- Finite m_t/m_b in $gg \to H$ production (especially relevant for SUSY Higgs),
- $pp \to (t \to H^+b)\bar{t}$, including a treatment of $t \to H^+b$ decay with the same level of accuracy achieved in $t \to W + b$ in MC@NLO and POWHEG,
- $pp \to t\bar{t}H$ and $pp \to b\bar{b}H$,
- $pp \to bH$.

For background MC generators, main processes needed to be implemented at NLO are (listed in order of implementation complexity):

- $q\bar{q} \to ZZ^*$ (now available without gamma interference),
- $Vb\bar{b}$,
- $t\bar{t}b\bar{b}$, $t\bar{t}$+jets, and V+jets In particular, V+jets processes are the most urgent since they have the largest expected cross section of the three. It is however already possible to perform precise measurements of V+jets production with the LHC data and test the theoretical predictions given the expected high luminosity in the next year. This will help understanding vector-boson production in association with jets for better understanding of the crucial background process to many Higgs search channels.

Finally, for the optimization of the experimental Higgs searches and their interpretation, there are two main issues: signal and background predictions and the estimation of their uncertainties both inclusively and as a function of most important quantities used to separate signal from background in the experimental selections.

For signal expectations, we have to rely on theoretical predictions. It is recommended to use as much as possible all available higher-order MC generators, rather than using K-factors. In many cases

---

[20]For example, for a simulation based on PYTHIA 6, the exact version number PYTHIA 6.xxx *plus* the properly documented underlying event tune, like DW, must be indicated. Similarly, when interfaced with ALPGEN, the results should be called "ALPGEN 2.xxx+PYTHIA 6.yyy (DW)" or similar.

[21]An unreleased patch of HERWIG is available for NLO corrections to $H \to b\bar{b}$ decay. For the experimental collaborations, it would be ideal to have this process implemented in the official HERWIG++ release. ME+PS corrections to $H \to b\bar{b}$ decay can be easily implemented also in SHERPA in which these corrections are already implemented for t decays.

NLO MC generators exist, as described in this section, thus there is no reason to use LO MC tools and apply K-factors NLO/LO to correct the LO predictions to NLO. In some cases NNLO calculations exist for SM Higgs production (ggH differential cross-section calculators) , but not a full event generator. In this case, in collaboration with the authors, the NLO MC team will provide values of the re-weighting factors NNLO/NLO for the Higgs momentum and pseudo-rapidity distributions.

The NLO MC team will also provide guidelines on how to estimate the theoretical uncertainties on signal production predictions as a function of most important measurable quantities used to discriminate signal from background in the experimental analyses (based on the compilation of the common set of variables and cuts by the experimental collaborations).

Future work of the NLO MC team will be devoted to the following open questions: Can we devise methods to test the signal predictions before the signal itself is measured, by using similar and already measurable SM processes? For example, how a precisely the measurement of the $t\bar{t}$ cross section may help to reduce the uncertainty on Higgs production via gg fusion (such as ggH)? More generally what measurable processes may serve as the benchmark and the validation of the signal predictions?

For background predictions, a number of processes can and will be measured with the data collected during the current and coming years at the LHC. V+jets and $V b\bar{b}$ predictions are urgent because they can be studied already with the LHC data. For all background processes, experimentalists should review methods to measure these processes in some control regions where data statistics is abundant and to extrapolate the background predictions in some signal regions where data statistics is expected to be small. The theoretical predictions should give guidance and improve the precision of the extrapolated results. For this, the NLO MC team will provide prescriptions on how to assign theoretical uncertainties to background predictions in the signal regions.

10.6 Further issues and studies

10.6.1 Which tools to use?

With the advent of better and more precise tools it becomes increasingly important to understand which tool to pick for a given study, in order to optimally use the best tools. Obviously it is very hard to find a solution that fits all eventualities, but we believe it is still worthwhile to formulate a few guidelines:

– Never use one tool alone.
Clearly, different tools have different accuracies and they may employ different approximations. This in turn may lead to systematic uncertainties, which can only be addressed by using different tools. Prime examples for this are uncertainties related to the underlying event or hadronisation, which involve a big amount of modelling. While it is tempting to simply use only various tunes of the same generator it may be important to see if various models (e.g. PYTHIA 8 vs. HERWIG++) lead to systematically different outcomes. The same also holds true for uncertainties related to parton showering etc.

– Employ the accuracy dictated by your analysis:
For very inclusive studies, like e.g. the rapidity distribution of the Higgs boson, NNLO accuracy is available and should be used. For exclusive final states, the best accuracy available at the moment is given by the codes employing the POWHEG and MC@NLO techniques, which would yield NLO accuracy for relatively inclusive quantities such as the Higgs-boson rapidity, LO accuracy for more exclusive quantities such as the p_T distribution of the first jet, and PS accuracy for all further jets. In contrast ME+PS tools yield LO accuracy for all jets, as long as the corresponding MEs have been employed. Thus, if an analysis relies on the correct description of many jets, employing the ME+PS tools is preferred, while the NLO+PS tools are the tools of choice for more inclusive quantities. Conversely, this suggest that pure PS tools should typically not be used.

10.6.2 Choice of parton distribution functions

For hadron colliders, parton distribution functions (PDFs) play an important role in determining the outcome of theoretical predictions. Common lore suggests that the order of the PDFs must be consistent with the order of the predictions. For leading-order predictions, LO PDFs should be used while for NLO predictions, NLO series of PDFs need to be used. This simple picture, however, is somewhat blurred by the parton showers, since they partially include higher-order effects, as discussed above.

This issues is further obfuscated by the often large impact the PDF has on the underlying event simulation. It is therefore important to ensure that the PDFs are used in a conscientious way – changing a PDF without changing other parameters may lead to huge and unphysical effects. Therefore, in order to assess PDF uncertainties by comparing apples to apples, it would be paramount to have at hand various tunes for the underlying event etc.

10.6.3 Interfacing codes

Many of the tools discussed in this section are based on interfacing a parton-level calculation at leading (ALPGEN and MADGRAPH/MADEVENT) or next-to leading order (POWHEG BOX and MC@NLO) to a full event generator that includes the parton showers, the underlying-event simulation, and hadronisation. While most likely uncritical for very inclusive observables such as cross section, a number of issues may arise for more exclusive observables such as jet production, jet spectra, and jet vetoes. Since they have not been studied in details, it may be worth pointing out a few of these issues:

– Typically, for NLO calculations, an NLO PDF is used, and the strong coupling constant of this PDF is employed, to guarantee the theoretical consistency of the calculation. In a similar fashion, already on the tree-level choices concerning PDFs and α_s are made. When interfacing such parton-level codes with their choice of PDFs etc. with a parton-shower code such as PYTHIA or HERWIG in a specific tune, which also includes a definition of PDFs and α_s. This renders the evaluation of PDF and scale uncertainties a tricky task, for which no prescription has been defined yet.

– In this context it is worth noting that for ME+PS tools, which *sit* on a full event generator, the merging algorithm often employs the Sudakov form factors of the underlying parton shower. This may then lead to the counter-intuitive effect that a *harder* tune for the parton shower yields softer jets when interfaced with parton-level MEs.

– As discussed above, quantities such as the central-jet veto in VBF depend on resummation properties – typically the realm of the parton showers in the simulations currently used by experimenters. It would therefore be worthwhile to check for these effects in different interfaced codes, including the impact of the underlying event in a more complete fashion.

10.7 Conclusions

As we are entering the LHC running phase, we have available several very accurate *theoretical-style* predictions in the form of parton-level integrators that can output histograms for any IR-safe observable. On the other hand, Monte Carlo event generators with NLO accuracy are now (or will be soon) available for all the relevant Higgs production processes. A systematic comparison between various implementations, PS programs and fixed or improved *theoretical-style* calculations is now possible.

In this brief note we have listed the available tools and also given an example (taken from Ref. [350]) on how such comparisons can be made.

The tunes for the various Monte Carlos need to be re-established as components relevant to assess, for instance, systematic uncertainties due to PDFs. We expect this to be a continuous process as the implemented order of calculations change and new codes and physics processes become available. Finally, it is important to establish

– a consistent set of Standard Model parameters for MC tools (the MC4LHC group is to provide a suggested set of these parameters),
– a consistent and complete way to reference the tools used,
– a common code repository,
– procedures to cross compare and validate different codes and implementations,
– procedures to assess systematic uncertainties of the theoretical predictions and simulations.

11 Higgs pseudo-observables[22]

11.1 Introduction

Recent years have witnessed dramatic advances in technologies for computing production and decay of Higgs bosons, critical to the program of calculations for collider physics. The main goals of this Report have been to calculate inclusive cross sections for on-shell Higgs-boson production and Higgs-boson branching ratios (BRs). Therefore, Higgs-boson decays are considered, in the experimental analyses, as on-shell Higgs bosons decaying according to their BR's, including higher-order effects. However, the quantities that can be directly measured in the (LHC) experiments are cross sections, asymmetries, etc., called *Realistic Observables* (RO, see below). The obtained results depend on the specific set of experimental cuts that have been applied and are influenced by detector effects and other details of the experimental setup. In order to determine quantities like Higgs-boson masses, partial widths, or couplings from the RO a deconvolution procedure (unfolding some of the higher-order corrections, interference contributions etc.) has to be applied. These secondary quantities are called *Pseudo Observables* (PO, see below). It should be kept in mind that the procedure of going from RO to the PO results in a slight model dependence.

11.2 Formulation of the problem

With respect to the measurement of Higgs-boson quantities at the LHC, some of the above mentioned aspects are mostly neglected so far. Sophisticated issues, such as off-shell effects of Higgs and interference between background and signal, have not been included in experimental analysis since it is assumed that they should not be so relevant for $M_{\mathrm{H}} < 200$ GeV, within the SM. (The case of the most popular extension of the SM, the Minimal Supersymmetric SM (MSSM) will be briefly discussed later.) It should be noted that the statement on low importance of off-shellness for the regime of low Higgs masses just comes from naive analysis of the ratio $\Gamma_{\mathrm{H}}/M_{\mathrm{H}}$: for a SM Higgs boson below 200 GeV, the natural width is much below the experimental resolution; and on certain assumptions about the vanishing of imaginary parts in the amplitudes. However, in our opinion, one should analyze more carefully how much this ratio banishes the off-shellness, given an increase in gg luminosity at small values of x. In any case, the experimental strategy for searching a light Higgs boson has always been to produce an on-shell Higgs and model its decay in a Monte Carlo (MC) generator. No effort has been devoted to analyze how MCs such as PYTHIA, HERWIG, or SHERPA are treating the Higgs-boson width internally. Especially for heavier Higgs bosons, we expect studies that include the interference, but it is clear that most probably this will only be done at LO with MC generators for $pp \to n$ fermions.

There are few examples of theoretical studies as well: quite a while ago, Ref. [357] presented a study of the interference of a light Higgs boson with the continuum background in $gg \to H \to \gamma\gamma$. Although the effect turned out to be fairly small, there may be other cases where such interference effects might be sizable, maybe even in channels where there will be earlier sensitivity to SM Higgs.

While the implementation of higher-order corrections to Higgs production cross sections and Higgs decays does not represent a problem anymore, very little effort has been devoted in analyzing the interference effect between Higgs-resonant and background diagrams. ATLAS and CMS studies have been done with full simulation, but without the interferences.

11.3 Examples of pseudo-observables

In the following we define the relevant quantities from a more general way of looking at this question. Let us split *signal* (S) from *background* (B) at the diagrammatic level. In principle one could refer to some *idealized* experimental cross section, but here we advocate another road, the one to define universal quantities that have the same meaning in all schemes and models, see Ref. [358]. Therefore, we go from

---

[22]S. Heinemeyer and G. Passarino.

data to *predictions* which are made of $| S \oplus B |^2$. Usually S and B come from different sources, and B is not always complete, e.g. the best prediction is reserved for S (usually including as many loops as possible) while often B is only known at LO; furthermore, $S \otimes B$ is usually discarded.

In order to pin down the theoretical uncertainty as much as possible all calculations of S are based on a consistent procedure; one does not use α_s at four loops in any LO calculation etc. In the end one is interested in the extraction of Higgs-boson masses, widths etc. by comparing experimental measurements with theory predictions. Therefore, the main question that we are going to address in this section is about the meaning of any future comparison (theory versus data) where, for instance, $\Gamma(H \to \gamma\gamma)$ computed at n loops is compared with something extracted from the data with much less precision and, sometimes, in a way that is not completely documented. Without loss of generality and to continue our discussion it will be useful to introduce an elementary glossary of terms:

RD =	real data
RO =	going from *real data* to distributions with cuts defines RO_{exp},
	e.g. from diphoton pairs (E, p) to $M(\gamma\gamma)$; given a model, e.g. SM,
	RO_{th} can be computed
PO =	transform the *universal intuition* of a *non-existing* quantity into an *archetype*,
	e.g. $\sigma(gg \to H), \Gamma(H \to \gamma\gamma), RO_{th}(M_H, \Gamma(H \to \gamma\gamma), \dots)$
	fitted to RO_{exp} (e.g. $RO_{exp} = M(\gamma\gamma)$) defines and extracts M_H etc.

Examples of POs used at LEP can be found in Ref. [359], for LHC (e.g. $gg \to 4$ fermions) see Ref. [360]. In calculations performed to date the background $pp \to 4\,f$ is generated at LO, the production cross section (e.g. $gg \to H$) is known at NNLO, and the on-shell decay is known at NLO, including electroweak effects. Ideally one should extract the p_T information from production and boost the decay rate computed in the Higgs rest frame in order to have a consistent matching in production $\times$ decay $(P \otimes D)$. Next step is the replacement of $P \otimes D$ with a Breit–Wigner, next-to-next the correct folding with a Dyson re-summed Higgs propagator. It is worth nothing that there is still a mismatch between background (LO) and signal (NNLO $\times$ NLO) and that for this channel we have more than one unstable particle. This leads us to consider the following, recommended, strategy: to go via idealized (model-independent?) RO distributions and from there then going to the POs, with the following steps:

- Step 0) Use a (new) MC tool – the PO code – to fit ROs;
- Step 1) understand differences with a *standard* event generator plus detector simulation plus calibrating the method/event generator used (which differ from the PO code in its theoretical content);
- Step ≥ 2) document the results of the analysis and understand implications.

11.4 Experimental overview with theoretical eyes

MC generators are usually selected for specific processes and used for all relevant final states. MC generators for Higgs production and decay, e.g. in CMS, are PYTHIA and POWHEG; for description and differences see Ref. [320]. For Higgs production PYTHIA is similar to POWHEG, the main difference being normalization which is LO in PYTHIA and NLO in POWHEG.

The strategy of describing Higgs signal as production $\otimes$ decay is based on the small value of width/mass (for a light Higgs) but also on the scalar nature of the Higgs resonance, i.e. there are no spin correlations, opposite to the case of W/Z bosons. Therefore the typical experimental strategy for analyzing the Higgs signal is based on generating events with POWHEG, storing them and using PYTHIA for the remaining shower. The correct definition of production $\otimes$ decay is better formulated as follows: the MC *produces* a scalar resonance, the Higgs boson, with a momentum distributed according

to a Breit–Wigner where peak and width are related to the on-shell mass and width of the Higgs boson. In other words what has been done amounts to generating Higgs virtuality, $\hat{s}$, according to the replacement

$$\delta\left(\hat{s} - M_{\mathrm{H}}^2\right) \rightarrow \begin{cases} \dfrac{1}{\pi}\dfrac{M_{\mathrm{H}}\,\Gamma_{\mathrm{H}}}{\left(\hat{s} - M_{\mathrm{H}}^2\right)^2 + \left(M_{\mathrm{H}}\,\Gamma_{\mathrm{H}}\right)^2} & \text{MC@NLO} \\[2em] \dfrac{1}{\pi}\dfrac{\hat{s}\,\Gamma_{\mathrm{H}}/M_{\mathrm{H}}}{\left(\hat{s} - M_{\mathrm{H}}^2\right)^2 + \left(\hat{s}\,\Gamma_{\mathrm{H}}/M_{\mathrm{H}}\right)^2} & \text{Pythia/POWHEG} \end{cases}$$

where $M_{\mathrm{H}}, \Gamma_{\mathrm{H}}$ are the on-shell mass and width. Furthermore, Higgs-boson production (e.g. via gg fusion) is also computed at $\hat{s}$, a procedure which does not guarantee gauge invariance at higher orders if the background is not included at the same order. As a consequence of this approach, no Higgs-boson propagator appears and the most important quantity at LHC – the Higgs-boson *mass* – appears only through the peak position of the momentum distribution in Higgs production.

It is not the aim of this section to discuss how the shower is performed or the NLO accuracy of the MC; we focus here on the treatment of the invariant-mass distribution, e.g. the way a Breit–Wigner distribution is implemented. For instance, POWHEG uses a running-width scheme for the resonance while MC@NLO implements a fixed-width scheme, $\Gamma_{\mathrm{H}}(M_{\mathrm{H}})$; therefore, the different treatments are sensitive to thresholds (e.g. $\overline{\mathrm{t}}\mathrm{t}$), a fact that becomes relevant for high Higgs-boson masses where, in any case, the whole procedure is ambiguous since the Higgs-boson width becomes larger and larger.

The main point here is that both schemes are equally inadequate if the Higgs boson is not light and propagator effects should be included. When talking about NLO or NNLO effects most people visualize them as a lot of gluon lines attached to the production triangle in gg fusion; there is an often forgot place where NLO effects show up, the propagator function. The unusual aspect of these corrections is that they manifest themselves in the denominator (the *propagator*), transforming a *bare* mass into a *complex pole*, a basic property of the S-matrix.

11.5 Theoretical background

Our review here will mention only the minimal material needed for the description of the proposed solution. To summarize, extraction of POs depends on many details, experimental cuts, detector effects etc., and requires deconvolution/unfolding. There are also different priorities: from the theory side we need a *crystal clear* definition, e.g. what is the correct definition of mass for an unstable particle. The quest for a proper treatment of a relativistic description of unstable particles dates back to the sixties and to the work of Veltman [361]; more recently the question has been readdressed by Sirlin and collaborators [362].

The Higgs boson, as well as the W or Z bosons, are unstable particles; as such they should be removed from in/out bases in the Hilbert space, without changing the unitarity of the theory. Concepts as the production of an unstable particle or its partial decay widths, not having a precise meaning, are only an approximation of a more complete description, see Refs. [360, 363]. From the experimental side priorities are on how to extract couplings (can couplings be extracted?) etc. For a comprehensive analysis of the problem see Ref. [54].

Concerning the definition of the Higgs-boson mass the object we have to deal with is the complex pole of the Dyson re-summed propagator, whereas all MC implementations have been done with the on-shell mass definition. In order to have these deviations under control it would be required to (a) investigate what is included in the MC tools actually used by the experiments and (b) to compare this to the results obtained from an MC tools using the correct mass definition. However, right now this cannot be done with realistic ATLAS/CMS distributions. Hence, the strategy should be limited to: take latest ATLAS/CMS MC tools, use (at most) a box detector (acceptance cuts, no resolutions) and try for a closure test with state-of-the-art tools and document the findings.

There is no perfect solution to the problem but our suggestions are as follows. As an example we take a process $i \rightarrow f$, e.g. gg $\rightarrow$ H $\rightarrow \gamma\gamma$ that is already described by a two-loop set of diagrams, and

parametrize the amplitude as

$$A\left(i \to f\right) = A_{\mathrm{H}}\left(i \to \mathrm{H} \to f\right) + A_{\mathrm{back}}\left(i \to f\right), \qquad A_{\mathrm{H}}\left(i \to \mathrm{H} \to f\right) = \frac{S_i(\hat{s})\, S_f(\hat{s})}{\hat{s} - s_{\mathrm{H}}}, \qquad (27)$$

where s_{H} is a complex quantity, the Higgs complex pole, usually parametrized as

$$s_{\mathrm{H}} = \mu_{\mathrm{H}}^2 - i\, \mu_{\mathrm{H}}\, \gamma_{\mathrm{H}}. \qquad (28)$$

It is the tough life of an unstable state whose energy (even in a non-relativistic theory) is doomed to be complex. Kinematics, of course, is always real, and s is the corresponding invariant at the parton level. $S_{i,f}$ are the matrix elements for the process $\mathrm{gg} \to \mathrm{H}^*$ and $\mathrm{H}^* \to \gamma\gamma$. Theoretically speaking, these matrix elements alone are ill-defined quantities if s is arbitrary and this reflects the intuition that only poles, their residues and non-resonant parts are well defined, e.g. they respect gauge invariance. Therefore, it is better to perform the following split in the amplitude:

$$A_{\mathrm{H}} = \frac{S_i(s_{\mathrm{H}})\, S_f(s_{\mathrm{H}})}{\hat{s} - s_{\mathrm{H}}} + \frac{S_i(\hat{s}) - S_i(s_{\mathrm{H}})}{\hat{s} - s_{\mathrm{H}}}\, S_f(s_{\mathrm{H}}) + \frac{S_f(\hat{s}) - S_f(s_{\mathrm{H}})}{\hat{s} - s_{\mathrm{H}}}\, S_i(s_{\mathrm{H}})$$

$$+ \frac{\left[S_i(\hat{s}) - S_i(s_{\mathrm{H}})\right]\left[S_f(\hat{s}) - S_f(s_{\mathrm{H}})\right]}{\hat{s} - s_{\mathrm{H}}} = A_{\mathrm{H,signal}} + A_{\mathrm{H,non-res}}, \qquad (29)$$

and to include $A_{\mathrm{H,non-res}}$ in A_{back}, the latter given by all diagrams contributing to $\mathrm{pp} \to \gamma\gamma$ that are not H-resonant. They can be classified as follows:

– LO $\bar{\mathrm{q}}\mathrm{q} \to \gamma\gamma$,
– beyond LO $\bar{\mathrm{q}}\mathrm{q} \to \gamma\gamma$ and $\mathrm{gg} \to \gamma\gamma$.

In case NLO is included one should worry about additional photons in the final state and this influences, inevitably, the POs definition. After that, let us define

$$\frac{1}{\hat{s}} \int dPS \left| \frac{S_i(s_{\mathrm{H}})\, S_f(s_{\mathrm{H}})}{\hat{s} - s_{\mathrm{H}}} \right|^2 = \frac{\mu_{\mathrm{H}}^5}{\hat{s} \mid \hat{s} - s_{\mathrm{H}} \mid^2}\, \sigma_{\mathrm{gg} \to \mathrm{H}}(\mu_{\mathrm{H}}) \otimes \Gamma_{\mathrm{H} \to \gamma\gamma}(\mu_{\mathrm{H}}). \qquad (30)$$

where the Higgs-boson mass is set (by convention) to μ_{H}, but other options are available as well. The phase space is always with real momenta while the Mandelstam invariant is made complex through the substitution $\hat{s} \to s_{\mathrm{H}}$, a procedure that can be genaralized to processes with more final-state legs. At this point we have four parameters, all of them Pseudo-Observables,

$$\mu_{\mathrm{H}}, \quad \gamma_{\mathrm{H}}, \quad \sigma_{\mathrm{gg} \to \mathrm{H}}(\mu_{\mathrm{H}}), \quad \Gamma_{\mathrm{H} \to \gamma\gamma}(\mu_{\mathrm{H}}), \qquad (31)$$

that we want to use in a fit to the (box-detector) experimental distribution (of course, after folding with PDFs). These quantities are universal, uniquely defined, and in one-to-one correspondence with *corrected* experimental data. After that one could start comparing the results of the fit with a SM calculation. The way this calculation has to be performed is also uniquely fixed.

The breakdown of a process into products of POs can be generalized to include unstable particles in the final state; an example is given by $\mathrm{pp} \to 4$ leptons; the amplitude can be written as

$$A\left(\mathrm{pp} \to 4\mathrm{l}\right) = A_{\mathrm{back}}\left(\mathrm{pp} \to 4\mathrm{l}\right) + A_{\mathrm{H}}\left(\mathrm{pp} \to \mathrm{H} \to \mathrm{ZZ} \to 4\mathrm{l}\right) + A_{\mathrm{H}}\left(\mathrm{pp} \to \mathrm{H} \to 4\mathrm{l}\right). \qquad (32)$$

The first and third amplitudes in Eq. (32) are subtracted by using SM (or MSSM) calculations while the second (triply resonant) can be parametrized in terms of POs and a fit to $M(\mathrm{llll})$ attempted. The (triply resonant) signal in $\mathrm{gg} \to 4\mathrm{l}$ is split into a chain $\mathrm{gg} \to \mathrm{H}$ (production), $\mathrm{H} \to \mathrm{ZZ}$ (decay), and $\mathrm{Z} \to \bar{l}l$ (decays) with a careful treatment of (W/Z) spin correlation. In this way we can also introduce the

folowing PO: $\Gamma(\mathrm{H} \to \mathrm{ZZ})$. It is worth noting that the introduction of complex poles allows us to split multi-leg processes into simple building blocks through the mechanism of separating gauge-invariant parts, once again, the complex pole, its residue, and the regular part. How else can we stand against the temptation of introducing a quantity like $\Gamma(\mathrm{H} \to \mathrm{ZZ})$ where three unstable particles occur in the in/out states?

For processes which are relevant for the LHC and, in particular, for $\mathrm{H} \to \bar{\mathrm{b}}\mathrm{b}, \gamma\gamma, \mathrm{gg}$, and $\mathrm{gg} \to \mathrm{H}$ etc., it is possible to define three different schemes and compare their results. The schemes are:

- the RMRP scheme which is the usual on-shell scheme where all masses and all Mandelstam invariants are real;
- the CMRP scheme [364], the complex-mass scheme [365] with complex internal W and Z poles (extendable to top complex pole) but with real, external, on-shell Higgs, etc. legs and with the standard LSZ wave-function renormalization;
- the CMCP scheme, the (complete) complex-mass scheme with complex, external, Higgs (W, Z, etc.) where the LSZ procedure is carried out at the Higgs complex pole (on the second Riemann sheet).

The introduction of three different schemes does not reflect a theoretical uncertainty; only the CMCP scheme is fully consistent when one wants to separate production and decay; therefore, comparisons only serve the purpose of quantifying deviations of more familiar schemes from the CMCP scheme. Example of how to apply the ideas presented in this section can be found in Ref. [360].

The usual objection against moving Standard Model Higgs POs into the second Riemann sheet of the S-matrix is that a light Higgs boson, say below 140 GeV, has a very narrow width and the effects induced are tiny. Admittedly, it is a well taken point for all practical consequences but one should remember that the Higgs-boson width rapidly increases after the opening of the WW and ZZ channels and, because of this, the on-shell treatment of an external Higgs particle becomes inadequate as a description of data if the Higgs boson is not (very) light. On top of all practical implications one should admit that it is hard to sustain a wrong theoretical description of experimental data.

It is also important to establish the proper connection between Higgs-boson propagator and Breit–Wigner distribution. Given the complex pole $s_{\mathrm{H}} = \mu_{\mathrm{H}}^2 - i\,\mu_{\mathrm{H}}\,\gamma_{\mathrm{H}}$, define new quantities (up tho higher orders, HO) as follows:

$$\overline{M}_{\mathrm{H}}^2 = \mu_{\mathrm{H}}^2 + \gamma_{\mathrm{H}}^2 + \mathrm{HO}, \quad \mu_{\mathrm{H}}\,\gamma_{\mathrm{H}} = \overline{M}_{\mathrm{H}}\,\overline{\Gamma}_{\mathrm{H}}\left(1 - \frac{\overline{\Gamma}_{\mathrm{H}}^2}{\overline{M}_{\mathrm{H}}^2}\right) + \mathrm{HO}. \tag{33}$$

At this order it can be shown that

$$\frac{1}{s - s_{\mathrm{H}}} = \left(1 + i\,\frac{\overline{\Gamma}_{\mathrm{H}}}{\overline{M}_{\mathrm{H}}}\right)\left(s - \overline{M}_{\mathrm{H}}^2 + i\,\frac{\overline{\Gamma}_{\mathrm{H}}}{\overline{M}_{\mathrm{H}}}\,s\right)^{-1}, \tag{34}$$

which one should compare with the Breit–Wigner implementation in MC tools. The practical recipe for introducing the Higgs complex pole in the Higgs-resonant amplitude $\mathrm{gg} \to \mathrm{H} \to f$ is as follows:

$$\sigma_{\mathrm{gg} \to \mathrm{H}}(M_{\mathrm{H}})\,\frac{\hat{s}^2}{\left(\hat{s} - M_{\mathrm{H}}^2\right)^2 + \left(\hat{s}\,\Gamma_{\mathrm{H}}/M_{\mathrm{H}}\right)^2}\,\frac{\Gamma_{\mathrm{H} \to f}(M_{\mathrm{H}})}{M_{\mathrm{H}}} \;\to\; \sigma_{\mathrm{gg} \to \mathrm{H}}(s_{\mathrm{H}})\,\frac{\hat{s}^2}{\left|\hat{s} - s_{\mathrm{H}}\right|^2}\,\frac{\Gamma_{\mathrm{H} \to f}(s_{\mathrm{H}})}{s_{\mathrm{H}}^{1/2}}. \tag{35}$$

It is worth noting that in any BSM scenario there will be interdependence among Higgs-boson masses and the simultaneous renormalization at the exact complex poles will also introduce consistency checks.

11.6 Extensions of the SM

Extensions of the SM allow for more complex Higgs sectors. Problems that can be avoided in the SM can easily be encountered in new-physics models. For instance, heavy SM-like Higgs bosons with a relatively large width naturally occur in models with an additional $U(1)$ symmetry and a corresponding Z$'$ boson.

Here we briefly describe the situation in the MSSM, where the Higgs sector consists of two Higgs doublets, leading to one light CP-even Higgs, h, one heavy CP-even Higgs, H, one CP-odd Higgs, A and two charged Higgs bosons, H$^{\pm}$. At tree level the Higgs sector is described by M_A and $\tan\beta$ (the ratio of the two vacuum expectation values). In general, concerning the determination of the MSSM parameters, additional complications arise compared to the SM case. Firstly, the unfolding procedure often involves the assumption of the SM. Using this data within the MSSM (or any other extension of the SM) is obviously only justified if the new-physics contributions to the subtraction terms and the implemented higher-order corrections are negligible. Secondly, the model dependence is relatively small for masses (see below). For couplings (beyond the SM-like gauge couplings), mixing angles, etc., on the other hand, the model dependence is relatively large. In contrast to the SM, many of the MSSM parameters are not closely related to one particular observable (for instance $\tan\beta$), resulting in a relatively large model dependence. Therefore the approach of extracting PO with only a fairly small model dependence seems not to be transferable ot the case of the MSSM. Eventually the MSSM parameters will have to be determined in a global fit of the full MSSM to a large set of observables, taking into account *consistently* higher-order corrections.

As mentioned above, the Higgs-boson masses in general constitute a smaller problem, even compared to the SM case. For large parts of the parameters space $M_A > 2M_Z$, the light CP-even Higgs boson is SM-like, while all other Higgs bosons are nearly mass degenerate [366]. Furthermore the upper limit of M_h is about 135 GeV [150]. Consequently, here the width of the h is also SM-like and small. Exceptions can occur for low M_A and large $\tan\beta$. Here the hb$\bar{\text{b}}$ coupling can grow with $\tan\beta$, so the width can grow with $\tan^2\beta$. On the other hand, in this part of the parameter space the hWW coupling is reduced, so that the decay h $\to$ WW$^{(*)}$ contributes less than in the SM. All in all for low M_A and large $\tan\beta$ one can find a strong enhancement with respect to the SM, but no large value of Γ_h/M_h.

The situation is different for the H and A. For heavy H, A, $M_A \gtrsim 150$ GeV, H and A have no substantial couplings to SM gauge bosons, so there is not the typical growth with M_H. Again here the H/Ab$\bar{\text{b}}$ coupling goes with $\tan\beta$, leading to an enhancement of the widths, but not to very large values of $\Gamma_{H/A}/M_{H/A}$ as in the SM for masses above ~ 200 GeV. Only for intermediate masses $M_A \sim 150$ GeV the enhancement in the coupling to b quarks can overcompensate the reduced coupling to gauge bosons, depending on $\tan\beta$.

11.7 Conclusions

In conclusion, the only purpose of this section has been to state the problem and the possible way to solutions, conventional but unique. Therefore, the work in this section is quite plainly an interlude and an actuate all at the same time. In any case it is worth noting that one of the goals of LHC will be to discover or exclude a SM Higgs boson up to 600 GeV. Already at 500 GeV the effect of using the complex pole instead of the on-shell mass on the gg $\to$ H cross section is large and comparable to higher-order QCD corrections. Using on-shell Higgs-boson also for high values of M_H can only be a very first step (i.e. a first guess, as taken elsewhere in this Report) and a truely quantitative analysis should do much better. But it is not the previous strategies that are important this time – it is normal that in the start-up phase of a new machine, strategies will fall like autumn leaves – what's significant here is that the LHC's performance significantly calls for further theoretical improvement. POs, they're the only things we can pay.

12 Parametric and theoretical uncertainties[23]

12.1 Introduction

In this note we address the following questions: definition of theoretical uncertainties (THU) for LHC predictions, their statistical meaning, inclusion of parametric uncertainties (PU), their combination. For the latter we want to stress that the solution (how to combine) relies on some implicit assumptions; any variation in the assumptions leads to a somehow different solution. In this case intuition may still help to qualitatively guess how the value of the measurement is affected.

The first step that we need to do is establish the definition of PUs and THUs. Following this we need to describe the issue (problem) of combination.

12.2 Parametric uncertainties

In our attempt to encode an acceptable definition of theoretical uncertainty for observables at the LHC we differentiate parametric uncertainties – those related to the value of input parameters – from true theoretical uncertainties reflecting our lack of knowledge about higher orders in perturbation theory.

 - **PU**, Parametric uncertainties, will always be there, but eventually reduced when more precise experiments produce improved results. They should not be mixed with THU, but listed as

$$\mathcal{O} = x.xxx \pm 0.00y \text{ (param) } {}^{+0.00a}_{-0.00b} \text{ (th)}. \tag{36}$$

Ideally and assuming that the central value will not change significantly, the better way of dealing with future improvements is as follows:

 1. Produce for each observable $\mathcal{O}$, which is a function of parameters $\{p_1 \ldots p_n\}$, the central value

$$\mathcal{O}\left(p_1^c \ldots p_n^c\right), \tag{37}$$

 2. Provide derivatives

$$\frac{d\mathcal{O}}{dp_i}, \qquad \forall i. \tag{38}$$

In this way users will not have to re-run codes as soon as an improved measurement of p_i is available.

Here, the recommendation is that parametric errors cannot be neglected and calculations should include them in their final estimate.

The main difference between PU and THU is that PU are distributed according to a known (usually Gaussian) distribution while the statistical interpretation of THU is less clear, and they are arguably distributed according to a flat distribution. Sometimes the uncertainty on α_s (say) is added in quadrature to the scale uncertainty (see Section 12.4.1), which is questionable if the former is Gaussian and the latter is flat. It is worth mentioning that we are discussing essentially Standard Model PUs.

12.3 THU, understanding the origin of the problem

In this and the next section we are going to discuss two separate issues [367] that are sometimes mixed:

 - What is the optimal choice for QCD scales?
 - Can one use scale variation to estimate higher-order corrections?

We begin by addressing the first question. Let us for a moment concentrate on the uncertainty induced by variations of the renormalization scale, μ_R, and of the factorization scale, μ_F. The question

---

[23]A. Denner, S. Dittmaier, S. Forte and G. Passarino.

is: Do we have a μ_R problem in QED? The answer is *yes*, but is it a real problem? This time the answer is *no*, because we have a *physical* subtraction point, $q^2 = 0$, for photons with momentum transfer q, which defines the Thomson limit. The next question is: Do we have a μ_R problem in the electroweak (EW) theory? Yes, but it is not a real problem since, once again, we have a *physical* subtraction point(s), since the electromagnetic coupling can still be fixed in the Thomson limit and the weak mixing angle can be tied to the ratio of the W- and Z-boson masses. Stated in other words, our calculations depend on μ_R, but once Lagrangian parameters (masses and couplings) are replaced by data (according to the renormalization program) this dependence disappears. Of course, in perturbation theory, the numerical output depends on the set of data that we have chosen, therefore the next question will be: Do we have large logs in our radiative corrections? The answer is *yes* for all cases where the coupling is related to a EW gauge boson, i.e. γ, W, or Z, with momentum transfer at the EW scale or higher. In the EW part of our theory the first step of the solution will be: Use the G_F-scheme, not $\alpha(0)$, which is equivalent to say *resum* large logarithms that are connected to the running of $\alpha(q^2)$ from $q^2 = 0$ to the EW scale. In the G_F scheme, G_F and the gauge-boson masses are used as input parameters and the electromagnetic coupling is derived according to $\alpha_{G_F} = \sqrt{2}G_F M_W^2(1 - M_W^2/M_Z^2)/\pi$. Actually, the message would be: For an observable at a scale s do not use an input parameter set at a scale $s_0 \ll s$ unless you know how to resum large logarithms. Of course, there may be more logarithms of large scale ratios connected to effects other than the running of α in addition (collinear photon radiation, EW Sudakov logarithms, etc.). Furthermore, the G_F scheme should not be used for couplings that concern external photons where $\alpha(0)$ is appropriate.

What to do in QCD? Resummation is the keyword [18] but, admittedly, apart from the running of the strong coupling it is not always available. There, the most useful keyword will be *minimization*. To understand the problem consider a physical observable which is affected by (large) QCD corrections. Since we have no analogue of G_F in QCD, our LO calculation will always contain logarithms $\ln(s/\mu_R)$ where s is the scale where we want to study the process. Ideally, one should find a scale s_0 where some data is available and renormalization means the replacement $\ln(s/\mu_R) \to \ln(s/s_0)$ and s_0 should not be far away from s. This is not (yet) possible in QCD, so the question will translate into, *how do I choose* μ_R? The guideline will be *set μ_R to s*, i.e. to evolve the coupling to scale s with renormalization group equations, or, in other words, make sure that you do not change much by going to the next order. This is easy in a one-scale process but in any multi-scale process one will have other additional large logarithms, say of argument s/s'. What to do?

- Select μ_R and μ_F, process by process, in such a way that when going from N^nLO to N^{n+1}LO you minimize the effect of the new corrections. In many cases a phase-space-dependent choice is needed in order to achieve this in differential cross sections. The recipe is the best simulation of a subtraction at some physical point close to the relevant scale. In jargon this is called *dynamical scale*.

12.4 THU uncertainties

In this section we will briefly discuss different sources of THU, starting with QCD scale variation.

12.4.1 QCD scale variation

Once the dynamical scale has been selected (process by process) we can address the second question mentioned in the beginning of Section 12.3. Namely, how do we understand our approximation in terms of scale variation, e.g. $s/n < \mu_{R,F} < ns$? The idea is as follows: In the *full* theory there is no scale dependence and order by order in perturbation theory we should be able to see this asymptotic limit. Therefore, variation of the scale(s) is a pragmatic way of understanding how far we are from controlling the theory. In practice, this means *which value do I choose* for n?

The recommendation, in this case, should be as follows: at a given order look for a plateau in the scale dependence and fix n to be such that the plateau is included. Therefore:

– Allow each calculation to set the range of scale variation (it is a matter of experience), but check that nobody is allowing for too small or too large variations just to bring the *error* in the range foreseen by their religion.
– Check that different calculations and different choices give consistent results.
– Drop extreme choices which are too far away from *common* understanding of the problem.

Renormalization scale and factorization scale have different origins and there is no good argument according to which we should set $\mu_F = \mu_R$. Once again we invoke the *minimization principle*, i.e. when going from N^{n}LO to N^{n+1}LO the choice should minimize the effect of the new corrections. Sometimes the estimate of the uncertainty is based on a diagonal scan, sometimes anti-diagonal directions are included. There is also another recipe, a two-dimensional scan with $1/n < \mu_R/\mu_F < n$. One should also mention that an independent variation of the two scales introduces large logarithmic corrections that are cancelled by the next order in perturbation theory. Our recommendation here is for a one-dimensional scan, monitoring at the same time large differences induced by the two-dimensional one.

A word of caution is needed at this point: there are examples where one can see that it is easy to optimize the scale choice, but scale variation becomes a very poor way to estimate higher-order corrections (HO) (in fact at LO it misses even the order of magnitude). Being pragmatic we should state that while there may be an optimal scale choice (i.e. one that minimizes higher-order corrections), one should be careful that this does not then bias the results of estimating higher orders by scale variation. To be more specific, nobody would object to the suggestion that μ_R and μ_F should be chosen in such a way that higher-order corrections are minimized, but in practice the recipe is not always meaningful. It remains true that if we do know the higher order, we will use it, and if we do not know it, we cannot estimate the scale which minimizes the difference. Therefore, what we are suggesting here is to use the last two known orders for the search of stability and for minimizing corrections (if reasonable), which is – at best – a *rule of thumb*. Looking for a *plateau* simply means looking for a stationary point in the dependence of the observable on scale. If there is a stationary point it suggests greater reliability. How to trust a calculation if there is no stationary point remains an highly questionable point. To summarize, one searches the region of the minimum of the higher-order corrections, and for distributions a dynamical scale that stays near the minimum in the whole condsidered range, so that the K-factor does not drift away

12.4.2 PDF

For PDFs, theoretical uncertainties in the sense defined above are unknown and have never been estimated (see section 8 and Refs. [45, 260, 368]). The known PDF uncertainties are

– PDF uncertainties, which are propagated data uncertainties (PDF uncertainty, henceforth);
– parametric uncertainties, of which the one due to propagation of the uncertainty on the value of α_s (α_s uncertainty henceforth) has been studied systematically by several groups, while the uncertainties due to the value of the heavy-quark masses are being gradually included.

While we refer to Section 8 for a more detailed discussion, we note that the recommendation given there for the determination of PDF uncertainties provides a result that already includes the combination of the PDF uncertainty and the α_s uncertainty. One option could have been to keep them separated but it was the PDF community recommendation to provide only the combination of these two. For future studies it might be more advantageous to keep them separate in that this would give more flexibility to the user. It should be understood clearly that other parametric uncertainties are thus not included in this prescription. It is interesting to note that the Gaussian behaviour of PDF uncertainties has been checked

explicitly within the HERAPDF and NNPDF PDF determinations (see Section 3.2 in Ref. [369] and Ref. [134]).

12.4.3 Other sources of THU

Other potential sources of THU are:

- Pole masses vs. running masses? Whenever we know which mass (including its scale) is to be taken the uncertainty should not enter the game. This means that, in general, we do not recommend inclusion of these effects in THU.

- In the scheme production $\otimes$ decay the Higgs shape is, usually, represented by a Breit–Wigner distribution. Differences induced by using fixed-width scheme vs. running width scheme should not enter the THU. If the difference matters (e.g. at large values of the Higgs mass) one should try to understand the difference and compare results with the complex-mass scheme.

- EW uncertainties; we have renormalization scheme dependence, but also an uncertainty associated to inclusion of EW effect in a QCD NNLO calculation [35]. If the QCD K-factor is large it will make some difference to multiply δ_{EW} by the full K-factor (complete factorization [30]) or to include it only at LO (as the conservative recipe of partial factorization would suggest). The most conservative recipe for mixed EW–QCD effects is the vary between complete and partial factorization, but an estimate should be given in any case.

- Full top mass dependence [10] vs. large m_t-approximation in the production $\sigma\,(\mathrm{H} \to \mathrm{gg})$. The correct recipe is as follows: at NLO one should take the full top mass dependence and the estimate of the approximation at NNLO should go into the THU [370].

- Inclusion of the bottom-quark loop in gluon–gluon fusion, complete factorization ($|$ top+bottom $|^2$ with full NNLO K-factor) or partial one ($|$ bottom $|^2$ and top–bottom interference with NLO K-factor)?

- Missing higher-order corrections not related to scale uncertainties. Sometimes LO predictions lack some scale uncertainty that appears only in higher orders (e.g. no QCD renormalization scale in the Drell–Yan process in LO), sometimes new channels open in higher orders, which is also a systematic effect that has nothing to do with scales (e.g. gg channel for WW+jet production). In particular, the THU resulting from missing higher-order EW corrections cannot be estimated via scale uncertainties. NNLO EW corrections can be estimated to some extent based on the known structure and size of the NLO corrections combined with power counting of EW couplings and logarithms. Here we are discussing mostly SM, at the moment no special recommendation is available for MSSM and one should include THU, whenever possible, by scaling the corresponding SM THU.

12.5 How to combine THU

The main question we want to discuss here is: *Are THU confidence intervals?* And also: *Do we have statistical meaning for THU?* There are different opinions on the subject; some of us think that THU *should* be confidence intervals, though of course being a distribution of true values they must be interpreted in a Bayesian sense. Obviously, given that they refer to a distribution of the values there is no reason to think that they are Gaussian, and it might be more reasonable to take them as flat distributions. This said, they should be combined using the rules of Bayesian inference. The envelope method is then the correct rule to combine probability intervals from flat distributions.

No matter which opinion one has, it seems obvious that if THU come from flat distributions, then they should be added linearly, and if from Gaussian, in quadrature. It is more reasonable and more conservative to think that THU are flat, and thus to add them linearly. As already stated, PDF uncertainties are most certainly Gaussian uncertainties, they have been explicitly checked to be Gaussian, and should

therefore be treated as such. Therefore, there is enough evidence that the PDF + α_s uncertainty should be added in quadrature to all other PU. The way the total PU is then combined with the THU comes down to the best way of combining a Gaussian and flat distributions (which is less obvious). Of course, whenever a theoretical uncertainty dominates (typically the QCD scale uncertainty, e.g. for gluon–gluon fusion) the problem becomes less relevant.

If only one observable is needed each code should provide a set of options

$$\{o_1, \ldots, o_m\}, \qquad \text{with values} \quad o_i = \{o_i^1, \ldots, o_i^k\} \tag{39}$$

where, for instance, o_i is QCD μ_R dependence and $\{o_i^1, o_i^2, o_i^3\}$ refer to $\mu_R = \text{scale}/2$, scale, $2\,\text{scale}$. After running the observable $\mathcal{O}$ over all options one determines $\mathcal{O}_{\min}$, $\mathcal{O}_c$, and $\mathcal{O}_{\max}$, where the central value is fixed by the author's taste, defining the *preferred* setup.

If several observables have to be combined one has to take into account that, given m options with multiple values, some of them are correlated, e.g. all options concerning production via gg fusion should not be varied independently in all observables. This means do not compute $\mathcal{O}_i$ with scale/2 and $\mathcal{O}_j$ with $2\,\text{scale}$ if both come from gg fusion. Even here we have two possibilities:

– Vary one option at the time and add the effects;
– vary all options (taking into account correlations) and find the absolute minimum and maximum in the allowed range of variation.

The first choice has the virtue that experimentalists can decide, later on, on error combination; the second one is more clean and reflects the true status of THU.

All this said, one has to face the problem of how to combine different determinations of uncertainties, e.g., from different groups which provide different uncertainty estimates for the same observable. Assume for definiteness that the two groups provide the probability distribution for an observable $\mathcal{O}$ as $p_1(\mathcal{O})$ and $p_2(\mathcal{O})$, for example by saying that the distributions are gaussian and providing their means and standard deviations m_i and σ_i. In the case of statistical uncertainties, two attitudes are possible:

– The different determinations differ due to statistical reasons. In such case, the best value is found as the weighted average. In the above example, the combined determination $\bar{p}(\mathcal{O})$ is a gaussian, with mean m equal to the weighted average of the means of the two starting distributions and standard deviation equal to the standard deviation of the mean, $\sigma^2 = \frac{\sigma_1^2 + \sigma_2^2}{2}$. In this case, the error on the combined determination is always smaller than the error on each of the determinations that go into it.
– The different determinations are exclusive, i.e. either one or the other is correct, and they should be combined in a Bayesian way by assigning an a priori reliability to each of them. In this case the combined probability is $\bar{p}(\mathcal{O}) = \frac{p_1(\mathcal{O}) + p_2(\mathcal{O})}{2}$, and the error on the combined determination is not necessarily smaller, and in fact typically larger than the error of each of the determinations that go into it. Indeed, in practice, unless the probability distributions that are being combined are very inconsistent (e.g. if their respective means differ by many standard deviations) this Bayesian combination is very close to the envelope of the distributions which are being combined (compare the method for the combination of PDF uncertainties discussed in Section 8).

The case of theoretical uncertainties is rather less obvious and it will be discussed in the next section.

12.5.1 Possibilities for option combination

Consider a given observable $\mathcal{O}$ whose calculation is characterized by a set of options $\{o_1, \ldots, o_n\}$. A typical result, showing all components of THU will be as follows:

$$\mathcal{O} = \mathcal{O}_c \,{}^{+\,o_1^{\max}}_{-\,o_1^{\min}} [o_1] \cdots {}^{+\,o_n^{\max}}_{-\,o_n^{\min}} [o_n]. \tag{40}$$

The question is on the combination of different sources. There are three options:

L) Linear combination:

$$\mathcal{O} = \mathcal{O}_{\text{c}}\,{}^{+\Delta_+^L\mathcal{O}}_{-\Delta_-^L\mathcal{O}}, \qquad \Delta_+^L\mathcal{O} = \sum_{i=1}^n o_i^{\max}, \quad \Delta_-^L\mathcal{O} = \sum_{i=1}^n o_i^{\min}, \tag{41}$$

Q) Quadratic combination:

$$\mathcal{O} = \mathcal{O}_{\text{c}}\,{}^{+\Delta_+^Q\mathcal{O}}_{-\Delta_-^Q\mathcal{O}}, \qquad \Delta_+^Q\mathcal{O} = \Big[\sum_{i=1}^n \big(o_i^{\max}\big)^2\Big]^{1/2}, \quad \Delta_-^Q\mathcal{O} = \Big[\sum_{i=1}^n \big(o_i^{\min}\big)^2\Big]^{1/2}, \tag{42}$$

E) Envelope combination:

$$\mathcal{O} = \mathcal{O}_{\text{c}}\,{}^{+\Delta_+^E\mathcal{O}}_{-\Delta_-^E\mathcal{O}}, \quad \Delta_+^E\mathcal{O} = \max_{o_1,\dots,o_n}\mathcal{O}\left(\{o\}\right) - \mathcal{O}_{\text{c}}, \quad \Delta_-^E\mathcal{O} = \mathcal{O}_{\text{c}} - \min_{o_1,\dots,o_n}\mathcal{O}\left(\{o\}\right), \tag{43}$$

where "c" refers to the preferred setup for all options. A loop over all options that are not correlated is indeed needed, all options that are independent should be varied simultaneously. When a specific set of PDFs is used, it should be kept fixed at its central value when computing the various THU. The PDF uncertainty (which is not a THU as discussed above) is computed along with other statistical and parametric uncertainties. Let us now assume that all options correspond to uncertainties which are known to be THU. Clearly addition in quadrature is then not appropriate. In an ideal case, all sources of THU should be recorded, with correlated options not be varied independently but rather in the correlated way discussed previously. The final ensuing uncorrelated THUs can then be just combined linearly. Moreover, in the future, combination can be repeated when some uncertainty is reduced or some improved strategy is found. To this purpose, all authors should provide information on each source of THU.

Unfortunately, this is not usually done, so, lacking detailed information, the problem of combining uncertainties arises. To be more concrete, let us consider an observable $\mathcal{O}$ and two different predictions, $\mathcal{O}_A$ and $\mathcal{O}_B$, both with asymmetric error (with for definiteness $\mathcal{O}_A > \mathcal{O}_B$). The precise meaning of error here is not obvious; however, we can assume that an error of $\pm\Delta_A$ means that the observable has a constant probability of being in the range $\mathcal{O}_A - \Delta_A < \mathcal{O} < \mathcal{O}_A + \Delta_A$ (with the obvious generalization when the error is asymmetric). Note that the standard deviation of such a probability distribution is equal to $\sigma = \frac{\Delta}{\sqrt{3}}$. The rationale for this choice is that if a calculation is performed by using the state-of-art of the present technology, the meaning of the error band is then: *I don't know about higher-order effects, I haven't computed them, but I know that it is almost impossible that they will change my result more than what I have indicated.* Thus, the true result should be within the shown interval.

Given two predictions $\mathcal{O}_{A,B}$ with asymmetric errors $\Delta A_\pm$ and $\Delta B_\pm$ the central value (this result rests on the assumption that the upper limit is due to A and the lower due to B) can be defined as

$$\langle\mathcal{O}\rangle = \frac{1}{2}\left(\mathcal{O}_A + \mathcal{O}_B + \Delta B_+ - \Delta A_-\right) \tag{44}$$

i.e. at the centre of the overlapping band (or at the centre of the gap in case of no overlap). If the two uncertainties are treated as completely independent and they are added linearly, the width of the band then is

$$W = \Delta A_+ + \Delta A_- + \Delta B_+ + \Delta B_-. \tag{45}$$

This is a very conservative estimate, which contradicts the above philosophy according to which the two intervals $\Delta A_+ + \Delta A_-$ and $\Delta B_+ + \Delta B_-$ should already be "maximal" ranges of variation. Furthermore, it neglects the fact that in practice the ranges of variation given by different authors will include several common effects.

One could then alternatively argue in the following way: the two determinations provide each a maximal range of variation, however the two different estimates of the range of variation include some common effects. The total range of variation should then be smaller than W, Eq. (45), to account for these common effects. For example, suppose A does not include the β-effect and estimates the corresponding uncertainty, but includes the α-effect. The opposite for B. If it is thought that a smaller W reflects a genuine progress, then an ideal solution would be that A and B include both the α- and β-effects. However, sometimes this is not possible, for example if B considers the α-effect to be wrong or questionable. Even so, a less conservative than just using Eq. (45) is possible. Namely, assuming that the possible inclusion of common effects is responsible for the fact that the two bands overlap, and the difference in central values is due to effects not included in both determinations, one should subtract from the uncertainty band the width

$$d = \max\{\, 0,\, \mathcal{O}_B - \mathcal{O}_A + \Delta B_+ + \Delta A_- \} \tag{46}$$

of the region of overlap of the two bands, thereby getting an uncertainty band with width

$$W' = W - d. \tag{47}$$

If the bands have a nonzero overlap, so $d > 0$, W' Eq. (47) is just the envelope of the two bands, namely $W' = W''$, with.

$$W'' = \Delta A_+ + \Delta B_- + \left(\mathcal{O}_A - \mathcal{O}_B \right). \tag{48}$$

If the bands do not overlap the envelope Eq. (48) is wider than the linear sum of the uncertainties Eq. (45): $W'' > W$. In this case, the lack of overlap of the two bands suggests that either or both of two determinations are missing some source of uncertainty, and the envelope prescription, which is now more conservative than the linear sum, seems more advisable.

Hence we conclude that it is in general advisable to adopt the envelope uncertainty estimate Eq. (48). To formulate our recommendation in full generality we define

$$
\begin{aligned}
O_- &= \max\left\{ \mathcal{O}_B - \Delta B_-,\ \mathcal{O}_A - \Delta A_- \right\}, \\
O_+ &= \min\left\{ \mathcal{O}_B + \Delta B_+,\ \mathcal{O}_A + \Delta A_+ \right\}, \\
E_- &= \min\left\{ \mathcal{O}_B - \Delta B_-,\ \mathcal{O}_A - \Delta A_- \right\}, \\
E_+ &= \max\left\{ \mathcal{O}_B + \Delta B_+,\ \mathcal{O}_A + \Delta A_+ \right\}.
\end{aligned} \tag{49}
$$

Our recommendation is thus to use as best prediction for the observable the central value

$$\langle \mathcal{O} \rangle = \frac{1}{2} \left(O_+ + O_- \right), \tag{50}$$

with an uncertainty band with envelope width

$$W'' = E_+ - E_- \tag{51}$$

[generalization of Eq. (48)], namely:

$$\mathcal{O} = \langle \mathcal{O} \rangle^{+\{E_+ - \langle \mathcal{O} \rangle\}}_{-\{\langle \mathcal{O} \rangle - E_-\}}. \tag{52}$$

Finally, we note that a similar conclusion is reached if we assume that the two determinations under discussion should be taken as exclusive and with equal a priori probability. Indeed if $p_A(\mathcal{O})$ and $p_B(\mathcal{O})$ are two flat probability distributions for the observable $\mathcal{O}$, then the combined distribution $\bar{p}(\mathcal{O}) = (p_A(\mathcal{O}) + p_B(\mathcal{O}))/2$ has an effect very similar to a flat distribution with width equal to the envelope of $p_A(\mathcal{O})$ and $p_B(\mathcal{O})$, as long as the two bands at least touch each other.

If the starting determinations distributions are inconsistent, i.e. $\mathcal{O}_B + \Delta B_+ \ll \mathcal{O}_A - \Delta A_-$ none of these methods seems adequate, and in such case one should question the reliability of the results which are being combined. In all other cases, we conclude that the envelope method Eq. (52) provides a conservative but not overly conservative way of combining THU, though it could overestimate a bit the combined THU.

12.5.2 Conclusions

The concept of THU and its use require few basic rules and an agreement within the community:

– Sets of options in different calculations should be homogeneous; if one calculation includes a *new* option its physical origin should be motivated and its inclusion accepted, in which case all codes should include it. If a calculation is based on options that inflate (or deflate) the THU without a general consensus or a solid theoretical basis, it should not be included in the average. Controversial assumptions should be put on a waiting list and included only when the issue is fully clarified. Our recommendation for central value is the midpoint of the overlapping region, Eq.(50).

– If different calculations include homogeneous sets of options the difference between central values should be considered with particular care, unless the central value itself reflects a specific choice for the *preferred setup* with different choices in different calculations. If all options, including the preferred setup, are congruent then differences in the central values cannot be justified by THU.

To summarize our recommendations we suggest that:

– Parametric uncertainties that are distributed according to a known (usually Gaussian) distribution should be added in quadrature.

– For the choice of central QCD scales we are suggesting to use the last two known orders for the search of stability and for minimizing corrections (if reasonable), which is – at best – a *rule of thumb*. The corresponding theoretical uncertainty, which of course should be assessed by investigating the highest known order, is arguably distributed according to a flat distribution. Problems related to incompatible data are more the rule than an exception for THU and, in principle, THUs should be considered case by case; this is this is particularly true whenever the two error bands are far apart, and also the envelope (the standard method for incompatible statistical uncertainties) becomes questionable. In order to formulate a global recommendation we suggest that THU should be combined according to the envelope method: therefore, define the central value according to Eq.(50) with uncertainty given by Eq.(52).

– One should keep in mind that there are additional sources of THU, e.g. the THU resulting from missing higher-order EW corrections, that cannot be estimated via scale uncertainties. Therefore scale variation uncertainties (SU) are a relevant portion of the global THU but do not exhaust the THU. It is our recommendation that all sources of THU, not only SU, and their origin should always be documented.

– The way the total PU is then combined with the THU comes down to the best way of combining a Gaussian and flat distributions. As general rule that is sufficiently conservative only the linear combination of those errors can be recommended.

– To stress our point let us repeat that the PDF + α_{s} (plus other parametric uncertainties, such as heavy-quark masses) are added in quadrature to each other (i.e. if one wants to add heavy-quark mass effects, this has to be done in quadrature to PDF + α_{s}, which is already the sum in quadrature of PDF + α_{s}), but then they are added *only once* at the end to the THU. Thus if one has two different estimates of the PDF + α_{s} uncertainty, A and B, the recommendation is on averaging these two estimates (which is the same as the uncertainty on two fully correlated measurements) before combining with the THU. A remaining source of uncertainty, i.e. the scale dependence of PDF, cannot be estimated at present.

13   Summary[24]

The present document is the result of a workshop that started in January 2010 as a new joint effort between ATLAS, CMS, LHCb, and the theory community. In this Report we have presented the state of the art for SM and MSSM Higgs cross-section and branching-ratio calculations.

Here we summarize the Higgs production cross sections which are obtained following the recommendation of Section 8 for the choice of parton distribution functions (PDFs) and their combined uncertainty assessment together with the one for the strong coupling constant α_s (PDF4LHC recipe). Moreover, we combine this PDF + α_s uncertainty with the theoretical uncertainty (THU) according to the prescription of Section 12. In detail, given two calculations $\mathcal{O}_{1,2}$ with THU uncertainties $\Delta_{i,\pm}^{\mathrm{THU}}$ and PDF + α_s uncertainties (according to the PDF4LHC recipe) $\Delta_{i,\pm}^{\mathrm{PU}}$, we

– define the corresponding central value as

$$\langle \mathcal{O} \rangle = \frac{1}{2}\left(O_+ + O_-\right), \tag{53}$$

where $O_\pm$ give the boundaries of the overlap,

$$O_+ = \min\{\mathcal{O}_1 + \Delta_{1,+}^{\mathrm{THU}}, \mathcal{O}_2 + \Delta_{2,+}^{\mathrm{THU}}\}, \qquad O_- = \max\{\mathcal{O}_1 - \Delta_{1,-}^{\mathrm{THU}}, \mathcal{O}_2 - \Delta_{2,-}^{\mathrm{THU}}\}, \tag{54}$$

– compute combined THU uncertainty

$$T^+ = E_+ - \langle \mathcal{O} \rangle, \quad T^- = \langle \mathcal{O} \rangle - E_-, \tag{55}$$

where $E_\pm$ give the boundaries of the envelope,

$$E_+ = \max\{\mathcal{O}_1 + \Delta_{1,+}^{\mathrm{THU}}, \mathcal{O}_2 + \Delta_{2,+}^{\mathrm{THU}}\}, \qquad E_- = \min\{\mathcal{O}_1 - \Delta_{1,-}^{\mathrm{THU}}, \mathcal{O}_2 - \Delta_{2,-}^{\mathrm{THU}}\}, \tag{56}$$

– compute combined PDF + α_s uncertainty

$$P^\pm = \frac{1}{2}\left(\Delta_{1,\pm}^{\mathrm{PU}} + \Delta_{2,\pm}^{\mathrm{PU}}\right) \tag{57}$$

– define total errors, $T^\pm + P^\pm$.

The combined numbers in this Summary, for the gg-fusion process, are based on the two predictions (ABPS and dFG) of Section 2; work is in progress to understand the numerical impact of (possibly) remaining THUs with the inclusion of other analyses (e.g. the BD calculation of Section 2.4).

The total cross section at $\sqrt{s} = 7$ TeV and 14 TeV is shown in Fig. 40. The SM Higgs production cross sections for the individual channels are shown in Fig. 41 for $\sqrt{s} = 7$ TeV and in Fig. 42 for $\sqrt{s} = 14$ TeV, with the combined parametric and theoretical uncertainties, PU + THU, illustrated by bands. The labels on the bands briefly indicated the type of radiative corrections that are included in the predictions. For details of the calculations and individual components of the error (THU, PDF + α_s, etc.) we refer the reader to the main text, e.g. to Section 2 for the gg-fusion results. In Tables 37–40 the cross sections and associated total errors for different production channels are summarized together with the total inclusive Higgs production cross sections.

The branching ratios for the SM Higgs boson are shown in Fig. 43. Tables containing explicit numbers on partial widths, branching ratios, and on the total width can be found in Section 9 and Appendix B. As already pointed out in Section 9, a full error analysis of the Higgs branching ratio is still in progress (see Ref. [40] for a recent independent analysis).

The results shown in this section will be regularly updated at our webpage[25].

---

[24]S. Dittmaier, C. Mariotti, G. Passarino and R. Tanaka.

[25]*https://twiki.cern.ch/twiki/bin/view/LHCPhysics/CrossSections*
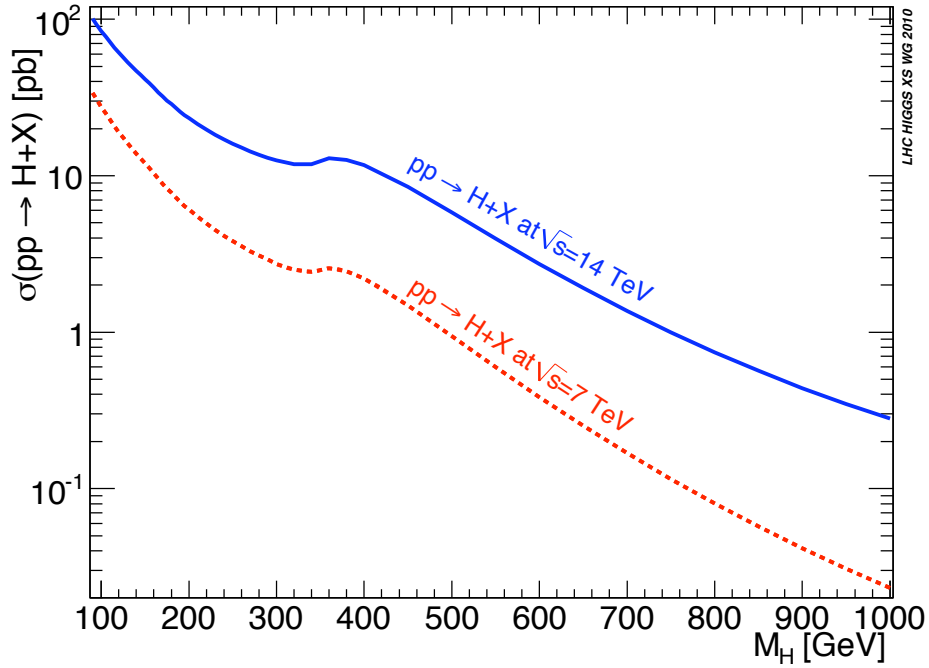
Fig. 40: The total SM Higgs production cross section at $\sqrt{s} = 7$ TeV and 14 TeV.

Each experiment is recommended to use the common Standard Model input parameters (Appendix A), the best known NNLO(NLO) cross sections and branching ratios reported in this Report as common basis for Higgs physics at LHC.

Beyond the goals of this Report remains the agreement between NLO MC predictions and NNLO calculations within the acceptance of the detectors. The next step in the activities of this working group will be the computation of cross sections that include acceptance cuts and differential distributions for all final states that will be considered in the Higgs search at the LHC. Preferably this should be carried out with the same set of (benchmark) cuts for ATLAS and CMS. The goal is to understand how the K-factors from (N)LO to (N)NLO will change after introduction of cuts and to compare the NNLO differential distributions with the ones from Monte Carlo generators at NLO.

There is a final comment concerning the SM background: We plan to estimate theoretical predictions for the most important backgrounds in the signal regions. This means that a *background control region* has to be defined, and there the experiments will measure a given source of background, directly from data. The *control region* can be in the bulk of the background production phase space, but can also be in the tail of the distributions. Thus it is important to define the precision with which the SM background will be measured and the theoretical precision available for that particular region. Then the background uncertainty should be extrapolated back to the *signal region*, using available theoretical predictions and their uncertainty. It will be important to compute the interference between signal and background and try to access this at NLO. The (N)LO Monte Carlos will be used to simulate this background and determine how the K-factor is changing with the chosen kinematic cuts.

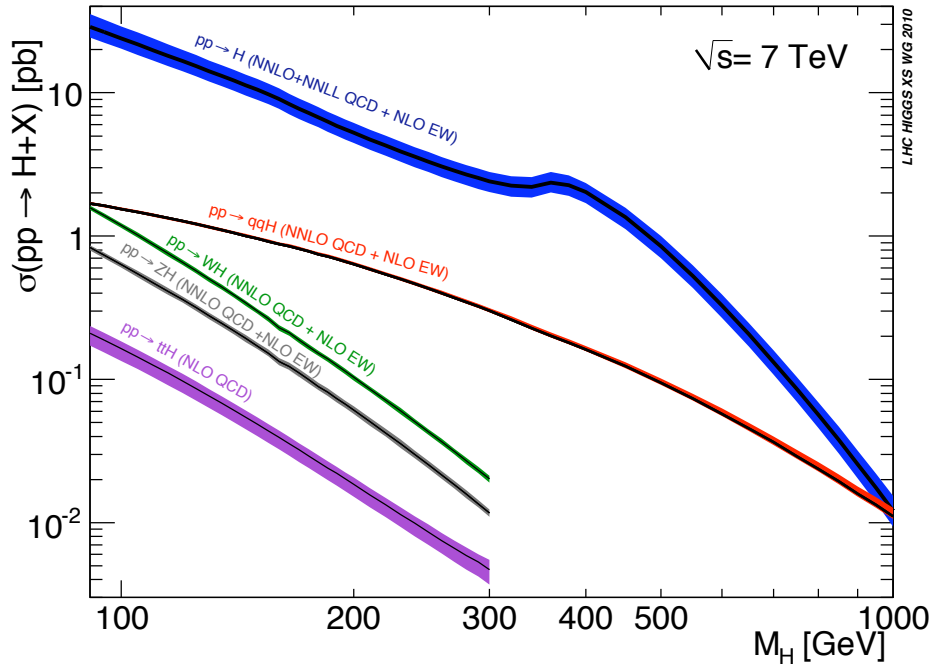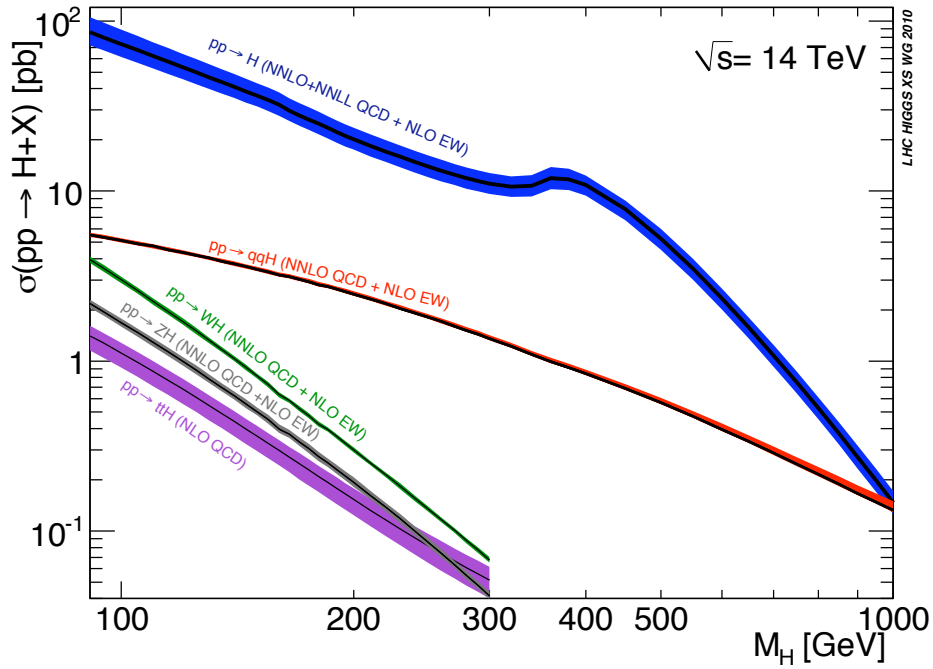**Fig. 41:** The SM Higgs production cross section at $\sqrt{s} = 7$ TeV.

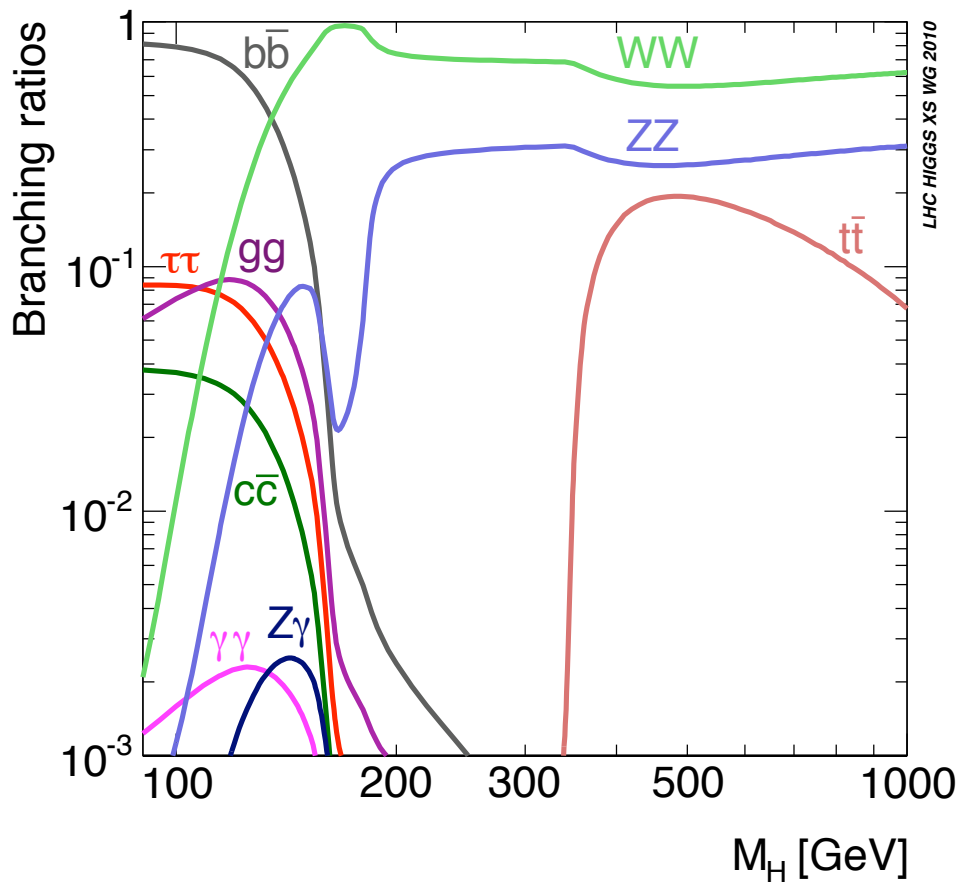**Fig. 42:** The SM Higgs production cross section at $\sqrt{s} = 14$ TeV.

Fig. 43: The SM Higgs branching ratios as a function of the Higgs-boson mass.

Table 37: SM Higgs-boson production cross section at $\sqrt{s} = 7$ TeV: light Higgs boson.

M_{H} [GeV]	ggF σ[pb]	error [%]	VBF σ[pb]	error [%]	WH σ[pb]	error [%]	ZH σ[pb]	error [%]	ttH σ[pb]	error [%]	Total σ[pb]
90	29.47	+22.9 −15.6	1.710	+2.7 −2.3	1.640	+3.3 −3.8	0.8597	+3.9 −4.0	0.2162	+12.5 −18.1	33.90
95	26.58	+21.9 −15.9	1.628	+2.5 −2.5	1.392	+3.3 −4.1	0.7348	+4.6 −4.7	0.1880	+12.4 −18.0	30.52
100	24.02	+21.2 −15.6	1.546	+2.6 −2.4	1.186	+4.0 −3.9	0.6313	+4.5 −4.6	0.1638	+12.3 −18.0	27.55
105	21.78	+20.8 −15.5	1.472	+2.5 −2.4	1.018	+3.8 −4.3	0.5449	+5.0 −5.3	0.1433	+12.1 −17.9	24.96
110	19.84	+20.4 −15.3	1.398	+2.8 −2.3	0.8754	+4.1 −4.5	0.4721	+5.3 −5.3	0.1257	+12.1 −18.0	22.71
115	18.13	+20.0 −15.3	1.332	+2.5 −2.3	0.7546	+4.3 −4.7	0.4107	+5.5 −5.4	0.1106	+11.9 −17.8	20.74
120	16.63	+19.7 −15.1	1.269	+2.8 −2.5	0.6561	+3.8 −4.1	0.3598	+5.0 −4.7	0.09756	+11.8 −17.8	19.01
125	15.31	+19.5 −15.1	1.211	+2.7 −2.4	0.5729	+3.7 −4.3	0.3158	+4.9 −5.1	0.08634	+11.8 −17.8	17.50
130	14.12	+19.2 −15.1	1.154	+2.8 −2.3	0.5008	+3.8 −4.3	0.2778	+5.2 −5.1	0.07658	+11.6 −17.7	16.13
135	13.08	+18.9 −15.0	1.100	+3.0 −2.2	0.4390	+4.1 −3.8	0.2453	+5.3 −5.0	0.06810	+11.5 −17.6	14.93
140	12.13	+18.8 −14.9	1.052	+2.8 −2.2	0.3857	+4.0 −4.0	0.2172	+5.2 −5.3	0.06072	+11.4 −17.6	13.85
145	11.27	+18.7 −14.9	1.004	+3.1 −2.1	0.3406	+4.0 −4.6	0.1930	+5.8 −5.8	0.05435	+11.4 −17.6	12.86
150	10.50	+18.7 −14.9	0.9617	+2.9 −2.2	0.3001	+3.7 −4.1	0.1713	+5.4 −5.2	0.04869	+11.3 −17.5	11.98
155	9.795	+18.5 −15.0	0.9180	+3.1 −2.1	0.2646	+4.0 −4.3	0.1525	+5.7 −5.2	0.04374	+11.4 −17.7	11.17
160	9.080	+18.6 −15.0	0.8787	+2.9 −2.3	0.2291	+4.3 −4.5	0.1334	+6.0 −5.7	0.03942	+11.4 −17.7	10.36
165	8.319	+18.1 −14.7	0.8517	+3.1 −2.1	0.2107	+4.1 −4.3	0.1233	+6.2 −5.8	0.03559	+11.3 −17.7	9.540
170	7.729	+17.9 −14.9	0.8173	+3.1 −2.2	0.1883	+4.3 −4.5	0.1106	+6.4 −6.1	0.03219	+11.3 −17.6	8.877
175	7.211	+17.9 −14.8	0.7814	+3.2 −2.1	0.1689	+4.1 −4.9	0.09950	+6.2 −6.0	0.02918	+11.2 −17.6	8.290
180	6.739	+18.1 −14.7	0.7480	+3.1 −2.4	0.1521	+4.1 −4.1	0.08917	+6.0 −5.7	0.02652	+11.2 −17.6	7.755
185	6.295	+17.4 −15.0	0.7193	+3.4 −2.2	0.1387	+3.9 −4.4	0.08139	+6.1 −5.8	0.02414	+11.3 −17.7	7.259
190	5.896	+17.3 −15.0	0.6925	+3.3 −2.2	0.1253	+4.2 −4.4	0.07366	+6.1 −6.0	0.02206	+11.3 −17.7	6.810
195	5.551	+17.2 −15.1	0.6643	+3.4 −2.5	0.1138	+4.4 −4.3	0.06699	+6.3 −5.9	0.02016	+11.3 −17.7	6.416
200	5.249	+17.2 −15.2	0.6371	+3.4 −2.3	0.1032	+4.2 −4.8	0.06096	+6.4 −6.0	0.01849	+11.3 −17.8	6.069
210	4.723	+16.9 −15.3	0.5869	+3.5 −2.4	0.08557	+4.2 −4.4	0.05068	+6.3 −6.2	0.01562	+11.7 −18.1	5.462
220	4.288	+16.8 −15.3	0.5420	+3.5 −2.5	0.07142	+4.0 −4.6	0.04235	+6.4 −6.1	0.01330	+11.8 −18.2	4.957
230	3.908	+16.6 −15.5	0.5011	+3.8 −2.4	0.06006	+5.2 −5.2	0.03560	+6.9 −6.7	0.01143	+12.2 −18.4	4.516
240	3.581	+16.7 −15.4	0.4641	+3.8 −2.5	0.05075	+4.5 −4.7	0.02999	+6.3 −6.2	0.009873	+12.3 −18.6	4.136
250	3.312	+16.5 −15.6	0.4304	+4.0 −2.6	0.04308	+4.5 −4.7	0.02540	+6.2 −5.8	0.008593	+12.6 −18.8	3.819
260	3.072	+16.2 −15.9	0.3988	+4.3 −2.4	0.03674	+4.8 −4.7	0.02158	+6.3 −6.2	0.007524	+12.9 −18.9	3.537
270	2.864	+16.2 −15.8	0.3715	+4.2 −2.6	0.03146	+4.4 −4.7	0.01839	+6.0 −6.0	0.006636	+13.6 −19.4	3.292
280	2.696	+16.0 −16.2	0.3461	+4.3 −2.7	0.02700	+4.8 −5.4	0.01575	+6.5 −6.2	0.005889	+14.2 −19.9	3.091
290	2.546	+16.1 −16.1	0.3226	+4.5 −2.6	0.02333	+4.9 −5.0	0.01355	+6.0 −5.8	0.005256	+14.9 −20.3	2.911
300	2.418	+16.1 −16.1	0.3010	+4.6 −2.7	0.02018	+5.1 −5.4	0.01169	+6.4 −6.2	0.004719	+15.6 −20.9	2.756

Table 38: SM Higgs-boson production cross section at $\sqrt{s} = 7$ TeV: heavy Higgs boson.

M_{H}	ggF		VBF		Total
[GeV]	σ[pb]	error [%]	σ[pb]	error [%]	σ[pb]
320	2.248	+16.3 −16.2	0.2622	+4.9 −2.7	2.510
340	2.199	+17.6 −15.7	0.2286	+5.1 −2.9	2.428
360	2.359	+19.1 −14.8	0.2018	+5.3 −3.0	2.561
380	2.263	+16.9 −15.8	0.1807	+5.7 −3.0	2.444
400	2.035	+15.3 −16.6	0.1619	+5.9 −3.0	2.197
450	1.356	+16.4 −17.4	0.1235	+6.6 −3.2	1.479
500	0.8497	+17.6 −17.5	0.09491	+7.2 −3.4	0.9446
550	0.5259	+18.4 −17.6	0.07356	+7.9 −3.5	0.5995
600	0.3275	+19.3 −17.8	0.05763	+8.6 −3.8	0.3851
650	0.2064	+19.8 −17.9	0.04556	+9.3 −3.8	0.2520
700	0.1320	+20.5 −18.2	0.03635	+9.9 −4.0	0.1683
750	0.08587	+21.4 −18.5	0.02924	+10.7 −4.2	0.1151
800	0.05665	+22.1 −19.0	0.02371	+11.3 −4.3	0.08036
850	0.03786	+23.1 −19.6	0.01937	+11.9 −4.5	0.05723
900	0.02561	+24.3 −20.4	0.01595	+12.6 −4.6	0.04156
950	0.01752	+25.5 −21.4	0.01321	+13.4 −4.8	0.03073
1000	0.01210	+27.1 −22.6	0.01103	+14.2 −4.9	0.02313

Table 39: SM Higgs-boson production cross section at $\sqrt{s} = 14$ TeV: light Higgs boson.

M_H [GeV]	ggF σ[pb]	ggF error [%]	VBF σ[pb]	VBF error [%]	WH σ[pb]	WH error [%]	ZH σ[pb]	ZH error [%]	ttH σ[pb]	ttH error [%]	Total σ[pb]
90	87.55	+23.0 −16.4	5.569	+2.9 −3.0	4.090	+4.3 −4.6	2.245	+5.3 −5.7	1.449	+14.9 −18.0	100.9
95	79.83	+22.3 −16.0	5.338	+3.0 −3.1	3.499	+4.4 −4.5	1.941	+5.2 −5.2	1.268	+14.8 −18.0	91.88
100	73.27	+21.5 −16.0	5.114	+2.8 −3.1	3.002	+4.5 −4.3	1.683	+5.7 −5.3	1.114	+14.8 −18.0	84.18
105	67.34	+21.1 −15.6	4.900	+3.2 −2.9	2.596	+4.1 −4.0	1.468	+5.4 −5.4	0.9816	+14.7 −18.0	77.29
110	62.16	+20.6 −15.3	4.750	+2.2 −3.9	2.246	+4.1 −4.6	1.283	+6.1 −5.6	0.8681	+14.8 −18.1	71.31
115	57.57	+20.2 −15.0	4.520	+2.9 −3.0	1.952	+4.5 −4.0	1.130	+6.2 −5.2	0.7699	+14.8 −18.1	65.94
120	53.49	+20.0 −14.8	4.361	+2.5 −3.5	1.710	+4.4 −4.1	0.9967	+6.0 −5.4	0.6850	+14.7 −18.1	61.24
125	49.85	+19.6 −14.6	4.180	+2.8 −3.0	1.504	+4.1 −4.4	0.8830	+6.4 −5.5	0.6113	+14.8 −18.2	57.03
130	46.55	+19.5 −14.4	4.029	+2.5 −3.1	1.324	+3.8 −3.7	0.7846	+6.3 −5.2	0.5472	+14.8 −18.2	53.23
135	43.61	+19.1 −14.2	3.862	+3.1 −2.8	1.167	+3.5 −3.4	0.6981	+5.9 −5.2	0.4910	+14.8 −18.2	49.83
140	40.93	+18.9 −13.9	3.732	+2.6 −3.3	1.034	+3.3 −3.8	0.6256	+5.8 −5.2	0.4419	+14.8 −18.2	46.76
145	38.49	+18.8 −13.7	3.590	+3.0 −3.0	0.9200	+3.8 −3.7	0.5601	+6.7 −5.5	0.3989	+14.9 −18.3	43.96
150	36.27	+18.7 −13.5	3.460	+2.8 −3.0	0.8156	+3.0 −3.3	0.5016	+6.0 −4.7	0.3609	+14.9 −18.3	41.41
155	34.22	+18.6 −13.6	3.332	+2.9 −3.0	0.7255	+3.5 −3.7	0.4513	+6.5 −5.6	0.3275	+14.9 −18.4	39.06
160	32.10	+18.6 −13.7	3.198	+3.1 −2.8	0.6341	+3.3 −3.6	0.3986	+6.6 −5.5	0.2980	+15.0 −18.5	36.63
165	29.77	+17.8 −13.4	3.137	+3.0 −2.9	0.5850	+2.6 −3.0	0.3705	+6.4 −4.9	0.2718	+15.1 −18.5	34.13
170	27.93	+17.7 −13.3	3.033	+2.8 −3.0	0.5260	+3.1 −3.5	0.3355	+6.5 −5.4	0.2487	+15.7 −18.9	32.07
175	26.36	+17.7 −13.4	2.922	+3.5 −2.8	0.4763	+3.4 −3.2	0.3044	+6.6 −5.7	0.2279	+15.8 −18.9	30.29
180	24.92	+17.8 −13.4	2.805	+3.3 −2.8	0.4274	+3.2 −3.4	0.2744	+6.7 −5.8	0.2095	+15.8 −19.0	28.64
185	23.49	+17.2 −13.4	2.740	+2.8 −2.9	0.3963	+2.9 −3.2	0.2524	+6.1 −5.5	0.1930	+15.8 −19.0	27.07
190	22.21	+17.1 −13.2	2.652	+2.7 −2.9	0.3600	+3.0 −3.4	0.2301	+6.5 −5.9	0.1783	+16.0 −19.2	25.63
195	21.10	+17.0 −13.2	2.566	+2.9 −2.9	0.3291	+3.0 −3.4	0.2112	+6.4 −5.8	0.1650	+16.0 −19.2	24.37
200	20.16	+16.8 −13.2	2.472	+3.2 −2.7	0.3004	+3.4 −3.5	0.1936	+6.7 −6.1	0.1532	+16.2 −19.4	23.28
210	18.49	+16.6 −13.3	2.315	+3.2 −2.7	0.2526	+2.8 −3.3	0.1628	+6.5 −5.1	0.1329	+16.4 −19.5	21.35
220	17.08	+16.4 −13.3	2.171	+2.9 −3.1	0.2138	+3.4 −3.3	0.1380	+6.3 −5.6	0.1162	+16.7 −19.8	19.72
230	15.86	+16.3 −13.2	2.036	+3.2 −2.8	0.1826	+3.9 −4.0	0.1173	+7.0 −6.2	0.1025	+17.1 −20.0	18.30
240	14.82	+16.1 −13.2	1.918	+3.0 −2.7	0.1561	+3.7 −3.8	0.09996	+6.5 −5.9	0.09109	+17.3 −20.3	17.09
250	13.92	+16.0 −13.2	1.807	+2.9 −3.0	0.1343	+3.2 −3.7	0.08540	+6.2 −5.5	0.08156	+17.7 −20.5	16.03
260	13.14	+15.9 −13.3	1.711	+2.9 −3.7	0.1161	+3.0 −3.5	0.07341	+6.1 −5.2	0.07351	+18.1 −20.8	15.11
270	12.47	+15.7 −13.1	1.606	+3.0 −2.9	0.1009	+3.1 −3.2	0.06325	+5.3 −4.7	0.06667	+18.5 −21.1	14.31
280	11.90	+15.7 −13.1	1.514	+3.2 −2.7	0.08781	+3.4 −3.6	0.05474	+5.7 −5.0	0.06081	+19.0 −21.4	13.62
290	11.43	+15.4 −13.2	1.436	+3.2 −2.8	0.07714	+3.5 −3.8	0.04769	+5.4 −4.7	0.05575	+19.4 −21.7	13.05
300	11.05	+15.3 −13.0	1.358	+3.2 −2.9	0.06755	+3.9 −3.8	0.04156	+5.6 −5.2	0.05133	+19.8 −21.9	12.57

Table 40: SM Higgs-boson production cross section at $\sqrt{s} = 14$ TeV: heavy Higgs boson.

M_{H}	ggF		VBF		Total
[GeV]	σ[pb]	error [%]	σ[pb]	error [%]	σ[pb]
320	10.59	+15.4 −12.9	1.220	+3.2 −2.8	11.81
340	10.72	+15.9 −13.4	1.094	+3.3 −2.8	11.81
360	11.91	+16.5 −13.8	0.9930	+3.3 −2.8	12.90
380	11.72	+15.3 −13.3	0.9148	+3.4 −2.7	12.63
400	10.87	+13.2 −13.6	0.8422	+3.6 −2.7	11.71
450	7.790	+12.6 −13.7	0.6893	+3.8 −3.0	8.479
500	5.255	+13.7 −13.9	0.5684	+4.0 −2.9	5.823
550	3.493	+14.2 −14.1	0.4724	+4.4 −3.0	3.965
600	2.332	+14.5 −14.0	0.3965	+4.7 −3.1	2.728
650	1.576	+14.5 −13.8	0.3360	+4.9 −3.2	1.912
700	1.078	+15.2 −14.1	0.2872	+5.2 −3.4	1.365
750	0.7498	+15.5 −13.9	0.2476	+5.6 −3.5	0.9974
800	0.5280	+15.6 −14.0	0.2155	+5.8 −3.7	0.7435
850	0.3766	+15.9 −14.2	0.1885	+6.3 −3.6	0.5651
900	0.2723	+16.3 −14.5	0.1666	+6.5 −3.8	0.4389
950	0.1987	+16.8 −14.5	0.1484	+6.6 −4.0	0.3471
1000	0.1472	+16.8 −14.6	0.1330	+7.0 −4.0	0.2802

Acknowledgements

References

[1] P. W. Higgs, *Broken symmetries, massless particles and gauge fields*, Phys. Lett. **12** (1964) 132–133.

[2] P. W. Higgs, *Broken symmetries and the masses of gauge bosons*, Phys. Rev. Lett. **13** (1964) 508–509.

[3] P. W. Higgs, *Spontaneous symmetry breakdown without massless bosons*, Phys. Rev. **145** (1966) 1156–1163.

[4] F. Englert and R. Brout, *Broken symmetry and the mass of gauge vector mesons*, Phys. Rev. Lett. **13** (1964) 321–323.

[5] G. Guralnik, C. Hagen, and T. Kibble, *Global conservation laws and massless particles*, Phys. Rev. Lett. **13** (1964) 585–587.

[6] H. M. Georgi, S. L. Glashow, M. E. Machacek, and D. V. Nanopoulos, *Higgs bosons from two gluon annihilation in proton proton collisions*, Phys. Rev. Lett. **40** (1978) 692.

[7] S. Dawson, *Radiative corrections to Higgs boson production*, Nucl. Phys. **B359** (1991) 283–300.

[8] A. Djouadi, M. Spira, and P. M. Zerwas, *Production of Higgs bosons in proton colliders: QCD corrections*, Phys. Lett. **B264** (1991) 440–446.

[9] D. Graudenz, M. Spira, and P. Zerwas, *QCD corrections to Higgs boson production at proton proton colliders*, Phys. Rev. Lett. **70** (1993) 1372–1375.

[10] M. Spira, A. Djouadi, D. Graudenz, and P. M. Zerwas, *Higgs boson production at the LHC*, Nucl. Phys. **B453** (1995) 17–82, `hep-ph/9504378`.

[11] R. V. Harlander, *Virtual corrections to $gg \rightarrow H$ to two loops in the heavy top limit*, Phys. Lett. **B492** (2000) 74–80, `arXiv:hep-ph/0007289`.

[12] S. Catani, D. de Florian, and M. Grazzini, *Higgs production in hadron collisions: Soft and virtual QCD corrections at NNLO*, JHEP **05** (2001) 025, `arXiv:hep-ph/0102227`.

[13] R. V. Harlander and W. B. Kilgore, *Soft and virtual corrections to pp → H+X at NNLO*, Phys. Rev. **D64** (2001) 013015, `arXiv:hep-ph/0102241`.

[14] R. V. Harlander and W. B. Kilgore, *Next-to-next-to-leading order Higgs production at hadron colliders*, Phys. Rev. Lett. **88** (2002) 201801, `arXiv:hep-ph/0201206`.

[15] C. Anastasiou and K. Melnikov, *Higgs boson production at hadron colliders in NNLO QCD*, Nucl. Phys. **B646** (2002) 220–256, `arXiv:hep-ph/0207004`.

[16] V. Ravindran, J. Smith, and W. L. van Neerven, *NNLO corrections to the total cross section for Higgs boson production in hadron hadron collisions*, Nucl. Phys. **B665** (2003) 325–366, `arXiv:hep-ph/0302135`.

[17] J. Blümlein and V. Ravindran, *Mellin moments of the next-to-next-to leading order coefficient functions for the Drell-Yan process and hadronic Higgs-boson production*, Nucl. Phys. **B716** (2005) 128–172, `arXiv:hep-ph/0501178`.

[18] S. Catani, D. de Florian, M. Grazzini, and P. Nason, *Soft-gluon resummation for Higgs boson production at hadron colliders*, JHEP **07** (2003) 028, `hep-ph/0306211`.

[19] S. Moch and A. Vogt, *Higher-order soft corrections to lepton pair and Higgs boson production*, Phys. Lett. **B631** (2005) 48–57, `hep-ph/0508265`.

[20] E. Laenen and L. Magnea, *Threshold resummation for electroweak annihilation from DIS data*, Phys. Lett. **B632** (2006) 270–276, `hep-ph/0508284`.

[21] A. Idilbi, X.-d. Ji, J.-P. Ma, and F. Yuan, *Threshold resummation for Higgs production in effective field theory*, Phys. Rev. **D73** (2006) 077501, `hep-ph/0509294`.

[22] V. Ravindran, *On Sudakov and soft resummations in QCD*, Nucl. Phys. **B746** (2006) 58–76, `arXiv:hep-ph/0512249 [hep-ph]`.

[23] V. Ravindran, *Higher-order threshold effects to inclusive processes in QCD*, Nucl. Phys. **B752** (2006) 173–196, `arXiv:hep-ph/0603041`.

[24] S. Marzani, R. D. Ball, V. Del Duca, S. Forte, and A. Vicini, *Higgs production via gluon-gluon fusion with finite top mass beyond next-to-leading order*, Nucl. Phys. **B800** (2008) 127–145, `arXiv:arXiv:0801.2544 [hep-ph]`.

[25] R. V. Harlander and K. J. Ozeren, *Top mass effects in Higgs production at next-to-next-to-leading order QCD: virtual corrections*, Phys. Lett. **B679** (2009) 467–472, `arXiv:0907.2997 [hep-ph]`.

[26] R. V. Harlander and K. J. Ozeren, *Finite top mass effects for hadronic Higgs production at next-to-next-to-leading order*, JHEP **11** (2009) 088, `arXiv:0909.3420 [hep-ph]`.

[27] R. V. Harlander, H. Mantler, S. Marzani, and K. J. Ozeren, *Higgs production in gluon fusion at next-to-next-to-leading order QCD for finite top mass*, Eur. Phys. J. **C66** (2010) 359–372, `arXiv:0912.2104 [hep-ph]`.

[28] A. Pak, M. Rogal, and M. Steinhauser, *Virtual three-loop corrections to Higgs boson production in gluon fusion for finite top quark mass*, Phys. Lett. **B679** (2009) 473–477, `arXiv:0907.2998 [hep-ph]`.

[29] A. Pak, M. Rogal, and M. Steinhauser, *Finite top quark mass effects in NNLO Higgs boson production at LHC*, JHEP **02** (2010) 025, `arXiv:0911.4662 [hep-ph]`.

[30] C. Anastasiou, R. Boughezal, and F. Petriello, *Mixed QCD-electroweak corrections to Higgs boson production in gluon fusion*, JHEP **04** (2009) 003, `arXiv:0811.3458 [hep-ph]`.

[31] A. Djouadi and P. Gambino, *Leading electroweak correction to Higgs boson production at proton colliders*, Phys. Rev. Lett. **73** (1994) 2528–2531, `hep-ph/9406432`.

[32] U. Aglietti, R. Bonciani, G. Degrassi, and A. Vicini, *Two-loop light fermion contribution to Higgs production and decays*, Phys. Lett. **B595** (2004) 432–441, `arXiv:hep-ph/0404071`.

[33] G. Degrassi and F. Maltoni, *Two-loop electroweak corrections to Higgs production at hadron*

colliders, Phys. Lett. **B600** (2004) 255–260, `arXiv:hep-ph/0407249`.

[34] S. Actis, G. Passarino, C. Sturm, and S. Uccirati, *NNLO computational techniques: the cases* $H \to \gamma\gamma$ *and* $H \to gg$, Nucl. Phys. **B811** (2009) 182–273, `arXiv:0809.3667 [hep-ph]`.

[35] S. Actis, G. Passarino, C. Sturm, and S. Uccirati, *NLO electroweak corrections to Higgs boson production at hadron colliders*, Phys. Lett. **B670** (2008) 12–17, `arXiv:0809.1301 [hep-ph]`.

[36] W.-Y. Keung and F. J. Petriello, *Electroweak and finite quark-mass effects on the Higgs boson transverse momentum distribution*, Phys. Rev. **D80** (2009) 013007, `arXiv:0905.2775 [hep-ph]`.

[37] O. Brein, *Electroweak and bottom quark contributions to Higgs boson plus jet production*, Phys. Rev. **D81** (2010) 093006, `arXiv:1003.4438 [hep-ph]`.

[38] D. de Florian and M. Grazzini, *Higgs production through gluon fusion: updated cross sections at the Tevatron and the LHC*, Phys. Lett. **B674** (2009) 291–294, `arXiv:0901.2427 [hep-ph]`.

[39] J. Baglio and A. Djouadi, *Predictions for Higgs production at the Tevatron and the associated uncertainties*, JHEP **10** (2010) 064, `arXiv:1003.4266 and addendum 1009.1363 [hep-ph]`.

[40] J. Baglio and A. Djouadi, *Higgs production at the LHC*, `arXiv:1012.0530 [hep-ph]`.

[41] A. D. Martin, W. J. Stirling, R. S. Thorne, and G. Watt, *Parton distributions for the LHC*, Eur. Phys. J. **C63** (2009) 189–285, `arXiv:0901.0002 [hep-ph]`.

[42] M. Grazzini, *Higgs production at hadron colliders: online calculators*, `http://theory.fi.infn.it/grazzini/hcalculators.html`, 2010.

[43] A. D. Martin, R. G. Roberts, W. J. Stirling, and R. S. Thorne, *Uncertainties of predictions from parton distributions. 1: Experimental errors*, Eur. Phys. J. **C28** (2003) 455–473, `arXiv:hep-ph/0211080`.

[44] A. D. Martin, W. J. Stirling, R. S. Thorne, and G. Watt, *Uncertainties on* α_s *in global PDF analyses and implications for predicted hadronic cross sections*, Eur. Phys. J. **C64** (2009) 653–680, `arXiv:0905.3531 [hep-ph]`.

[45] *PDF4LHC steering committee*, `http://www.hep.ucl.ac.uk/pdf4lhc/`, 2010.

[46] S. Alekhin, J. Blümlein, S. Klein, and S. Moch, *The 3-, 4-, and 5-flavor NNLO parton from deep-inelastic-scattering data and at hadron colliders*, Phys. Rev. **D81** (2010) 014032, `arXiv:0908.2766 [hep-ph]`.

[47] P. Jimenez-Delgado and E. Reya, *Variable flavor number parton distributions and weak gauge and Higgs boson production at hadron colliders at NNLO of QCD*, Phys. Rev. **D80** (2009) 114011, `arXiv:0909.1711 [hep-ph]`.

[48] A. M. Cooper-Sarkar, *HERAPDF fits including* $F_2(charm)$ *data*, `arXiv:1006.4471 [hep-ph]`.

[49] V. Ahrens, T. Becher, M. Neubert, and L. L. Yang, *Updated predictions for Higgs production at the Tevatron and the LHC*, `arXiv:1008.3162 [hep-ph]`.

[50] V. Ahrens, T. Becher, M. Neubert, and L. L. Yang, *Origin of the large perturbative corrections to Higgs production at hadron colliders*, Phys. Rev. **D79** (2009) 033013, `arXiv:0808.3008 [hep-ph]`.

[51] V. Ahrens, T. Becher, M. Neubert, and L. L. Yang, *Renormalization-group improved prediction for Higgs production at hadron colliders*, Eur. Phys. J. **C62** (2009) 333–353, `arXiv:0809.4283 [hep-ph]`.

[52] S. Asai et al., *Prospects for the search for a standard model Higgs boson in ATLAS using vector boson fusion*, Eur. Phys. J. **C32S2** (2004) 19–54, `arXiv:hep-ph/0402254`.

[53] S. Abdullin et al., *Summary of the CMS potential for the Higgs boson discovery*, Eur. Phys. J. **C39S2** (2005) 41–61.

[54] M. Dührssen et al., *Extracting Higgs boson couplings from LHC data*, Phys. Rev. **D70** (2004) 113009, `arXiv:hep-ph/0406323`.

[55] V. Hankele, G. Klamke, D. Zeppenfeld, and T. Figy, *Anomalous Higgs boson couplings in vector boson fusion at the CERN LHC*, Phys. Rev. **D74** (2006) 095001, arXiv:hep-ph/0609075.

[56] V. Del Duca, W. Kilgore, C. Oleari, C. Schmidt, and D. Zeppenfeld, *Gluon-fusion contributions to H + 2-jet production*, Nucl. Phys. **B616** (2001) 367–399, arXiv:hep-ph/0108030.

[57] J. M. Campbell, R. K. Ellis, and G. Zanderighi, *Next-to-leading order Higgs + 2-jet production via gluon fusion*, JHEP **10** (2006) 028, arXiv:hep-ph/0608194.

[58] V. D. Barger, R. J. N. Phillips, and D. Zeppenfeld, *Mini-jet veto: A tool for the heavy Higgs search at the LHC*, Phys. Lett. **B346** (1995) 106–114, arXiv:hep-ph/9412276.

[59] D. L. Rainwater and D. Zeppenfeld, *Searching for $H \to \gamma\gamma$ in weak boson fusion at the LHC*, JHEP **12** (1997) 005, arXiv:hep-ph/9712271.

[60] D. L. Rainwater, D. Zeppenfeld, and K. Hagiwara, *Searching for $H \to \tau\tau$ in weak boson fusion at the LHC*, Phys. Rev. **D59** (1999) 014037, arXiv:hep-ph/9808468.

[61] D. L. Rainwater and D. Zeppenfeld, *Observing $H \to W^{(*)}W^{(*)} \to e^{\pm}\mu^{\mp}p\!\!\!/_T$ in weak boson fusion with dual forward jet tagging at the CERN LHC*, Phys. Rev. **D60** (1999) 113004, arXiv:hep-ph/9906218.

[62] V. Del Duca et al., *Monte Carlo studies of the jet activity in Higgs + 2-jet events*, JHEP **10** (2006) 016, arXiv:hep-ph/0608158.

[63] A. Nikitenko and M. L. Vazquez Acosta, *Monte Carlo study of $gg \to H$+jets contribution to vector boson fusion Higgs production at the LHC*, arXiv:0705.3585 [hep-ph].

[64] M. Spira, *QCD effects in Higgs physics*, Fortschr. Phys. **46** (1998) 203–284, arXiv:hep-ph/9705337.

[65] T. Han, G. Valencia, and S. Willenbrock, *Structure function approach to vector boson scattering in pp collisions*, Phys. Rev. Lett. **69** (1992) 3274–3277, arXiv:hep-ph/9206246.

[66] T. Figy, C. Oleari, and D. Zeppenfeld, *Next-to-leading order jet distributions for Higgs boson production via weak-boson fusion*, Phys. Rev. **D68** (2003) 073005, arXiv:hep-ph/0306109.

[67] T. Figy and D. Zeppenfeld, *QCD corrections to jet correlations in weak boson fusion*, Phys. Lett. **B591** (2004) 297–303, arXiv:hep-ph/0403297.

[68] E. L. Berger and J. M. Campbell, *Higgs boson production in weak boson fusion at next-to-leading order*, Phys. Rev. **D70** (2004) 073011, arXiv:hep-ph/0403194.

[69] M. Ciccolini, A. Denner, and S. Dittmaier, *Strong and electroweak corrections to the production of Higgs + 2-jets via weak interactions at the LHC*, Phys. Rev. Lett. **99** (2007) 161803, arXiv:0707.0381 [hep-ph].

[70] M. Ciccolini, A. Denner, and S. Dittmaier, *Electroweak and QCD corrections to Higgs production via vector-boson fusion at the LHC*, Phys. Rev. **D77** (2008) 013002, arXiv:0710.4749 [hep-ph].

[71] A. Denner, S. Dittmaier, and A. Mück, *HAWK: A Monte Carlo generator for the production of Higgs bosons Attached to WeaK bosons at hadron colliders*, http://omnibus.uni-freiburg.de/~sd565/programs/hawk/hawk.html, 2010.

[72] K. Arnold et al., *VBFNLO: A parton level Monte Carlo for processes with electroweak bosons*, Comput. Phys. Commun. **180** (2009) 1661–1670, arXiv:0811.4559 [hep-ph].

[73] M. Spira, *VV2H*, http://people.web.psi.ch/spira/vv2h, 2007.

[74] N. Adam, T. Aziz, J. Andersen, A. Belyaev, T. Binoth, et al., *Higgs working group summary report*, arXiv:0803.1154 [hep-ph].

[75] P. Bolzoni, F. Maltoni, S.-O. Moch, and M. Zaro, *Higgs production via vector-boson fusion at NNLO in QCD*, Phys. Rev. Lett. **105** (2010) 011801, arXiv:1003.4451 [hep-ph].

[76] A. Ghinculov, *Two loop heavy Higgs correction to Higgs decay into vector bosons*, Nucl. Phys. **B455** (1995) 21–38, arXiv:hep-ph/9507240 [hep-ph].

[77] A. Frink, B. A. Kniehl, D. Kreimer, and K. Riesselmann, *Heavy Higgs lifetime at two loops*, Phys. Rev. **D54** (1996) 4548–4560, `arXiv:hep-ph/9606310 [hep-ph]`.

[78] K. Arnold et al., *VBFNLO: A parton level Monte Carlo for processes with electroweak bosons*, `http://www-itp.particle.uni-karlsruhe.de/~vbfnloweb`, 2009.

[79] J. Alwall et al., *A standard format for Les Houches event files*, Comput. Phys. Commun. **176** (2007) 300–304, `arXiv:hep-ph/0609017`.

[80] J. R. Andersen, T. Binoth, G. Heinrich, and J. M. Smillie, *Loop induced interference effects in Higgs boson plus two jet production at the LHC*, JHEP **02** (2008) 057, `arXiv:0709.3513 [hep-ph]`.

[81] A. Bredenstein, K. Hagiwara, and B. Jager, *Mixed QCD-electroweak contributions to Higgs-plus-dijet production at the LHC*, Phys. Rev. **D77** (2008) 073004, `arXiv:0801.4231 [hep-ph]`.

[82] T. Figy, S. Palmer, and G. Weiglein, *Higgs production via weak boson fusion in the standard model and the MSSM*, `arXiv:1012.4789 [hep-ph]`.

[83] W. A. Bardeen, A. J. Buras, D. W. Duke, and T. Muta, *Deep inelastic scattering beyond the leading order in asymptotically free gauge theories*, Phys. Rev. **D18** (1978) 3998.

[84] D. I. Kazakov, A. V. Kotikov, G. Parente, O. A. Sampayo, and J. Sanchez Guillen, *Complete quartic (α_s^2) correction to the deep inelastic longitudinal structure function F(L) in QCD*, Phys. Rev. Lett. **65** (1990) 1535–1538.

[85] E. B. Zijlstra and W. L. van Neerven, *Order α_s^2 correction to the structure function F3 (x, Q^2) in deep inelastic neutrino-hadron scattering*, Phys. Lett. **B297** (1992) 377–384.

[86] E. B. Zijlstra and W. L. van Neerven, *Order α_s^2 QCD corrections to the deep inelastic proton structure functions F2 and F(L)*, Nucl. Phys. **B383** (1992) 525–574.

[87] S. Moch and J. A. M. Vermaseren, *Deep inelastic structure functions at two loops*, Nucl. Phys. **B573** (2000) 853–907, `arXiv:hep-ph/9912355`.

[88] W. L. van Neerven and J. A. M. Vermaseren, *The role of the five point function in radiative corrections to two photon physics*, Phys. Lett. **B142** (1984) 80.

[89] J. Blümlein, G. J. van Oldenborgh, and R. Rückl, *QCD and QED corrections to Higgs boson production in charged current ep scattering*, Nucl. Phys. **B395** (1993) 35–59, `arXiv:hep-ph/9209219`.

[90] T. Figy, V. Hankele, and D. Zeppenfeld, *Next-to-leading order QCD corrections to Higgs plus three jet production in vector-boson fusion*, JHEP **02** (2008) 076, `arXiv:0710.5621 [hep-ph]`.

[91] R. V. Harlander, J. Vollinga, and M. M. Weber, *Gluon-induced weak boson fusion*, Phys. Rev. **D77** (2008) 053010, `arXiv:0801.3355 [hep-ph]`.

[92] P. Bolzoni, F. Maltoni, S.-O. Moch, and M. Zaro, *VBF@NNLO: cross-section calculator*, `http://vbf-nnlo.phys.ucl.ac.be/vbf.html`, 2010.

[93] H. Baer and J. D. Wells, *Trilepton Higgs signal at hadron colliders*, Phys. Rev. **D57** (1998) 4446–4452, `arXiv:hep-ph/9710368`.

[94] The ATLAS Collaboration, *Detector and physics performance technical design report*, CERN/LHCC/99-14/15, 1999.

[95] K. Jakobs, *A study of the associated production WH, $H \rightarrow WW \rightarrow l\nu l\nu$*, ATLAS Note ATL-PHYS-2000-008, 2000.

[96] The ATLAS Collaboration, G. Aad et al., *Expected performance of the ATLAS experiment-detector, trigger and physics*, `hep-ex:arXiv:0901.0512`.

[97] E. Richter-Was, *Prospects for the observability of the WH and ZH, $H \rightarrow bb$ channel in 14 TeV pp and 2 TeV ppbar collisions ($E_T^{miss} + bb$ final state)*, ATLAS Note ATL-PHYS-2000-023, 2000.

[98] E. Richter-Was, *Revisiting the observability of the WH and ZH, $H \rightarrow bb$ channel in the 14 TeV*

pp and 2 TeV ppbar collisions (lbb and llbb final states), ATLAS Note ATL-PHYS-2000-024, 2000.

[99] J. M. Butterworth, A. R. Davison, M. Rubin, and G. P. Salam, *Jet substructure as a new Higgs search channel at the LHC*, Phys. Rev. Lett. **100** (2008) 242001, arXiv:0802.2470 [hep-ph].

[100] J. M. Butterworth, A. R. Davison, K. Jakobs, V. E. Oezcan, G. Piacquadio, and C. Weiser, *ATLAS sensitivity to the standard model Higgs in the HW and HZ channels at high transverse momenta*, ATLAS Note ATL-PHYS-PUB-2009-088, 2009.

[101] The ATLAS Collaboration, *ATLAS sensitivity prospects for Higgs boson production at the LHC running at 7, 8 or 9 TeV*, ATLAS Note ATL-PHYS-PUB-2010-015, 2010.

[102] The CMS Collaboration. https://twiki.cern.ch/twiki/bin/view/CMSPublic/ PhysicsResultsHIGStandardModelProjections, 2010.

[103] G. Piacquadio, *Identification of b-jets and investigation of the discovery potential of a Higgs boson in the $WH \rightarrow l\nu b\bar{b}$ channel with the ATLAS experiment*. PhD thesis, Albert-Ludwigs-Universität Freiburg, CERN-THESIS-2010-027, 2010.

[104] T. Han and S. Willenbrock, *QCD correction to the $pp \rightarrow WH$ and ZH total cross-sections*, Phys. Lett. **B273** (1991) 167–172.

[105] H. Baer, B. Bailey, and J. F. Owens, *$\mathcal{O}(\alpha_s)$ Monte Carlo approach to W+Higgs associated production at hadron supercolliders*, Phys. Rev. **D47** (1993) 2730–2734.

[106] J. Ohnemus and W. J. Stirling, *Order α_s corrections to the differential cross-section for the WH intermediate mass Higgs signal*, Phys. Rev. **D47** (1993) 2722–2729.

[107] R. Hamberg, W. L. van Neerven, and T. Matsuura, *A complete calculation of the order α_s^2 correction to the Drell-Yan K factor*, Nucl. Phys. **B359** (1991) 343–405.

[108] O. Brein, A. Djouadi, and R. Harlander, *NNLO QCD corrections to the Higgs-strahlung processes at hadron colliders*, Phys. Lett. **B579** (2004) 149–156, arXiv:hep-ph/0307206.

[109] M. L. Ciccolini, S. Dittmaier, and M. Krämer, *Electroweak radiative corrections to associated WH and ZH production at hadron colliders*, Phys. Rev. **D68** (2003) 073003, arXiv:hep-ph/0306234.

[110] O. Brein et al., *Precision calculations for associated WH and ZH production at hadron colliders*, arXiv:hep-ph/0402003.

[111] M. Spira, *V2HV*, http://people.web.psi.ch/spira/v2hv, 2007.

[112] J. Campbell and K. Ellis, *MCFM-Monte Carlo for FeMtobarn processes*, http://mcfm.fnal.gov, 2010.

[113] R. Raitio and W. W. Wada, *Higgs boson production at large transverse momentum in QCD*, Phys. Rev. **D19** (1979) 941.

[114] J. N. Ng and P. Zakarauskas, *A QCD parton calculation of conjoined production of Higgs bosons and heavy flavors in $p\bar{p}$ collision*, Phys. Rev. **D29** (1984) 876.

[115] Z. Kunszt, *Associated production of heavy Higgs boson with top quarks*, Nucl. Phys. **B247** (1984) 339.

[116] J. F. Gunion, *Associated $t\bar{t}$ Higgs production as a large source of WH events: Implications for Higgs detection in the lepton neutrino gamma gamma final state*, Phys. Lett. **B261** (1991) 510–517.

[117] W. J. Marciano and F. E. Paige, *Associated production of Higgs bosons with $t\bar{t}$ pairs*, Phys. Rev. Lett. **66** (1991) 2433–2435.

[118] M. Spira, *HQQ*, http://people.web.psi.ch/spira/hqq, 2006.

[119] T. Stelzer and W. F. Long, *Automatic generation of tree level helicity amplitudes*, Nucl. Phys. Proc. Suppl. **37B** (1994) 158–162.

[120] J. Alwall et al., *MadGraph/MadEvent*, http://madgraph.hep.uiuc.edu, 2010.

[121] T. Sjöstrand, S. Ask, R. Corke, S. Mrenna, and P. Skands, *PYTHIA*, `http://home.thep.lu.se/~torbjorn/Pythia.html`, 2010.

[122] W. Beenakker et al., *Higgs radiation off top quarks at the Tevatron and the LHC*, Phys. Rev. Lett. **87** (2001) 201805, `arXiv:hep-ph/0107081`.

[123] W. Beenakker et al., *NLO QCD corrections to t$\bar{\text{t}}$ H production in hadron collisions. ((U))*, Nucl. Phys. **B653** (2003) 151–203, `arXiv:hep-ph/0211352`.

[124] L. Reina and S. Dawson, *Next-to-leading order results for t$\bar{\text{t}}$ h production at the Tevatron*, Phys. Rev. Lett. **87** (2001) 201804, `arXiv:hep-ph/0107101`.

[125] S. Dawson, L. H. Orr, L. Reina, and D. Wackeroth, *Associated top quark Higgs boson production at the LHC*, Phys. Rev. **D67** (2003) 071503, `arXiv:hep-ph/0211438`.

[126] S. Dawson and L. Reina, *QCD corrections to associated Higgs boson production*, Phys. Rev. **D57** (1998) 5851–5859, `arXiv:hep-ph/9712400`.

[127] A. Bredenstein, A. Denner, S. Dittmaier, and S. Pozzorini, *NLO QCD corrections to pp → t$\bar{\text{t}}$ b$\bar{\text{b}}$ + X at the LHC*, Phys. Rev. Lett. **103** (2009) 012002, `arXiv:0905.0110 [hep-ph]`.

[128] A. Bredenstein, A. Denner, S. Dittmaier, and S. Pozzorini, *NLO QCD corrections to t$\bar{\text{t}}$ b$\bar{\text{b}}$ production at the LHC: 1. quark-antiquark annihilation*, JHEP **08** (2008) 108, `arXiv:0807.1248 [hep-ph]`.

[129] A. Bredenstein, A. Denner, S. Dittmaier, and S. Pozzorini, *NLO QCD corrections to t$\bar{\text{t}}$ b$\bar{\text{b}}$ production at the LHC: 2. full hadronic results*, JHEP **03** (2010) 021, `arXiv:1001.4006 [hep-ph]`.

[130] G. Bevilacqua, M. Czakon, C. G. Papadopoulos, R. Pittau, and M. Worek, *Assault on the NLO wishlist: pp → tt bb*, JHEP **09** (2009) 109, `arXiv:0907.4723 [hep-ph]`.

[131] SM and NLO Multileg Working Group Collaboration, J. R. Andersen et al., *The SM and NLO multileg working group: Summary report*, `arXiv:1003.1241 [hep-ph]`.

[132] G. Bevilacqua, M. Czakon, C. G. Papadopoulos, and M. Worek, *Dominant QCD backgrounds in Higgs boson analyses at the LHC: A study of pp → t$\bar{\text{t}}$ + 2 jets at next-to-leading order*, Phys. Rev. Lett. **104** (2010) 162002, `arXiv:1002.4009 [hep-ph]`.

[133] J. Pumplin et al., *New generation of parton distributions with uncertainties from global QCD analysis*, JHEP **07** (2002) 012, `arXiv:hep-ph/0201195`.

[134] R. D. Ball et al., *A first unbiased global NLO determination of parton distributions and their uncertainties*, Nucl. Phys. **B838** (2010) 136–206, `arXiv:1002.4407 [hep-ph]`.

[135] L. J. Hall, R. Rattazzi, and U. Sarid, *The Top quark mass in supersymmetric SO(10) unification*, Phys. Rev. **D50** (1994) 7048–7065, `arXiv:hep-ph/9306309`.

[136] R. Hempfling, *Yukawa coupling unification with supersymmetric threshold corrections*, Phys. Rev. **D49** (1994) 6168–6172.

[137] M. S. Carena, M. Olechowski, S. Pokorski, and C. E. M. Wagner, *Electroweak symmetry breaking and bottom-top Yukawa unification*, Nucl. Phys. **B426** (1994) 269–300, `arXiv:hep-ph/9402253`.

[138] D. M. Pierce, J. A. Bagger, K. T. Matchev, and R.-j. Zhang, *Precision corrections in the minimal supersymmetric standard model*, Nucl. Phys. **B491** (1997) 3–67, `arXiv:hep-ph/9606211`.

[139] M. S. Carena, D. Garcia, U. Nierste, and C. E. M. Wagner, *Effective Lagrangian for the $\bar{t}bH^+$ interaction in the MSSM and charged Higgs phenomenology*, Nucl. Phys. **B577** (2000) 88–120, `arXiv:hep-ph/9912516`.

[140] J. Guasch, P. Häfliger, and M. Spira, *MSSM Higgs decays to bottom quark pairs revisited*, Phys. Rev. **D68** (2003) 115001, `arXiv:hep-ph/0305101`.

[141] D. Noth and M. Spira, *Higgs boson couplings to bottom quarks: two-loop supersymmetry-QCD corrections*, Phys. Rev. Lett. **101** (2008) 181801, `arXiv:0808.0087 [hep-ph]`.

[142] D. Noth and M. Spira, *Supersymmetric Higgs Yukawa couplings to bottom quarks at next-to-next-to-leading order*, arXiv:1001.1935 [hep-ph].

[143] L. Mihaila and C. Reisser, *$O(\alpha_s^2)$ corrections to fermionic Higgs decays in the MSSM*, JHEP **1008** (2010) 021, arXiv:arXiv:1007.0693 [hep-ph].

[144] L. Hofer, U. Nierste, and D. Scherer, *Resummation of tan-beta-enhanced supersymmetric loop corrections beyond the decoupling limit*, JHEP **10** (2009) 081, arXiv:0907.5408 [hep-ph].

[145] LEP Working Group for Higgs boson searches Collaboration, R. Barate et al., *Search for the standard model Higgs boson at LEP*, Phys. Lett. **B565** (2003) 61–75, arXiv:hep-ex/0306033.

[146] ALEPH Collaboration, S. Schael et al., *Search for neutral MSSM Higgs bosons at LEP*, Eur. Phys. J. **C47** (2006) 547–587, arXiv:hep-ex/0602042.

[147] M. S. Carena, S. Heinemeyer, C. E. M. Wagner, and G. Weiglein, *Suggestions for benchmark scenarios for MSSM Higgs boson searches at hadron colliders*, Eur. Phys. J. **C26** (2003) 601–607, arXiv:hep-ph/0202167.

[148] S. Heinemeyer, W. Hollik, and G. Weiglein, *FeynHiggs: a program for the calculation of the masses of the neutral CP-even Higgs bosons in the MSSM*, Comput. Phys. Commun. **124** (2000) 76–89, arXiv:hep-ph/9812320.

[149] S. Heinemeyer, W. Hollik, and G. Weiglein, *The masses of the neutral CP-even Higgs bosons in the MSSM: accurate analysis at the two loop level*, Eur. Phys. J. **C9** (1999) 343–366, arXiv:hep-ph/9812472.

[150] G. Degrassi, S. Heinemeyer, W. Hollik, P. Slavich, and G. Weiglein, *Towards high-precision predictions for the MSSM Higgs sector*, Eur. Phys. J. **C28** (2003) 133–143, arXiv:hep-ph/0212020.

[151] M. Frank et al., *The Higgs boson masses and mixings of the complex MSSM in the Feynman-diagrammatic approach*, JHEP **02** (2007) 047, arXiv:hep-ph/0611326.

[152] J. S. Lee et al., *CPsuperH: a computational tool for Higgs phenomenology in the minimal supersymmetric standard model with explicit CP violation*, Comput. Phys. Commun. **156** (2004) 283–317, arXiv:hep-ph/0307377.

[153] J. S. Lee, M. Carena, J. Ellis, A. Pilaftsis, and C. E. M. Wagner, *CPsuperH2.0: an improved computational tool for Higgs phenomenology in the MSSM with explicit CP violation*, Comput. Phys. Commun. **180** (2009) 312–331, arXiv:0712.2360 [hep-ph].

[154] M. S. Carena et al., *Reconciling the two-loop diagrammatic and effective field theory computations of the mass of the lightest CP-even Higgs boson in the MSSM*, Nucl. Phys. **B580** (2000) 29–57, arXiv:hep-ph/0001002.

[155] A. Djouadi, J. Kalinowski, and M. Spira, *HDECAY: A program for Higgs boson decays in the standard model and its supersymmetric extension*, Comput. Phys. Commun. **108** (1998) 56–74, arXiv:hep-ph/9704448.

[156] A. Djouadi, J. Kalinowski, M. Mühlleitner, and M. Spira, *An update of the program HDECAY*, in *The Les Houches 2009 workshop on TeV colliders: The tools and Monte Carlo working group summary report*. 2010. arXiv:1003.1643 [hep-ph].

[157] S. Dawson, A. Djouadi, and M. Spira, *QCD corrections to SUSY Higgs production: The role of squark loops*, Phys. Rev. Lett. **77** (1996) 16–19, arXiv:hep-ph/9603423 [hep-ph].

[158] R. P. Kauffman and W. Schaffer, *QCD corrections to production of Higgs pseudoscalars*, Phys. Rev. **D49** (1994) 551–554, arXiv:hep-ph/9305279 [hep-ph].

[159] S. Dawson and R. Kauffman, *QCD corrections to Higgs boson production: nonleading terms in the heavy quark limit*, Phys. Rev. **D49** (1994) 2298–2309, arXiv:hep-ph/9310281 [hep-ph].

[160] M. Spira, A. Djouadi, D. Graudenz, and P. Zerwas, *SUSY Higgs production at proton colliders*, Phys. Lett. **B318** (1993) 347–353.

[161] R. Harlander and P. Kant, *Higgs production and decay: analytic results at next-to-leading order QCD*, JHEP **0512** (2005) 015, `arXiv:hep-ph/0509189` [`hep-ph`].

[162] C. Anastasiou, S. Beerli, S. Bucherer, A. Daleo, and Z. Kunszt, *Two-loop amplitudes and master integrals for the production of a Higgs boson via a massive quark and a scalar-quark loop*, JHEP **0701** (2007) 082, `arXiv:hep-ph/0611236` [`hep-ph`].

[163] U. Aglietti, R. Bonciani, G. Degrassi, and A. Vicini, *Analytic results for virtual QCD corrections to Higgs production and decay*, JHEP **01** (2007) 021, `arXiv:hep-ph/0611266`.

[164] R. Bonciani, G. Degrassi, and A. Vicini, *Scalar particle contribution to Higgs production via gluon fusion at NLO*, JHEP **11** (2007) 095, `arXiv:0709.4227` [`hep-ph`].

[165] M. Krämer, E. Laenen, and M. Spira, *Soft gluon radiation in Higgs boson production at the LHC*, Nucl. Phys. **B511** (1998) 523–549, `arXiv:hep-ph/9611272` [`hep-ph`].

[166] A. Djouadi, *The anatomy of electro-weak symmetry breaking. I: the Higgs boson in the standard model*, Phys. Rep. **457** (2008) 1–216, `arXiv:hep-ph/0503172` [`hep-ph`].

[167] A. Djouadi, *The anatomy of electro-weak symmetry breaking. II: the Higgs bosons in the minimal supersymmetric model*, Phys. Rep. **459** (2008) 1–241, `arXiv:hep-ph/0503173`.

[168] R. V. Harlander and W. B. Kilgore, *Production of a pseudoscalar Higgs boson at hadron colliders at next-to-next-to leading order*, JHEP **0210** (2002) 017, `arXiv:hep-ph/0208096` [`hep-ph`].

[169] C. Anastasiou and K. Melnikov, *Pseudoscalar Higgs boson production at hadron colliders in NNLO QCD*, Phys. Rev. **D67** (2003) 037501, `arXiv:hep-ph/0208115` [`hep-ph`].

[170] M. Mühlleitner and M. Spira, *Higgs boson production via gluon fusion: squark loops at NLO QCD*, Nucl. Phys. **B790** (2008) 1–27, `arXiv:hep-ph/0612254` [`hep-ph`].

[171] R. V. Harlander and M. Steinhauser, *Hadronic Higgs production and decay in supersymmetry at next-to-leading order*, Phys. Lett. **B574** (2003) 258–268, `arXiv:hep-ph/0307346` [`hep-ph`].

[172] R. Harlander and M. Steinhauser, *Effects of SUSY QCD in hadronic Higgs production at next-to-next-to-leading order*, Phys. Rev. **D68** (2003) 111701, `arXiv:hep-ph/0308210` [`hep-ph`].

[173] R. V. Harlander and M. Steinhauser, *Supersymmetric Higgs production in gluon fusion at next-to-leading order*, JHEP **0409** (2004) 066, `arXiv:hep-ph/0409010` [`hep-ph`].

[174] R. V. Harlander and F. Hofmann, *Pseudo-scalar Higgs production at next-to-leading order SUSY-QCD*, JHEP **0603** (2006) 050, `arXiv:hep-ph/0507041` [`hep-ph`].

[175] G. Degrassi and P. Slavich, *On the NLO QCD corrections to Higgs production and decay in the MSSM*, Nucl. Phys. **B805** (2008) 267–286, `arXiv:0806.1495` [`hep-ph`].

[176] M. Mühlleitner, H. Rzehak, and M. Spira, *MSSM Higgs boson production via gluon fusion: the large gluino mass limit*, JHEP **0904** (2009) 023, `arXiv:0812.3815` [`hep-ph`].

[177] G. Degrassi and P. Slavich, *NLO QCD bottom corrections to Higgs boson production in the MSSM*, `arXiv:1007.3465` [`hep-ph`].

[178] C. Anastasiou, S. Beerli, and A. Daleo, *The two-loop QCD amplitude gg → h,H in the minimal supersymmetric standard model*, Phys. Rev. Lett. **100** (2008) 241806, `arXiv:0803.3065` [`hep-ph`].

[179] M. Mühlleitner, H. Rzehak, and M. Spira, *SUSY-QCD corrections to MSSM Higgs boson production via gluon fusion*, PoS **RADCOR2009** (2010) 043, `arXiv:1001.3214` [`hep-ph`].

[180] R. Cahn and S. Dawson, *Production of very massive Higgs bosons*, Phys. Lett. **B136** (1984) 196.

[181] K.-I. Hikasa, *Heavy Higgs production in e^+e^- and e^-e^- collisions*, Phys. Lett. **B164** (1985) 385.

[182] G. Altarelli, B. Mele, and F. Pitolli, *Heavy Higgs production at future colliders*, Nucl. Phys. **B287** (1987) 205–224.

[183] A. Djouadi and M. Spira, *SUSY-QCD corrections to Higgs boson production at hadron colliders*, Phys. Rev. **D62** (2000) 014004, `arXiv:hep-ph/9912476` [`hep-ph`].

[184] W. Hollik, T. Plehn, M. Rauch, and H. Rzehak, *Supersymmetric Higgs bosons in weak boson fusion*, Phys. Rev. Lett. **102** (2009) 091802, `arXiv:0804.2676 [hep-ph]`.

[185] S. Glashow, D. V. Nanopoulos, and A. Yildiz, *Associated production of Higgs bosons and Z particles*, Phys. Rev. **D18** (1978) 1724–1727.

[186] Z. Kunszt, Z. Trocsanyi, and W. Stirling, *Clear signal of intermediate mass Higgs boson production at LHC and SSC*, Phys. Lett. **B271** (1991) 247–255.

[187] W. Peng, M. Wen-Gan, H. Hong-Sheng, Z. Ren-You, H. Liang, et al., *NLO supersymmetric QCD corrections to $t\bar{t}h^0$ associated production at hadron colliders*, Phys. Lett. **B618** (2005) 209–220, `arXiv:hep-ph/0505086 [hep-ph]`.

[188] W. Hollik and M. Rauch, *Higgs-Boson production in association with heavy quarks*, AIP Conf. Proc. **903** (2007) 117–120, `arXiv:hep-ph/0610340 [hep-ph]`.

[189] P. Häfliger, *Associated MSSM Higgs production with heavy quarks: SUSY-QCD corrections and impact of A0 on the mSUGRA parameter space*. PhD thesis, ETH (Zürich) DISS-ETH-16970, 2006.

[190] M. Walser, *NLO QCD and SUSY-QCD corrections to associated MSSM Higgs production with heavy quarks at hadron colliders*. PhD thesis, ETH (Zürich) DISS-ETH-17592, 2008.

[191] S. Dittmaier, M. Krämer, and M. Spira, *Higgs radiation off bottom quarks at the Tevatron and the LHC*, Phys. Rev. **D70** (2004) 074010, `arXiv:hep-ph/0309204`.

[192] S. Dawson, C. Jackson, L. Reina, and D. Wackeroth, *Exclusive Higgs boson production with bottom quarks at hadron colliders*, Phys. Rev. **D69** (2004) 074027, `arXiv:hep-ph/0311067 [hep-ph]`.

[193] D. A. Dicus and S. Willenbrock, *Higgs boson production from heavy quark fusion*, Phys. Rev. **D39** (1989) 751.

[194] D. Dicus, T. Stelzer, Z. Sullivan, and S. Willenbrock, *Higgs boson production in association with bottom quarks at next-to-leading order*, Phys. Rev. **D59** (1999) 094016, `arXiv:hep-ph/9811492 [hep-ph]`.

[195] C. Balazs, H.-J. He, and C. Yuan, *QCD corrections to scalar production via heavy quark fusion at hadron colliders*, Phys. Rev. **D60** (1999) 114001, `arXiv:hep-ph/9812263 [hep-ph]`.

[196] R. V. Harlander and W. B. Kilgore, *Higgs boson production in bottom quark fusion at next-to-next-to leading order*, Phys. Rev. **D68** (2003) 013001, `arXiv:hep-ph/0304035 [hep-ph]`.

[197] J. M. Campbell et al., *Higgs boson production in association with bottom quarks*, `arXiv:hep-ph/0405302`.

[198] S. Dawson, C. B. Jackson, L. Reina, and D. Wackeroth, *Higgs production in association with bottom quarks at hadron colliders*, Mod. Phys. Lett. **A21** (2006) 89–110, `arXiv:hep-ph/0508293`.

[199] J. M. Campbell, R. Ellis, F. Maltoni, and S. Willenbrock, *Higgs-Boson production in association with a single bottom quark*, Phys. Rev. **D67** (2003) 095002, `arXiv:hep-ph/0204093 [hep-ph]`.

[200] S. Dawson, C. Jackson, L. Reina, and D. Wackeroth, *Higgs boson production with one bottom quark jet at hadron colliders*, Phys. Rev. Lett. **94** (2005) 031802, `arXiv:hep-ph/0408077 [hep-ph]`.

[201] M. Beccaria, G. Dovier, G. Macorini, E. Mirabella, L. Panizzi, et al., *Semi-inclusive bottom-Higgs production at LHC: The complete one-loop electroweak effect in the MSSM*, Phys. Rev. **D82** (2010) 093018, `arXiv:1005.0759 [hep-ph]`.

[202] S. Dawson and C. Jackson, *SUSY QCD corrections to associated Higgs-bottom quark production*, Phys. Rev. **D77** (2008) 015019, `arXiv:0709.4519 [hep-ph]`.

[203] M. Spira, *HIGLU: A program for the calculation of the total Higgs production cross-section at hadron colliders via gluon fusion including QCD corrections*, `arXiv:hep-ph/9510347 [hep-ph]`.

[204] S. Dittmaier, M. Krämer, A. Muck, and T. Schluter, *MSSM Higgs-boson production in bottom-quark fusion: electroweak radiative corrections*, JHEP **03** (2007) 114, `arXiv:hep-ph/0611353`.

[205] A. D. Martin, W. J. Stirling, R. S. Thorne, and G. Watt, *Heavy-quark mass dependence in global PDF analyses and 3- and 4-flavour parton distributions*, `arXiv:1007.2624 [hep-ph]`.

[206] ALEPH Collaboration, A. Heister et al., *Search for charged Higgs bosons in e^+e^- collisions at energies up to $\sqrt{s}$ = 209-GeV*, Phys. Lett. **B543** (2002) 1–13, `arXiv:hep-ex/0207054`.

[207] J. F. Gunion and A. Turski, *Renormalization of Higgs boson mass sum rules and screening*, Phys. Rev. **D39** (1989) 2701.

[208] A. Brignole, *Radiative corrections to the supersymmetric charged Higgs boson mass*, Phys. Lett. **B277** (1992) 313–323.

[209] M. A. Diaz and H. E. Haber, *One loop radiative corrections to the charged Higgs mass of the minimal supersymmetric model*, Phys. Rev. **D45** (1992) 4246–4260.

[210] CDF Collaboration, T. Aaltonen et al., *Search for charged Higgs bosons in decays of top quarks in $p - \bar{p}$ collisions at $\sqrt{s} = 1.96$ TeV*, Phys. Rev. Lett. **103** (2009) 101803, `arXiv:0907.1269 [hep-ex]`.

[211] D0 Collaboration, V. M. Abazov et al., *Search for charged Higgs bosons in top quark decays*, Phys. Lett. **B682** (2009) 278–286, `arXiv:0908.1811 [hep-ex]`.

[212] S. Dittmaier, G. Hiller, T. Plehn, and M. Spannowsky, *Charged-Higgs collider signals with or without flavor*, Phys. Rev. **D77** (2008) 115001, `arXiv:0708.0940 [hep-ph]`.

[213] D. Eriksson, S. Hesselbach, and J. Rathsman, *Associated charged Higgs and W boson production in the MSSM at the CERN large hadron collider*, Eur. Phys. J. **C53** (2008) 267–280, `arXiv:hep-ph/0612198`.

[214] A. Alves and T. Plehn, *Charged Higgs boson pairs at the LHC*, Phys. Rev. **D71** (2005) 115014, `arXiv:hep-ph/0503135`.

[215] O. Brein and W. Hollik, *Pair production of charged MSSM Higgs bosons by gluon fusion*, Eur. Phys. J. **C13** (2000) 175–184, `arXiv:hep-ph/9908529`.

[216] M. S. Carena, S. Heinemeyer, C. E. M. Wagner, and G. Weiglein, *MSSM Higgs boson searches at the Tevatron and the LHC: impact of different benchmark scenarios*, Eur. Phys. J. **C45** (2006) 797–814, `arXiv:hep-ph/0511023`.

[217] J. M. Campbell, R. K. Ellis, and F. Tramontano, *Single top production and decay at next-to-leading order*, Phys. Rev. **D70** (2004) 094012, `arXiv:hep-ph/0408158`.

[218] K. G. Chetyrkin, R. Harlander, T. Seidensticker, and M. Steinhauser, *Second order QCD corrections to the top decay rate*, `arXiv:hep-ph/9910339`.

[219] M. S. Carena, J. R. Ellis, S. Mrenna, A. Pilaftsis, and C. E. M. Wagner, *Collider probes of the MSSM Higgs sector with explicit CP violation*, Nucl. Phys. **B659** (2003) 145–178, `arXiv:hep-ph/0211467`.

[220] J. Ellis, R. N. Hodgkinson, J. S. Lee, and A. Pilaftsis, *Flavour geometry and effective Yukawa couplings in the MSSM*, JHEP **02** (2010) 016, `arXiv:0911.3611 [hep-ph]`.

[221] R. M. Barnett, H. E. Haber, and D. E. Soper, *Ultraheavy particle production from heavy partons at hadron colliders*, Nucl. Phys. **B306** (1988) 697.

[222] C. Buttar et al., *Les Houches physics at TeV colliders 2005, standard model and Higgs working group: Summary report*, `arXiv:hep-ph/0604120`.

[223] S.-h. Zhu, *Complete next-to-leading order QCD corrections to charged Higgs boson associated*

production with top quark at the CERN large hadron collider, Phys. Rev. **D67** (2003) 075006, `arXiv:hep-ph/0112109`.

[224] G.-p. Gao, G.-r. Lu, Z.-h. Xiong, and J. M. Yang, *Loop effects and non-decoupling property of SUSY QCD in $gb \to tH^-$*, Phys. Rev. **D66** (2002) 015007, `arXiv:hep-ph/0202016`.

[225] T. Plehn, *Charged Higgs boson production in bottom gluon fusion*, Phys. Rev. **D67** (2003) 014018, `arXiv:hep-ph/0206121`.

[226] E. L. Berger, T. Han, J. Jiang, and T. Plehn, *Associated production of a top quark and a charged Higgs boson*, Phys. Rev. **D71** (2005) 115012, `arXiv:hep-ph/0312286`.

[227] N. Kidonakis, *Charged Higgs production: higher-order corrections*, PoS **HEP2005** (2006) 336, `arXiv:hep-ph/0511235`.

[228] W. Peng et al., *NLO supersymmetric QCD corrections to the $t\bar{b}H^-$ associated production at hadron colliders*, Phys. Rev. **D73** (2006) 015012, `arXiv:hep-ph/0601069`.

[229] M. Beccaria, G. Macorini, L. Panizzi, F. M. Renard, and C. Verzegnassi, *Associated production of charged Higgs and top at LHC: the role of the complete electroweak supersymmetric contribution*, Phys. Rev. **D80** (2009) 053011, `arXiv:0908.1332 [hep-ph]`.

[230] N. Kidonakis, *Two-loop soft anomalous dimensions for single top quark associated production with a W^- or H^-*, Phys. Rev. **D82** (2010) 054018, `arXiv:1005.4451 [hep-ph]`.

[231] C. Weydert et al., *Charged Higgs boson production in association with a top quark in MC@NLO*, Eur. Phys. J. **C67** (2010) 617–636, `arXiv:0912.3430 [hep-ph]`.

[232] J. L. Diaz-Cruz and O. A. Sampayo, *Contribution of gluon fusion to the production of charged Higgs at hadron colliders*, Phys. Rev. **D50** (1994) 6820–6823.

[233] F. Borzumati, J.-L. Kneur, and N. Polonsky, *Higgs-strahlung and R-parity violating slepton-strahlung at hadron colliders*, Phys. Rev. **D60** (1999) 115011, `arXiv:hep-ph/9905443`.

[234] D. J. Miller, 2, S. Moretti, D. P. Roy, and W. J. Stirling, *Detecting heavy charged Higgs bosons at the CERN LHC with four b quark tags*, Phys. Rev. **D61** (2000) 055011, `arXiv:hep-ph/9906230`.

[235] S. Dittmaier, M. Krämer, M. Spira, and M. Walser, *Charged-Higgs-boson production at the LHC: NLO supersymmetric QCD corrections*, `arXiv:0906.2648 [hep-ph]`.

[236] S. Frixione, F. Stoeckli, P. Torrielli, B. R. Webber, and C. D. White, *The MC@NLO 4.0 event generator*, `arXiv:1010.0819 [hep-ph]`.

[237] J. M. Campbell, R. Frederix, F. Maltoni, and F. Tramontano, *Next-to-leading-order predictions for t-channel single-top production at hadron colliders*, Phys. Rev. Lett. **102** (2009) 182003, `arXiv:0903.0005 [hep-ph]`.

[238] A. D. Martin, R. G. Roberts, W. J. Stirling, and R. S. Thorne, *Physical gluons and high E(T) jets*, Phys. Lett. **B604** (2004) 61–68, `arXiv:hep-ph/0410230`.

[239] P. M. Nadolsky et al., *Implications of CTEQ global analysis for collider observables*, Phys. Rev. **D78** (2008) 013004, `arXiv:0802.0007 [hep-ph]`.

[240] M. Glück, P. Jimenez-Delgado, and E. Reya, *Dynamical parton distributions of the nucleon and very small-x physics*, Eur. Phys. J. **C53** (2008) 355–366, `arXiv:0709.0614 [hep-ph]`.

[241] M. Glück, P. Jimenez-Delgado, E. Reya, and C. Schuck, *On the role of heavy flavor parton distributions at high energy colliders*, Phys. Lett. **B664** (2008) 133–138, `arXiv:0801.3618 [hep-ph]`.

[242] H1 and ZEUS Collaboration, F. D. Aaron et al., *Combined measurement and QCD analysis of the inclusive ep scattering cross sections at HERA*, JHEP **01** (2010) 109, `arXiv:0911.0884 [hep-ex]`.

[243] P. Jimenez-Delgado and E. Reya, *Dynamical NNLO parton distributions*, Phys. Rev. **D79** (2009) 074023, `arXiv:0810.4274 [hep-ph]`.

[244] S. Moch, J. A. M. Vermaseren, and A. Vogt, *The three-loop splitting functions in QCD: the non-singlet case*, Nucl. Phys. **B688** (2004) 101–134, `arXiv:hep-ph/0403192`.

[245] A. Vogt, S. Moch, and J. A. M. Vermaseren, *The three-loop splitting functions in QCD: the singlet case*, Nucl. Phys. **B691** (2004) 129–181, `arXiv:hep-ph/0404111`.

[246] H.-L. Lai et al., *New parton distributions for collider physics*, `arXiv:1007.2241 [hep-ph]`.

[247] S. Alekhin, J. Blümlein, and S.-O. Moch, *Update of the NNLO PDFs in the 3-, 4-, and 5-flavour scheme*, `arXiv:1007.3657 [hep-ph]`.

[248] J. Rojo et al., *The impact of heavy quark mass effects in the NNPDF global analysis*, `arXiv:1007.0354 [hep-ph]`.

[249] R. S. Thorne, A. D. Martin, W. J. Stirling, and G. Watt, *The effects of combined HERA and recent Tevatron W → lepton neutrino charge asymmetry data on the MSTW PDFs*, `arXiv:1006.2753 [hep-ph]`.

[250] D. Stump et al., *Uncertainties of predictions from parton distribution functions. 1. The Lagrange multiplier method*, Phys. Rev. **D65** (2001) 014012, `arXiv:hep-ph/0101051`.

[251] J. Pumplin et al., *Uncertainties of predictions from parton distribution functions. 2. The Hessian method*, Phys. Rev. **D65** (2001) 014013, `arXiv:hep-ph/0101032`.

[252] NNPDF Collaboration, R. D. Ball et al., *A determination of parton distributions with faithful uncertainty estimation*, Nucl. Phys. **B809** (2009) 1–63, `arXiv:0808.1231 [hep-ph]`.

[253] A. Guffanti and J. Rojo, *Top production at the LHC: the impact of PDF uncertainties and correlations*, `arXiv:1008.4671 [hep-ph]`.

[254] A. D. Martin, R. G. Roberts, W. J. Stirling, and R. S. Thorne, *Parton distributions incorporating QED contributions*, Eur. Phys. J. **C39** (2005) 155–161, `arXiv:hep-ph/0411040`.

[255] F. Demartin, S. Forte, E. Mariani, J. Rojo, and A. Vicini, *The impact of PDF and α_s uncertainties on Higgs production in gluon fusion at hadron colliders*, Phys. Rev. **D82** (2010) 014002, `arXiv:1004.0962 [hep-ph]`.

[256] H.-L. Lai et al., *Uncertainty induced by QCD coupling in the CTEQ global analysis of parton distributions*, `arXiv:1004.4624 [hep-ph]`.

[257] G. Watt, *presented at the PDF4LHC meeting of March 26, (CERN). Plots from*, `http://projects.hepforge.org/mstwpdf/pdf4lhc/`, 2010.

[258] *International workshop "QCD at the LHC 2010", organized by J. Blümlein, H. Fritzsch, and M. Mangano, ECT* Trento, Italy, Sept. 26-Oct. 1 2010*, `http://indico.cern.ch/conferenceDisplay.py?confId=93790`.

[259] *PDF4LHC meeting, DESY, Hamburg, Germany, Nov. 29 2010*, `http://indico.cern.ch/conferenceDisplay.py?confId=103872`.

[260] *PDF4LHC working group*, `https://wiki.terascale.de/index.php?title=PDF4LHC\_WIKI`, 2010.

[261] S. Alekhin, J. Blümlein, P. Jimenez-Delgado, S. Moch, and E. Reya, *NNLO benchmarks for gauge and Higgs boson production at TeV hadron colliders*, `arXiv:1011.6259 [hep-ph]`.

[262] M. Ubiali et al., *Combined PDF and strong coupling uncertainties at the LHC with NNPDF2.0*, `arXiv:1005.0397 [hep-ph]`.

[263] U. Aglietti, R. Bonciani, G. Degrassi, and A. Vicini, *Master integrals for the two-loop light fermion contributions to gg → H and H → γγ*, Phys. Lett. **B600** (2004) 57–64, `arXiv:hep-ph/0407162`.

[264] G. Degrassi and F. Maltoni, *Two-loop electroweak corrections to the Higgs-boson decay H→ γγ*, Nucl. Phys. **B724** (2005) 183–196, `arXiv:hep-ph/0504137`.

[265] A. Bredenstein, A. Denner, S. Dittmaier, and M. M. Weber, *Precise predictions for the Higgs-boson decay H → WW/ZZ → 4 leptons*, Phys. Rev. **D74** (2006) 013004,

`arXiv:hep-ph/0604011`.

[266] A. Bredenstein, A. Denner, S. Dittmaier, and M. Weber, *Radiative corrections to the semileptonic and hadronic Higgs-boson decays H →W W / Z Z→ 4 fermions*, JHEP **0702** (2007) 080, `arXiv:hep-ph/0611234 [hep-ph]`.

[267] A. Bredenstein, A. Denner, S. Dittmaier, A. Mück, and M. M. Weber, *Prophecy4f: A Monte Carlo generator for a proper description of the Higgs decay into 4 fermions*, `http://omnibus.uni-freiburg.de/~sd565/programs/prophecy4f/prophecy4f.html`, 2010.

[268] U. Aglietti et al., *Tevatron for LHC report: Higgs*, `arXiv:hep-ph/0612172`.

[269] J. Fleischer and F. Jegerlehner, *Radiative corrections to Higgs decays in the extended Weinberg-Salam model*, Phys. Rev. **D23** (1981) 2001–2026.

[270] D. Bardin, B. Vilensky, and P. Khristova, *Calculation of the Higgs boson decay width into fermion pairs*, Sov. J. Nucl. Phys. **53** (1991) 152–158.

[271] A. Dabelstein and W. Hollik, *Electroweak corrections to the fermionic decay width of the standard Higgs boson*, Z. Phys. **C53** (1992) 507–516.

[272] B. A. Kniehl, *Radiative corrections for H→ f f̄ (γ) in the standard model*, Nucl. Phys. **B376** (1992) 3–28.

[273] ECFA/DESY LC physics working group Collaboration, E. Accomando et al., *Physics with e^+e^- linear colliders*, Phys. Rep. **299** (1998) 1–78, `arXiv:hep-ph/9705442 [hep-ph]`.

[274] E. Braaten and J. P. Leveille, *Higgs boson decay and the running mass*, Phys. Rev. **D22** (1980) 715.

[275] N. Sakai, *Perturbative QCD corrections to the hadronic decay width of the Higgs boson*, Phys. Rev. **D22** (1980) 2220.

[276] T. Inami and T. Kubota, *Renormalization group estimate of the hadronic decay width of the Higgs boson*, Nucl. Phys. **B179** (1981) 171.

[277] S. Gorishnii, A. Kataev, and S. Larin, *The width of Higgs boson decay into hadrons: three loop corrections of strong interactions*, Sov. J. Nucl. Phys. **40** (1984) 329–334.

[278] M. Drees and K.-i. Hikasa, *Heavy quark thresholds in Higgs physics*, Phys. Rev. **D41** (1990) 1547.

[279] M. Drees and K.-i. Hikasa, *Note on QCD corrections to hadronic Higgs decay*, Phys. Lett. **B240** (1990) 455.

[280] M. Drees and K.-i. Hikasa, *Erratum: Note on QCD corrections to hadronic Higgs decay*, Phys. Lett. **B262** (1991) 497.

[281] S. Gorishnii, A. Kataev, S. Larin, and L. Surguladze, *Corrected three loop QCD correction to the correlator of the quark scalar current and $\Gamma_{tot}(H \to hadrons)$*, Mod. Phys. Lett. **A5** (1990) 2703–2712.

[282] S. Gorishnii, A. Kataev, S. Larin, and L. Surguladze, *Scheme dependence of the next to next-to-leading QCD corrections to $\Gamma_{tot}(H \to hadrons)$ and the spurious QCD infrared fixed point*, Phys. Rev. **D43** (1991) 1633–1640.

[283] A. L. Kataev and V. T. Kim, *The effects of the QCD corrections to $\Gamma(H \to b\bar{b})$*, Mod. Phys. Lett. **A9** (1994) 1309–1326. Revised version of ENSLAPP-A-407-92.

[284] L. R. Surguladze, *Quark mass effects in fermionic decays of the Higgs boson in $O(\alpha_s^2)$ perturbative QCD*, Phys. Lett. **B341** (1994) 60–72, `arXiv:hep-ph/9405325 [hep-ph]`.

[285] S. Larin, T. van Ritbergen, and J. Vermaseren, *The large top quark mass expansion for Higgs boson decays into bottom quarks and into gluons*, Phys. Lett. **B362** (1995) 134–140, `arXiv:hep-ph/9506465 [hep-ph]`.

[286] K. Chetyrkin and A. Kwiatkowski, *Second order QCD corrections to scalar and pseudoscalar*

Higgs decays into massive bottom quarks, Nucl. Phys. **B461** (1996) 3–18, `arXiv:hep-ph/9505358 [hep-ph]`.

[287] K. Chetyrkin, *Correlator of the quark scalar currents and* $\Gamma_{tot}(H \to hadrons)$ *at* $O\,(\alpha_s^3)$ *in pQCD*, Phys. Lett. **B390** (1997) 309–317, `arXiv:hep-ph/9608318 [hep-ph]`.

[288] A. Ghinculov, *Two loop heavy Higgs corrections to the Higgs fermionic width*, Phys. Lett. **B337** (1994) 137–140, `arXiv:hep-ph/9405394 [hep-ph]`.

[289] A. Ghinculov, *Erratum: Two loop heavy Higgs corrections to the Higgs fermionic width*, Phys. Lett. **B346** (1995) 426, `arXiv:hep-ph/9405394 [hep-ph]`.

[290] L. Durand, K. Riesselmann, and B. A. Kniehl, *Onset of strong interactions in the Higgs sector of the standard model:* $H \to f\bar{f}$ *at two loops*, Phys. Rev. Lett. **72** (1994) 2534–2537.

[291] L. Durand, K. Riesselmann, and B. A. Kniehl, *Erratum:Onset of strong interactions in the Higgs sector of the standard model:* $H \to f\bar{f}$ *at two loops*, Phys. Rev. Lett. **74** (1995) 1699.

[292] L. Durand, B. A. Kniehl, and K. Riesselmann, *Two loop* $O\,(G_F^2 M_H^4)$ *corrections to the fermionic decay rates of the Higgs boson*, Phys. Rev. **D51** (1995) 5007–5015, `arXiv:hep-ph/9412311 [hep-ph]`.

[293] V. Borodulin and G. Jikia, *Analytic evaluation of two loop renormalization constants of enhanced electroweak strength in the Higgs sector of the standard model*, Phys. Lett. **B391** (1997) 434–440, `arXiv:hep-ph/9609447 [hep-ph]`.

[294] T. Inami, T. Kubota, and Y. Okada, *Effective gauge theory and the effect of heavy quarks in Higgs boson decay*, Z. Phys. **C18** (1983) 69.

[295] K. Chetyrkin, B. A. Kniehl, and M. Steinhauser, *Hadronic Higgs decay to order* α_s^4, Phys. Rev. Lett. **79** (1997) 353–356, `arXiv:hep-ph/9705240 [hep-ph]`.

[296] P. Baikov and K. Chetyrkin, *Higgs decay into hadrons to order* α_s^5, Phys. Rev. Lett. **97** (2006) 061803, `arXiv:hep-ph/0604194 [hep-ph]`.

[297] H.-Q. Zheng and D.-D. Wu, *First order QCD corrections to the decay of the Higgs boson into two photons*, Phys. Rev. **D42** (1990) 3760–3763.

[298] A. Djouadi, M. Spira, J. van der Bij, and P. Zerwas, *QCD corrections to* $\gamma\gamma$ *decays of Higgs particles in the intermediate mass range*, Phys. Lett. **B257** (1991) 187–190.

[299] S. Dawson and R. Kauffman, *QCD corrections to* $H \to \gamma\gamma$, Phys. Rev. **D47** (1993) 1264–1267.

[300] A. Djouadi, M. Spira, and P. Zerwas, *Two photon decay widths of Higgs particles*, Phys. Lett. **B311** (1993) 255–260, `arXiv:hep-ph/9305335 [hep-ph]`.

[301] K. Melnikov and O. I. Yakovlev, *Higgs* → *two photon decay: QCD radiative correction*, Phys. Lett. **B312** (1993) 179–183, `arXiv:hep-ph/9302281 [hep-ph]`.

[302] M. Inoue, R. Najima, T. Oka, and J. Saito, *QCD corrections to two photon decay of the Higgs boson and its reverse process*, Mod. Phys. Lett. **A9** (1994) 1189–1194.

[303] A. Firan and R. Stroynowski, *Internal conversions in Higgs decays to two photons*, Phys. Rev. **D76** (2007) 057301, `arXiv:0704.3987 [hep-ph]`.

[304] S. Frixione and B. R. Webber, *Matching NLO QCD computations and parton shower simulations*, JHEP **06** (2002) 029, `arXiv:hep-ph/0204244`.

[305] S. Frixione, P. Nason, and B. R. Webber, *Matching NLO QCD and parton showers in heavy flavour production*, JHEP **08** (2003) 007, `arXiv:hep-ph/0305252`.

[306] S. Frixione, E. Laenen, P. Motylinski, and B. R. Webber, *Single-top production in MC@NLO*, JHEP **03** (2006) 092, `arXiv:hep-ph/0512250`.

[307] S. Frixione and B. R. Webber, *The MC@NLO 3.3 event generator*, `arXiv:hep-ph/0612272`.

[308] S. Frixione, E. Laenen, P. Motylinski, and B. R. Webber, *Angular correlations of lepton pairs from vector boson and top quark decays in Monte Carlo simulations*, JHEP **04** (2007) 081, `arXiv:hep-ph/0702198`.

[309] S. Frixione, E. Laenen, P. Motylinski, B. R. Webber, and C. D. White, *Single-top hadroproduction in association with a W boson*, JHEP **07** (2008) 029, `arXiv:0805.3067 [hep-ph]`.

[310] O. Latunde-Dada, *Herwig Monte Carlo at next-to-leading order for e^+e^- annihilation and lepton pair production*, JHEP **11** (2007) 040, `arXiv:0708.4390 [hep-ph]`.

[311] P. Nason, *A new method for combining NLO QCD with shower Monte Carlo algorithms*, JHEP **11** (2004) 040, `arXiv:hep-ph/0409146`.

[312] P. Nason and G. Ridolfi, *A positive-weight next-to-leading-order Monte Carlo for Z pair hadroproduction*, JHEP **08** (2006) 077, `arXiv:hep-ph/0606275`.

[313] S. Frixione, P. Nason, and G. Ridolfi, *The POWHEG-hvq manual version 1.0*, `arXiv:0707.3081 [hep-ph]`.

[314] S. Frixione, P. Nason, and C. Oleari, *Matching NLO QCD computations with parton shower simulations: the POWHEG method*, JHEP **11** (2007) 070, `arXiv:0709.2092 [hep-ph]`.

[315] S. Frixione, P. Nason, and G. Ridolfi, *A positive-weight next-to-leading-order Monte Carlo for heavy flavour hadroproduction*, JHEP **09** (2007) 126, `arXiv:0707.3088 [hep-ph]`.

[316] O. Latunde-Dada, S. Gieseke, and B. Webber, *A positive-weight next-to-leading-order Monte Carlo for e^+e^- annihilation to hadrons*, JHEP **02** (2007) 051, `arXiv:hep-ph/0612281`.

[317] K. Hamilton, P. Richardson, and J. Tully, *A positive-weight next-to-leading order Monte Carlo simulation of Drell-Yan vector boson production*, JHEP **10** (2008) 015, `arXiv:0806.0290 [hep-ph]`.

[318] K. Hamilton, P. Richardson, and J. Tully, *A positive-weight next-to-leading order Monte Carlo simulation for Higgs boson production*, JHEP **04** (2009) 116, `arXiv:0903.4345 [hep-ph]`.

[319] S. Alioli, P. Nason, C. Oleari, and E. Re, *NLO vector-boson production matched with shower in POWHEG*, JHEP **07** (2008) 060, `arXiv:0805.4802 [hep-ph]`.

[320] S. Alioli, P. Nason, C. Oleari, and E. Re, *NLO Higgs boson production via gluon fusion matched with shower in POWHEG*, JHEP **04** (2009) 002, `arXiv:0812.0578 [hep-ph]`.

[321] S. Alioli, P. Nason, C. Oleari, and E. Re, *NLO single-top production matched with shower in POWHEG: s- and t-channel contributions*, JHEP **09** (2009) 111, `arXiv:0907.4076 [hep-ph]`.

[322] O. Latunde-Dada, *Applying the POWHEG method to top pair production and decays at the ILC*, Eur. Phys. J. **C58** (2008) 543–554, `arXiv:0806.4560 [hep-ph]`.

[323] M. L. Mangano, M. Moretti, and R. Pittau, *Multijet matrix elements and shower evolution in hadronic collisions: $Wb\bar{b} + n$ jets as a case study*, Nucl. Phys. **B632** (2002) 343–362, `arXiv:hep-ph/0108069`.

[324] S. Catani, F. Krauss, R. Kuhn, and B. R. Webber, *QCD matrix elements + parton showers*, JHEP **11** (2001) 063, `arXiv:hep-ph/0109231`.

[325] L. Lonnblad, *Correcting the colour-dipole cascade model with fixed order matrix elements*, JHEP **05** (2002) 046, `arXiv:hep-ph/0112284`.

[326] F. Krauss, *Matrix elements and parton showers in hadronic interactions*, JHEP **08** (2002) 015, `arXiv:hep-ph/0205283`.

[327] S. Mrenna and P. Richardson, *Matching matrix elements and parton showers with HERWIG and PYTHIA*, JHEP **05** (2004) 040, `arXiv:hep-ph/0312274`.

[328] A. Schälicke and F. Krauss, *Implementing the ME+PS merging algorithm*, JHEP **07** (2005) 018, `arXiv:hep-ph/0503281`.

[329] J. Alwall et al., *Comparative study of various algorithms for the merging of parton showers and matrix elements in hadronic collisions*, Eur. Phys. J. **C53** (2008) 473–500, `arXiv:0706.2569 [hep-ph]`.

[330] S. Höche, F. Krauss, S. Schumann, and F. Siegert, *QCD matrix elements and truncated showers*,

JHEP **05** (2009) 053, `arXiv:0903.1219 [hep-ph]`.

[331] K. Hamilton, P. Richardson, and J. Tully, *A modified CKKW matrix element merging approach to angular-ordered parton showers*, JHEP **11** (2009) 038, `arXiv:0905.3072 [hep-ph]`.

[332] T. Sjöstrand, S. Mrenna, and P. Z. Skands, *PYTHIA 6.4 physics and manual*, JHEP **05** (2006) 026, `arXiv:hep-ph/0603175`.

[333] T. Sjöstrand, S. Mrenna, and P. Z. Skands, *A brief Introduction to PYTHIA 8.1*, Comput. Phys. Commun. **178** (2008) 852–867, `arXiv:0710.3820 [hep-ph]`.

[334] G. Corcella et al., *HERWIG 6: an event generator for hadron emission reactions with interfering gluons (including supersymmetric processes)*, JHEP **01** (2001) 010, `arXiv:hep-ph/0011363`.

[335] M. Bahr et al., *Herwig++ physics and manual*, Eur. Phys. J. **C58** (2008) 639–707, `arXiv:0803.0883 [hep-ph]`.

[336] T. Gleisberg et al., *SHERPA 1.alpha, a proof-of-concept version*, JHEP **02** (2004) 056, `arXiv:hep-ph/0311263`.

[337] M. Bengtsson and T. Sjöstrand, *Coherent parton showers versus matrix elements: implications of PETRA-PEP data*, Phys. Lett. **B185** (1987) 435.

[338] G. Gustafson and U. Pettersson, *Dipole formulation of QCD cascades*, Nucl. Phys. **B306** (1988) 746.

[339] M. H. Seymour, *A simple prescription for first-order corrections to quark scattering and annihilation processes*, Nucl. Phys. **B436** (1995) 443–460, `arXiv:hep-ph/9410244`.

[340] M. H. Seymour, *Matrix-element corrections to parton shower algorithms*, Comput. Phys. Commun. **90** (1995) 95–101, `hep-ph/9410414`.

[341] G. Miu and T. Sjöstrand, *W production in an improved parton-shower approach*, Phys. Lett. **B449** (1999) 313–320, `arXiv:hep-ph/9812455`.

[342] L. Lönnblad, *Small x effects in W + jets production at the Tevatron*, Nucl. Phys. **B458** (1996) 215–230, `hep-ph/9508261`.

[343] P. Torrielli and S. Frixione, *Matching NLO QCD computations with PYTHIA using MC@NLO*, JHEP **1004** (2010) 110, `arXiv:1002.4293 [hep-ph]`.

[344] S. Alioli, P. Nason, C. Oleari, and E. Re, *A general framework for implementing NLO calculations in shower Monte Carlo programs: the POWHEG BOX*, JHEP **1006** (2010) 043, `arXiv:1002.2581 [hep-ph]`.

[345] S. Höche, F. Krauss, M. Schönherr, and F. Siegert, *Automating the POWHEG method in Sherpa*, `arXiv:1008.5399 [hep-ph]`.

[346] J. Alwall, S. de Visscher, and F. Maltoni, *QCD radiation in the production of heavy colored particles at the LHC*, JHEP **02** (2009) 017, `arXiv:0810.5350 [hep-ph]`.

[347] K. Hamilton and P. Nason, *Improving NLO-parton shower matched simulations with higher order matrix elements*, JHEP **1006** (2010) 039, `arXiv:1004.1764 [hep-ph]`.

[348] S. Höche, F. Krauss, M. Schönherr, and F. Siegert, *NLO matrix elements and truncated showers*, `arXiv:1009.1127 [hep-ph]`.

[349] S. Catani and M. Grazzini, *An NNLO subtraction formalism in hadron collisions and its application to Higgs boson production at the LHC*, Phys. Rev. Lett. **98** (2007) 222002, `hep-ph/0703012`.

[350] J. M. Butterworth et al., *The Les Houches 2009 workshop on TeV colliders: The tools and Monte Carlo working group summary report*,, `arXiv:1003.1643 [hep-ph]`.

[351] G. Bozzi, S. Catani, D. de Florian, and M. Grazzini, *Transverse-momentum resummation and the spectrum of the Higgs boson at the LHC*, Nucl. Phys. **B737** (2006) 73–120, `arXiv:hep-ph/0508068 [hep-ph]`.

[352] F. Stöckli, A. G. Holzner, and G. Dissertori, *Study of perturbative QCD predictions at*

next-to-leading order and beyond for $pp \to H \to \gamma\gamma + X$, JHEP **0510** (2005) 079, `arXiv:hep-ph/0509130 [hep-ph]`.

[353] C. Anastasiou, G. Dissertori, F. Stoeckli, and B. R. Webber, *QCD radiation effects on the* $H \to WW \to l\nu l\nu$ *signal at the LHC*, `arXiv:0801.2682 [hep-ph]`.

[354] J. Butterworth, J. R. Forshaw, and M. Seymour, *Multiparton interactions in photoproduction at HERA*, Z. Phys. **C72** (1996) 637–646, `arXiv:hep-ph/9601371 [hep-ph]`.

[355] P. Nason and C. Oleari, *NLO Higgs boson production via vector-boson fusion matched with shower in POWHEG*, JHEP **02** (2010) 037, `arXiv:0911.5299 [hep-ph]`.

[356] J. M. Campbell, R. Ellis, and C. Williams, *Hadronic production of a Higgs boson and two jets at next-to-leading order*, Phys. Rev. **D81** (2010) 074023, `arXiv:1001.4495 [hep-ph]`.

[357] L. J. Dixon and M. S. Siu, *Resonance-continuum interference in the di-photon Higgs signal at the LHC*, Phys. Rev. Lett. **90** (2003) 252001, `arXiv:hep-ph/0302233`.

[358] G. Passarino, *Higgs pseudo-observables*, Nucl. Phys. B. Proc. Suppl. **205-206** (2010) 16–19.

[359] D. Y. Bardin, M. Grunewald, and G. Passarino, *Precision calculation project report*, `arXiv:hep-ph/9902452`.

[360] G. Passarino, C. Sturm, and S. Uccirati, *Higgs pseudo-observables, second Riemann sheet and all that*, Nucl. Phys. **B834** (2010) 77–115, `arXiv:1001.3360 [hep-ph]`.

[361] M. J. G. Veltman, *Unitarity and causality in a renormalizable field theory with unstable particles*, Physica **29** (1963) 186–207.

[362] P. A. Grassi, B. A. Kniehl, and A. Sirlin, *Width and partial widths of unstable particles*, Phys. Rev. Lett. **86** (2001) 389–392, `arXiv:hep-th/0005149`.

[363] S. Actis and G. Passarino, *Two-loop renormalization in the standard model. III: Renormalization equations and their solutions*, Nucl. Phys. **B777** (2007) 100–156, `arXiv:hep-ph/0612124`.

[364] S. Actis, G. Passarino, C. Sturm, and S. Uccirati, *Two-loop threshold singularities, unstable particles and complex masses*, Phys. Lett. **B669** (2008) 62–68, `arXiv:0809.1302 [hep-ph]`.

[365] A. Denner, S. Dittmaier, M. Roth, and L. Wieders, *Electroweak corrections to charged-current* $e^+e^- \to 4$ *fermion processes: Technical details and further results*, Nucl. Phys. **B724** (2005) 247–294, `arXiv:hep-ph/0505042 [hep-ph]`.

[366] J. F. Gunion, H. E. Haber, G. L. Kane, and S. Dawson, *The Higgs Hunter's Guide*, (Perseus, Cambridge, Mass., 2000).

[367] J. C. Collins, *Choosing the factorization / renormalization scale in perturbative QCD calculations*, Proc. of 25th Rencontre de Moriond: High energy hadronic interactions, Les Arcs, France, Mar. 11-17, 1990.

[368] S. Forte, *Parton distributions at the dawn of the LHC*, `arXiv:1011.5247 [hep-ph]`.

[369] M. Dittmar, S. Forte, A. Glazov, and S. Moch, *Parton distributions*, `arXiv:0901.2504 [hep-ph]`.

[370] C. Anastasiou, S. Bucherer, and Z. Kunszt, *HPro: A NLO Monte Carlo for Higgs production via gluon fusion with finite heavy quark masses*, JHEP **10** (2009) 068, `arXiv:0907.2362 [hep-ph]`.

Appendices

A   The Standard Model input parameter set

The production cross sections and decay branching ratios of the Higgs bosons depend on a large number of Standard Model parameters. Unless otherwise specified, the following *default* parameter sets[26] are used as listed in Table A.

The strong coupling constant α_s is in general taken to be the value from the PDF set used. MSTW2008 determines the α_s value as part of its PDF fit: $\alpha_\mathrm{s}(M_\mathrm{Z}^2) = 0.1394$ at LO, 0.1202 at NLO and 0.1171 at NNLO. The CTEQ collaboration uses the world average values ($\alpha_\mathrm{s}(M_\mathrm{Z}^2) = 0.130$ at LO and $\alpha_\mathrm{s}(M_\mathrm{Z}^2) = 0.118$ at NLO) for its PDF fits. The NNPDF collaboration uses $\alpha_\mathrm{s}(M_\mathrm{Z}^2) = 0.119$ at NLO.

Table A.1: The Standard Model input parameters for particle masses and widths for computing cross section and branching ratios as presented in this Report.

Parameter	Value±Error
electron mass	0.510998910(13) MeV
muon mass	105.658367(4) MeV
tau mass	1776.84(17) MeV
u quark mass	190 MeV
d quark mass	190 MeV
s quark mass	190 MeV
c quark mass	1.40 GeV
b quark mass	4.75 GeV
t quark mass	172.5 ± 2.5 GeV
$\overline{\mathrm{MS}}$ scheme c mass	1.28 GeV
$\overline{\mathrm{MS}}$ scheme b mass	4.16 GeV
c pole mass 1-loop	1.41 GeV
c pole mass 2-loop	1.55 GeV
b pole mass 1-loop	4.49 GeV
b pole mass 2-loop	4.69 GeV
W mass	80.398 ± 0.025 GeV
Γ_W	2.141 ± 0.041 GeV
NLO Γ_W	2.08872 GeV
Z mass	91.1876 ± 0.0021 GeV
Γ_Z	2.4952 ± 0.0023 GeV
NLO Γ_Z	2.49595 GeV
G_F	$1.16637(1) \times 10^{-5}$ GeV^{-2}

---

[26]These parameters can be found at *https://twiki.cern.ch/twiki/bin/view/LHCPhysics/SMInputParameter*

B SM Higgs-boson partial widths

SM Higgs boson partial widths[27] for all relevant 2-particle decay channels are listed in Tables B.1–B.4. In Tables B.5–B.9 we list the partial widths of the SM Higgs boson decaying into 4-fermion final states, where leptons include $l = e, \mu, \tau, \nu_e, \nu_\mu, \nu_\tau$, and quarks $q = u, d, s, c, b$. Since all fermion masses are neglected, the branching ratios are identical for different flavours e, μ or τ. We display results for various 4-lepton final states ($H \rightarrow e^+e^-e^+e^-$, $e^+e^-\mu^+\mu^-$, $l^+l^-l^+l^-$, $e^+\nu_e e^-\overline{\nu}_e$, $e^+\nu_e \mu^-\overline{\nu}_\mu$, $l^+l^-\nu_l\overline{\nu}_l$) in Tables B.5–B.7. Results for final states with 2 leptons and 2 quarks ($H \rightarrow l^+l^-q\overline{q}$, $l^+\nu_l q\overline{q}'$, $\nu_l\overline{\nu}_l q\overline{q}$), 4 arbitrary quarks ($H \rightarrow qqqq$), and for all possible 4-fermion final states ($H \rightarrow ffff$) are provided in Tables B.8–B.9.

---

[27]Full listings can be found at *https://twiki.cern.ch/twiki/bin/view/LHCPhysics/CERNYellowReportPageBR*

Table B.1: SM Higgs-boson partial widths [GeV] in fermionic final states, for the low- and intermediate-mass range.

M_{H} [GeV]	$H \to b\bar{b}$	$H \to \tau\tau$	$H \to \mu\mu$	$H \to s\bar{s}$	$H \to c\bar{c}$	$H \to t\bar{t}$
90	$1.79 \cdot 10^{-3}$	$1.85 \cdot 10^{-4}$	$6.43 \cdot 10^{-7}$	$1.36 \cdot 10^{-6}$	$8.32 \cdot 10^{-5}$	0.00
95	$1.87 \cdot 10^{-3}$	$1.95 \cdot 10^{-4}$	$6.79 \cdot 10^{-7}$	$1.42 \cdot 10^{-6}$	$8.68 \cdot 10^{-5}$	0.00
100	$1.95 \cdot 10^{-3}$	$2.06 \cdot 10^{-4}$	$7.14 \cdot 10^{-7}$	$1.48 \cdot 10^{-6}$	$9.04 \cdot 10^{-5}$	0.00
105	$2.02 \cdot 10^{-3}$	$2.16 \cdot 10^{-4}$	$7.50 \cdot 10^{-7}$	$1.54 \cdot 10^{-6}$	$9.40 \cdot 10^{-5}$	0.00
110	$2.10 \cdot 10^{-3}$	$2.26 \cdot 10^{-4}$	$7.85 \cdot 10^{-7}$	$1.60 \cdot 10^{-6}$	$9.75 \cdot 10^{-5}$	0.00
115	$2.18 \cdot 10^{-3}$	$2.37 \cdot 10^{-4}$	$8.21 \cdot 10^{-7}$	$1.66 \cdot 10^{-6}$	$1.01 \cdot 10^{-4}$	0.00
120	$2.25 \cdot 10^{-3}$	$2.47 \cdot 10^{-4}$	$8.56 \cdot 10^{-7}$	$1.72 \cdot 10^{-6}$	$1.05 \cdot 10^{-4}$	0.00
125	$2.33 \cdot 10^{-3}$	$2.57 \cdot 10^{-4}$	$8.92 \cdot 10^{-7}$	$1.77 \cdot 10^{-6}$	$1.08 \cdot 10^{-4}$	0.00
130	$2.40 \cdot 10^{-3}$	$2.67 \cdot 10^{-4}$	$9.28 \cdot 10^{-7}$	$1.83 \cdot 10^{-6}$	$1.11 \cdot 10^{-4}$	0.00
135	$2.48 \cdot 10^{-3}$	$2.78 \cdot 10^{-4}$	$9.63 \cdot 10^{-7}$	$1.89 \cdot 10^{-6}$	$1.15 \cdot 10^{-4}$	0.00
140	$2.55 \cdot 10^{-3}$	$2.88 \cdot 10^{-4}$	$9.99 \cdot 10^{-7}$	$1.94 \cdot 10^{-6}$	$1.18 \cdot 10^{-4}$	0.00
145	$2.63 \cdot 10^{-3}$	$2.98 \cdot 10^{-4}$	$1.03 \cdot 10^{-6}$	$2.00 \cdot 10^{-6}$	$1.22 \cdot 10^{-4}$	0.00
150	$2.70 \cdot 10^{-3}$	$3.08 \cdot 10^{-4}$	$1.07 \cdot 10^{-6}$	$2.05 \cdot 10^{-6}$	$1.25 \cdot 10^{-4}$	0.00
155	$2.77 \cdot 10^{-3}$	$3.19 \cdot 10^{-4}$	$1.11 \cdot 10^{-6}$	$2.11 \cdot 10^{-6}$	$1.28 \cdot 10^{-4}$	0.00
160	$2.85 \cdot 10^{-3}$	$3.29 \cdot 10^{-4}$	$1.14 \cdot 10^{-6}$	$2.17 \cdot 10^{-6}$	$1.32 \cdot 10^{-4}$	0.00
165	$2.92 \cdot 10^{-3}$	$3.39 \cdot 10^{-4}$	$1.18 \cdot 10^{-6}$	$2.22 \cdot 10^{-6}$	$1.35 \cdot 10^{-4}$	0.00
170	$2.99 \cdot 10^{-3}$	$3.50 \cdot 10^{-4}$	$1.21 \cdot 10^{-6}$	$2.27 \cdot 10^{-6}$	$1.38 \cdot 10^{-4}$	0.00
175	$3.06 \cdot 10^{-3}$	$3.60 \cdot 10^{-4}$	$1.25 \cdot 10^{-6}$	$2.33 \cdot 10^{-6}$	$1.42 \cdot 10^{-4}$	0.00
180	$3.13 \cdot 10^{-3}$	$3.70 \cdot 10^{-4}$	$1.28 \cdot 10^{-6}$	$2.38 \cdot 10^{-6}$	$1.45 \cdot 10^{-4}$	0.00
185	$3.20 \cdot 10^{-3}$	$3.80 \cdot 10^{-4}$	$1.32 \cdot 10^{-6}$	$2.44 \cdot 10^{-6}$	$1.48 \cdot 10^{-4}$	0.00
190	$3.27 \cdot 10^{-3}$	$3.91 \cdot 10^{-4}$	$1.35 \cdot 10^{-6}$	$2.49 \cdot 10^{-6}$	$1.51 \cdot 10^{-4}$	0.00
195	$3.34 \cdot 10^{-3}$	$4.01 \cdot 10^{-4}$	$1.39 \cdot 10^{-6}$	$2.54 \cdot 10^{-6}$	$1.55 \cdot 10^{-4}$	0.00
200	$3.41 \cdot 10^{-3}$	$4.11 \cdot 10^{-4}$	$1.43 \cdot 10^{-6}$	$2.59 \cdot 10^{-6}$	$1.58 \cdot 10^{-4}$	0.00
210	$3.55 \cdot 10^{-3}$	$4.32 \cdot 10^{-4}$	$1.50 \cdot 10^{-6}$	$2.70 \cdot 10^{-6}$	$1.64 \cdot 10^{-4}$	0.00
220	$3.69 \cdot 10^{-3}$	$4.53 \cdot 10^{-4}$	$1.57 \cdot 10^{-6}$	$2.80 \cdot 10^{-6}$	$1.70 \cdot 10^{-4}$	0.00
230	$3.83 \cdot 10^{-3}$	$4.73 \cdot 10^{-4}$	$1.64 \cdot 10^{-6}$	$2.91 \cdot 10^{-6}$	$1.77 \cdot 10^{-4}$	0.00
240	$3.96 \cdot 10^{-3}$	$4.94 \cdot 10^{-4}$	$1.71 \cdot 10^{-6}$	$3.01 \cdot 10^{-6}$	$1.83 \cdot 10^{-4}$	0.00
250	$4.10 \cdot 10^{-3}$	$5.15 \cdot 10^{-4}$	$1.78 \cdot 10^{-6}$	$3.11 \cdot 10^{-6}$	$1.89 \cdot 10^{-4}$	0.00
260	$4.23 \cdot 10^{-3}$	$5.35 \cdot 10^{-4}$	$1.86 \cdot 10^{-6}$	$3.21 \cdot 10^{-6}$	$1.95 \cdot 10^{-4}$	$2.45 \cdot 10^{-7}$
270	$4.36 \cdot 10^{-3}$	$5.56 \cdot 10^{-4}$	$1.93 \cdot 10^{-6}$	$3.31 \cdot 10^{-6}$	$2.02 \cdot 10^{-4}$	$1.27 \cdot 10^{-5}$
280	$4.50 \cdot 10^{-3}$	$5.77 \cdot 10^{-4}$	$2.00 \cdot 10^{-6}$	$3.42 \cdot 10^{-6}$	$2.08 \cdot 10^{-4}$	$7.00 \cdot 10^{-5}$
290	$4.63 \cdot 10^{-3}$	$5.98 \cdot 10^{-4}$	$2.07 \cdot 10^{-6}$	$3.52 \cdot 10^{-6}$	$2.14 \cdot 10^{-4}$	$2.26 \cdot 10^{-4}$
300	$4.76 \cdot 10^{-3}$	$6.18 \cdot 10^{-4}$	$2.14 \cdot 10^{-6}$	$3.62 \cdot 10^{-6}$	$2.20 \cdot 10^{-4}$	$5.79 \cdot 10^{-4}$
310	$4.90 \cdot 10^{-3}$	$6.39 \cdot 10^{-4}$	$2.22 \cdot 10^{-6}$	$3.72 \cdot 10^{-6}$	$2.26 \cdot 10^{-4}$	$1.32 \cdot 10^{-3}$
320	$5.02 \cdot 10^{-3}$	$6.60 \cdot 10^{-4}$	$2.29 \cdot 10^{-6}$	$3.81 \cdot 10^{-6}$	$2.32 \cdot 10^{-4}$	$2.86 \cdot 10^{-3}$
330	$5.16 \cdot 10^{-3}$	$6.81 \cdot 10^{-4}$	$2.36 \cdot 10^{-6}$	$3.91 \cdot 10^{-6}$	$2.38 \cdot 10^{-4}$	$6.31 \cdot 10^{-3}$
340	$5.29 \cdot 10^{-3}$	$7.02 \cdot 10^{-4}$	$2.43 \cdot 10^{-6}$	$4.01 \cdot 10^{-6}$	$2.44 \cdot 10^{-4}$	$1.62 \cdot 10^{-2}$
350	$5.42 \cdot 10^{-3}$	$7.23 \cdot 10^{-4}$	$2.50 \cdot 10^{-6}$	$4.11 \cdot 10^{-6}$	$2.50 \cdot 10^{-4}$	$2.37 \cdot 10^{-1}$
360	$5.55 \cdot 10^{-3}$	$7.44 \cdot 10^{-4}$	$2.58 \cdot 10^{-6}$	$4.21 \cdot 10^{-6}$	$2.56 \cdot 10^{-4}$	$9.07 \cdot 10^{-1}$
370	$5.68 \cdot 10^{-3}$	$7.65 \cdot 10^{-4}$	$2.65 \cdot 10^{-6}$	$4.31 \cdot 10^{-6}$	$2.62 \cdot 10^{-4}$	1.69
380	$5.81 \cdot 10^{-3}$	$7.86 \cdot 10^{-4}$	$2.72 \cdot 10^{-6}$	$4.41 \cdot 10^{-6}$	$2.68 \cdot 10^{-4}$	2.54
390	$5.94 \cdot 10^{-3}$	$8.07 \cdot 10^{-4}$	$2.80 \cdot 10^{-6}$	$4.51 \cdot 10^{-6}$	$2.74 \cdot 10^{-4}$	3.43
400	$6.07 \cdot 10^{-3}$	$8.28 \cdot 10^{-4}$	$2.87 \cdot 10^{-6}$	$4.61 \cdot 10^{-6}$	$2.80 \cdot 10^{-4}$	4.34
410	$6.20 \cdot 10^{-3}$	$8.49 \cdot 10^{-4}$	$2.94 \cdot 10^{-6}$	$4.70 \cdot 10^{-6}$	$2.86 \cdot 10^{-4}$	5.25
420	$6.32 \cdot 10^{-3}$	$8.70 \cdot 10^{-4}$	$3.02 \cdot 10^{-6}$	$4.80 \cdot 10^{-6}$	$2.92 \cdot 10^{-4}$	6.16
430	$6.45 \cdot 10^{-3}$	$8.92 \cdot 10^{-4}$	$3.09 \cdot 10^{-6}$	$4.90 \cdot 10^{-6}$	$2.98 \cdot 10^{-4}$	7.06
440	$6.58 \cdot 10^{-3}$	$9.13 \cdot 10^{-4}$	$3.16 \cdot 10^{-6}$	$4.99 \cdot 10^{-6}$	$3.04 \cdot 10^{-4}$	7.96
450	$6.71 \cdot 10^{-3}$	$9.34 \cdot 10^{-4}$	$3.24 \cdot 10^{-6}$	$5.09 \cdot 10^{-6}$	$3.09 \cdot 10^{-4}$	8.85
460	$6.84 \cdot 10^{-3}$	$9.55 \cdot 10^{-4}$	$3.31 \cdot 10^{-6}$	$5.19 \cdot 10^{-6}$	$3.15 \cdot 10^{-4}$	9.73
470	$6.96 \cdot 10^{-3}$	$9.77 \cdot 10^{-4}$	$3.38 \cdot 10^{-6}$	$5.29 \cdot 10^{-6}$	$3.21 \cdot 10^{-4}$	10.6
480	$7.09 \cdot 10^{-3}$	$9.98 \cdot 10^{-4}$	$3.46 \cdot 10^{-6}$	$5.38 \cdot 10^{-6}$	$3.27 \cdot 10^{-4}$	11.4
490	$7.22 \cdot 10^{-3}$	$1.02 \cdot 10^{-3}$	$3.53 \cdot 10^{-6}$	$5.48 \cdot 10^{-6}$	$3.33 \cdot 10^{-4}$	12.3

Table B.2: SM Higgs-boson partial widths [GeV] in fermionic final states, for the high-mass range.

M_{H} [GeV]	H → b$\bar{\mathrm{b}}$	H → ττ	H → μμ	H → s$\bar{\mathrm{s}}$	H → c$\bar{\mathrm{c}}$	H → t$\bar{\mathrm{t}}$
500	$7.35 \cdot 10^{-3}$	$1.04 \cdot 10^{-3}$	$3.60 \cdot 10^{-6}$	$5.57 \cdot 10^{-6}$	$3.39 \cdot 10^{-4}$	13.1
510	$7.47 \cdot 10^{-3}$	$1.06 \cdot 10^{-3}$	$3.68 \cdot 10^{-6}$	$5.67 \cdot 10^{-6}$	$3.45 \cdot 10^{-4}$	13.9
520	$7.60 \cdot 10^{-3}$	$1.08 \cdot 10^{-3}$	$3.75 \cdot 10^{-6}$	$5.77 \cdot 10^{-6}$	$3.50 \cdot 10^{-4}$	14.8
530	$7.72 \cdot 10^{-3}$	$1.10 \cdot 10^{-3}$	$3.83 \cdot 10^{-6}$	$5.86 \cdot 10^{-6}$	$3.56 \cdot 10^{-4}$	15.5
540	$7.85 \cdot 10^{-3}$	$1.13 \cdot 10^{-3}$	$3.90 \cdot 10^{-6}$	$5.96 \cdot 10^{-6}$	$3.62 \cdot 10^{-4}$	16.3
550	$7.98 \cdot 10^{-3}$	$1.15 \cdot 10^{-3}$	$3.97 \cdot 10^{-6}$	$6.05 \cdot 10^{-6}$	$3.68 \cdot 10^{-4}$	17.1
560	$8.10 \cdot 10^{-3}$	$1.17 \cdot 10^{-3}$	$4.05 \cdot 10^{-6}$	$6.15 \cdot 10^{-6}$	$3.73 \cdot 10^{-4}$	17.8
570	$8.23 \cdot 10^{-3}$	$1.19 \cdot 10^{-3}$	$4.12 \cdot 10^{-6}$	$6.24 \cdot 10^{-6}$	$3.79 \cdot 10^{-4}$	18.6
580	$8.35 \cdot 10^{-3}$	$1.21 \cdot 10^{-3}$	$4.20 \cdot 10^{-6}$	$6.34 \cdot 10^{-6}$	$3.85 \cdot 10^{-4}$	19.3
590	$8.48 \cdot 10^{-3}$	$1.23 \cdot 10^{-3}$	$4.27 \cdot 10^{-6}$	$6.43 \cdot 10^{-6}$	$3.91 \cdot 10^{-4}$	20.1
600	$8.60 \cdot 10^{-3}$	$1.25 \cdot 10^{-3}$	$4.35 \cdot 10^{-6}$	$6.53 \cdot 10^{-6}$	$3.96 \cdot 10^{-4}$	20.8
610	$8.72 \cdot 10^{-3}$	$1.28 \cdot 10^{-3}$	$4.42 \cdot 10^{-6}$	$6.62 \cdot 10^{-6}$	$4.02 \cdot 10^{-4}$	21.5
620	$8.85 \cdot 10^{-3}$	$1.30 \cdot 10^{-3}$	$4.49 \cdot 10^{-6}$	$6.71 \cdot 10^{-6}$	$4.08 \cdot 10^{-4}$	22.2
630	$8.97 \cdot 10^{-3}$	$1.32 \cdot 10^{-3}$	$4.57 \cdot 10^{-6}$	$6.81 \cdot 10^{-6}$	$4.13 \cdot 10^{-4}$	22.9
640	$9.10 \cdot 10^{-3}$	$1.34 \cdot 10^{-3}$	$4.64 \cdot 10^{-6}$	$6.90 \cdot 10^{-6}$	$4.19 \cdot 10^{-4}$	23.6
650	$9.22 \cdot 10^{-3}$	$1.36 \cdot 10^{-3}$	$4.72 \cdot 10^{-6}$	$6.99 \cdot 10^{-6}$	$4.25 \cdot 10^{-4}$	24.2
660	$9.34 \cdot 10^{-3}$	$1.38 \cdot 10^{-3}$	$4.79 \cdot 10^{-6}$	$7.08 \cdot 10^{-6}$	$4.30 \cdot 10^{-4}$	24.9
670	$9.46 \cdot 10^{-3}$	$1.40 \cdot 10^{-3}$	$4.86 \cdot 10^{-6}$	$7.18 \cdot 10^{-6}$	$4.36 \cdot 10^{-4}$	25.6
680	$9.58 \cdot 10^{-3}$	$1.43 \cdot 10^{-3}$	$4.94 \cdot 10^{-6}$	$7.27 \cdot 10^{-6}$	$4.42 \cdot 10^{-4}$	26.2
690	$9.70 \cdot 10^{-3}$	$1.45 \cdot 10^{-3}$	$5.01 \cdot 10^{-6}$	$7.36 \cdot 10^{-6}$	$4.47 \cdot 10^{-4}$	26.8
700	$9.83 \cdot 10^{-3}$	$1.47 \cdot 10^{-3}$	$5.09 \cdot 10^{-6}$	$7.45 \cdot 10^{-6}$	$4.53 \cdot 10^{-4}$	27.5
710	$9.95 \cdot 10^{-3}$	$1.49 \cdot 10^{-3}$	$5.16 \cdot 10^{-6}$	$7.54 \cdot 10^{-6}$	$4.58 \cdot 10^{-4}$	28.1
720	$1.01 \cdot 10^{-2}$	$1.51 \cdot 10^{-3}$	$5.23 \cdot 10^{-6}$	$7.64 \cdot 10^{-6}$	$4.64 \cdot 10^{-4}$	28.7
730	$1.02 \cdot 10^{-2}$	$1.53 \cdot 10^{-3}$	$5.31 \cdot 10^{-6}$	$7.73 \cdot 10^{-6}$	$4.69 \cdot 10^{-4}$	29.4
740	$1.03 \cdot 10^{-2}$	$1.55 \cdot 10^{-3}$	$5.38 \cdot 10^{-6}$	$7.82 \cdot 10^{-6}$	$4.75 \cdot 10^{-4}$	29.9
750	$1.04 \cdot 10^{-2}$	$1.57 \cdot 10^{-3}$	$5.45 \cdot 10^{-6}$	$7.91 \cdot 10^{-6}$	$4.80 \cdot 10^{-4}$	30.6
760	$1.05 \cdot 10^{-2}$	$1.60 \cdot 10^{-3}$	$5.53 \cdot 10^{-6}$	$8.00 \cdot 10^{-6}$	$4.86 \cdot 10^{-4}$	31.2
770	$1.07 \cdot 10^{-2}$	$1.62 \cdot 10^{-3}$	$5.60 \cdot 10^{-6}$	$8.08 \cdot 10^{-6}$	$4.91 \cdot 10^{-4}$	31.7
780	$1.08 \cdot 10^{-2}$	$1.64 \cdot 10^{-3}$	$5.67 \cdot 10^{-6}$	$8.17 \cdot 10^{-6}$	$4.96 \cdot 10^{-4}$	32.3
790	$1.09 \cdot 10^{-2}$	$1.66 \cdot 10^{-3}$	$5.75 \cdot 10^{-6}$	$8.26 \cdot 10^{-6}$	$5.02 \cdot 10^{-4}$	32.9
800	$1.10 \cdot 10^{-2}$	$1.68 \cdot 10^{-3}$	$5.82 \cdot 10^{-6}$	$8.35 \cdot 10^{-6}$	$5.07 \cdot 10^{-4}$	33.5
810	$1.11 \cdot 10^{-2}$	$1.70 \cdot 10^{-3}$	$5.89 \cdot 10^{-6}$	$8.44 \cdot 10^{-6}$	$5.12 \cdot 10^{-4}$	34.1
820	$1.12 \cdot 10^{-2}$	$1.72 \cdot 10^{-3}$	$5.96 \cdot 10^{-6}$	$8.52 \cdot 10^{-6}$	$5.18 \cdot 10^{-4}$	34.6
830	$1.14 \cdot 10^{-2}$	$1.74 \cdot 10^{-3}$	$6.03 \cdot 10^{-6}$	$8.61 \cdot 10^{-6}$	$5.23 \cdot 10^{-4}$	35.2
840	$1.15 \cdot 10^{-2}$	$1.76 \cdot 10^{-3}$	$6.10 \cdot 10^{-6}$	$8.69 \cdot 10^{-6}$	$5.28 \cdot 10^{-4}$	35.7
850	$1.16 \cdot 10^{-2}$	$1.78 \cdot 10^{-3}$	$6.17 \cdot 10^{-6}$	$8.78 \cdot 10^{-6}$	$5.33 \cdot 10^{-4}$	36.2
860	$1.17 \cdot 10^{-2}$	$1.80 \cdot 10^{-3}$	$6.24 \cdot 10^{-6}$	$8.86 \cdot 10^{-6}$	$5.38 \cdot 10^{-4}$	36.8
870	$1.18 \cdot 10^{-2}$	$1.82 \cdot 10^{-3}$	$6.31 \cdot 10^{-6}$	$8.95 \cdot 10^{-6}$	$5.43 \cdot 10^{-4}$	37.3
880	$1.19 \cdot 10^{-2}$	$1.84 \cdot 10^{-3}$	$6.38 \cdot 10^{-6}$	$9.03 \cdot 10^{-6}$	$5.48 \cdot 10^{-4}$	37.8
890	$1.20 \cdot 10^{-2}$	$1.86 \cdot 10^{-3}$	$6.45 \cdot 10^{-6}$	$9.11 \cdot 10^{-6}$	$5.53 \cdot 10^{-4}$	38.3
900	$1.21 \cdot 10^{-2}$	$1.88 \cdot 10^{-3}$	$6.52 \cdot 10^{-6}$	$9.19 \cdot 10^{-6}$	$5.58 \cdot 10^{-4}$	38.9
910	$1.22 \cdot 10^{-2}$	$1.90 \cdot 10^{-3}$	$6.58 \cdot 10^{-6}$	$9.27 \cdot 10^{-6}$	$5.63 \cdot 10^{-4}$	39.4
920	$1.23 \cdot 10^{-2}$	$1.92 \cdot 10^{-3}$	$6.66 \cdot 10^{-6}$	$9.35 \cdot 10^{-6}$	$5.67 \cdot 10^{-4}$	39.9
930	$1.24 \cdot 10^{-2}$	$1.94 \cdot 10^{-3}$	$6.72 \cdot 10^{-6}$	$9.43 \cdot 10^{-6}$	$5.72 \cdot 10^{-4}$	40.4
940	$1.25 \cdot 10^{-2}$	$1.96 \cdot 10^{-3}$	$6.79 \cdot 10^{-6}$	$9.51 \cdot 10^{-6}$	$5.77 \cdot 10^{-4}$	40.8
950	$1.26 \cdot 10^{-2}$	$1.98 \cdot 10^{-3}$	$6.85 \cdot 10^{-6}$	$9.58 \cdot 10^{-6}$	$5.82 \cdot 10^{-4}$	41.3
960	$1.27 \cdot 10^{-2}$	$2.00 \cdot 10^{-3}$	$6.92 \cdot 10^{-6}$	$9.66 \cdot 10^{-6}$	$5.86 \cdot 10^{-4}$	41.8
970	$1.28 \cdot 10^{-2}$	$2.01 \cdot 10^{-3}$	$6.98 \cdot 10^{-6}$	$9.74 \cdot 10^{-6}$	$5.90 \cdot 10^{-4}$	42.2
980	$1.29 \cdot 10^{-2}$	$2.03 \cdot 10^{-3}$	$7.04 \cdot 10^{-6}$	$9.81 \cdot 10^{-6}$	$5.95 \cdot 10^{-4}$	42.7
990	$1.30 \cdot 10^{-2}$	$2.05 \cdot 10^{-3}$	$7.11 \cdot 10^{-6}$	$9.88 \cdot 10^{-6}$	$6.00 \cdot 10^{-4}$	43.2
1000	$1.31 \cdot 10^{-2}$	$2.07 \cdot 10^{-3}$	$7.17 \cdot 10^{-6}$	$9.95 \cdot 10^{-6}$	$6.04 \cdot 10^{-4}$	43.6

Table B.3: SM Higgs-boson partial widths [GeV] in bosonic final states, for the low- and intermediate-mass range.

M_{H} [GeV]	H → gg	H → γγ	H → Zγ	H → WW	H → ZZ
90	$1.35 \cdot 10^{-4}$	$2.71 \cdot 10^{-6}$	0.00	$4.60 \cdot 10^{-6}$	$9.27 \cdot 10^{-7}$
95	$1.57 \cdot 10^{-4}$	$3.26 \cdot 10^{-6}$	$1.05 \cdot 10^{-8}$	$1.10 \cdot 10^{-5}$	$1.56 \cdot 10^{-6}$
100	$1.81 \cdot 10^{-4}$	$3.91 \cdot 10^{-6}$	$1.22 \cdot 10^{-7}$	$2.72 \cdot 10^{-5}$	$2.79 \cdot 10^{-6}$
105	$2.08 \cdot 10^{-4}$	$4.67 \cdot 10^{-6}$	$4.54 \cdot 10^{-7}$	$6.36 \cdot 10^{-5}$	$5.63 \cdot 10^{-6}$
110	$2.38 \cdot 10^{-4}$	$5.55 \cdot 10^{-6}$	$1.11 \cdot 10^{-6}$	$1.36 \cdot 10^{-4}$	$1.24 \cdot 10^{-5}$
115	$2.71 \cdot 10^{-4}$	$6.59 \cdot 10^{-6}$	$2.21 \cdot 10^{-6}$	$2.68 \cdot 10^{-4}$	$2.70 \cdot 10^{-5}$
120	$3.06 \cdot 10^{-4}$	$7.81 \cdot 10^{-6}$	$3.88 \cdot 10^{-6}$	$4.95 \cdot 10^{-4}$	$5.57 \cdot 10^{-5}$
125	$3.45 \cdot 10^{-4}$	$9.27 \cdot 10^{-6}$	$6.26 \cdot 10^{-6}$	$8.73 \cdot 10^{-4}$	$1.07 \cdot 10^{-4}$
130	$3.87 \cdot 10^{-4}$	$1.10 \cdot 10^{-5}$	$9.55 \cdot 10^{-6}$	$1.49 \cdot 10^{-3}$	$1.95 \cdot 10^{-4}$
135	$4.33 \cdot 10^{-4}$	$1.31 \cdot 10^{-5}$	$1.40 \cdot 10^{-5}$	$2.47 \cdot 10^{-3}$	$3.38 \cdot 10^{-4}$
140	$4.82 \cdot 10^{-4}$	$1.57 \cdot 10^{-5}$	$2.01 \cdot 10^{-5}$	$4.10 \cdot 10^{-3}$	$5.62 \cdot 10^{-4}$
145	$5.35 \cdot 10^{-4}$	$1.91 \cdot 10^{-5}$	$2.83 \cdot 10^{-5}$	$6.86 \cdot 10^{-3}$	$9.06 \cdot 10^{-4}$
150	$5.93 \cdot 10^{-4}$	$2.36 \cdot 10^{-5}$	$4.00 \cdot 10^{-5}$	$1.21 \cdot 10^{-2}$	$1.43 \cdot 10^{-3}$
155	$6.52 \cdot 10^{-4}$	$3.02 \cdot 10^{-5}$	$5.78 \cdot 10^{-5}$	$2.41 \cdot 10^{-2}$	$2.22 \cdot 10^{-3}$
160	$7.10 \cdot 10^{-4}$	$4.42 \cdot 10^{-5}$	$9.56 \cdot 10^{-5}$	$7.53 \cdot 10^{-2}$	$3.44 \cdot 10^{-3}$
165	$7.66 \cdot 10^{-4}$	$5.66 \cdot 10^{-5}$	$1.34 \cdot 10^{-4}$	$2.36 \cdot 10^{-1}$	$5.47 \cdot 10^{-3}$
170	$8.29 \cdot 10^{-4}$	$6.01 \cdot 10^{-5}$	$1.52 \cdot 10^{-4}$	$3.67 \cdot 10^{-1}$	$8.98 \cdot 10^{-3}$
175	$8.99 \cdot 10^{-4}$	$6.13 \cdot 10^{-5}$	$1.69 \cdot 10^{-4}$	$4.80 \cdot 10^{-1}$	$1.62 \cdot 10^{-2}$
180	$9.72 \cdot 10^{-4}$	$6.44 \cdot 10^{-5}$	$1.87 \cdot 10^{-4}$	$5.88 \cdot 10^{-1}$	$3.80 \cdot 10^{-2}$
185	$1.05 \cdot 10^{-3}$	$6.73 \cdot 10^{-5}$	$2.03 \cdot 10^{-4}$	$7.02 \cdot 10^{-1}$	$1.25 \cdot 10^{-1}$
190	$1.13 \cdot 10^{-3}$	$7.01 \cdot 10^{-5}$	$2.20 \cdot 10^{-4}$	$8.17 \cdot 10^{-1}$	$2.18 \cdot 10^{-1}$
195	$1.22 \cdot 10^{-3}$	$7.28 \cdot 10^{-5}$	$2.36 \cdot 10^{-4}$	$9.36 \cdot 10^{-1}$	$2.95 \cdot 10^{-1}$
200	$1.31 \cdot 10^{-3}$	$7.54 \cdot 10^{-5}$	$2.51 \cdot 10^{-4}$	1.06	$3.66 \cdot 10^{-1}$
210	$1.53 \cdot 10^{-3}$	$8.01 \cdot 10^{-5}$	$2.81 \cdot 10^{-4}$	1.33	$5.06 \cdot 10^{-1}$
220	$1.77 \cdot 10^{-3}$	$8.45 \cdot 10^{-5}$	$3.10 \cdot 10^{-4}$	1.65	$6.54 \cdot 10^{-1}$
230	$2.05 \cdot 10^{-3}$	$8.86 \cdot 10^{-5}$	$3.36 \cdot 10^{-4}$	2.00	$8.16 \cdot 10^{-1}$
240	$2.37 \cdot 10^{-3}$	$9.23 \cdot 10^{-5}$	$3.62 \cdot 10^{-4}$	2.39	$9.97 \cdot 10^{-1}$
250	$2.73 \cdot 10^{-3}$	$9.58 \cdot 10^{-5}$	$3.85 \cdot 10^{-4}$	2.83	1.20
260	$3.13 \cdot 10^{-3}$	$9.90 \cdot 10^{-5}$	$4.08 \cdot 10^{-4}$	3.32	1.42
270	$3.60 \cdot 10^{-3}$	$1.02 \cdot 10^{-4}$	$4.29 \cdot 10^{-4}$	3.87	1.67
280	$4.13 \cdot 10^{-3}$	$1.05 \cdot 10^{-4}$	$4.48 \cdot 10^{-4}$	4.47	1.95
290	$4.74 \cdot 10^{-3}$	$1.07 \cdot 10^{-4}$	$4.67 \cdot 10^{-4}$	5.12	2.25
300	$5.45 \cdot 10^{-3}$	$1.09 \cdot 10^{-4}$	$4.85 \cdot 10^{-4}$	5.83	2.59
310	$6.28 \cdot 10^{-3}$	$1.12 \cdot 10^{-4}$	$5.01 \cdot 10^{-4}$	6.60	2.95
320	$7.26 \cdot 10^{-3}$	$1.14 \cdot 10^{-4}$	$5.16 \cdot 10^{-4}$	7.44	3.34
330	$8.46 \cdot 10^{-3}$	$1.16 \cdot 10^{-4}$	$5.31 \cdot 10^{-4}$	8.32	3.76
340	$1.00 \cdot 10^{-2}$	$1.18 \cdot 10^{-4}$	$5.44 \cdot 10^{-4}$	9.26	4.19
350	$1.22 \cdot 10^{-2}$	$1.16 \cdot 10^{-4}$	$5.54 \cdot 10^{-4}$	10.3	4.66
360	$1.48 \cdot 10^{-2}$	$1.07 \cdot 10^{-4}$	$5.58 \cdot 10^{-4}$	11.4	5.22
370	$1.73 \cdot 10^{-2}$	$9.82 \cdot 10^{-5}$	$5.59 \cdot 10^{-4}$	12.7	5.81
380	$1.96 \cdot 10^{-2}$	$8.92 \cdot 10^{-5}$	$5.59 \cdot 10^{-4}$	14.1	6.45
390	$2.19 \cdot 10^{-2}$	$8.05 \cdot 10^{-5}$	$5.58 \cdot 10^{-4}$	15.5	7.13
400	$2.40 \cdot 10^{-2}$	$7.22 \cdot 10^{-5}$	$5.55 \cdot 10^{-4}$	17.0	7.85
410	$2.60 \cdot 10^{-2}$	$6.45 \cdot 10^{-5}$	$5.52 \cdot 10^{-4}$	18.6	8.62
420	$2.80 \cdot 10^{-2}$	$5.73 \cdot 10^{-5}$	$5.49 \cdot 10^{-4}$	20.2	9.43
430	$2.98 \cdot 10^{-2}$	$5.06 \cdot 10^{-5}$	$5.45 \cdot 10^{-4}$	22.0	10.3
440	$3.16 \cdot 10^{-2}$	$4.44 \cdot 10^{-5}$	$5.42 \cdot 10^{-4}$	23.9	11.2
450	$3.32 \cdot 10^{-2}$	$3.88 \cdot 10^{-5}$	$5.38 \cdot 10^{-4}$	25.8	12.2
460	$3.48 \cdot 10^{-2}$	$3.37 \cdot 10^{-5}$	$5.33 \cdot 10^{-4}$	27.9	13.2
470	$3.63 \cdot 10^{-2}$	$2.90 \cdot 10^{-5}$	$5.29 \cdot 10^{-4}$	30.0	14.2
480	$3.78 \cdot 10^{-2}$	$2.49 \cdot 10^{-5}$	$5.25 \cdot 10^{-4}$	32.3	15.3
490	$3.92 \cdot 10^{-2}$	$2.12 \cdot 10^{-5}$	$5.20 \cdot 10^{-4}$	34.6	16.5

Table B.4: SM Higgs-boson partial widths [GeV] in bosonic final states, for the low- and intermediate-mass range.

M_{H} [GeV]	$H \to gg$	$H \to \gamma\gamma$	$H \to Z\gamma$	$H \to WW$	$H \to ZZ$
500	$4.05 \cdot 10^{-2}$	$1.80 \cdot 10^{-5}$	$5.16 \cdot 10^{-4}$	37.1	17.7
510	$4.18 \cdot 10^{-2}$	$1.52 \cdot 10^{-5}$	$5.11 \cdot 10^{-4}$	39.7	19.0
520	$4.31 \cdot 10^{-2}$	$1.28 \cdot 10^{-5}$	$5.07 \cdot 10^{-4}$	42.4	20.4
530	$4.42 \cdot 10^{-2}$	$1.08 \cdot 10^{-5}$	$5.02 \cdot 10^{-4}$	45.2	21.8
540	$4.54 \cdot 10^{-2}$	$9.17 \cdot 10^{-6}$	$4.98 \cdot 10^{-4}$	48.1	23.2
550	$4.65 \cdot 10^{-2}$	$7.93 \cdot 10^{-6}$	$4.93 \cdot 10^{-4}$	51.2	24.7
560	$4.76 \cdot 10^{-2}$	$7.07 \cdot 10^{-6}$	$4.89 \cdot 10^{-4}$	54.4	26.3
570	$4.85 \cdot 10^{-2}$	$6.56 \cdot 10^{-6}$	$4.84 \cdot 10^{-4}$	57.7	28.0
580	$4.95 \cdot 10^{-2}$	$6.40 \cdot 10^{-6}$	$4.80 \cdot 10^{-4}$	61.2	29.7
590	$5.05 \cdot 10^{-2}$	$6.57 \cdot 10^{-6}$	$4.75 \cdot 10^{-4}$	64.8	31.5
600	$5.14 \cdot 10^{-2}$	$7.08 \cdot 10^{-6}$	$4.71 \cdot 10^{-4}$	68.5	33.4
610	$5.23 \cdot 10^{-2}$	$7.92 \cdot 10^{-6}$	$4.67 \cdot 10^{-4}$	72.4	35.4
620	$5.31 \cdot 10^{-2}$	$9.06 \cdot 10^{-6}$	$4.63 \cdot 10^{-4}$	76.5	37.4
630	$5.40 \cdot 10^{-2}$	$1.05 \cdot 10^{-5}$	$4.59 \cdot 10^{-4}$	80.7	39.5
640	$5.48 \cdot 10^{-2}$	$1.23 \cdot 10^{-5}$	$4.55 \cdot 10^{-4}$	85.0	41.7
650	$5.56 \cdot 10^{-2}$	$1.44 \cdot 10^{-5}$	$4.51 \cdot 10^{-4}$	89.6	44.0
660	$5.63 \cdot 10^{-2}$	$1.68 \cdot 10^{-5}$	$4.47 \cdot 10^{-4}$	94.3	46.3
670	$5.71 \cdot 10^{-2}$	$1.94 \cdot 10^{-5}$	$4.44 \cdot 10^{-4}$	99.1	48.8
680	$5.78 \cdot 10^{-2}$	$2.24 \cdot 10^{-5}$	$4.40 \cdot 10^{-4}$	104	51.3
690	$5.84 \cdot 10^{-2}$	$2.57 \cdot 10^{-5}$	$4.36 \cdot 10^{-4}$	109	53.9
700	$5.91 \cdot 10^{-2}$	$2.92 \cdot 10^{-5}$	$4.33 \cdot 10^{-4}$	115	56.7
710	$5.98 \cdot 10^{-2}$	$3.30 \cdot 10^{-5}$	$4.30 \cdot 10^{-4}$	120	59.5
720	$6.04 \cdot 10^{-2}$	$3.72 \cdot 10^{-5}$	$4.27 \cdot 10^{-4}$	126	62.4
730	$6.11 \cdot 10^{-2}$	$4.16 \cdot 10^{-5}$	$4.24 \cdot 10^{-4}$	132	65.5
740	$6.16 \cdot 10^{-2}$	$4.62 \cdot 10^{-5}$	$4.20 \cdot 10^{-4}$	139	68.6
750	$6.22 \cdot 10^{-2}$	$5.12 \cdot 10^{-5}$	$4.18 \cdot 10^{-4}$	145	71.9
760	$6.28 \cdot 10^{-2}$	$5.65 \cdot 10^{-5}$	$4.15 \cdot 10^{-4}$	152	75.2
770	$6.34 \cdot 10^{-2}$	$6.19 \cdot 10^{-5}$	$4.12 \cdot 10^{-4}$	159	78.7
780	$6.39 \cdot 10^{-2}$	$6.77 \cdot 10^{-5}$	$4.10 \cdot 10^{-4}$	166	82.3
790	$6.45 \cdot 10^{-2}$	$7.38 \cdot 10^{-5}$	$4.08 \cdot 10^{-4}$	173	86.1
800	$6.50 \cdot 10^{-2}$	$8.02 \cdot 10^{-5}$	$4.06 \cdot 10^{-4}$	181	89.9
810	$6.55 \cdot 10^{-2}$	$8.68 \cdot 10^{-5}$	$4.04 \cdot 10^{-4}$	189	93.9
820	$6.60 \cdot 10^{-2}$	$9.37 \cdot 10^{-5}$	$4.01 \cdot 10^{-4}$	197	98.0
830	$6.65 \cdot 10^{-2}$	$1.01 \cdot 10^{-4}$	$4.00 \cdot 10^{-4}$	206	102
840	$6.70 \cdot 10^{-2}$	$1.08 \cdot 10^{-4}$	$3.98 \cdot 10^{-4}$	214	107
850	$6.75 \cdot 10^{-2}$	$1.16 \cdot 10^{-4}$	$3.96 \cdot 10^{-4}$	223	111
860	$6.80 \cdot 10^{-2}$	$1.24 \cdot 10^{-4}$	$3.95 \cdot 10^{-4}$	233	116
870	$6.84 \cdot 10^{-2}$	$1.32 \cdot 10^{-4}$	$3.94 \cdot 10^{-4}$	242	121
880	$6.88 \cdot 10^{-2}$	$1.41 \cdot 10^{-4}$	$3.93 \cdot 10^{-4}$	252	126
890	$6.93 \cdot 10^{-2}$	$1.50 \cdot 10^{-4}$	$3.92 \cdot 10^{-4}$	263	131
900	$6.97 \cdot 10^{-2}$	$1.59 \cdot 10^{-4}$	$3.91 \cdot 10^{-4}$	273	137
910	$7.01 \cdot 10^{-2}$	$1.68 \cdot 10^{-4}$	$3.91 \cdot 10^{-4}$	284	142
920	$7.05 \cdot 10^{-2}$	$1.78 \cdot 10^{-4}$	$3.90 \cdot 10^{-4}$	296	148
930	$7.09 \cdot 10^{-2}$	$1.88 \cdot 10^{-4}$	$3.90 \cdot 10^{-4}$	308	154
940	$7.13 \cdot 10^{-2}$	$1.98 \cdot 10^{-4}$	$3.90 \cdot 10^{-4}$	320	160
950	$7.17 \cdot 10^{-2}$	$2.09 \cdot 10^{-4}$	$3.90 \cdot 10^{-4}$	332	166
960	$7.21 \cdot 10^{-2}$	$2.20 \cdot 10^{-4}$	$3.90 \cdot 10^{-4}$	345	173
970	$7.25 \cdot 10^{-2}$	$2.31 \cdot 10^{-4}$	$3.91 \cdot 10^{-4}$	359	180
980	$7.29 \cdot 10^{-2}$	$2.43 \cdot 10^{-4}$	$3.92 \cdot 10^{-4}$	373	187
990	$7.32 \cdot 10^{-2}$	$2.54 \cdot 10^{-4}$	$3.92 \cdot 10^{-4}$	387	194
1000	$7.36 \cdot 10^{-2}$	$2.66 \cdot 10^{-4}$	$3.94 \cdot 10^{-4}$	402	201

Table B.5: SM Higgs-boson partial widths [GeV] for 4-fermion final states for the low-mass range. We list results for the specific final states $e^+e^-e^+e^-$ and $e^+e^-\mu^+\mu^-$, for final states with 4 arbitrary charged leptons, $e^+\nu_e e^-\bar\nu_e$ and $e^+\nu_e\mu^-\bar\nu_\mu$, and for final states $l^+l^-\nu_l\bar\nu_l$ with 2 charged leptons plus 2 neutrinos (ν_l represents any type of neutrinos).

M_H [GeV]	$H \to e^+e^-e^+e^-$	$H \to e^+e^-\mu^+\mu^-$	$H \to l^+l^-l^+l^-$ (l = e or μ)	$H \to l^+l^-l^+l^-$ (l = e, μ or τ)	$H \to e^+\nu_e e^-\bar\nu_e$	$H \to e^+\nu_e\mu^-\bar\nu_\mu$	$H \to l^+l^-\nu_l\bar\nu_l$ (l = e or μ)	$H \to l^+l^-\nu_l\bar\nu_l$ (l = e, μ or τ)
90	$1.56 \cdot 10^{-9}$	$2.07 \cdot 10^{-9}$	$5.19 \cdot 10^{-9}$	$1.09 \cdot 10^{-8}$	$3.89 \cdot 10^{-8}$	$5.40 \cdot 10^{-8}$	$2.03 \cdot 10^{-7}$	$4.66 \cdot 10^{-7}$
95	$2.58 \cdot 10^{-9}$	$3.47 \cdot 10^{-9}$	$8.62 \cdot 10^{-9}$	$1.81 \cdot 10^{-8}$	$1.04 \cdot 10^{-7}$	$1.29 \cdot 10^{-7}$	$4.93 \cdot 10^{-7}$	$1.13 \cdot 10^{-6}$
100	$4.43 \cdot 10^{-9}$	$6.19 \cdot 10^{-9}$	$1.51 \cdot 10^{-8}$	$3.19 \cdot 10^{-8}$	$2.79 \cdot 10^{-7}$	$3.20 \cdot 10^{-7}$	$1.25 \cdot 10^{-6}$	$2.83 \cdot 10^{-6}$
105	$8.40 \cdot 10^{-9}$	$1.25 \cdot 10^{-8}$	$2.93 \cdot 10^{-8}$	$6.28 \cdot 10^{-8}$	$6.86 \cdot 10^{-7}$	$7.47 \cdot 10^{-7}$	$2.97 \cdot 10^{-6}$	$6.69 \cdot 10^{-6}$
110	$1.72 \cdot 10^{-8}$	$2.76 \cdot 10^{-8}$	$6.20 \cdot 10^{-8}$	$1.34 \cdot 10^{-7}$	$1.51 \cdot 10^{-6}$	$1.60 \cdot 10^{-6}$	$6.44 \cdot 10^{-6}$	$1.44 \cdot 10^{-5}$
115	$3.55 \cdot 10^{-8}$	$6.03 \cdot 10^{-8}$	$1.31 \cdot 10^{-7}$	$2.88 \cdot 10^{-7}$	$3.05 \cdot 10^{-6}$	$3.15 \cdot 10^{-6}$	$1.29 \cdot 10^{-5}$	$2.88 \cdot 10^{-5}$
120	$7.06 \cdot 10^{-8}$	$1.25 \cdot 10^{-7}$	$2.66 \cdot 10^{-7}$	$5.86 \cdot 10^{-7}$	$5.74 \cdot 10^{-6}$	$5.83 \cdot 10^{-6}$	$2.41 \cdot 10^{-5}$	$5.37 \cdot 10^{-5}$
125	$1.33 \cdot 10^{-7}$	$2.41 \cdot 10^{-7}$	$5.08 \cdot 10^{-7}$	$1.12 \cdot 10^{-6}$	$1.03 \cdot 10^{-5}$	$1.03 \cdot 10^{-5}$	$4.30 \cdot 10^{-5}$	$9.53 \cdot 10^{-5}$
130	$2.38 \cdot 10^{-7}$	$4.39 \cdot 10^{-7}$	$9.16 \cdot 10^{-7}$	$2.03 \cdot 10^{-6}$	$1.76 \cdot 10^{-5}$	$1.75 \cdot 10^{-5}$	$7.37 \cdot 10^{-5}$	$1.63 \cdot 10^{-4}$
135	$4.07 \cdot 10^{-7}$	$7.61 \cdot 10^{-7}$	$1.57 \cdot 10^{-6}$	$3.50 \cdot 10^{-6}$	$2.96 \cdot 10^{-5}$	$2.91 \cdot 10^{-5}$	$1.24 \cdot 10^{-4}$	$2.73 \cdot 10^{-4}$
140	$6.70 \cdot 10^{-7}$	$1.27 \cdot 10^{-6}$	$2.61 \cdot 10^{-6}$	$5.81 \cdot 10^{-6}$	$4.93 \cdot 10^{-5}$	$4.82 \cdot 10^{-5}$	$2.05 \cdot 10^{-4}$	$4.52 \cdot 10^{-4}$
145	$1.07 \cdot 10^{-6}$	$2.04 \cdot 10^{-6}$	$4.19 \cdot 10^{-6}$	$9.35 \cdot 10^{-6}$	$8.28 \cdot 10^{-5}$	$8.09 \cdot 10^{-5}$	$3.44 \cdot 10^{-4}$	$7.58 \cdot 10^{-4}$
150	$1.68 \cdot 10^{-6}$	$3.22 \cdot 10^{-6}$	$6.59 \cdot 10^{-6}$	$1.47 \cdot 10^{-5}$	$1.46 \cdot 10^{-4}$	$1.42 \cdot 10^{-4}$	$6.01 \cdot 10^{-4}$	$1.33 \cdot 10^{-3}$
155	$2.61 \cdot 10^{-6}$	$5.01 \cdot 10^{-6}$	$1.02 \cdot 10^{-5}$	$2.29 \cdot 10^{-5}$	$2.90 \cdot 10^{-4}$	$2.84 \cdot 10^{-4}$	$1.19 \cdot 10^{-3}$	$2.63 \cdot 10^{-3}$
160	$4.02 \cdot 10^{-6}$	$7.76 \cdot 10^{-6}$	$1.58 \cdot 10^{-5}$	$3.53 \cdot 10^{-5}$	$8.99 \cdot 10^{-4}$	$8.88 \cdot 10^{-4}$	$3.64 \cdot 10^{-3}$	$8.12 \cdot 10^{-3}$
165	$6.35 \cdot 10^{-6}$	$1.23 \cdot 10^{-5}$	$2.50 \cdot 10^{-5}$	$5.60 \cdot 10^{-5}$	$2.81 \cdot 10^{-3}$	$2.79 \cdot 10^{-3}$	$1.13 \cdot 10^{-2}$	$2.53 \cdot 10^{-2}$
170	$1.04 \cdot 10^{-5}$	$2.02 \cdot 10^{-5}$	$4.10 \cdot 10^{-5}$	$9.18 \cdot 10^{-5}$	$4.36 \cdot 10^{-3}$	$4.32 \cdot 10^{-3}$	$1.75 \cdot 10^{-2}$	$3.92 \cdot 10^{-2}$
175	$1.86 \cdot 10^{-5}$	$3.64 \cdot 10^{-5}$	$7.36 \cdot 10^{-5}$	$1.65 \cdot 10^{-4}$	$5.72 \cdot 10^{-3}$	$5.65 \cdot 10^{-3}$	$2.30 \cdot 10^{-2}$	$5.15 \cdot 10^{-2}$
180	$4.32 \cdot 10^{-5}$	$8.55 \cdot 10^{-5}$	$1.72 \cdot 10^{-4}$	$3.86 \cdot 10^{-4}$	$7.09 \cdot 10^{-3}$	$6.93 \cdot 10^{-3}$	$2.87 \cdot 10^{-2}$	$6.39 \cdot 10^{-2}$
185	$1.41 \cdot 10^{-4}$	$2.82 \cdot 10^{-4}$	$5.64 \cdot 10^{-4}$	$1.27 \cdot 10^{-3}$	$8.83 \cdot 10^{-3}$	$8.28 \cdot 10^{-3}$	$3.65 \cdot 10^{-2}$	$7.95 \cdot 10^{-2}$
190	$2.46 \cdot 10^{-4}$	$4.91 \cdot 10^{-4}$	$9.82 \cdot 10^{-4}$	$2.21 \cdot 10^{-3}$	$1.06 \cdot 10^{-2}$	$9.63 \cdot 10^{-3}$	$4.44 \cdot 10^{-2}$	$9.55 \cdot 10^{-2}$
195	$3.32 \cdot 10^{-4}$	$6.64 \cdot 10^{-4}$	$1.33 \cdot 10^{-3}$	$2.99 \cdot 10^{-3}$	$1.23 \cdot 10^{-2}$	$1.10 \cdot 10^{-2}$	$5.21 \cdot 10^{-2}$	$1.11 \cdot 10^{-1}$
200	$4.12 \cdot 10^{-4}$	$8.24 \cdot 10^{-4}$	$1.65 \cdot 10^{-3}$	$3.71 \cdot 10^{-3}$	$1.41 \cdot 10^{-2}$	$1.25 \cdot 10^{-2}$	$5.99 \cdot 10^{-2}$	$1.27 \cdot 10^{-1}$
210	$5.70 \cdot 10^{-4}$	$1.14 \cdot 10^{-3}$	$2.28 \cdot 10^{-3}$	$5.13 \cdot 10^{-3}$	$1.80 \cdot 10^{-2}$	$1.57 \cdot 10^{-2}$	$7.65 \cdot 10^{-2}$	$1.62 \cdot 10^{-1}$
220	$7.36 \cdot 10^{-4}$	$1.47 \cdot 10^{-3}$	$2.94 \cdot 10^{-3}$	$6.62 \cdot 10^{-3}$	$2.23 \cdot 10^{-2}$	$1.94 \cdot 10^{-2}$	$9.51 \cdot 10^{-2}$	$2.01 \cdot 10^{-1}$
230	$9.19 \cdot 10^{-4}$	$1.84 \cdot 10^{-3}$	$3.67 \cdot 10^{-3}$	$8.27 \cdot 10^{-3}$	$2.72 \cdot 10^{-2}$	$2.35 \cdot 10^{-2}$	$1.16 \cdot 10^{-1}$	$2.45 \cdot 10^{-1}$
240	$1.12 \cdot 10^{-3}$	$2.24 \cdot 10^{-3}$	$4.49 \cdot 10^{-3}$	$1.01 \cdot 10^{-2}$	$3.26 \cdot 10^{-2}$	$2.82 \cdot 10^{-2}$	$1.39 \cdot 10^{-1}$	$2.94 \cdot 10^{-1}$
250	$1.35 \cdot 10^{-3}$	$2.70 \cdot 10^{-3}$	$5.40 \cdot 10^{-3}$	$1.21 \cdot 10^{-2}$	$3.87 \cdot 10^{-2}$	$3.34 \cdot 10^{-2}$	$1.66 \cdot 10^{-1}$	$3.49 \cdot 10^{-1}$
260	$1.60 \cdot 10^{-3}$	$3.21 \cdot 10^{-3}$	$6.41 \cdot 10^{-3}$	$1.44 \cdot 10^{-2}$	$4.55 \cdot 10^{-2}$	$3.92 \cdot 10^{-2}$	$1.95 \cdot 10^{-1}$	$4.10 \cdot 10^{-1}$
270	$1.89 \cdot 10^{-3}$	$3.77 \cdot 10^{-3}$	$7.54 \cdot 10^{-3}$	$1.70 \cdot 10^{-2}$	$5.31 \cdot 10^{-2}$	$4.56 \cdot 10^{-2}$	$2.27 \cdot 10^{-1}$	$4.78 \cdot 10^{-1}$
280	$2.20 \cdot 10^{-3}$	$4.39 \cdot 10^{-3}$	$8.78 \cdot 10^{-3}$	$1.98 \cdot 10^{-2}$	$6.13 \cdot 10^{-2}$	$5.26 \cdot 10^{-2}$	$2.63 \cdot 10^{-1}$	$5.52 \cdot 10^{-1}$
290	$2.54 \cdot 10^{-3}$	$5.07 \cdot 10^{-3}$	$1.01 \cdot 10^{-2}$	$2.28 \cdot 10^{-2}$	$7.04 \cdot 10^{-2}$	$6.03 \cdot 10^{-2}$	$3.02 \cdot 10^{-1}$	$6.34 \cdot 10^{-1}$
300	$2.91 \cdot 10^{-3}$	$5.82 \cdot 10^{-3}$	$1.16 \cdot 10^{-2}$	$2.62 \cdot 10^{-2}$	$8.03 \cdot 10^{-2}$	$6.87 \cdot 10^{-2}$	$3.44 \cdot 10^{-1}$	$7.22 \cdot 10^{-1}$

Table B.6: SM Higgs-boson partial widths [GeV] for 4-fermion final states for the intermediate-mass range. We list results for the specific final states $e^+e^-e^+e^-$ and $e^+e^-\mu^+\mu^-$, for final states with 4 arbitrary charged leptons, $e^+\nu_e e^-\bar{\nu}_e$ and $e^+\nu_e\mu^-\bar{\nu}_\mu$, and for final states $l^+l^-\nu_l\bar{\nu}_l$ with 2 charged leptons plus 2 neutrinos (ν_l represents any type of neutrinos).

M_H [GeV]	$H \to e^+e^-e^+e^-$	$H \to e^+e^-\mu^+\mu^-$	$H \to l^+l^-l^+l^-$ (l = e or μ)	$H \to l^+l^-l^+l^-$ (l = e, μ or τ)	$H \to e^+\nu_e e^-\bar{\nu}_e$	$H \to e^+\nu_e\mu^-\bar{\nu}_\mu$	$H \to l^+l^-\nu_l\bar{\nu}_l$ (l = e or μ)	$H \to l^+l^-\nu_l\bar{\nu}_l$ (l = e, μ or τ)
310	$3.32 \cdot 10^{-3}$	$6.63 \cdot 10^{-3}$	$1.33 \cdot 10^{-2}$	$2.98 \cdot 10^{-2}$	$9.10 \cdot 10^{-2}$	$7.78 \cdot 10^{-2}$	$3.90 \cdot 10^{-1}$	$8.19 \cdot 10^{-1}$
320	$3.76 \cdot 10^{-3}$	$7.51 \cdot 10^{-3}$	$1.50 \cdot 10^{-2}$	$3.38 \cdot 10^{-2}$	$1.03 \cdot 10^{-1}$	$8.75 \cdot 10^{-2}$	$4.40 \cdot 10^{-1}$	$9.23 \cdot 10^{-1}$
330	$4.23 \cdot 10^{-3}$	$8.44 \cdot 10^{-3}$	$1.69 \cdot 10^{-2}$	$3.80 \cdot 10^{-2}$	$1.15 \cdot 10^{-1}$	$9.80 \cdot 10^{-2}$	$4.93 \cdot 10^{-1}$	1.03
340	$4.72 \cdot 10^{-3}$	$9.43 \cdot 10^{-3}$	$1.89 \cdot 10^{-2}$	$4.24 \cdot 10^{-2}$	$1.28 \cdot 10^{-1}$	$1.09 \cdot 10^{-1}$	$5.49 \cdot 10^{-1}$	1.15
350	$5.24 \cdot 10^{-3}$	$1.05 \cdot 10^{-2}$	$2.10 \cdot 10^{-2}$	$4.72 \cdot 10^{-2}$	$1.42 \cdot 10^{-1}$	$1.21 \cdot 10^{-1}$	$6.08 \cdot 10^{-1}$	1.27
360	$5.87 \cdot 10^{-3}$	$1.17 \cdot 10^{-2}$	$2.35 \cdot 10^{-2}$	$5.28 \cdot 10^{-2}$	$1.58 \cdot 10^{-1}$	$1.35 \cdot 10^{-1}$	$6.79 \cdot 10^{-1}$	1.42
370	$6.54 \cdot 10^{-3}$	$1.31 \cdot 10^{-2}$	$2.62 \cdot 10^{-2}$	$5.88 \cdot 10^{-2}$	$1.76 \cdot 10^{-1}$	$1.50 \cdot 10^{-1}$	$7.55 \cdot 10^{-1}$	1.58
380	$7.26 \cdot 10^{-3}$	$1.45 \cdot 10^{-2}$	$2.90 \cdot 10^{-2}$	$6.53 \cdot 10^{-2}$	$1.94 \cdot 10^{-1}$	$1.66 \cdot 10^{-1}$	$8.36 \cdot 10^{-1}$	1.75
390	$8.03 \cdot 10^{-3}$	$1.60 \cdot 10^{-2}$	$3.21 \cdot 10^{-2}$	$7.22 \cdot 10^{-2}$	$2.14 \cdot 10^{-1}$	$1.82 \cdot 10^{-1}$	$9.21 \cdot 10^{-1}$	1.93
400	$8.84 \cdot 10^{-3}$	$1.77 \cdot 10^{-2}$	$3.54 \cdot 10^{-2}$	$7.96 \cdot 10^{-2}$	$2.35 \cdot 10^{-1}$	$2.00 \cdot 10^{-1}$	1.01	2.12
410	$9.71 \cdot 10^{-3}$	$1.94 \cdot 10^{-2}$	$3.88 \cdot 10^{-2}$	$8.74 \cdot 10^{-2}$	$2.58 \cdot 10^{-1}$	$2.19 \cdot 10^{-1}$	1.11	2.32
420	$1.06 \cdot 10^{-2}$	$2.12 \cdot 10^{-2}$	$4.25 \cdot 10^{-2}$	$9.56 \cdot 10^{-2}$	$2.81 \cdot 10^{-1}$	$2.39 \cdot 10^{-1}$	1.21	2.53
430	$1.16 \cdot 10^{-2}$	$2.32 \cdot 10^{-2}$	$4.64 \cdot 10^{-2}$	$1.04 \cdot 10^{-1}$	$3.06 \cdot 10^{-1}$	$2.60 \cdot 10^{-1}$	1.32	2.75
440	$1.26 \cdot 10^{-2}$	$2.52 \cdot 10^{-2}$	$5.05 \cdot 10^{-2}$	$1.14 \cdot 10^{-1}$	$3.32 \cdot 10^{-1}$	$2.82 \cdot 10^{-1}$	1.43	2.99
450	$1.37 \cdot 10^{-2}$	$2.74 \cdot 10^{-2}$	$5.48 \cdot 10^{-2}$	$1.23 \cdot 10^{-1}$	$3.59 \cdot 10^{-1}$	$3.05 \cdot 10^{-1}$	1.55	3.23
460	$1.48 \cdot 10^{-2}$	$2.97 \cdot 10^{-2}$	$5.93 \cdot 10^{-2}$	$1.34 \cdot 10^{-1}$	$3.88 \cdot 10^{-1}$	$3.29 \cdot 10^{-1}$	1.67	3.49
470	$1.60 \cdot 10^{-2}$	$3.21 \cdot 10^{-2}$	$6.41 \cdot 10^{-2}$	$1.44 \cdot 10^{-1}$	$4.18 \cdot 10^{-1}$	$3.54 \cdot 10^{-1}$	1.80	3.76
480	$1.73 \cdot 10^{-2}$	$3.46 \cdot 10^{-2}$	$6.91 \cdot 10^{-2}$	$1.56 \cdot 10^{-1}$	$4.50 \cdot 10^{-1}$	$3.81 \cdot 10^{-1}$	1.94	4.05
490	$1.86 \cdot 10^{-2}$	$3.72 \cdot 10^{-2}$	$7.44 \cdot 10^{-2}$	$1.67 \cdot 10^{-1}$	$4.83 \cdot 10^{-1}$	$4.09 \cdot 10^{-1}$	2.08	4.35
500	$2.00 \cdot 10^{-2}$	$4.00 \cdot 10^{-2}$	$7.99 \cdot 10^{-2}$	$1.80 \cdot 10^{-1}$	$5.18 \cdot 10^{-1}$	$4.38 \cdot 10^{-1}$	2.23	4.66
510	$2.14 \cdot 10^{-2}$	$4.29 \cdot 10^{-2}$	$8.57 \cdot 10^{-2}$	$1.93 \cdot 10^{-1}$	$5.54 \cdot 10^{-1}$	$4.68 \cdot 10^{-1}$	2.39	4.98
520	$2.29 \cdot 10^{-2}$	$4.59 \cdot 10^{-2}$	$9.18 \cdot 10^{-2}$	$2.07 \cdot 10^{-1}$	$5.92 \cdot 10^{-1}$	$5.00 \cdot 10^{-1}$	2.55	5.33
530	$2.45 \cdot 10^{-2}$	$4.91 \cdot 10^{-2}$	$9.81 \cdot 10^{-2}$	$2.21 \cdot 10^{-1}$	$6.31 \cdot 10^{-1}$	$5.34 \cdot 10^{-1}$	2.72	5.68
540	$2.62 \cdot 10^{-2}$	$5.24 \cdot 10^{-2}$	$1.05 \cdot 10^{-1}$	$2.36 \cdot 10^{-1}$	$6.73 \cdot 10^{-1}$	$5.68 \cdot 10^{-1}$	2.90	6.05
550	$2.79 \cdot 10^{-2}$	$5.58 \cdot 10^{-2}$	$1.12 \cdot 10^{-1}$	$2.51 \cdot 10^{-1}$	$7.16 \cdot 10^{-1}$	$6.04 \cdot 10^{-1}$	3.08	6.44
560	$2.97 \cdot 10^{-2}$	$5.94 \cdot 10^{-2}$	$1.19 \cdot 10^{-1}$	$2.67 \cdot 10^{-1}$	$7.61 \cdot 10^{-1}$	$6.42 \cdot 10^{-1}$	3.28	6.84
570	$3.16 \cdot 10^{-2}$	$6.32 \cdot 10^{-2}$	$1.26 \cdot 10^{-1}$	$2.84 \cdot 10^{-1}$	$8.07 \cdot 10^{-1}$	$6.81 \cdot 10^{-1}$	3.48	7.27
580	$3.36 \cdot 10^{-2}$	$6.71 \cdot 10^{-2}$	$1.34 \cdot 10^{-1}$	$3.02 \cdot 10^{-1}$	$8.56 \cdot 10^{-1}$	$7.22 \cdot 10^{-1}$	3.69	7.70
590	$3.56 \cdot 10^{-2}$	$7.12 \cdot 10^{-2}$	$1.42 \cdot 10^{-1}$	$3.20 \cdot 10^{-1}$	$9.07 \cdot 10^{-1}$	$7.65 \cdot 10^{-1}$	3.91	8.16
600	$3.77 \cdot 10^{-2}$	$7.54 \cdot 10^{-2}$	$1.51 \cdot 10^{-1}$	$3.39 \cdot 10^{-1}$	$9.59 \cdot 10^{-1}$	$8.09 \cdot 10^{-1}$	4.14	8.63
610	$3.99 \cdot 10^{-2}$	$7.98 \cdot 10^{-2}$	$1.60 \cdot 10^{-1}$	$3.59 \cdot 10^{-1}$	1.01	$8.55 \cdot 10^{-1}$	4.37	9.13
620	$4.22 \cdot 10^{-2}$	$8.44 \cdot 10^{-2}$	$1.69 \cdot 10^{-1}$	$3.80 \cdot 10^{-1}$	1.07	$9.03 \cdot 10^{-1}$	4.62	9.64
630	$4.46 \cdot 10^{-2}$	$8.92 \cdot 10^{-2}$	$1.78 \cdot 10^{-1}$	$4.01 \cdot 10^{-1}$	1.13	$9.53 \cdot 10^{-1}$	4.88	$1.02 \cdot 10^{1}$
640	$4.71 \cdot 10^{-2}$	$9.41 \cdot 10^{-2}$	$1.88 \cdot 10^{-1}$	$4.24 \cdot 10^{-1}$	1.19	1.00	5.14	$1.07 \cdot 10^{1}$
650	$4.96 \cdot 10^{-2}$	$9.93 \cdot 10^{-2}$	$1.99 \cdot 10^{-1}$	$4.47 \cdot 10^{-1}$	1.26	1.06	5.42	$1.13 \cdot 10^{1}$

Table B.7: SM Higgs-boson partial widths [GeV] for 4-fermion final states for the high-mass range. We list results for the specific final states $e^+e^-e^+e^-$ and $e^+e^-\mu^+\mu^-$, for final states with 4 arbitrary charged leptons, $e^+\nu_e e^-\bar{\nu}_e$ and $e^+\nu_e\mu^-\bar{\nu}_\mu$, and for final states $l^+l^-\nu_l\bar{\nu}_l$ with 2 charged leptons plus 2 neutrinos (ν_l represents any type of neutrinos).

M_H [GeV]	$H \to e^+e^-e^+e^-$	$H \to e^+e^-\mu^+\mu^-$	$H \to l^+l^-l^+l^-$ ($l = e$ or μ)	$H \to l^+l^-l^+l^-$ ($l = e, \mu$ or τ)	$H \to e^+\nu_e e^-\bar{\nu}_e$	$H \to e^+\nu_e\mu^-\bar{\nu}_\mu$	$H \to l^+l^-\nu_l\bar{\nu}_l$ ($l = e$ or μ)	$H \to l^+l^-\nu_l\bar{\nu}_l$ ($l = e, \mu$ or τ)
660	$5.23 \cdot 10^{-2}$	$1.05 \cdot 10^{-1}$	$2.09 \cdot 10^{-1}$	$4.71 \cdot 10^{-1}$	1.32	1.11	5.70	$1.19 \cdot 10^1$
670	$5.51 \cdot 10^{-2}$	$1.10 \cdot 10^{-1}$	$2.20 \cdot 10^{-1}$	$4.96 \cdot 10^{-1}$	1.39	1.17	6.00	$1.25 \cdot 10^1$
680	$5.80 \cdot 10^{-2}$	$1.16 \cdot 10^{-1}$	$2.32 \cdot 10^{-1}$	$5.22 \cdot 10^{-1}$	1.46	1.23	6.31	$1.32 \cdot 10^1$
690	$6.09 \cdot 10^{-2}$	$1.22 \cdot 10^{-1}$	$2.44 \cdot 10^{-1}$	$5.48 \cdot 10^{-1}$	1.54	1.29	6.63	$1.38 \cdot 10^1$
700	$6.40 \cdot 10^{-2}$	$1.28 \cdot 10^{-1}$	$2.56 \cdot 10^{-1}$	$5.76 \cdot 10^{-1}$	1.61	1.36	6.96	$1.45 \cdot 10^1$
710	$6.72 \cdot 10^{-2}$	$1.34 \cdot 10^{-1}$	$2.69 \cdot 10^{-1}$	$6.05 \cdot 10^{-1}$	1.69	1.42	7.30	$1.52 \cdot 10^1$
720	$7.05 \cdot 10^{-2}$	$1.41 \cdot 10^{-1}$	$2.82 \cdot 10^{-1}$	$6.35 \cdot 10^{-1}$	1.77	1.49	7.66	$1.60 \cdot 10^1$
730	$7.40 \cdot 10^{-2}$	$1.48 \cdot 10^{-1}$	$2.96 \cdot 10^{-1}$	$6.66 \cdot 10^{-1}$	1.86	1.56	8.02	$1.67 \cdot 10^1$
740	$7.75 \cdot 10^{-2}$	$1.55 \cdot 10^{-1}$	$3.10 \cdot 10^{-1}$	$6.98 \cdot 10^{-1}$	1.95	1.64	8.41	$1.75 \cdot 10^1$
750	$8.12 \cdot 10^{-2}$	$1.63 \cdot 10^{-1}$	$3.25 \cdot 10^{-1}$	$7.31 \cdot 10^{-1}$	2.04	1.72	8.80	$1.83 \cdot 10^1$
760	$8.51 \cdot 10^{-2}$	$1.70 \cdot 10^{-1}$	$3.40 \cdot 10^{-1}$	$7.66 \cdot 10^{-1}$	2.13	1.79	9.21	$1.92 \cdot 10^1$
770	$8.90 \cdot 10^{-2}$	$1.78 \cdot 10^{-1}$	$3.56 \cdot 10^{-1}$	$8.01 \cdot 10^{-1}$	2.23	1.88	9.63	$2.01 \cdot 10^1$
780	$9.31 \cdot 10^{-2}$	$1.86 \cdot 10^{-1}$	$3.73 \cdot 10^{-1}$	$8.38 \cdot 10^{-1}$	2.33	1.96	$1.01 \cdot 10^1$	$2.10 \cdot 10^1$
790	$9.74 \cdot 10^{-2}$	$1.95 \cdot 10^{-1}$	$3.89 \cdot 10^{-1}$	$8.76 \cdot 10^{-1}$	2.44	2.05	$1.05 \cdot 10^1$	$2.19 \cdot 10^1$
800	$1.02 \cdot 10^{-1}$	$2.04 \cdot 10^{-1}$	$4.07 \cdot 10^{-1}$	$9.16 \cdot 10^{-1}$	2.55	2.14	$1.10 \cdot 10^1$	$2.29 \cdot 10^1$
810	$1.06 \cdot 10^{-1}$	$2.13 \cdot 10^{-1}$	$4.25 \cdot 10^{-1}$	$9.57 \cdot 10^{-1}$	2.66	2.24	$1.15 \cdot 10^1$	$2.39 \cdot 10^1$
820	$1.11 \cdot 10^{-1}$	$2.22 \cdot 10^{-1}$	$4.44 \cdot 10^{-1}$	$9.99 \cdot 10^{-1}$	2.77	2.33	$1.20 \cdot 10^1$	$2.50 \cdot 10^1$
830	$1.16 \cdot 10^{-1}$	$2.32 \cdot 10^{-1}$	$4.63 \cdot 10^{-1}$	1.04	2.90	2.43	$1.25 \cdot 10^1$	$2.61 \cdot 10^1$
840	$1.21 \cdot 10^{-1}$	$2.42 \cdot 10^{-1}$	$4.83 \cdot 10^{-1}$	1.09	3.02	2.54	$1.30 \cdot 10^1$	$2.72 \cdot 10^1$
850	$1.26 \cdot 10^{-1}$	$2.52 \cdot 10^{-1}$	$5.04 \cdot 10^{-1}$	1.13	3.15	2.65	$1.36 \cdot 10^1$	$2.83 \cdot 10^1$
860	$1.31 \cdot 10^{-1}$	$2.63 \cdot 10^{-1}$	$5.26 \cdot 10^{-1}$	1.18	3.28	2.76	$1.42 \cdot 10^1$	$2.95 \cdot 10^1$
870	$1.37 \cdot 10^{-1}$	$2.74 \cdot 10^{-1}$	$5.48 \cdot 10^{-1}$	1.23	3.42	2.87	$1.48 \cdot 10^1$	$3.08 \cdot 10^1$
880	$1.43 \cdot 10^{-1}$	$2.85 \cdot 10^{-1}$	$5.71 \cdot 10^{-1}$	1.28	3.56	2.99	$1.54 \cdot 10^1$	$3.20 \cdot 10^1$
890	$1.49 \cdot 10^{-1}$	$2.97 \cdot 10^{-1}$	$5.94 \cdot 10^{-1}$	1.34	3.71	3.12	$1.60 \cdot 10^1$	$3.34 \cdot 10^1$
900	$1.55 \cdot 10^{-1}$	$3.09 \cdot 10^{-1}$	$6.19 \cdot 10^{-1}$	1.39	3.86	3.24	$1.67 \cdot 10^1$	$3.47 \cdot 10^1$
910	$1.61 \cdot 10^{-1}$	$3.22 \cdot 10^{-1}$	$6.44 \cdot 10^{-1}$	1.45	4.02	3.37	$1.73 \cdot 10^1$	$3.61 \cdot 10^1$
920	$1.68 \cdot 10^{-1}$	$3.35 \cdot 10^{-1}$	$6.71 \cdot 10^{-1}$	1.51	4.18	3.51	$1.80 \cdot 10^1$	$3.76 \cdot 10^1$
930	$1.74 \cdot 10^{-1}$	$3.49 \cdot 10^{-1}$	$6.98 \cdot 10^{-1}$	1.57	4.35	3.65	$1.88 \cdot 10^1$	$3.91 \cdot 10^1$
940	$1.81 \cdot 10^{-1}$	$3.63 \cdot 10^{-1}$	$7.26 \cdot 10^{-1}$	1.63	4.52	3.80	$1.95 \cdot 10^1$	$4.07 \cdot 10^1$
950	$1.89 \cdot 10^{-1}$	$3.77 \cdot 10^{-1}$	$7.54 \cdot 10^{-1}$	1.70	4.70	3.95	$2.03 \cdot 10^1$	$4.23 \cdot 10^1$
960	$1.96 \cdot 10^{-1}$	$3.92 \cdot 10^{-1}$	$7.84 \cdot 10^{-1}$	1.76	4.88	4.10	$2.11 \cdot 10^1$	$4.39 \cdot 10^1$
970	$2.04 \cdot 10^{-1}$	$4.08 \cdot 10^{-1}$	$8.15 \cdot 10^{-1}$	1.83	5.08	4.26	$2.19 \cdot 10^1$	$4.57 \cdot 10^1$
980	$2.12 \cdot 10^{-1}$	$4.24 \cdot 10^{-1}$	$8.47 \cdot 10^{-1}$	1.91	5.27	4.43	$2.28 \cdot 10^1$	$4.74 \cdot 10^1$
990	$2.20 \cdot 10^{-1}$	$4.40 \cdot 10^{-1}$	$8.80 \cdot 10^{-1}$	1.98	5.48	4.60	$2.37 \cdot 10^1$	$4.93 \cdot 10^1$
1000	$2.29 \cdot 10^{-1}$	$4.57 \cdot 10^{-1}$	$9.14 \cdot 10^{-1}$	2.06	5.69	4.78	$2.46 \cdot 10^1$	$5.12 \cdot 10^1$

Table B.8: SM Higgs-boson partial widths [GeV] for 4-fermion final states for the low- and intermediate-mass range. We list results for the specific final states for 2 charged leptons plus 2 quarks, $l^+\nu_l q\bar{q}'$ (not including charge conjugate state), 2 neutrinos plus 2 quarks, 4 quarks, as well as the result for arbitrary 4 fermions, where q = udscb and ν_l represents any type of neutrinos.

M_H [GeV]	$H \to l^+l^-q\bar{q}$ (l = e or μ)	$H \to l^+l^-q\bar{q}$ (l = e, μ or τ)	$H \to l^+\nu_l q\bar{q}'$ (l = e or μ)	$H \to \nu_l\bar{\nu}_l q\bar{q}$	$H \to qqqq$	$H \to ffff$
90	$8.70 \cdot 10^{-8}$	$1.31 \cdot 10^{-7}$	$6.74 \cdot 10^{-7}$	$2.62 \cdot 10^{-7}$	$2.34 \cdot 10^{-6}$	$5.28 \cdot 10^{-6}$
95	$1.46 \cdot 10^{-7}$	$2.19 \cdot 10^{-7}$	$1.61 \cdot 10^{-6}$	$4.39 \cdot 10^{-7}$	$5.43 \cdot 10^{-6}$	$1.21 \cdot 10^{-5}$
100	$2.59 \cdot 10^{-7}$	$3.89 \cdot 10^{-7}$	$3.99 \cdot 10^{-6}$	$7.80 \cdot 10^{-7}$	$1.33 \cdot 10^{-5}$	$2.94 \cdot 10^{-5}$
105	$5.23 \cdot 10^{-7}$	$7.85 \cdot 10^{-7}$	$9.31 \cdot 10^{-6}$	$1.57 \cdot 10^{-6}$	$3.09 \cdot 10^{-5}$	$6.82 \cdot 10^{-5}$
110	$1.15 \cdot 10^{-6}$	$1.72 \cdot 10^{-6}$	$1.99 \cdot 10^{-5}$	$3.45 \cdot 10^{-6}$	$6.66 \cdot 10^{-5}$	$1.47 \cdot 10^{-4}$
115	$2.51 \cdot 10^{-6}$	$3.77 \cdot 10^{-6}$	$3.92 \cdot 10^{-5}$	$7.53 \cdot 10^{-6}$	$1.33 \cdot 10^{-4}$	$2.92 \cdot 10^{-4}$
120	$5.19 \cdot 10^{-6}$	$7.79 \cdot 10^{-6}$	$7.25 \cdot 10^{-5}$	$1.56 \cdot 10^{-5}$	$2.50 \cdot 10^{-4}$	$5.47 \cdot 10^{-4}$
125	$1.00 \cdot 10^{-5}$	$1.51 \cdot 10^{-5}$	$1.28 \cdot 10^{-4}$	$3.00 \cdot 10^{-5}$	$4.46 \cdot 10^{-4}$	$9.75 \cdot 10^{-4}$
130	$1.83 \cdot 10^{-5}$	$2.74 \cdot 10^{-5}$	$2.17 \cdot 10^{-4}$	$5.46 \cdot 10^{-5}$	$7.65 \cdot 10^{-4}$	$1.67 \cdot 10^{-3}$
135	$3.16 \cdot 10^{-5}$	$4.74 \cdot 10^{-5}$	$3.62 \cdot 10^{-4}$	$9.45 \cdot 10^{-5}$	$1.28 \cdot 10^{-3}$	$2.80 \cdot 10^{-3}$
140	$5.26 \cdot 10^{-5}$	$7.89 \cdot 10^{-5}$	$6.00 \cdot 10^{-4}$	$1.57 \cdot 10^{-4}$	$2.13 \cdot 10^{-3}$	$4.64 \cdot 10^{-3}$
145	$8.49 \cdot 10^{-5}$	$1.27 \cdot 10^{-4}$	$1.01 \cdot 10^{-3}$	$2.53 \cdot 10^{-4}$	$3.55 \cdot 10^{-3}$	$7.75 \cdot 10^{-3}$
150	$1.34 \cdot 10^{-4}$	$2.01 \cdot 10^{-4}$	$1.77 \cdot 10^{-3}$	$3.99 \cdot 10^{-4}$	$6.16 \cdot 10^{-3}$	$1.35 \cdot 10^{-2}$
155	$2.08 \cdot 10^{-4}$	$3.13 \cdot 10^{-4}$	$3.52 \cdot 10^{-3}$	$6.22 \cdot 10^{-4}$	$1.20 \cdot 10^{-2}$	$2.63 \cdot 10^{-2}$
160	$3.23 \cdot 10^{-4}$	$4.84 \cdot 10^{-4}$	$1.10 \cdot 10^{-2}$	$9.63 \cdot 10^{-4}$	$3.59 \cdot 10^{-2}$	$7.87 \cdot 10^{-2}$
165	$5.12 \cdot 10^{-4}$	$7.68 \cdot 10^{-4}$	$3.46 \cdot 10^{-2}$	$1.53 \cdot 10^{-3}$	$1.10 \cdot 10^{-1}$	$2.42 \cdot 10^{-1}$
170	$8.42 \cdot 10^{-4}$	$1.26 \cdot 10^{-3}$	$5.37 \cdot 10^{-2}$	$2.51 \cdot 10^{-3}$	$1.71 \cdot 10^{-1}$	$3.75 \cdot 10^{-1}$
175	$1.52 \cdot 10^{-3}$	$2.27 \cdot 10^{-3}$	$7.03 \cdot 10^{-2}$	$4.53 \cdot 10^{-3}$	$2.26 \cdot 10^{-1}$	$4.96 \cdot 10^{-1}$
180	$3.56 \cdot 10^{-3}$	$5.34 \cdot 10^{-3}$	$8.61 \cdot 10^{-2}$	$1.06 \cdot 10^{-2}$	$2.86 \cdot 10^{-1}$	$6.26 \cdot 10^{-1}$
185	$1.17 \cdot 10^{-2}$	$1.76 \cdot 10^{-2}$	$1.03 \cdot 10^{-1}$	$3.50 \cdot 10^{-2}$	$3.80 \cdot 10^{-1}$	$8.27 \cdot 10^{-1}$
190	$2.04 \cdot 10^{-2}$	$3.07 \cdot 10^{-2}$	$1.20 \cdot 10^{-1}$	$6.11 \cdot 10^{-2}$	$4.78 \cdot 10^{-1}$	1.03
195	$2.77 \cdot 10^{-2}$	$4.15 \cdot 10^{-2}$	$1.37 \cdot 10^{-1}$	$8.27 \cdot 10^{-2}$	$5.69 \cdot 10^{-1}$	1.23
200	$3.44 \cdot 10^{-2}$	$5.15 \cdot 10^{-2}$	$1.55 \cdot 10^{-1}$	$1.03 \cdot 10^{-1}$	$6.61 \cdot 10^{-1}$	1.43
210	$4.75 \cdot 10^{-2}$	$7.12 \cdot 10^{-2}$	$1.96 \cdot 10^{-1}$	$1.42 \cdot 10^{-1}$	$8.54 \cdot 10^{-1}$	1.84
220	$6.13 \cdot 10^{-2}$	$9.20 \cdot 10^{-2}$	$2.41 \cdot 10^{-1}$	$1.83 \cdot 10^{-1}$	1.07	2.30
230	$7.66 \cdot 10^{-2}$	$1.15 \cdot 10^{-1}$	$2.92 \cdot 10^{-1}$	$2.29 \cdot 10^{-1}$	1.31	2.81
240	$9.35 \cdot 10^{-2}$	$1.40 \cdot 10^{-1}$	$3.50 \cdot 10^{-1}$	$2.79 \cdot 10^{-1}$	1.57	3.39
250	$1.12 \cdot 10^{-1}$	$1.69 \cdot 10^{-1}$	$4.15 \cdot 10^{-1}$	$3.36 \cdot 10^{-1}$	1.87	4.03
260	$1.34 \cdot 10^{-1}$	$2.00 \cdot 10^{-1}$	$4.87 \cdot 10^{-1}$	$3.99 \cdot 10^{-1}$	2.21	4.75
270	$1.57 \cdot 10^{-1}$	$2.36 \cdot 10^{-1}$	$5.66 \cdot 10^{-1}$	$4.69 \cdot 10^{-1}$	2.58	5.54
280	$1.83 \cdot 10^{-1}$	$2.75 \cdot 10^{-1}$	$6.54 \cdot 10^{-1}$	$5.47 \cdot 10^{-1}$	2.98	6.42
290	$2.12 \cdot 10^{-1}$	$3.17 \cdot 10^{-1}$	$7.50 \cdot 10^{-1}$	$6.32 \cdot 10^{-1}$	3.43	7.37
300	$2.43 \cdot 10^{-1}$	$3.64 \cdot 10^{-1}$	$8.54 \cdot 10^{-1}$	$7.25 \cdot 10^{-1}$	3.91	8.42
310	$2.76 \cdot 10^{-1}$	$4.15 \cdot 10^{-1}$	$9.67 \cdot 10^{-1}$	$8.26 \cdot 10^{-1}$	4.44	9.55
320	$3.13 \cdot 10^{-1}$	$4.70 \cdot 10^{-1}$	1.09	$9.36 \cdot 10^{-1}$	5.01	$1.08 \cdot 10^1$
330	$3.52 \cdot 10^{-1}$	$5.28 \cdot 10^{-1}$	1.22	1.05	5.62	$1.21 \cdot 10^1$
340	$3.93 \cdot 10^{-1}$	$5.90 \cdot 10^{-1}$	1.36	1.18	6.26	$1.35 \cdot 10^1$
350	$4.37 \cdot 10^{-1}$	$6.56 \cdot 10^{-1}$	1.50	1.31	6.94	$1.49 \cdot 10^1$
360	$4.89 \cdot 10^{-1}$	$7.34 \cdot 10^{-1}$	1.68	1.46	7.75	$1.67 \cdot 10^1$
370	$5.45 \cdot 10^{-1}$	$8.18 \cdot 10^{-1}$	1.86	1.63	8.62	$1.85 \cdot 10^1$
380	$6.05 \cdot 10^{-1}$	$9.08 \cdot 10^{-1}$	2.06	1.81	9.54	$2.05 \cdot 10^1$
390	$6.69 \cdot 10^{-1}$	1.00	2.27	2.00	$1.05 \cdot 10^1$	$2.26 \cdot 10^1$
400	$7.37 \cdot 10^{-1}$	1.11	2.49	2.20	$1.16 \cdot 10^1$	$2.48 \cdot 10^1$
410	$8.09 \cdot 10^{-1}$	1.21	2.72	2.42	$1.27 \cdot 10^1$	$2.72 \cdot 10^1$
420	$8.85 \cdot 10^{-1}$	1.33	2.97	2.64	$1.38 \cdot 10^1$	$2.97 \cdot 10^1$
430	$9.66 \cdot 10^{-1}$	1.45	3.22	2.88	$1.50 \cdot 10^1$	$3.23 \cdot 10^1$
440	1.05	1.58	3.50	3.14	$1.63 \cdot 10^1$	$3.51 \cdot 10^1$
450	1.14	1.71	3.78	3.41	$1.77 \cdot 10^1$	$3.80 \cdot 10^1$
460	1.24	1.85	4.08	3.69	$1.91 \cdot 10^1$	$4.10 \cdot 10^1$
470	1.33	2.00	4.40	3.99	$2.06 \cdot 10^1$	$4.43 \cdot 10^1$
480	1.44	2.16	4.73	4.30	$2.22 \cdot 10^1$	$4.76 \cdot 10^1$
490	1.55	2.32	5.08	4.63	$2.38 \cdot 10^1$	$5.12 \cdot 10^1$

Table B.9: SM Higgs-boson partial widths [GeV] for 4-fermion final states for the hig-mass range. We list results for the specific finalstates for 2 charged leptons plus 2 quarks, $l^+\nu_l q\overline{q}'$ (not including charge conjugate state), 2 neutrinos plus 2 quarks, 4 quarks, as well as the result for arbitrary 4 fermions, where $q = udscb$ and ν_l represents any type of neutrinos.

M_H [GeV]	$H \to l^+l^-q\overline{q}$ (l = e or μ)	$H \to l^+l^-q\overline{q}$ (l = e, μ or τ)	$H \to l^+\nu_l q\overline{q}'$ (l = e or μ)	$H \to \nu_l\overline{\nu}_l q\overline{q}$	$H \to qqqq$	$H \to ffff$
500	1.66	2.50	5.44	4.97	$2.55 \cdot 10^1$	$5.48 \cdot 10^1$
510	1.78	2.68	5.82	5.33	$2.73 \cdot 10^1$	$5.87 \cdot 10^1$
520	1.91	2.87	6.21	5.70	$2.92 \cdot 10^1$	$6.27 \cdot 10^1$
530	2.04	3.06	6.62	6.10	$3.12 \cdot 10^1$	$6.70 \cdot 10^1$
540	2.18	3.27	7.05	6.51	$3.32 \cdot 10^1$	$7.14 \cdot 10^1$
550	2.32	3.49	7.50	6.94	$3.53 \cdot 10^1$	$7.60 \cdot 10^1$
560	2.47	3.71	7.97	7.38	$3.76 \cdot 10^1$	$8.07 \cdot 10^1$
570	2.63	3.94	8.46	7.85	$3.99 \cdot 10^1$	$8.57 \cdot 10^1$
580	2.79	4.19	8.97	8.33	$4.23 \cdot 10^1$	$9.09 \cdot 10^1$
590	2.96	4.44	9.49	8.84	$4.48 \cdot 10^1$	$9.63 \cdot 10^1$
600	3.14	4.71	$1.00 \cdot 10^1$	9.37	$4.74 \cdot 10^1$	$1.02 \cdot 10^2$
610	3.32	4.98	$1.06 \cdot 10^1$	9.91	$5.02 \cdot 10^1$	$1.08 \cdot 10^2$
620	3.51	5.27	$1.12 \cdot 10^1$	$1.05 \cdot 10^1$	$5.30 \cdot 10^1$	$1.14 \cdot 10^2$
630	3.71	5.56	$1.18 \cdot 10^1$	$1.11 \cdot 10^1$	$5.59 \cdot 10^1$	$1.20 \cdot 10^2$
640	3.91	5.87	$1.25 \cdot 10^1$	$1.17 \cdot 10^1$	$5.89 \cdot 10^1$	$1.27 \cdot 10^2$
650	4.13	6.19	$1.31 \cdot 10^1$	$1.23 \cdot 10^1$	$6.21 \cdot 10^1$	$1.34 \cdot 10^2$
660	4.35	6.53	$1.38 \cdot 10^1$	$1.30 \cdot 10^1$	$6.54 \cdot 10^1$	$1.41 \cdot 10^2$
670	4.58	6.87	$1.45 \cdot 10^1$	$1.37 \cdot 10^1$	$6.88 \cdot 10^1$	$1.48 \cdot 10^2$
680	4.82	7.23	$1.53 \cdot 10^1$	$1.44 \cdot 10^1$	$7.23 \cdot 10^1$	$1.55 \cdot 10^2$
690	5.06	7.60	$1.60 \cdot 10^1$	$1.51 \cdot 10^1$	$7.60 \cdot 10^1$	$1.63 \cdot 10^2$
700	5.32	7.99	$1.68 \cdot 10^1$	$1.59 \cdot 10^1$	$7.98 \cdot 10^1$	$1.72 \cdot 10^2$
710	5.59	8.38	$1.77 \cdot 10^1$	$1.67 \cdot 10^1$	$8.37 \cdot 10^1$	$1.80 \cdot 10^2$
720	5.87	8.80	$1.85 \cdot 10^1$	$1.75 \cdot 10^1$	$8.78 \cdot 10^1$	$1.89 \cdot 10^2$
730	6.15	9.23	$1.94 \cdot 10^1$	$1.84 \cdot 10^1$	$9.20 \cdot 10^1$	$1.98 \cdot 10^2$
740	6.45	9.67	$2.03 \cdot 10^1$	$1.92 \cdot 10^1$	$9.64 \cdot 10^1$	$2.07 \cdot 10^2$
750	6.75	$1.01 \cdot 10^1$	$2.13 \cdot 10^1$	$2.01 \cdot 10^1$	$1.01 \cdot 10^2$	$2.17 \cdot 10^2$
760	7.07	$1.06 \cdot 10^1$	$2.22 \cdot 10^1$	$2.11 \cdot 10^1$	$1.06 \cdot 10^2$	$2.27 \cdot 10^2$
770	7.40	$1.11 \cdot 10^1$	$2.33 \cdot 10^1$	$2.21 \cdot 10^1$	$1.10 \cdot 10^2$	$2.37 \cdot 10^2$
780	7.74	$1.16 \cdot 10^1$	$2.43 \cdot 10^1$	$2.31 \cdot 10^1$	$1.15 \cdot 10^2$	$2.48 \cdot 10^2$
790	8.09	$1.21 \cdot 10^1$	$2.54 \cdot 10^1$	$2.41 \cdot 10^1$	$1.21 \cdot 10^2$	$2.59 \cdot 10^2$
800	8.45	$1.27 \cdot 10^1$	$2.65 \cdot 10^1$	$2.52 \cdot 10^1$	$1.26 \cdot 10^2$	$2.71 \cdot 10^2$
810	8.83	$1.32 \cdot 10^1$	$2.77 \cdot 10^1$	$2.63 \cdot 10^1$	$1.31 \cdot 10^2$	$2.83 \cdot 10^2$
820	9.22	$1.38 \cdot 10^1$	$2.89 \cdot 10^1$	$2.75 \cdot 10^1$	$1.37 \cdot 10^2$	$2.95 \cdot 10^2$
830	9.62	$1.44 \cdot 10^1$	$3.01 \cdot 10^1$	$2.87 \cdot 10^1$	$1.43 \cdot 10^2$	$3.08 \cdot 10^2$
840	$1.00 \cdot 10^1$	$1.51 \cdot 10^1$	$3.14 \cdot 10^1$	$2.99 \cdot 10^1$	$1.49 \cdot 10^2$	$3.21 \cdot 10^2$
850	$1.05 \cdot 10^1$	$1.57 \cdot 10^1$	$3.28 \cdot 10^1$	$3.12 \cdot 10^1$	$1.56 \cdot 10^2$	$3.35 \cdot 10^2$
860	$1.09 \cdot 10^1$	$1.64 \cdot 10^1$	$3.41 \cdot 10^1$	$3.25 \cdot 10^1$	$1.62 \cdot 10^2$	$3.49 \cdot 10^2$
870	$1.14 \cdot 10^1$	$1.71 \cdot 10^1$	$3.56 \cdot 10^1$	$3.39 \cdot 10^1$	$1.69 \cdot 10^2$	$3.63 \cdot 10^2$
880	$1.18 \cdot 10^1$	$1.78 \cdot 10^1$	$3.70 \cdot 10^1$	$3.53 \cdot 10^1$	$1.76 \cdot 10^2$	$3.78 \cdot 10^2$
890	$1.23 \cdot 10^1$	$1.85 \cdot 10^1$	$3.85 \cdot 10^1$	$3.68 \cdot 10^1$	$1.83 \cdot 10^2$	$3.94 \cdot 10^2$
900	$1.28 \cdot 10^1$	$1.93 \cdot 10^1$	$4.01 \cdot 10^1$	$3.83 \cdot 10^1$	$1.90 \cdot 10^2$	$4.10 \cdot 10^2$
910	$1.34 \cdot 10^1$	$2.00 \cdot 10^1$	$4.17 \cdot 10^1$	$3.99 \cdot 10^1$	$1.98 \cdot 10^2$	$4.27 \cdot 10^2$
920	$1.39 \cdot 10^1$	$2.09 \cdot 10^1$	$4.34 \cdot 10^1$	$4.15 \cdot 10^1$	$2.06 \cdot 10^2$	$4.44 \cdot 10^2$
930	$1.45 \cdot 10^1$	$2.17 \cdot 10^1$	$4.51 \cdot 10^1$	$4.31 \cdot 10^1$	$2.14 \cdot 10^2$	$4.62 \cdot 10^2$
940	$1.50 \cdot 10^1$	$2.26 \cdot 10^1$	$4.69 \cdot 10^1$	$4.49 \cdot 10^1$	$2.23 \cdot 10^2$	$4.80 \cdot 10^2$
950	$1.56 \cdot 10^1$	$2.35 \cdot 10^1$	$4.88 \cdot 10^1$	$4.66 \cdot 10^1$	$2.32 \cdot 10^2$	$4.99 \cdot 10^2$
960	$1.63 \cdot 10^1$	$2.44 \cdot 10^1$	$5.07 \cdot 10^1$	$4.85 \cdot 10^1$	$2.41 \cdot 10^2$	$5.18 \cdot 10^2$
970	$1.69 \cdot 10^1$	$2.53 \cdot 10^1$	$5.27 \cdot 10^1$	$5.04 \cdot 10^1$	$2.50 \cdot 10^2$	$5.39 \cdot 10^2$
980	$1.76 \cdot 10^1$	$2.63 \cdot 10^1$	$5.47 \cdot 10^1$	$5.23 \cdot 10^1$	$2.60 \cdot 10^2$	$5.59 \cdot 10^2$
990	$1.82 \cdot 10^1$	$2.74 \cdot 10^1$	$5.68 \cdot 10^1$	$5.44 \cdot 10^1$	$2.70 \cdot 10^2$	$5.81 \cdot 10^2$
1000	$1.89 \cdot 10^1$	$2.84 \cdot 10^1$	$5.90 \cdot 10^1$	$5.64 \cdot 10^1$	$2.80 \cdot 10^2$	$6.03 \cdot 10^2$